Department of Chemistry

THE UNIVERSITY
OF ADELAIDE
AUSTRALIA

FROM TWO AND BEYOND!

Synthesis and Chemistry of Group 8 Alkynyl Complexes

A Thesis Submitted Towards the Degree of Doctor of Philosophy.

By Gary James Perkins B.Sc. (Hons)

May 2006

Contents

Abstract.

Chapter One gives an introduction to the history of molecular electronics and its importance in future electronic devices. A brief overview of the four classes of transition metal complexes as possible models for molecular wires, and the three most common methods of evaluating these complexes is given. This thesis furthers the work in Group 8 transition metal yndiyl and poly-yndiyl complexes with particular interest in their potential as models for molecular wires.

Chapter Two describes the synthesis of three diyndiyl complexes Cp*(dppe)OsC≡CC≡CM(dppe)Cp* (where M = Fe, Ru, Os) along with the mono- and di-cations of {Cp*(dppe)Os}$_2$(μ–C≡CC≡C). Detailed examination of the electrochemistry of these complexes revealed the expected three or four one-electron oxidation steps. These redox events for osmium occur at intermediate values compared to other symmetrical Group 8 complexes, while those mixed complexes appear at intermediate values to the two corresponding symmetrical complexes.

Chapter Three summarises the syntheses of several yndiyl complexes of the general formula Cp(dppe)RuC$_2$M(dppe)Cp', prepared from [Cp'(dppe)M=C=CH$_2$] [PF$_6$] (where M = Fe, Ru, Os and Cp' = Cp, Cp*), and RuCl(dppe)Cp. Double deprotonation of [Cp'(dppe)M=C=CH$_2$][PF$_6$] with ^{n}BuLi yields the lithium salt Cp'(dppe)MC≡CLi, which can be further reacted with the ruthenium tetrahydrofuran cation to give the desired yndiyl complex. The electrochemistry of these complexes demonstrates the subtle variations in the three group 8 metals. Detailed examination of the metal-metal interactions also allows comparisons to be drawn about the effect of chain length on these interactions.

Chapter Four details the synthesis of several compounds containing the anthracene moiety. Starting from either TMSC≡CC$_{14}$H$_8$C≡CTMS or Cp*(dppe)FeC≡CC$_{14}$H$_8$ C≡CTIPS, treatment with RuCl(dppe)Cp* in the presence of a desilylating reagent gives the symmetrical or asymmetric complexes Cp*(dppe)RuC≡CC$_{14}$H$_8$C≡CM(dppe)Cp*

(where M = Ru, Fe). An NMR study of the derived di-cations revealed that there is no singlet-triplet state interconversion as demonstrated by the diamagnetic nature of the ^1H NMR. Also reported are the syntheses of several anthracene compounds en-route to the synthesis of an organo-iron complex with a possible trapped singlet state.

Chapter Five summarises some reactions of two yndiyl complexes, OsC≡CFc(dppe)Cp and 1,1'-{Cp[*m*-tol$_3$P]$_2$RuC≡C}$_2$Rc'. A detailed electrochemical study of the parent complexes revealed that the ferroceneayl and ruthenoceneayl moieties act as insulators to the metal-metal interactions observed in the straight chain diyndiyl complexes. Treatment of OsC≡CFc(dppe)Cp with TCNE resulted in addition of the electron-poor alkene across the electron-rich triple bond. The same reaction with 1,1'-(Cp[*m*-tol$_3$P]$_2$RuC≡C)$_2$Rc' resulted in a similar addition across the electron-rich triple bond together with displacement of one *m*-tol$_3$P ligand.

Chapter Six describes the synthesis of several osmium organometallic starting materials. Previously these starting materials have been synthesised from the extremely toxic osmium tetroxide. Starting from the stable potassium osmate, treatment with concentrated hydrochloric acid gives $K_2[OsCl_6]$. This material can be easily reduced in the presence of triphenylphosphine and then further reacted with LiCp to give OsCl(PPh$_3$)$_2$Cp. This starting material undergoes a ready ligand exchange with bis(diphenylphosphino)ethane to yield the desired starting material OsCl(dppe)Cp. Treatment of $K_2[OsCl_6]$ with pentamethylcyclopentadiene and then further with 1,5-cyclooctadiene yields OsCl(COD)Cp*. This complex also undergoes ready ligand exchange with bis(diphenylphosphino)ethane to give the desired OsCl(dppe)Cp*. The electrochemistry of these two complexes reveals lower first oxidation potentials when compared to both ruthenium analogues. X-ray crystal structure determinations are also reported for both of these novel starting materials. This chapter also summarises the advantages of using alcohol solvents in the synthesis of several known and novel organometallic vinylidene complexes.

Declaration.

This thesis contains no material which has been accepted for the award of any other degree or diploma in any university and to the best of my knowledge, contains no material previously published or written by another person except where due reference has been made.

I give consent for this thesis to be made available for photocopying and loan if applicable.

Signed:

Gary James Perkins

Date:

Department of Chemistry,
The University of Adelaide,
Adelaide, South Australia.

Acknowledgements.

Firstly I would like to acknowledge my supervisor Professor Michael Bruce for all his help throughout my PhD along with my co-supervisor Dr Marcus Cole. He has not only given me the opportunity to work within his lab but has encouraged me to extend myself as a chemist through a tough but rewarding project. I would like to acknowledge his collaborators Professor Claude Lapinte, Professor Jean-François Halet and Dr Paul Low, which allowed me to spend six months abroad in Professor Lapinte and Dr Low's Labs. I would also like to thank Professor Allan White and Dr Brian Skelton for the X-ray structures and data and Professor Brian Nicholson for the mass spectra.

I would also like to thank all the members of Lab 9 and 10 for all their help but especially Ben Ellis and Martyn Jevric who have taught me a lot about chemistry along with Natasha Zaitseva for her help with crystals. Also Maryka Gaudio, Paul Humphrey, Ben Hall, Christian Parker, Nancy Scoleri, Cassandra Mitchell and David Armitt who have not only helped in the lab, but were all willing to help make light of a tough situation. I can not forget the members of the french lab Gilles, Fred, Jen, Safaa, Fred and Gwen who made me feel at home despite my limited French.

For those that gave their time to read my thesis Professor Michael Bruce, Dr Ben Hall, Alison Perkins and Elizabeth Perkins I thankyou for giving up your time.

I must also thank the general staff of Graham, Peter and John who were always there to lend a hand on chemistry and non-chemistry matters.

I would like to thank my two best friends John, who despite studying med still have time to talk and Shanti who understood fully the ups and downs of a PhD. I will cherish your friendship for a lifetime to come.

I can't forget the Adelaide University Scuba Diving Club Committee of 2005. Dave, Tim, Andrea, Lesly, Lauren, Filip, Kris and Michael who gave me a release outside of chemistry to help keep me sane.

Last but definitely not least my family and extended family. My parents for all their support not just through my PhD, but through my entire career so far. My father Dale who taught me "you can't fight change but manage it to best suit yourself" and my mother Heather for her undeniable skill to make things look good no matter how bad they seem. My oldest sister Alison for her knowledge of the english language and her partner Cameron who despite moving to NZ can still make me laugh. My older brother Mark and his partner Anneliese who also moved, but to Brisbane, have been happy to have me up there and feed me without question. Also my younger sister Elizabeth who has put up with living with me through my PhD and for making a great dive buddy to get out of the house. I thank you seven most of all!

Abbreviations.

°	Degrees
°C	Degrees celsius
$[L_nM]$	General metal-ligand fragment
δ	Chemical shift
Å	Ångstrom
abs	Absorbance
Anal.	Analysis
Amp	Amperes
br	Broad
^{t}Bu	Tertiary butyl
C_α	Carbon bonded directly to the metal
C_β	Carbon bonded directly to C_α
C_γ	Carbon bonded directly to C_β
ca	Approximately
Calcd	Calculated
cm^{-1}	Wavenumbers
COD	1,5-Cyclooctadiene
Cp	Cyclopentadienyl
Cp*	Pentamethylcyclopentadienyl
CV	Cyclic Voltammetry
d	Doublet
dbu	1,8-Diazabicyclo[5.4.0]undec-7-ene
DFT	Density functional theory
dippe	ethylenebis(diisopropylphosphine)
DNA	Deoxyribonucleic acid
dppe	1,2-Bis(diphenylphosphino)ethane
E	Potential
$E_{1/2}$	Half-wave potential
ΔE	Potential difference

e^-	Electron
eg.	Example
eq	Equivalents
E°	Formal electrode potential
EtOH	Ethanol
ES-MS	Electrospray mass spectrum
eV	Electron volts
F	Faraday constant, 9.6485×10^4 C mol^{-1}
Fc	Ferrocenyl
h	Hour(s)
HOMO	Highest occupied molecular orbital
Hz	Hertz
I	Current
i_a	Anodic peak current
i_c	Cathodic peak current
IR	Infrared
IC	Integrated circuit
IVCT	Intervalence charge transfer
J	Coupling constant
K	Kelvin
K_c	Comproportination constant
L	Ligand or litre
m	Medium or multiplet
M	Metal or molarity
Me	Methyl, CH_3
MeOH	Methanol
mg	Milligrams
min	Minutes
mL	Millilitres
mmol	Millimoles
MO	Molecular orbital

MV	Mixed valence
MWCNT	Multi-walled carbon nanotube
m/z	Mass per unit charge
NIR	Near-infrared
ORTEP	Oak Ridge Thermal Ellipsoid Plot Program
OTf	Triflate, trifluoromethanesulfonate, $CF_3SO_3^-$
OTTLE	Optically transparent thin-layer electrochemical
Ph	Phenyl, $-C_6H_5$
PPh_3	Triphenylphosphine
ppm	Parts per million
pz	Pyrazine
R	Gas constant, 8.31451 J K^{-1} mol^{-1}
Rc	Ruthenocenyl
r.t.	Room temperature
s	Strong or singlet
SCE	Saturated calomel electrode
SWCNT	Single-walled carbon nanotube
TCNE	Tetracyanoethylene
THF	Tetrahydrofuran
TLC	Thin layer chromatography
tol	C_6H_4Me
TMS	Trimethylsilyl, $-Si(CH_3)_3$, $SiMe_3$
UV	Ultraviolet
V_{ab}	Electronic coupling parameter
VIS	Visible
vs	Very strong
w	Weak
X	Halide

Chapter One

Introduction

1.1. Molecular electronics.

Since 1958 and the first revolution of electronics with the invention of the integrated circuit, it has long been considered that the ultimate revolution would be performing these same logic and memory operations on a single molecule.[1]

At present, Electronics have been driven by a "top down" approach with design of progressively smaller integrated circuits culminating in the process called photolithography. An integrated circuit is a series of precisely patterned and positioned layers of dielectric and conduction materials. The process of photolithography allows areas of these layers, typically made from silicon, to be delineated for doping and internal connections.[2]

In 1965 Gordon Moore predicted a trend where the number of components on an integrated circuit would double every year. This blueprint still stands true today for the electronics industry, but many physical considerations have arisen. Such barriers include oxide layers at the three-atom thick level, which results in charge leakage due to inadequate insulation.[3] The other barrier for this "top down" approach is the cost of developing and constructing new fabrication lines for every new generation of integrated circuit. Using a "bottom up" approach with the use of individual molecules might give rise to the prospect for a rapid and cost effective means of producing these revolutionary circuits.

1.2. Molecular circuits.

Presently there has been increasing interest in the design of molecular components. Synthesis of many individual molecular components (see Figure 1.1) have been successful with molecular switches,[4-6] memories,[7,8] and diodes[9] reported. Before these individual components can be considered a molecular circuit they require molecular wires to tether these devices together.[10-13]

It was first suggested in 1974 that purely organic compounds could be used as molecular wires.[14] By definition a molecular wire is a "one-dimensional molecule allowing a through-bridge exchange of an electron/hole between its remote ends/terminal groups, themselves able to exchange electrons with the outside world".[12]

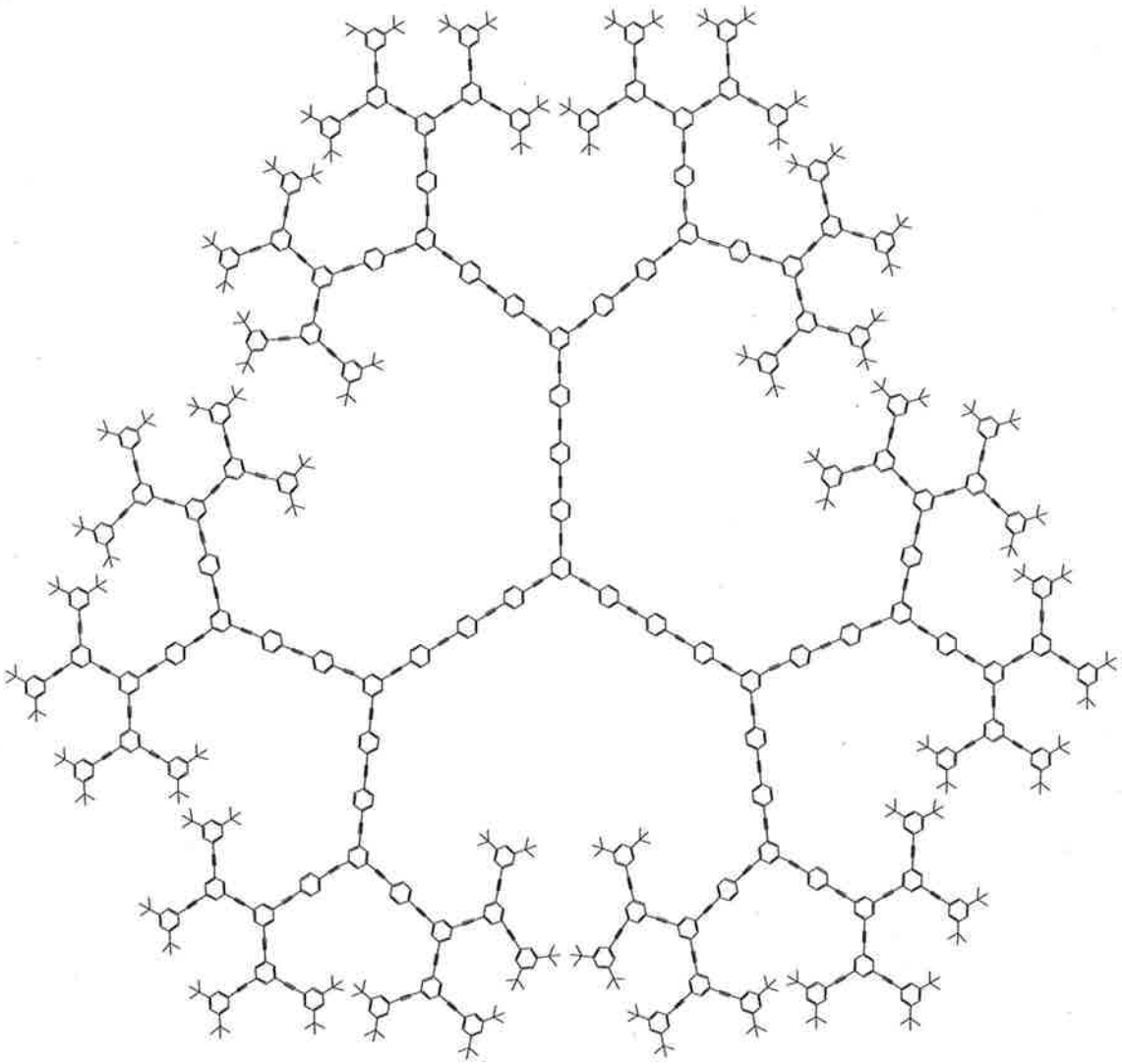

Figure 1.1. *Possible molecular device.*[15]

1.3. Molecular wires.

Molecular wires are the most basic component of any molecular circuit. There have been many suggestions for suitable compounds, such as conjugated organic compounds,[16,17] carbon nano-tubes,[18] redox-active complexes,[19] DNA[20] and oligomers,[21] as potential molecular wires. Even though the structures of these compounds vary widely they all possess the ability to allow the transport of an electron from a donor to an acceptor. Although they are the simplest component, this simplicity creates a basis around which all molecular components can be designed, allowing for the assembly of the molecular circuit.

1.3.1. Conjugated organic compounds.

Conjugated organic compounds have long been suggested as possible molecular wires because of their precise length and number of molecular constituents (see Figure 1.2).[16,22]

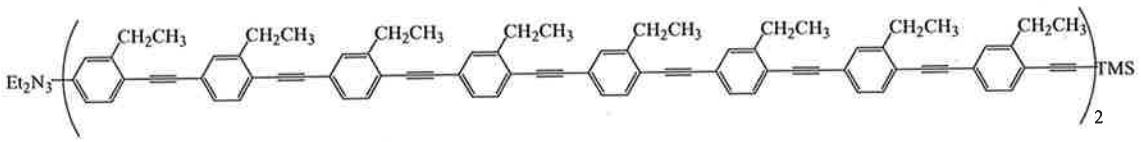

Figure 1.2. *Possible conjugated organic molecular wire.*

These conjugated systems also have a distinct advantage over non-conjugated systems with the continuous overlap of π-density. This π-overlap not only creates a through-bridge for utilisation in molecular circuits but also creates rigidity, which promotes the self-assembly of these molecular devices.[3] The great possibility lies not only in the wide range of known organic reactions but also in the diverse number of known organic compounds. Thiol moieties allow for the adhesion of these conjugated organic compounds onto gold surfaces by self-assembly.[3]

1.3.2. Carbon nano-tubes.

Since the discovery of carbon nanotubes in 1991,[23] they have been regarded as one of the most promising candidates for molecular wires.[24] Their great desirability arises from their mechanical stiffness and their electronic properties, such as their conductivity (See Figure 1.3).[25]

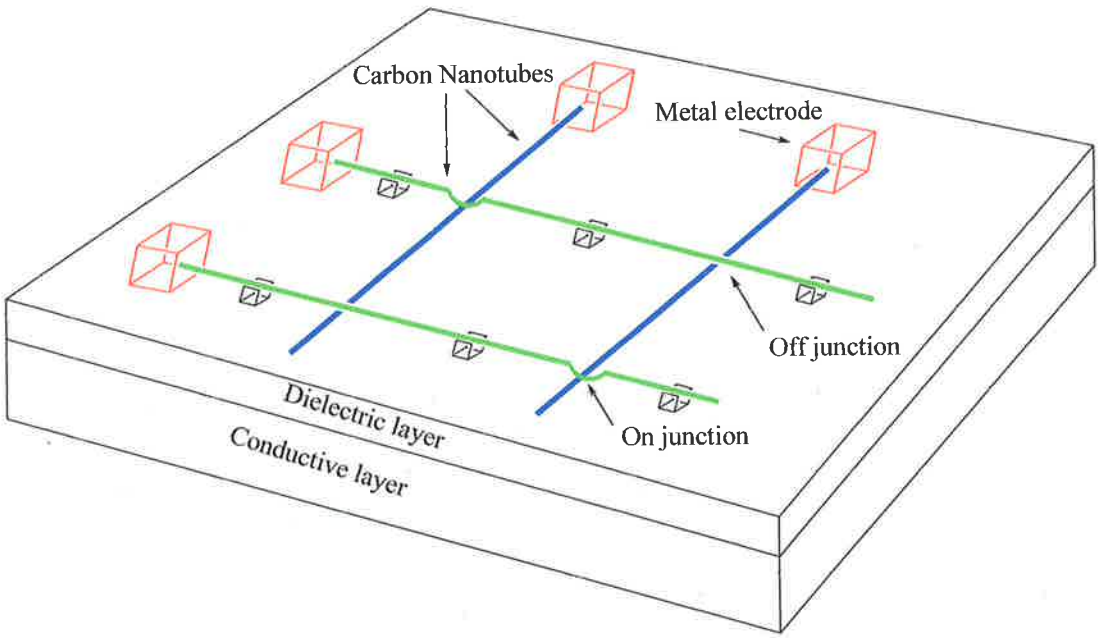

Figure 1.3. *3D view of a possible molecular device using carbon nanotubes.*[26]

There are two different types of carbon nanotubes, single-walled (SWNT) and multi-walled nanotubes (MWNT). In MWNT, which vary between two and 50 layers, it was found that the electronic properties of the individual tubes can differ dramatically due to interactions of adjacent layers.[25] SWNT have demonstrated a great potential as possible molecular wires.[25] The conductivity is one of the most important electronic considerations of any potential molecular wire. In a SWNT this depends on two factors, the tube diameter and wrapping angle (see Figure 1.4).[27] These can be altered to tune the conductivity of the SWNT. Furthermore through the use of scanning tunnelling microscopy, it is possible to relate these structural differences, and therefore predict the conductivity of any SWNT.[28]

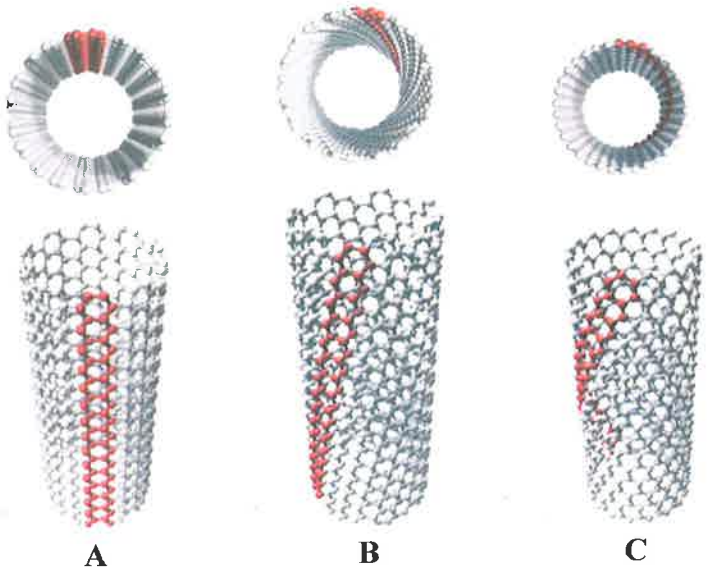

Figure 1.4. *Structural differences of carbon nanotubes. A. Armchair. B. Chiral. C. Zigzag.*

The biggest problem for carbon nanotubes at present is the selectivity inherent in their synthesis. There are four methods used:

1. carbon discharge;
2. pyrolysis of hydrocarbons or other carbon-containing molecules over metal catalysts;
3. laser vaporisation of graphite;
4. electrolysis using graphite electrodes immersed in molten ionic salts.[25]

Even though these methods are very effective in the synthesis of carbon nanotubes there is little control over the growth or thickness. This means that the desired nanotube must be separated from a mixture of unwanted nanotubes, which is virtually impossible on a large scale.

Defects such as pentagon-heptagon irregularities, called elbow connections, [25] within the SWNT can affect the conductivity allowing charge to flow in only one direction. These defects may have some advantages giving points at which the nanotube can be doped with other metals enhancing its potential as a molecular wire. Further suggestions have been made that SWNTs should be sheathed inside one another, with the first acting as a

conductor to carry the charge, while the second acting as an insulator to create a barrier from the effects of other adjacent wires.

1.3.3. Redox-active complexes.

In the successful synthesis of molecular wires there are several considerations. In recent decades chemists have begun to explore beyond the traditional strictly organic compounds and cap these all-carbon bridges with redox-active transition metal centres. These have the general formula $[ML_n]$-$(C)_x$-$[M'L_m]$, as possible models for molecular wires (where M is a redox active metal, L is the associated ligands of the metal, and $(C)_x$ is the all-carbon conjugated bridge). The capping of these organic bridges allows for "fine tuning" of the electronic properties of the molecule by substituting either electron donating or withdrawing ligands on the metal centres. This has been further extended to photoactive terminals to create storage devices.[29] As seen in conjugated organic compounds the π-overlap possess the ability to allow the transport of electrons, but this π-overlap must also interact with the appropriate d-orbitals of the metal to allow communication across the entire molecule. Furthermore there must be a free electron that can traverse through the π-overlap. This free electron is obtained by either, removal of an electron from the HOMO or addition of an electron into the LUMO of the neutral complex, leaving the two metal termini in different oxidation states, also known as a mixed-valence complex. The free electron can then reside on either metal terminal in these mixed-valence complexes (see Figure 1.5).

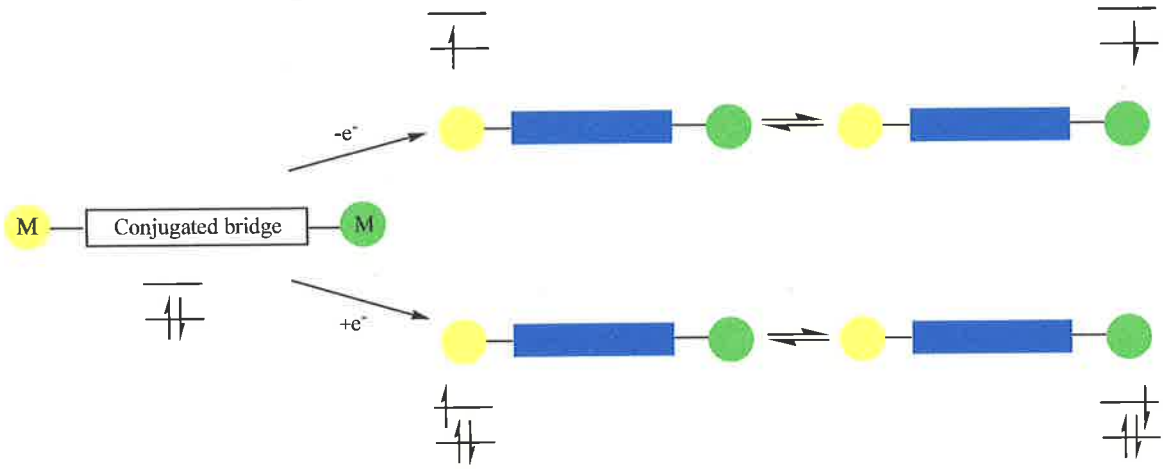

Figure 1.5. *Electron transport in a molecular wire containing two redox-active metal terminals.*

The Group 8 metals; iron,[30] ruthenium,[31] and osmium, have all shown strong metal-metal interactions allowing complete delocalisation of electrons. Calculations have further confirmed this delocalisation and orbital overlap.[32,33] The degree of overlap or interaction allows these complexes to be placed in one of three classes by the Robin-Day classification system,[34] further extended by Meyer and co-workers.[35]

Class I. Complexes in this class demonstrate no electronic interactions between the two terminal metal centres. In these cases the bridging ligand acts as a complete insulator. Symmetrical Class I complexes have identical oxidation and reduction potentials E^o, with the only difference a small statistical factor [$\Delta E^o = 2(RT/F)\ln 2$].

Class II. Complexes (eg. $\{Cp^*(dppe)Fe\}_2(\mu\text{-}C{\equiv}C\text{-}4,4'\text{-}\{1,1'\text{-}(C_6H_4)_2\}C{\equiv}C)$)[36] in this class have weakly interacting metal terminals. These metal termini can be distinguished by at least one spectroscopic method and show an intervalence charge transfer band (IVCT) in the near-infrared, which is the energy required to transmit the free electron from one terminal to the other. Care needs to be taken when assigning this IVCT band because it is often solvent dependent.

Class III. Complexes (eg. $\{Cp^*(dppe)Ru\}_2(\mu\text{-}C{\equiv}CC{\equiv}C)$)[31] in this class display strong electronic interactions. The bridging ligand in these cases is acting as a conductor. Oxidation or reduction in these complexes happens in a step-wise fashion due to the overlap between the two metal terminals and the bridging ligand, with ΔE^o greater than 200mV.

Presently the Robin-Day classification system has limited the description of a particular group of complexes that contain characteristics of both Class II and III.

Class II-III. Complexes (eg. $[\{(H_3N)_5Ru\}_2(\mu\text{-pz})]^{5+}$)[35] in this class possess characteristics of both Class II and Class III. They have an inter-valence charge transfer band that is not solvent dependent, which indicates a Class III type complex. However it is possible to determine some charge localisation through the use of IR and low temperature X-ray crystallography, which indicates a Class II complex.

1.4. Evaluation of molecular wires.

At present there are many different techniques for determining the degree of overlap between the two metal termini along the bridging ligand. The three most common techniques are direct measurement, cyclic voltammetry, and infrared (IR), UV/Vis and near-infrared (NIR) absorption spectroscopy.

1.4.1. Direct measurement.

Direct measurement offers the most accurate method for determining the resistance or ability of a molecule to transport electrons. The biggest problem with this type of measurement is that the molecular wire of interest must have the appropriate termini to interact with macroscopic electrodes. Also a great deal of control is needed with the ability to move the nano-junction electrodes in picometer increments.

Direct measurement can be achieved through the use of a break junction. A mechanically controlled break junction is typically created by slowly bending or extruding a microscopic piece of wire, generally made from gold. With the appropriate terminals, usually thiol groups, the molecule is coated onto this nano-junction in a self-assembly mono-layer. The gold tips are then moved closer together in picometer increments until the correct distance is achieved for a single molecule to bridge the gap (see Figure 1.6). A current can then be applied to one electrode and the current response can be measured for the single molecule.[37,38]

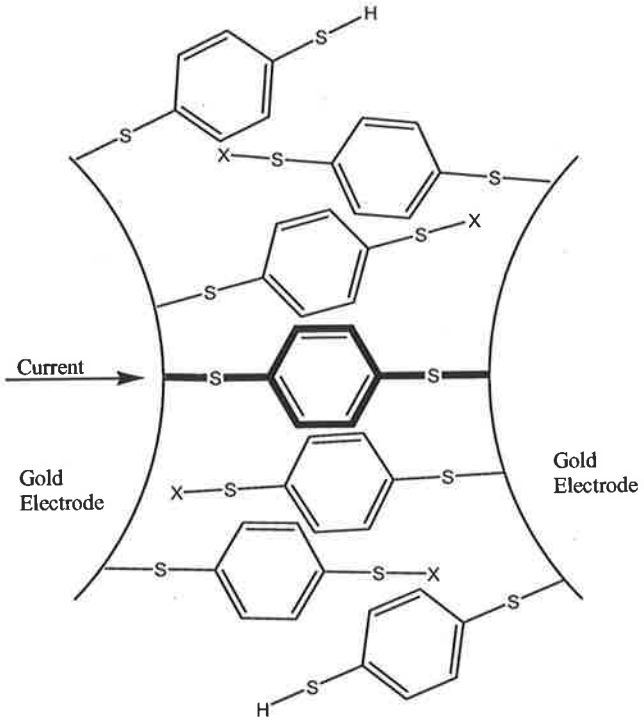

Figure 1.6. *Benzene-1,4-dithiolate spanning two gold electrodes (where X can either be H or Au, the Au potentially coming from the wire when the break junction was formed).*[39]

1.4.2. Cyclic voltammetry.

Cyclic voltammetry is a simple but effective method of evaluating the electronic interactions in redox-active complexes. Although cyclic voltammetry is a powerful and useful tool, care needs to be taken when describing the results as effects such as solvation,[40] electrostatic interactions[41] and structural distortion,[42] need to be considered. This method is not as powerful as direct measurement, but the cyclic voltammetry method allows for redox-active complexes to be categorised within the Robin-Day[34] and Meyer[35] classification systems.

Cyclic voltammetry requires a three-electrode system submerged into a solution of the desired complex and supporting electrolyte (see Figure 1.7). The working electrode, usually made from platinum, glassy carbon, or gold, is used to apply a potential across the solution, either reducing or oxidising. The counter-electrode is necessary to collect the current from the working electrode to complete the circuit. A redox reaction is also provoked by the counter-electrode opposite in nature, but equal in extent to that occurring at the working electrode. The reference electrode is needed because only differences in potential or current can be measured experimentally. Therefore the reference electrode must not pass current so that this difference can be accurately measured at the counter electrode.[43]

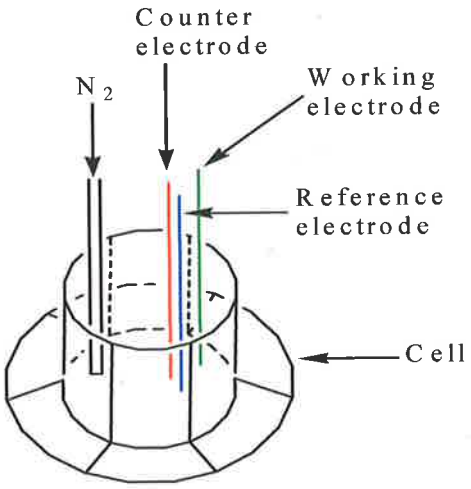

Figure 1.7. *Cyclic voltammetry cell setup containing the three relevant electrodes, working, counter, and reference.*

Cyclic voltammetry experiments begin at a potential which no current is measured, this being an arbitrary point for every complex. The potential is then swept in the forward direction recording the cathodic reaction, until it reaches the switching potential. At this point the potential is reversed and the sweep measures the anodic reaction, until it reaches the initial potential (see Figure 1.8). The cathodic and anodic current can be graphed as a function of potential giving the desired voltammogram (see Figure 8).[43]

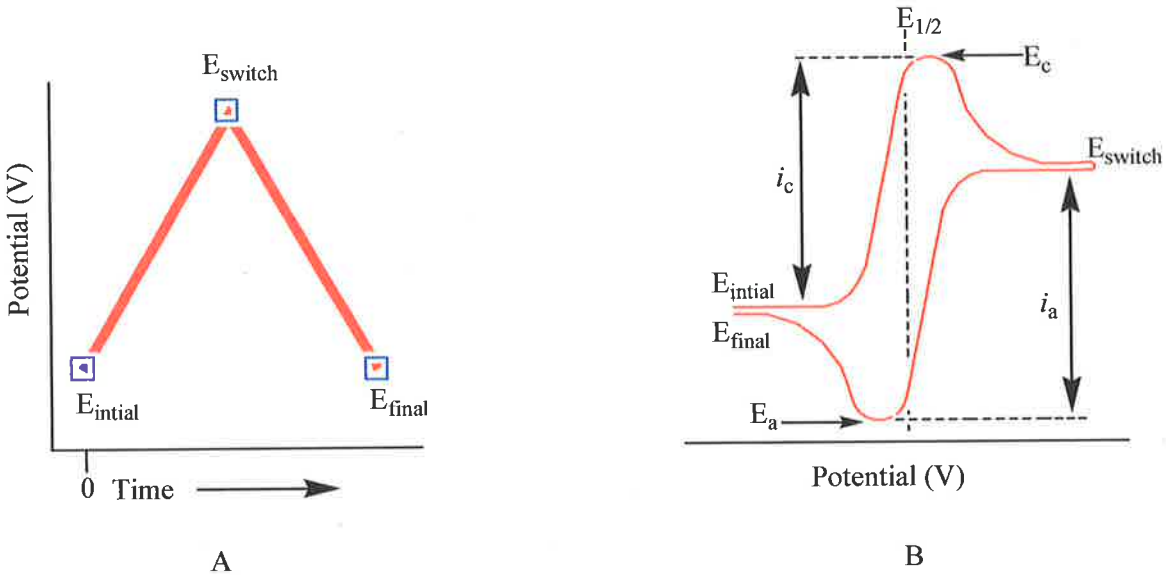

Figure 1.8. *A. Cyclic potential sweep. B. Theoretical trace of a fully reversible redox event.*

From the theoretical trace it is possible to measure not only the current intensities (peak height) of both the cathodic i_c, and anodic i_a process, but also $E_{1/2}$ which is the difference between the two redox events (see Equation 1.1).

$$E_{1/2} = |E_a - E_c| \qquad \textbf{Equation 1.1}$$

To obtain an accurate voltammogram, measurements must be taken under the conditions of a stationary working electrode and an unstirred solution. Furthermore the mass transport, the way in which the redox-active complexes move between the bulk solution and the interface double layer, must be controlled by diffusion (see Figure 1.9).[43]

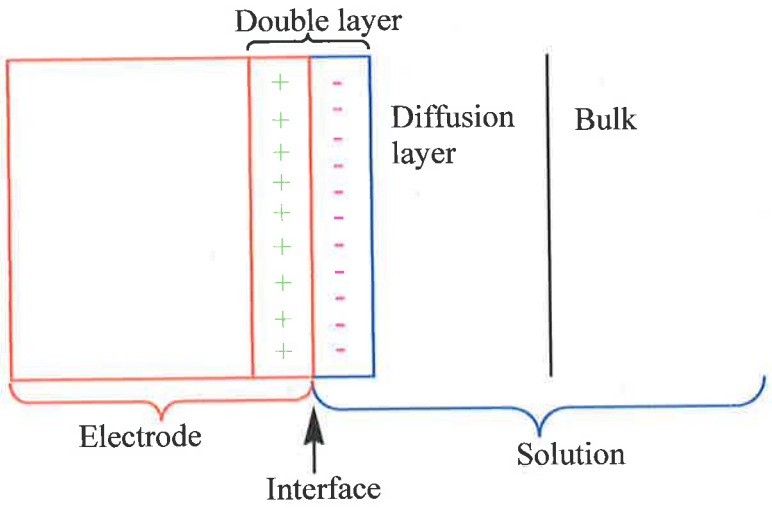

Figure 1.9. *Enlarged view of the area around the working electrode.*

If the mass transport is not controlled by diffusion, the complex at the interface will become depleted causing errors in the measured current. A simple test used to determine whether the mass transport of a complex is controlled by diffusion is to relate the current intensity (peak height of the relevant redox event) to the square-root of the scan rate (see Equation 1.2).[43]

$$i \quad \alpha \quad \sqrt{\nu} \qquad \textbf{Equation 1.2}$$

The peak shape of the cyclic voltammogram can also reveal information about the kinetics and thermodynamics of the relevant species. By comparing i_c to i_a, for a fully reversible redox event $i_a / i_c = 1$. For quasi-reversible events $1 > i_a / i_c > 0$, where as for fully non-reversible events $i_a / i_c = 0$ and is independent of scan rate.[43]

This can be further extended to class II and III mixed-valence complexes by measuring the comproportionation constant K_c of the relevant species in solution (see Equation 1.3, which simplifies to Equation 1.4).

$$K_c = \frac{[Ox - Red]^2}{[Ox - Ox]\,[Red - Red]} = \exp\left[\frac{\Delta E \times F}{RT}\right] \qquad \textbf{Equation 1.3}$$

$$K_c = \exp\left[\Delta E \times 38.94\right] \qquad \textbf{Equation 1.4}$$

Class II complexes have small K_c values whereas class III complexes have large K_c values. These large K_c values indicate the thermodynamic stability of the oxidised MV complex and the possibility of its isolation, without disproportionation into the doubly reduced, doubly oxidised species or decomposition (see Figure 1.10).

$$M^+ \overset{K_c}{\rightleftharpoons} M^0 + M^{2+}$$

Figure 1.10. *Disproportionation reaction.*

1.4.3. IR, UV/Vis, NIR spectroscopy.

The use of absorption spectroscopy, in particular in the regions of IR, UV/Vis, and NIR, allows the *in situ* investigation of electrochemically generated complexes, which is not always possible in the solid state for some complexes due to their instability.[44]

Through the use of infrared reflection-absorption spectroscopy (IRRAS)[45] in a modified solution IR cell it is possible to follow the bonding changes that occur in complexes due to oxidation or reduction. Both techniques (cyclic voltammetry and absorption spectroscopy) work on a three-electrode system, a working, reference, and counter-electrode (as seen for cyclic voltammetry). IRRAS uses a working electrode that is placed extremely close to an IR transparent window to form a 1 to 10 μm film. The IR beam is then directed through this film and is reflected by the working electrode to the detector (see Figure 1.11). Further modifications can be made to allow these measurements to be taken under an inert atmosphere and at low temperature. A solution

IR cell can also be built with these same three electrodes producing a simplified method where the transmittance can be measured instead (see Figure 1.11).

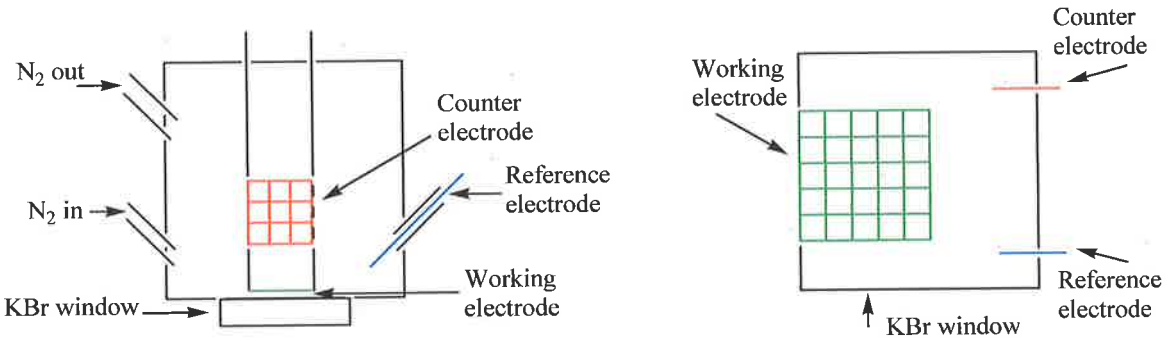

Figure 1.11. *IRRAS and solution cell setups.*

For polycarbon chains for example, IR has also proven an effective means of following these changes in the solid state with stable complexes. By focusing on the carbon-carbon bonds in the chain it is possible to observe the change in absorption from a carbon-carbon triple bond to a carbon-carbon double bond (see Figure 1.12) (also dicussed later).

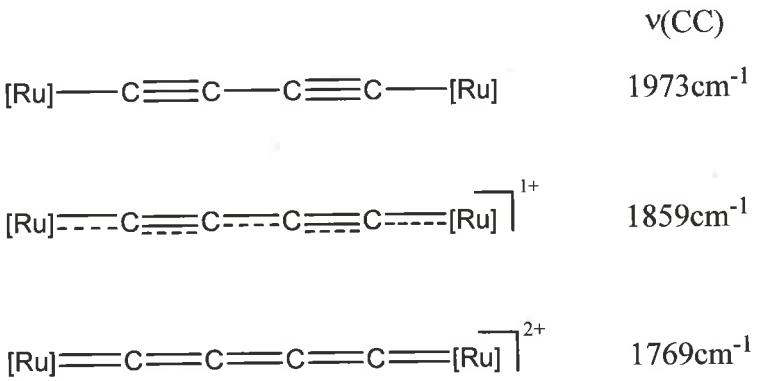

Figure 1.12. *Difference in electronic structure and in IR when oxidised from the neutral through to the dication (where [Ru] is Cp*(dppe)Ru).*

UV/Vis-NIR spectroscopy uses an optically transparent thin-layer electrode (OTTLE) cell, which again contains the three relevant electrodes (see Figure 1.13).[46]

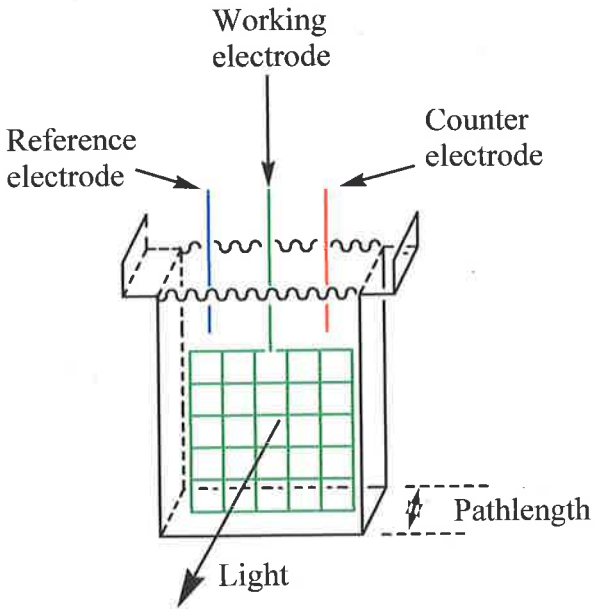

Figure 1.13. *An Optically Transparent Thin-Layer Electrode (OTTLE) cell.*

Guided by the CV data the working electrode is first held at a resting potential, where the complex in solution is neither oxidised or reduced. The appropriate potential is then applied to the working electrode to either oxidise or reduce the complex. The reversibility of this process is demonstrated by the recovery of the original spectra after completing the cycle and well-defined isosbestic points.[47]

Of greatest interest is the NIR region for mixed valence complexes. In the NIR region an inter-valence charge transfer band can be observed, which corresponds to the optically excited transfer of an electron between the two redox-active metal centres. This band is only observed in class II and III complexes and not in class I complexes as a result of the isolated behaviour of the two redox-active metal termini.[34] Detailed analysis of this band allows the electronic coupling parameter V_{ab} (or H_{ab}) to be determined.

For mono-oxidised or reduced class III complexes the coupling parameter V_{ab} is simply related to the energy of the NIR band (see equation 1.5).[19,48]

$$V_{ab} = \frac{\nu_{max}}{2} \qquad \textbf{Equation 1.5}$$

The relationship of the coupling parameter to the energy of the band can sometimes be difficult to interpret with the appearance of multiple overlapping bands in the NIR region, which can arise from either vibrational modes or multiple transitions.[12,31] Further interpretation of this band can become misleading also in class III complexes, as a result of the total delocalisation across the entire complex.[49]

A diagnostic test applied to determine whether a MV complex belongs in either class II or III involves the comparison of the observed bandwidth $\nu_{1/2}$ of the lowest energy electronic transfer to the theoretically determined value (see Equation 1.6).[48,50]

$$\nu_{1/2} = \sqrt{2310\nu_{max}} \qquad \textbf{Equation 1.6}$$

The IVCT band for class II complexes is either in good agreement or broader than that determined from the above relationship. Class III complexes give rise to an IVCT band which is relatively narrower than the theoretical value, but again care needs to be taken with the possible presence of multiple overlapping bands. These overlapping bands can be deconvoluted into Gaussian-shaped components allowing V_{ab} to be extracted.[51]

The coupling parameter for class II complexes can be also calculated based on the Hush theory (see Equation 1.7).[50]

$$V_{ab} = 2.05 \times 10^{-2} \frac{\sqrt{(\varepsilon\, \nu_{max}\, \Delta\nu_{1/2})}}{R_{MM'}} \qquad \textbf{Equation 1.7}$$

Where ε is the molar extinction coefficient ($M^{-1}cm^{-1}$), ν_{max} is the energy of the IVCT band (cm^{-1}), $\Delta\nu_{1/2}$ is the half-height width of the IVCT band, and $R_{MM'}$ is the through-space internuclear distance between the two redox-active centres (Å). Calculation of V_{ab}

allows direct comparisons of related complexes to be drawn, and evaluation of the effectiveness of the bridging ligand to mediate electron transfer.

1.5. Group 8 [M]-C_4-[M] complexes.

Given the definition of a molecular wire, complexes containing two redox-active metal termini bridged by either yndiyl (-C≡C-) or polyyndiyl [(-C≡C-)$_n$] fragments are obvious candidates. Transition metal complexes of the general formula [ML_n]-C_x-[$M'L'_m$] (where [ML_n] and [$M'L'_m$] represent the redox-active termini, and C_x represents the bridging fragment) have significant potential for use in molecular electronics.

Recent work has developed the synthesis of transition metal complexes containing successively longer carbon chains such as {Cp*(ON)(PPh_3)Re}$_2$(μ-C≡C)$_n$ (where n = 2 to 10) and {Ar(PAr_3)$_2$Pt}$_2$(μ-C≡C)$_n$ (where n = 2 to 14).[52-62]

Of particular interest to this thesis is the Group 8 complexes Cp*(dppe)MC≡CC≡C M(dppe)Cp* (where M = Fe, Ru, Os). The use of cyclic voltammetry and spectroelectrochemistry has allowed the electronic interactions of these complexes to be measured, which has generally confirmed that strong interactions do exist through the C_x bridging ligand. These interactions gradually decrease as the chain length is extended due to the increased resistance within the wire. Theoretical analysis of these complexes has furthered the understanding of the bonding between the metal termini and the linking carbon bridge. For a simple molcule {Cp(PH_3)$_2$Ru}$_2$(μ-C≡CC≡C) theoretical calculations have shown that there are strong σ-type interactions between the high-lying metallic frontier orbitals $3b_u$ and $3a_g$ and the low-lying C_4 orbtials $1b_u$ and $2a_g$ (see Figure 1.14).[47] The predominant interactions between the metal centres and the carbon-chain are filled/filled interactions, which stablise the C_4 chain and destabilise the metallic orbitals. Considering this the HOMO for the neutral complex is delocalised over the entire molecule and is well separated from the LUMO's. Therefore any oxidation, which involves loss of an electron, will not be exclusively metal centred and since these

HOMO's are anti-bonding between Ru and C_α and bonding between C_α and C_β, this supports the findings made in the IR with a lengthening in the C≡C bonds.

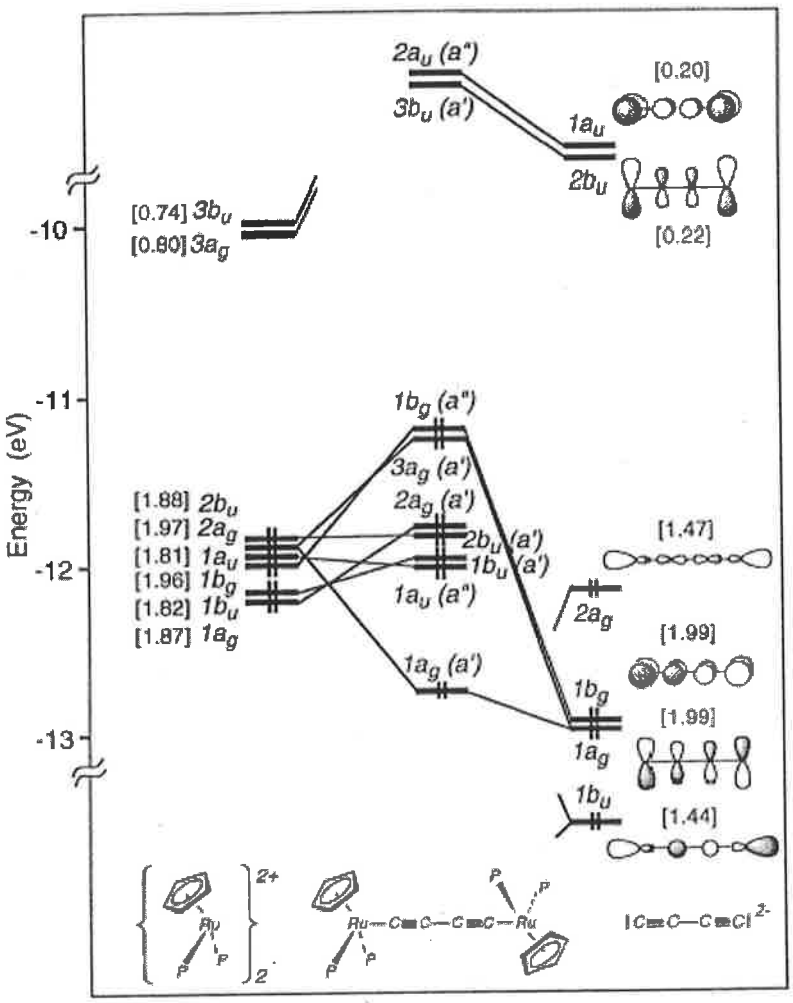

Figure 1.14. *Molecular orbital diagram of* $\{Cp(PH_3)_2Ru\}_2(\mu\text{-}C{\equiv}CC{\equiv}C)$.

1.6. Work described in this Thesis.

Work described in this thesis explores the synthesis of several different types of molecular wire models containing electron-rich Group 8 metal termini. Complexes containing the -C≡CC≡C- bridging ligand capped by the Os(dppe)Cp* are reported (see Figure 1.15). The use of this moiety allows for direct comparison of the through-bridge interaction in the MV complex to the analogous series containing the Fe(dppe)Cp* and Ru(dppe)Cp* termini through the use of cyclic voltammetry and NIR spectroscopy. This is the first comparative study of similar complexes containing all the three members of a transition metal Group.

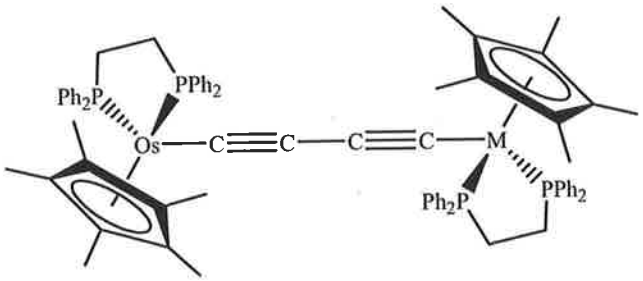

Figure 1.15 *Group 8 metal termini bridged by -C≡CC≡C- ligand (where M = Fe, Ru, Os).*

The effect of chain length on these electronic interactions are also investigated with the synthesis of several complexes containing –(C≡C)$_n$- (where n = 1, 2) bridging ligands. The oxidised derivatives of these complexes were isolated and where possible their electronic structure was investigated using both spectroscopic and structural characterisation. The electronic coupling parameter V_{ab} was also determined using NIR spectroscopy allowing comparisons to be made with longer chain analogues within a related series.

The effect of inserting organic fragments, such as 9,10-anthracenediyl, 1-ferrocenediyl and 1,1'-ruthenocenediyl (see Figure 1.16) into these *sp* carbon chains was investigated with Group 8 termini. Through the use of cyclic voltammetry the electronic interactions were measured allowing comparison to complexes with equivalent length straight carbon chains. The effect of the 9,10-anthracenediyl fragment on the singlet-triplet state

interconversion seen in several straight chain complexes was also investigated with approaches towards the synthesis of a Fe(dppe)Cp* complex containing a trapped electronic structure.

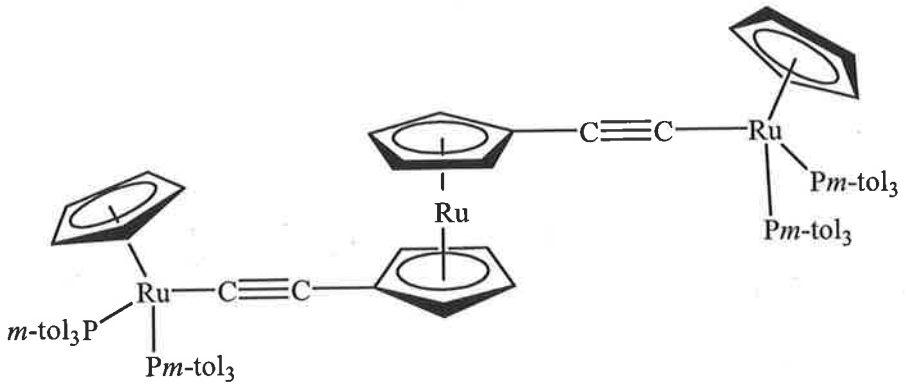

Figure 1.16 *Insertion of 1,1'-ruthenocenediyl into {Cp*(dppe)Ru}$_2$(μ-C≡CC≡C).*

At present most organometallic osmium starting materials involve the use of extremely toxic OsO_4. Due to the dangers associated with the transport of OsO_4 a novel general synthetic approach was investigated starting from the stable potassium osmate. Novel synthetic approaches were also found for several known and unknown Group 8 vinylidenes giving a more general approach to some Group 8 starting materials.

Chapter Two

Synthesis and Electronic Properties of Some Homo- and Hetero-metallic Osmium Diyndiyl Complexes

2.1. Introduction.

Group 8 complexes of the general formula $[ML_n]$-(C≡CC≡C)-$[M'L'_m]$ are of great interest with the synthesis of $\{Cp^*(dppe)Fe\}_2(\mu–C{\equiv}CC{\equiv}C)$ **(1)**,[63] $\{Cp^*(dppe)Ru\}_2(\mu–C{\equiv}CC{\equiv}C)$ **(2)**,[31] $Cp^*(dppe)FeC{\equiv}CC{\equiv}CRu(dppe)Cp^*$ **(3)**[32] previously reported. In these complexes strong metal-metal interactions along the carbon chain have been shown to exist by cyclic voltammetry. These complexes have been used as possible models for molecular wires where simple unsaturated carbon chains link redox-active metal centres.

Complexes of this type can be represented by one of three possible valence bond structures (see Figure 2.1). At present most complexes of this type are best represented by the valence structure **A**, which comprises alternating single and triple bonds. Structure **B** is also based on polyynes, while **C** shows a fully double-bonded cumulenic system.

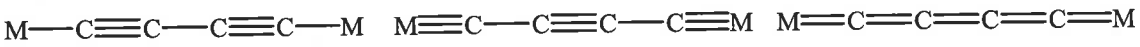

(A) **(B)** **(C)**

Figure 2.1. *Valence bond structures of complexes of the general formula MCCCCM.*

2.1.1. Synthetic strategies for diyndiyl complexes.

Diyndiyl complexes of the general formula $[ML_n]$-(C≡CC≡C)-$[M'L'_m]$ have been prepared through three main synthetic routes (see Scheme 2.1).

1. Coupling between a substituted C_4 fragment and two equivalents of the desired metal-ligand fragment.

2. Coupling between $[ML_n]$-C≡CC≡CR and another metal ligand fragment.

3. Homo coupling of two $[ML_n]$-C≡CH fragments.

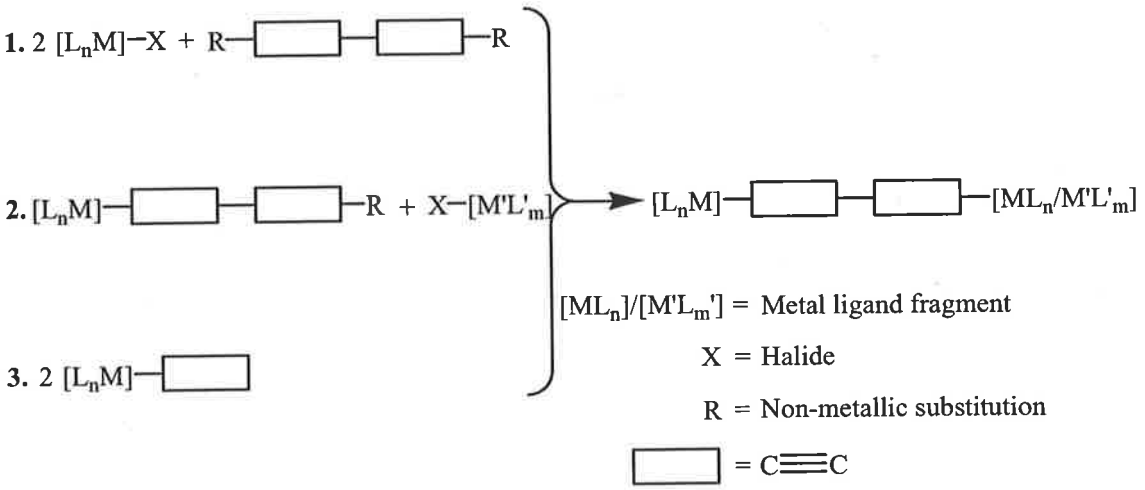

Scheme 2.1. *Synthetic strategies for complexes of the general formula $[ML_n]$-(C≡CC≡C)-$[M'L'_m]$.*

2.1.1.1. Synthetic strategy One. Coupling between a substituted C_4 fragment and two equivalents of the desired metal-ligand fragment.

Coupling between a substituted C_4 fragment and two equivalents of the desired metal-ligand fragment is the most widely used synthetic method due to the large number of accessible substituted C_4 compounds.

Buta-1,3-diyne (HC≡CC≡CH) is the simplest accessible C_4 fragment. This C_4 fragment is extremely reactive, which makes it a potential starting material, but it can only be kept at low temperatures for approximately a week in a THF solution before complete polymerisation occurs. Despite its reactivity and the dangers associated with its use, it has been used to synthesise several different diyndiyl complexes. [64,65]

Treatment of $\{RhCl(P^iPr_3)_2\}_2$ with buta-1,3-diyne at -78°C in pentane yields the homo-metallic complex $\{(P^iPr_3)_2Cl(H)Rh\}_2(\mu\text{-}C{\equiv}CC{\equiv}C)$ in 68% yield (see Scheme 2.2). This method is also adopted in the synthesis of $\{(P^iPr_3)_2Cl(H)Ir\}_2(\mu\text{-}C{\equiv}CC{\equiv}C)$ in 48% yield.

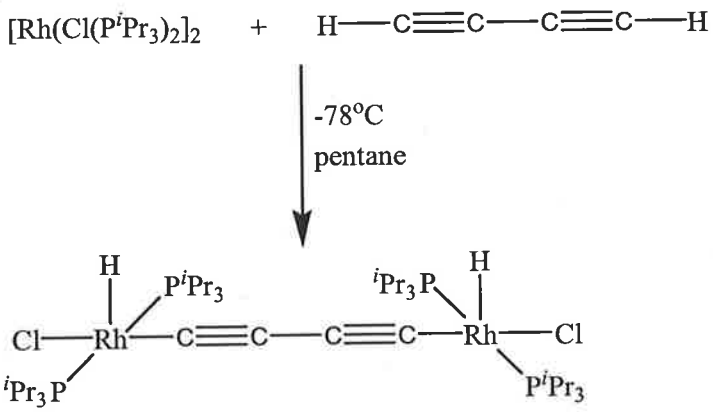

Scheme 2.2. *Synthesis of $\{(P^iPr_3)_2Cl(H)Rh\}_2(\mu\text{-}C{\equiv}CC{\equiv}C)$ using buta-1,3-diyne.*

The hazards associated with buta-1,3-diyne have lead to its replacement by TMSC≡CC≡CTMS. This white crystalline solid, 1,4-bis(trimethylsilyl)buta-1,3-diyne, which can be stored at room temperature has also proved to be a useful compound in the synthesis of these symmetrical complexes.

Treatment of 1,4-bis(trimethylsilyl)buta-1,3-diyne with $RuCl(PPh_3)_2Cp$ in refluxing methanol in the presence of KF yielded the desired symmetrical complex which precipitated from the hot methanol solution (see Scheme 2.3).[66]

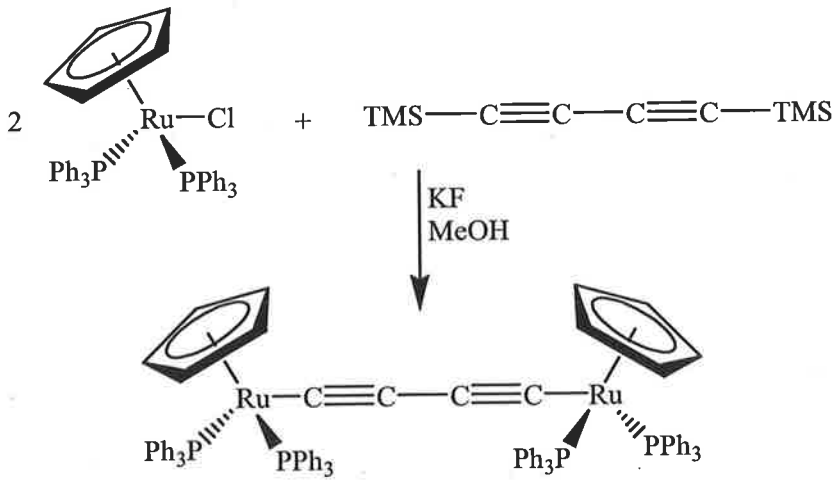

Scheme 2.3. *Synthetic route to $\{Cp(PPh_3)_2Ru\}_2(\mu\text{-}C{\equiv}CC{\equiv}C)$ using TMSC≡CC≡CTMS.*

2.1.1.2. Synthetic strategy two. Coupling between $[ML_n]$-C≡CC≡CR and another metal ligand fragment.

2.1.1.2.1. Synthesis of $[ML_n]$-C≡CC≡CR.

Coupling between a metal-ligand fragment that already contains the diyndiyl chain and another metal-ligand fragment gives a wide variety of homo- and hetero-metallic complexes. The synthetic strategy employed uses complexes that contain the diyndiyl chain already and depends on the chemistry of both the metal and organic starting material.

Catalytic condensation reactions using copper(I) iodide in the presence of an amine solvent is one of the most widely used methods to access these complexes. Treatment of buta-1,3-diyne with $WCl(CO)_3Cp^*$ and catalytic CuI in the presence of diethylamine affords the yellow complex $Cp^*(OC)_3WC{\equiv}CC{\equiv}CH$ after chromatography (alumina) in 77% yield (see Scheme 2.4).[67,68]

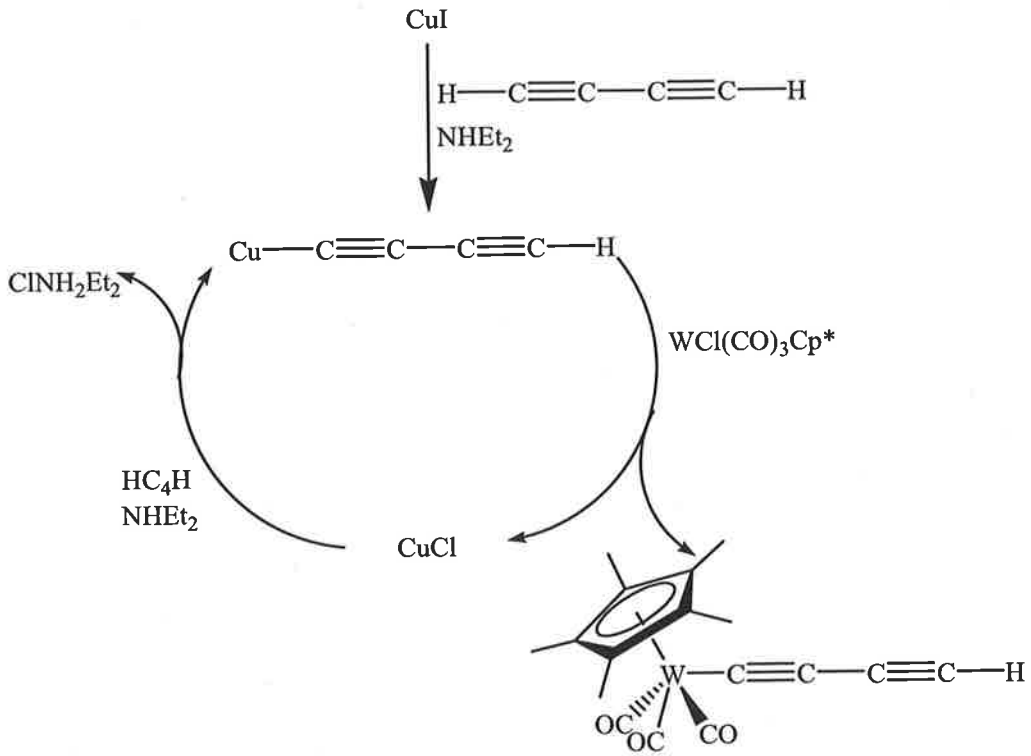

Scheme 2.4. *Catalysed condensation reaction to yield $Cp^*(OC)_3WC{\equiv}CC{\equiv}CH$.*

Organolithium reagents have also given a viable entry into these complexes by reaction with the appropriate metal halide, which results in precipitation of a lithium halide. Treatment of 1,4-bis(trimethylsilyl)buta-1,3-diyne with one equivalent of methyllithium results in the formation of LiC≡CC≡CTMS. This organolithium reagent further reacts with $FeI(CO)_2Cp^*$ to give the metal complex $Cp^*(OC)_2FeC{\equiv}CC{\equiv}CTMS$, which contains a TMS protected diynyl ligand which can be desilylated using potassium fluoride (see Scheme 2.5).[69]

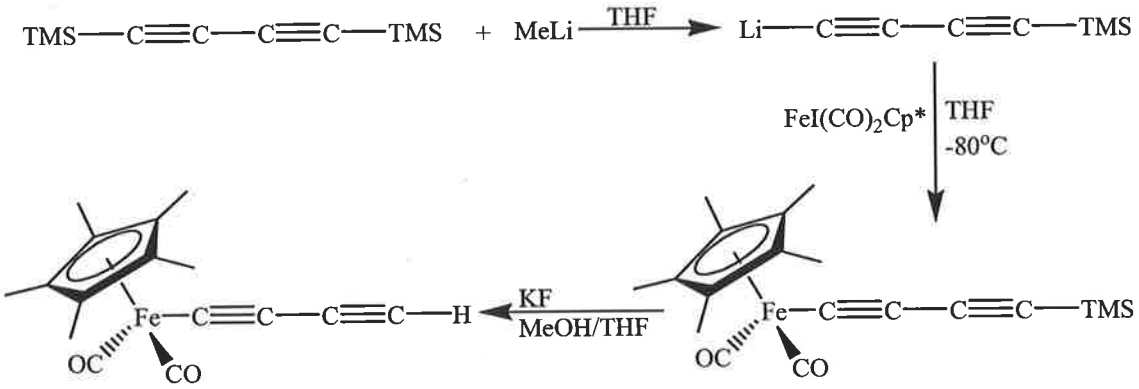

Scheme 2.5. *Synthetic route to $Cp^*(OC)_2FeC{\equiv}CC{\equiv}CH$ from $TMSC{\equiv}CC{\equiv}CTMS$.*

Where the two above procedures are not appropriate, complexation can be achieved through the mono-substituted TMS starting material HC≡CC≡CTMS. Reaction of RuCl(dppe)Cp* (**4**) with HC≡CC≡CTMS in the presence of $Na[BPh_4]$ in a NEt_3 / THF mixture gives Cp*(dppe)RuC≡CC≡CTMS (**5**) (see Scheme 2.6).[70] The presence of $Na[BPh_4]$ assists in the ionisation of the ruthenium-chlorine bond allowing complexation, a 1,4-hydrogen shift then occurs to give a butatrienylidene, as an unstable intermediate. The presence of NEt_3 deprotonates this reactive species affording the desired complex, which can be desilylated using $[Bu^n{}_4N]F$ to yield Cp*(dppe)RuC≡CC≡CH.

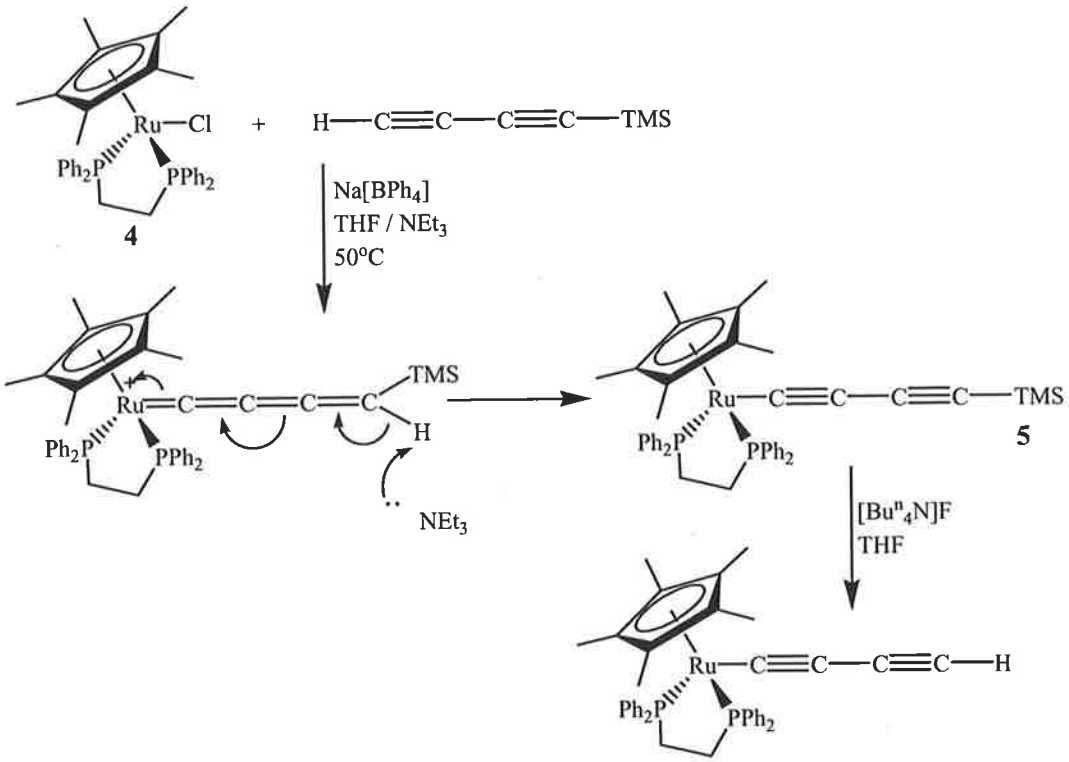

Scheme 2.6. *Synthetic route to Cp*(dppe)RuC≡CC≡CH from HC≡CC≡CTMS.*

2.1.1.2.2. Coupling between $[ML_n]$-C≡CC≡CR and another metal ligand fragment.

Treatment of $Cp^*(OC)_3WC{\equiv}CC{\equiv}CH$ with stoichiometric $WCl(CO)_3Cp^*$ and catalytic CuI in $NHEt_2$ results in the precipitation of the desired complex $\{Cp^*(CO)_3W\}_2(\mu\text{–}C{\equiv}CC{\equiv}C)$ (see Scheme 2.7).[71]

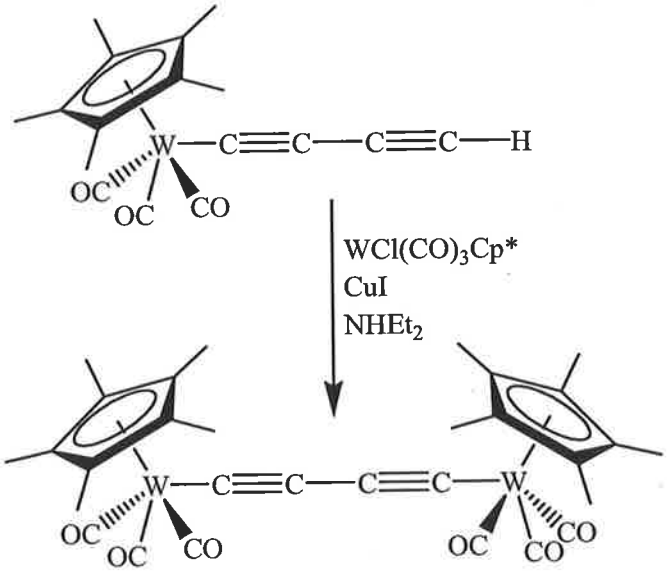

Scheme 2.7. *Synthetic route to {Cp*(OC)$_3$W}$_2$(μ-C≡CC≡C).*

The complex Cp*(dppe)RuC≡CC≡CH undergoes complexation with FeCl(dppe)Cp* in the presence of both Na[BPh$_4$] and NEt$_3$ / dbu, to give the heterometallic complex Cp*(dppe)RuC≡CC≡CFe(dppe)Cp* (see Scheme 2.8).[32]

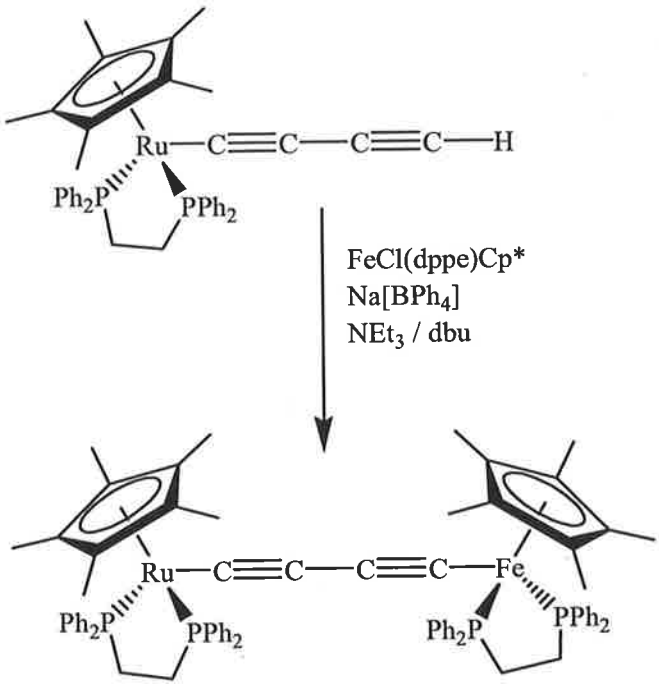

Scheme 2.8. *General synthetic method for Cp*(dppe)RuC≡CC≡CFe(dppe)Cp*.*

2.1.1.3. Synthetic strategy Three. Homo coupling between two $[ML_n]$-C≡CH fragments.

Oxidative homo-coupling of two metal ethynyl complexes has been used in the synthesis of several different complexes such as $\{Cp^*(ON)(p\text{-}tol_3P)Re\}_2(\mu\text{-}C{\equiv}CC{\equiv}C)$ and **2**, under varying reaction conditions.

The synthesis of $\{Cp^*(ON)(p\text{-}tol_3P)Re\}_2(\mu\text{-}C{\equiv}CC{\equiv}C)$ was achieved by heating the rhenium complex $Cp^*(ON)(p\text{-}tol_3P)ReC{\equiv}CH$ at 80°C in the presence of $Cu(OAc)_2$ in pyridine, which also acts as a base to deprotonate the bis(vinylidene) *in situ* (see Scheme 2.9).[54] Despite the high temperature conditions the C_4 complex is obtained in a good yield of 70%.

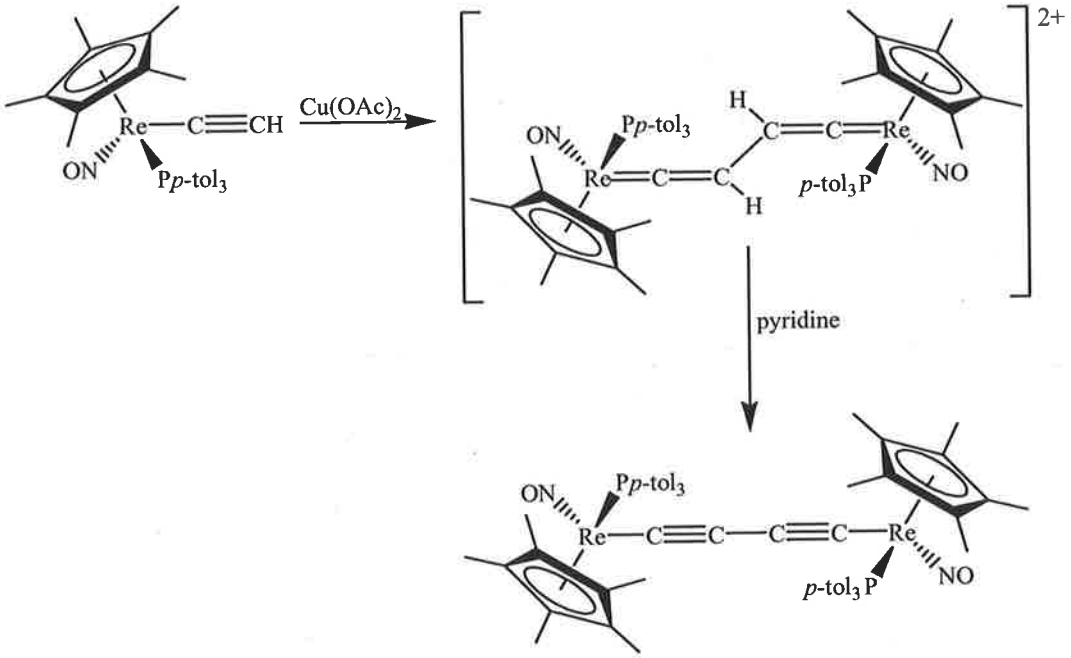

Scheme 2.9. *Homo coupling of Cp*(ON)(p-tol₃P)ReC≡CH.*

The synthesis of both **1** and **2** was achieved by radical dimerisation. This process was initiated by the addition of $[FeCp_2][PF_6]$ to a solution of corresponding metal ethynyl at –78°C. The $[FeCp_2][PF_6]$ removes an electron from the metal giving rise to a free radical on C_β. This free radical undergoes spontaneous carbon-carbon bond formation to afford

the coupled bis(vinylidene), which upon deprotonation with KO^{t}Bu yields the desired homo-metallic complex (see Scheme 2.10).[31]

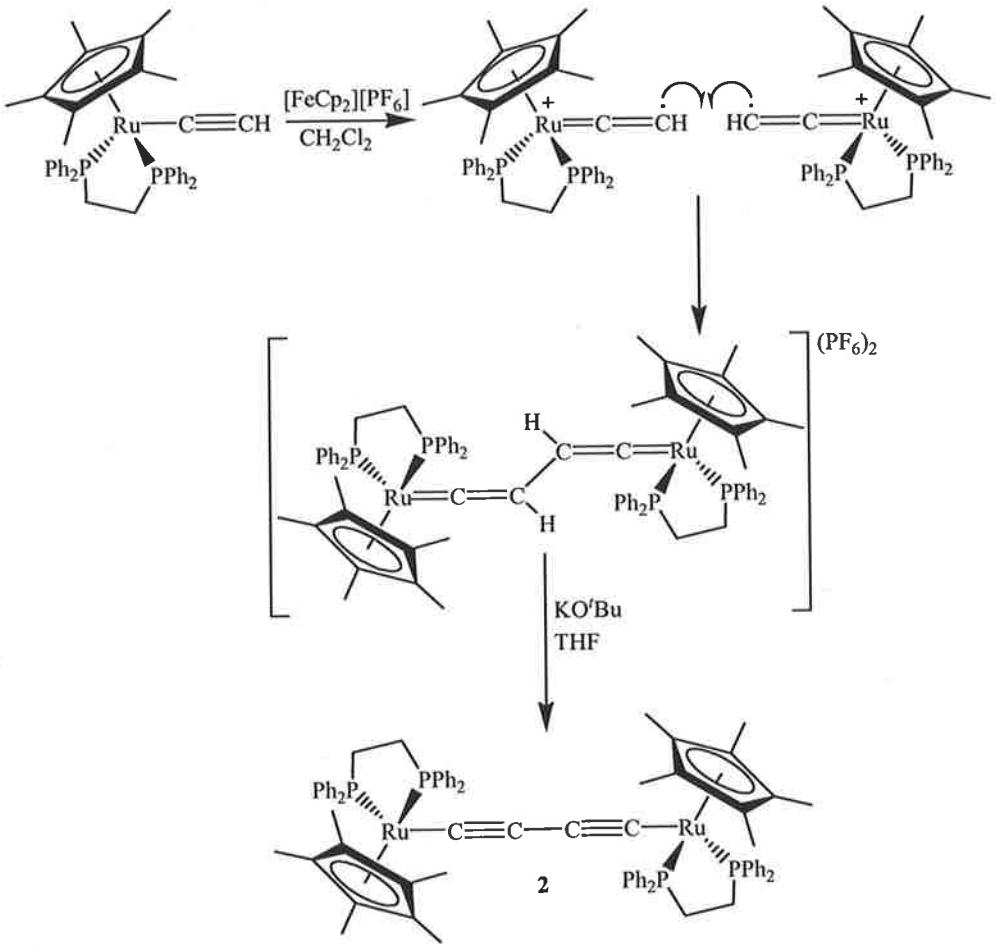

Scheme 2.10. *Radical dimerisation of Cp*(dppe)RuC≡CH.*

2.2. Aims of this work.

The primary aim of this work is to complete the series of Group 8 complexes containing the diynyl bridging ligand. The syntheses of $\{Cp^*(dppe)Fe\}_2(\mu\text{-}C{\equiv}CC{\equiv}C)$, $\{Cp^*(dppe)Ru\}_2(\mu\text{-}C{\equiv}CC{\equiv}C)$, and $Cp^*(dppe)FeC{\equiv}CC{\equiv}CRu(dppe)Cp^*$ have been reported previously.[31,32,63] These complexes show marked differences in their oxidation potentials with all complexes demonstrating strong electronic coupling between the two metals centres through the carbon chain. In the homo-metallic di-cations it has also been observed that there exists a triplet state for iron complex, which is not observed for the ruthenium complex.

This chapter reports the syntheses and characterisation of five new osmium diyndiyl complexes containing dppe and Cp* ligands including $\{Cp^*(dppe)Os\}_2(\mu\text{-}C{\equiv}CC{\equiv}C)$ (**6**). Of significant interest in this chapter are the oxidation potentials of these new hetero-metallic osmium complexes along with the electronic structure of the mono- and di-cations of $\{Cp^*(dppe)Os\}_2(\mu\text{-}C{\equiv}CC{\equiv}C)$, which can be followed by the use of IR spectroscopy.

2.3. Results and Discussion.

2.3.1. Synthesis and properties of {Cp*(dppe)Os}C≡CC≡C{M(dppe)Cp*}, where M = Fe, Ru.

The osmium diyndiyl complex was achieved using a synthetic method similar to the ruthenium and iron analogues (see Scheme 2.11).

The osmium bromo- or chloro- starting material undergoes complexation, in the presence of both TMSC≡CH and $[NH_4][PF_6]$ to yield the bright yellow vinylidene. Previous attempts of this reaction required heating at reflux in dichloromethane for 72 h, while in methanol the product precipitates directly from the hot methanol solution in three hours. As found with both the ruthenium and iron cases the presence of $[NH_4][PF_6]$ is needed to stabilise the vinylidene salt and to aid ionisation of the osmium-halide bond.

Deprotonation of $[Cp^*(dppe)Os{=}C{=}CH_2][PF_6]$ (**7**) with KO^{t}Bu in THF afforded the neutral acetylene complex Cp*(dppe)OsC≡CH (**8**), which undergoes oxidative coupling in the presence of $[FeCp_2][PF_6]$ in dichloromethane at -78^oC to give $[Cp^*(dppe)Os{=}C{=}CHCH{=}C{=}Os(dppe)Cp^*][PF_6]_2$ (**9**). Deprotonation of this product with KO^{t}Bu in THF affords the butadiyndiyl complex **6**.

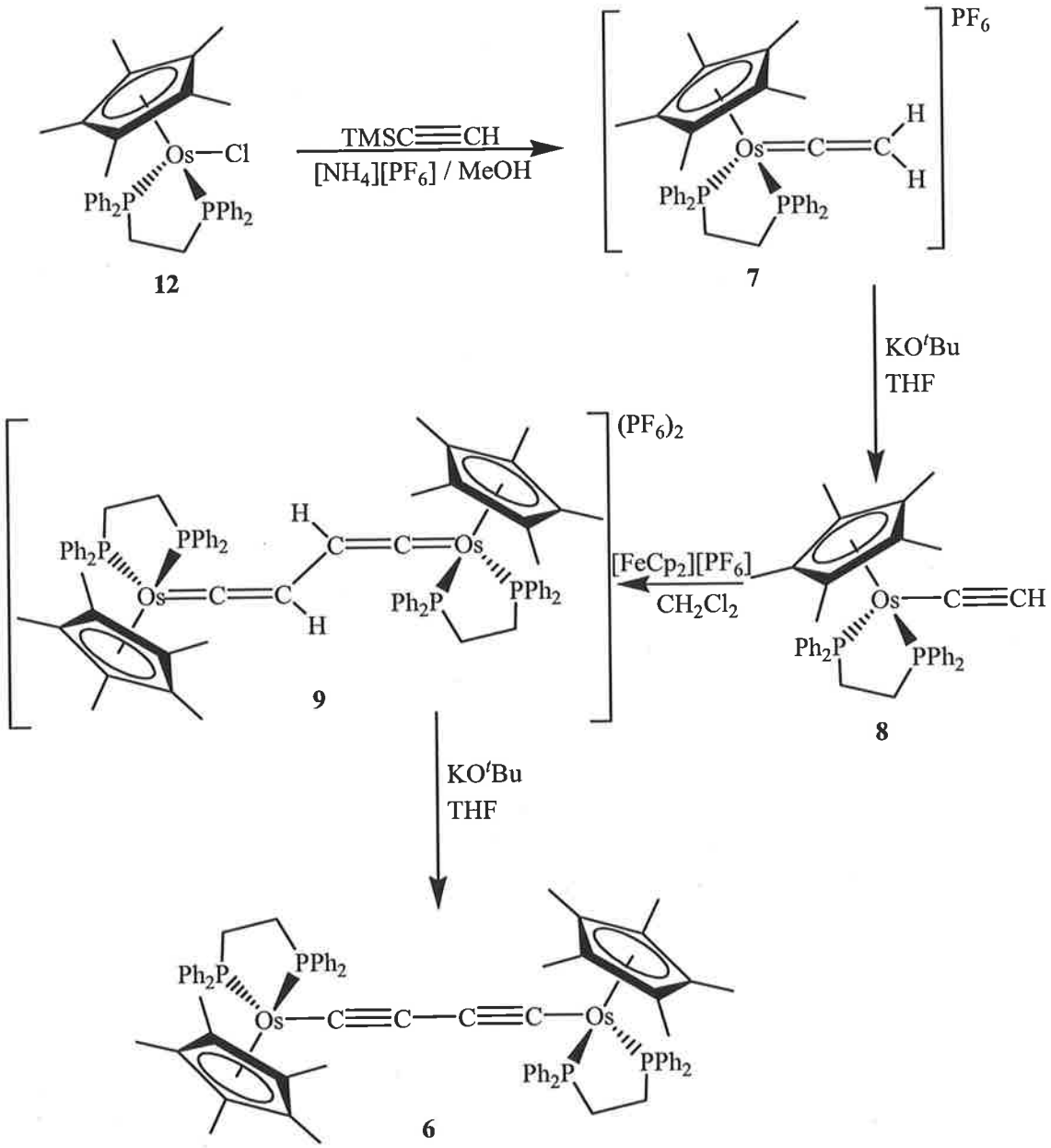

12 **7** **9** **8** **6**

Scheme 2.11. *Synthetic route to {Cp*(dppe)Os}$_2$(μ–C≡CC≡C).*

This method was successfully extended to the synthesis of both Cp*(dppe)OsC≡CC≡CRu(dppe)Cp* (**10**) and Cp*(dppe)OsC≡CC≡CFe(dppe)Cp* (**11**). Oxidative coupling of **8** with Cp*(dppe)MC≡CH (where M = Ru, Fe respectively), gave the bis(vinylidenes). Deprotonation of each bis(vinylidene) with KO^{t}Bu afforded the neutral C_4 complexes as an inseparable mixture with the two corresponding homo metallic complexes.

In the ^{1}H and ^{31}P NMR spectra of **10** and **11** two Cp* and dppe peaks were seen which indicates the presence of only the two homo-metallic complexes. For **10** the ^{31}P NMR spectrum showed peaks at δ 82.52 and 43.58, which corresponded to the homometallic complexes. This same trend is observed in the ^{1}H NMR with peaks at δ 8.01-7.07 corresponding to the aromatic protons in dppe, δ 2.78-2.63 and 2.02-1.95 corresponding to the CH_2CH_2 bridge in dppe. The peaks corresponding to the Cp* protons were found at δ 1.74 and 1.69. The mass spectrum however showed peaks for all three complexes at *m/z* 1317, 1408 and 1496, corresponding to $[M]^+$ for **2**, **10** and **6** respectively. The presence of all three complexes in the mass spectrum would indicate overlap in the ^{1}H and ^{31}P NMR spectra due to similar chemical environments or very little of the heterometallic species.

This was also observed for **11** with peaks in the ^{31}P NMR spectrum at δ 101.41 and 43.56. The ^{1}H NMR spectrum showed peaks at δ 8.12-7.06 (aromatic protons), 2.81-2.73 and 2.11-1.98 (CH_2CH_2 in dppe), and δ 1.73 and 1.56 corresponding to the Cp* protons. Again the mass spectrum showed the presence of all three complexes with peaks at *m/z* 1226, 1362 and 1496 corresponding to $[M]^+$ for **1**, **11**, and **6** respectively.

2.3.2. Synthesis and properties of Cp*(dppe)OsC≡CC≡CTMS.

Initial work towards the synthesis of both **10** and **11** centered around the preparation of Cp*(dppe)OsC≡CC≡CTMS (**12**). As shown previously for ruthenium, desilylation and

further coupling with the correct metal halide resulted in the desired hetero-metallic complex.[32] The synthesis of **12** was not achieved in large enough yields to make it a viable starting material for further organometallic reactions. Under similar conditions as those used for the successful synthesis of **5**,[70] OsCl(dppe)Cp* (**13**) was reacted with an excess of HC≡CC≡CTMS in the presence of $Na[BPh_4]$ in a THF / NEt_3 mixture at 50°C for 48 h. The procedure did not result in formation of the desired product but only the recovery of the starting chloro complex. This suggests that the ruthenium-chloride bond in **4** is weaker than the osmium-chloride bond in **13**.

As demonstrated in chapter six the use of different solvents can increase the lability and hence the reactivity of the metal-halide bond in the synthesis of vinylidenes. The reaction of **4** with an excess of HC≡CC≡CTMS in methanol has already been reported,[72] the product of which undergoes addition of methanol at C_γ. Taking this result into consideration the reaction of **4** with an excess of HC≡CC≡CTMS was performed in ^{t}BuOH.

Treatment of **4** with an excess of HC≡CC≡CTMS in the presence of both $Na[BPh_4]$ and proton sponge™ in ^{t}BuOH at 50°C for one hour resulted in the precipitation of the desired complex **5** in 86-95% yield. If the temperature exceeds 60°C in the course of the reaction then the formation of the cyclobutenylidene complex is observed (see Figure 2.2) by mass spectrum *m/z* 1441 $[M]^+$. This impurity can be removed by chromatography (basic alumina) loading with NEt_3 and eluting with hexane.[73]

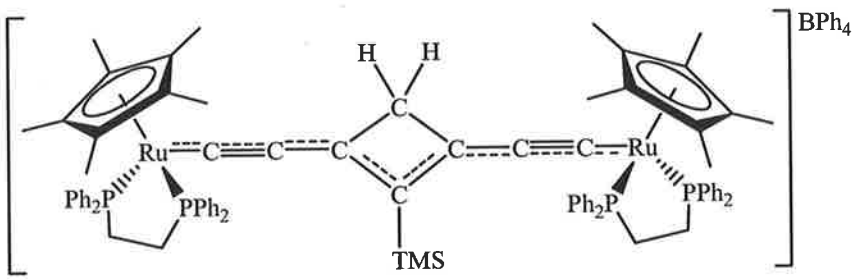

Figure 2.2. *Ruthenium cyclobutenylidene complex.*

With the successful synthesis of **5** under these new conditions, the same procedure was attempted using **13**. Treatment of **13** with an excess of HC≡CC≡CTMS in the presence

of $Na[BPh_4]$ and proton sponge^{TM} in ^tBuOH at 50°C results in the formation of only trace amounts of **12**, which could be extracted with hot hexane. The major product was identified by mass spectroscopy, which was found to be the cyclobutenylidene (**14**). The formation of **14** is thought to happen by a [2 + 2] cycloaddition between carbons C(3) and C(4) of adjacent complexes (see Scheme 2.12).

In order to minimize the formation of the cyclobutenylidene complex the reaction was repeated at a lower temperature, which resulted in the recovery of the starting chloro-complex and no observable product.

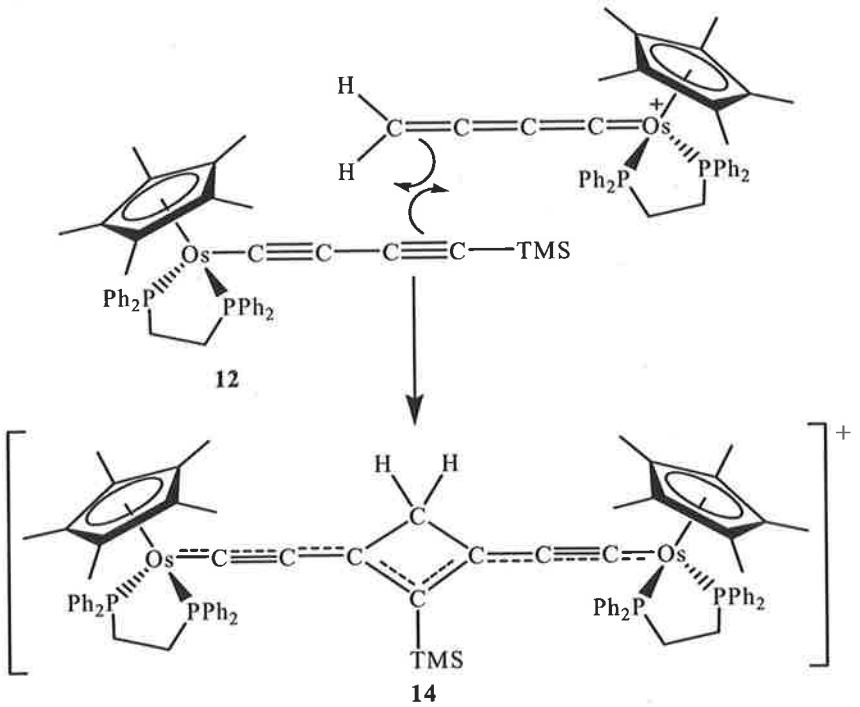

Scheme 2.12. *Proposed mechanism for the formation of the osmium cyclobutenylidene complex.*

2.3.3. Electrochemistry of Cp*(dppe)OsC≡CC≡CM(dppe)Cp*, where M = Fe, Ru, Os.

The redox potentials for complexes **1**, **2**, **6** and **10** were measured under similar conditions and are presented in Table 2.1.

The spectra of the symmetrical osmium complex **6** shows four oxidation waves. The first three redox events (E_1, E_2 and E_3) are fully reversible, (i_a / i_c = 1; current is proportional to the square root of the scan rate) while the E_4 event was only quasi-reversible (i_a / i_c = 0.7; current is proportional to the square root of the scan rate)(see Figure 2.3).

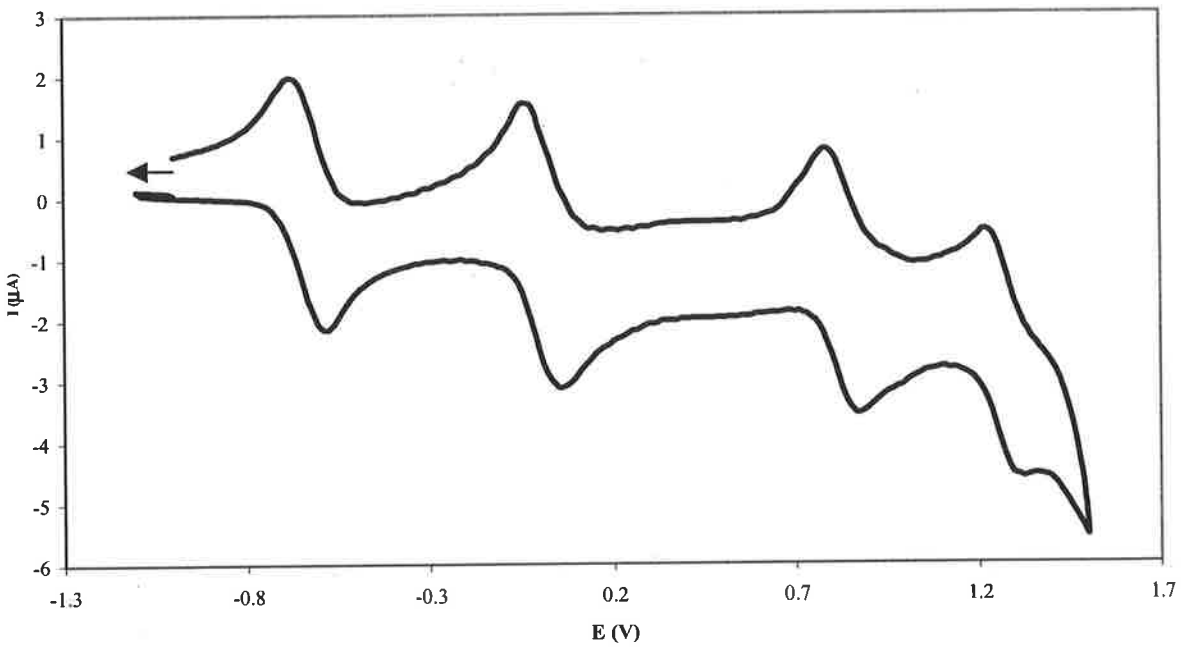

Figure 2.3. *Cyclic voltammogram of {Cp*(dppe)Os}$_2$(μ-C≡CC≡C), recorded in CH_2Cl_2, 0.1M [Bu$^n_4$N][PF$_6$] at 100mV s^{-1}.*

Further analysis of the electrochemical data provided an insight into the thermodynamic stabilities of the neutral complex and its oxidised states. The comproportionation constant, K_c (see Equation 1.4), can be determined by looking at the comproportionation reaction, which is the reaction of two molecules of the same complex in different oxidation states giving rise to a single species through electron transfer.

High thermodynamic stabilities are found for the oxidised species $[\mathbf{6}]^{n+}$ (where n = 1, 2, 3), as evident by the large separation between redox events giving rise to large K_c values (n = 1, $K_c = 2.07 \times 10^{10}$; n = 2, $K_c = 1.09 \times 10^{14}$; n = 3, $K_c = 2.76 \times 10^{7}$), which also

indicate a Class III complex by the Robin and Day classification system. Unfortunately these values only give an estimate of the thermodynamic stability of these oxidised complexes, but given the significant K_c values they were all considered viable synthetic targets.

The first oxidation potential (E_1) for **6** at –0.62 V, is much lower than that found for **2** at –0.43 V and is comparable to that of **1** at –0.69 V (see Figure 2.4). This result was not expected as it was predicted that the first oxidation would increase on descending Group 8 from iron to ruthenium to osmium as a result of initial theoretical studies.[74]

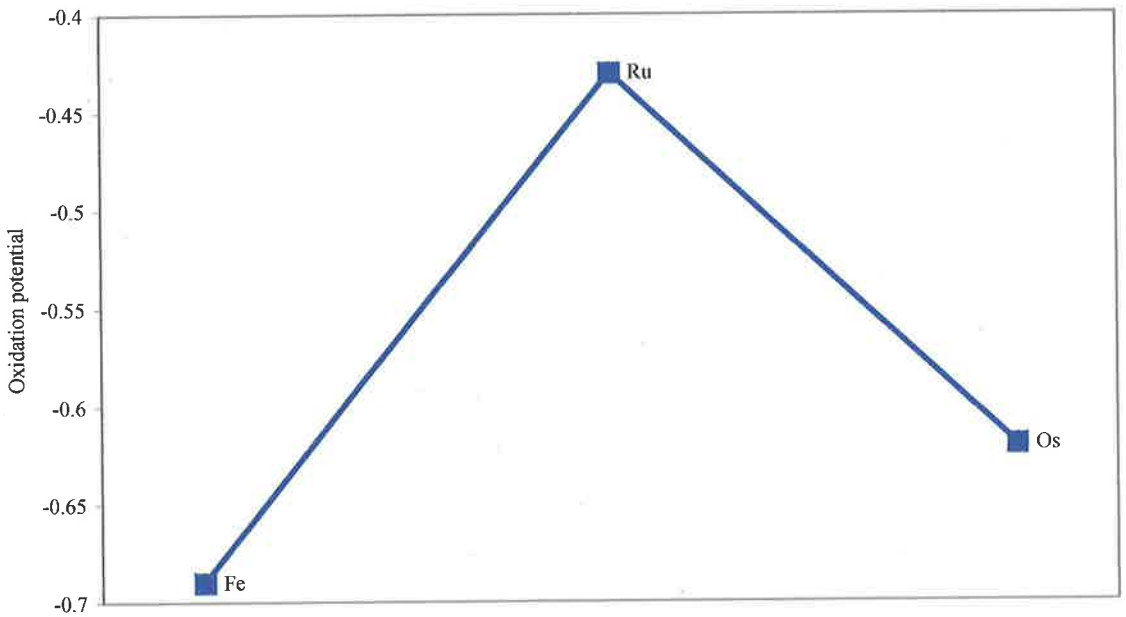

Figure 2.4. *First oxidation potentials for the Group 8 series {Cp*(dppe)M}$_2$(μ-C≡CC≡C) where M = Fe, Ru, Os.*

The oxidation potentials (E_1, E_2, E_3, E_4) for the heterometallic complex **10** were found to be intermediate to that observed for **6** and **2**, at –0.52 V, +0.11 V, +0.63 V and +0.92 V (see Figure 2.5).

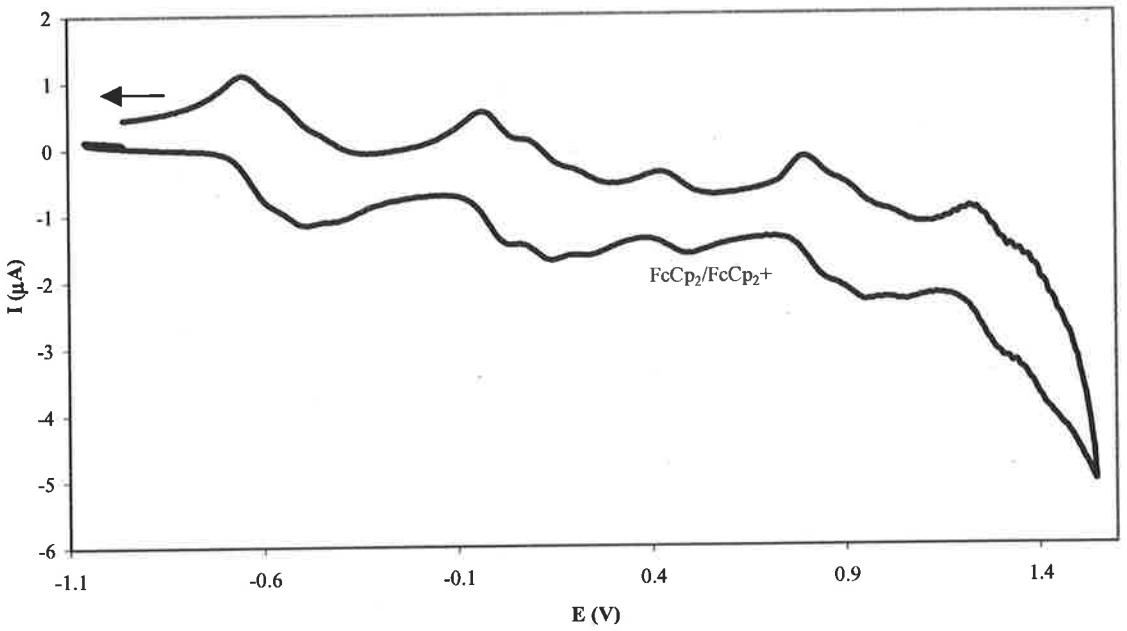

Figure 2.5. *Cyclic voltammogram of Cp*(dppe)OsC≡CC≡CRu(dppe)Cp*, recorded in CH_2Cl_2, 0.1M $[Bu^n{}_4N][PF_6]$ at 100 mV s^{-1}.*

Complex	[M]/[M']	E_1	E_2	$\Delta E_{1/2}$	E_3	E_4	$K_c(0/+1/+2)$	[REF]
1	Fe/Fe	-0.69	+0.03	0.72	+0.95		9.95×10^{11}	63
2	Ru/Ru	-0.43	+0.23	0.66	+1.02	$+1.51_a$	9.64×10^{10}	31
6	Os/Os	-0.62	-0.01	0.61	+0.82	$+1.26^a$	2.07×10^{10}	This work
3	Fe/Ru	-0.59	+0.18	0.77	+0.99			32
10	Ru/Os	-0.52	+0.11	0.63	+0.92	$+1.39^a$	4.51×10^{10}	This work

Table 2.1. *Electrochemical data for Cp*(dppe)MC≡CC≡CM'(dppe)Cp* recorded in CH_2Cl_2 0.1M $[Bu^n_4N][PF_6]$ and 100 mV s^{-1}. [a] peak potential of a quasi-reversible wave.*

2.3.4. Synthesis and properties of $[\{Cp^*(dppe)Os\}_2(\mu\text{-}C{\equiv}CC{\equiv}C)]^{n+}$, where n = 1, 2.

After examination of the CV of **6** (see Section 2.3.3), which contains three fully reversible and one quasi-reversible oxidation waves, it was thought that synthesis of the mono-, di-, and tri-cations should be possible through chemical oxidation.

Treatment of **6** with one equivalent of $[FeCp_2][PF_6]$ in dichloromethane caused a rapid colour change from orange to deep green. The mono-cation, **6**$[PF_6]$ was isolated by precipitation from the reaction mixture upon addition of hexane. The ^1H NMR spectrum showed broad peaks at δ 12.16 corresponding to the Cp* protons, δ 10.68 corresponding to the CH_2CH_2 in dppe and multiplets at δ 8.22-7.36 corresponding to the aromatic protons. Despite the broad nature of the ^1H NMR spectra, which was to be expected for the paramagnetic 35-electron complex, assignments could still be made based on the relative intensities of the observed peaks. No signal was seen in the ^{31}P NMR spectrum for dppe. The IR spectrum confirmed the presence of the PF_6 anion with a characteristic ν(PF) band at 839 cm^{-1}. The IR spectrum also contained a ν(CC) absorption at 1860 cm^{-1}, which is consistent with that observed for **2**$[PF_6]$ (1859 cm^{-1}),[31] with a decrease in the carbon-carbon bond order between C_α and C_β (see Figure 2.6). The mass spectrum also confirmed the presence of the mono-cation with a peak at *m/z* 1496 corresponding to $[M]^+$.

Treatment of **6** with two equivalents of $[FeCp_2][PF_6]$ in dichloromethane caused a rapid colour change through the deep green observed for the mono-cation to eventually give a deep blue solution. The di-cation **6**$[PF_6]_2$ was isolated by precipitation from the reaction mixture upon addition of hexane. The ^1H NMR spectrum of this 34-electron complex displayed sharp well-defined peaks at δ 7.80-6.99 (aromatic), 3.69-3.58 and 3.31-3.19 (CH_2CH_2), and 2.13 (Cp*) consistent with a diamagnetic complex. The ^{31}P NMR spectrum showed a slightly broadened singlet at δ 80.98 corresponding to the dppe and a septet at δ –143.01 corresponding to the PF_6 anion. A dramatic shift is observed from δ 43.58 for the neutral complex to δ 80.98 in the di-cation for the phosphorus nuclei of the dppe, which is consistent with the removal of electron density from the osmium centre and therefore the phosphorus

nuclei upon oxidation. The IR spectrum also indicates a change in the carbon-carbon bond order in the complex with a ν(C=C) absorption at 1781 cm^{-1} and an absorption at 836 cm^{-1} corresponding to ν(PF). This shift to shorter wavelengths for the ν(CC) absorption is indicative of further decrease in the C_α-C_β bond order towards a cumulenic structure (see Figure 2.6). The mass spectrum confirmed the presence of the di-cation with a peak at *m/z* 748 corresponding to $[M]^{2+}$.

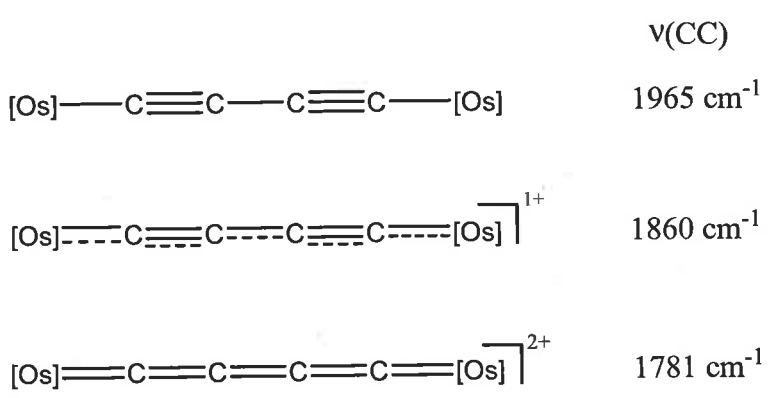

Figure 2.6. *Electronic structure of* $[\{Cp^*(dppe)Os\}_2(\mu\text{-}C{\equiv}CC{\equiv}C)]^{n+}$ *(where n = 0, 1, 2) as indicated by the IR spectrum.*

Attempts were also made to isolate **6**$[PF_6]_3$ using stronger oxidising agents such as Ag^+ ($E_{1/2}$ = +1.11 V in CH_2Cl_2),[75] but all reactions failed to give the desired complex. The cyclic voltammetry of the product from this reaction was not similar to those observed for $[Cp^*(dppe)OsCCCCOs(dppe)Cp^*]^{n+}$ (where n = 0, 1, 2). This suggested that the tri-cation has enhanced reactivity compared to that of the mono- and di-cations and undergoes a chemical transformation precluding its isolation. This problem might be overcome by the addition of stronger electron-donating ligands. In a related iron complex the isolation of $[\{Cp^*(dippe)Fe\}_2(CCCC)][PF_6]_3$,[76] was possible when the more electron-donating dippe ligand was used.

2.4. Conclusions.

The successful syntheses of three new diyndiyl complexes **6**, **10** and **11** was achieved along with the mono- and di-cationic species of **6**. Comparison of the IR spectra of **6**[PF_6] and **6**[PF_6]$_2$ with those observed for **2**[PF_6] and **2**[PF_6]$_2$, shows similar decreases in the bond order between C_α and C_β, consistent with a reorganisation of the electron density as indicated by the structures **A**-**C**.

Comparison of the electrochemistry of the five Group 8 diyndiyl complexes (**1**, **2**, **3**, **6** and **10**) shows that strong electronic interactions exist between the two metal termini in all complexes, which are all considered Class III by the Robin-Day classification system due to the large separation between the redox events.

Despite the novel synthetic approach used in the synthesis of **5** this could not be extended successfully to the synthesis of **12** due to the apparent strength of the osmium-chloride bond compared to the ruthenium-chloride bond. The [2 +2] cycloaddition of **12** that was previously observed for ruthenium was also confirmed by osmium, which undergoes the same process to give **14**.

2.5. Experimental.

All reactions were carried out under dry, high purity argon using standard Schlenk techniques. Solvents were purified as follows: THF, diethyl ether, pentane, and benzene were distilled form Na/benzophenone; CH_2Cl_2 and ^tBuOH were distilled from CaH_2; MeOH was distilled from Mg/I_2. Elemental analyses were performed by CMAS, Belmont, VIC, Australia. Despite several attempts accurate elemental analyses could not be obtained for **6**[PF_6] and **56**.

Instrumentation.

IR spectra were obtained on either a Perkin-Elmer 1720X FT IR spectrometer (4000-400 cm^{-1}) or on a Bruker IFS28 FT IR spectrometer (4000-400 cm^{-1}). Nujol mull spectra were obtained from samples mounted between NaCl discs.

NMR spectra were recorded on Varian 2000 instrument (^1H at 300.13 MHz, ^{13}C at 75.47 MHz, ^{31}P at 121.50 MHz,). Samples were contained within 5 mm sample tubes. Chemical shifts (δ) are given in ppm relative to internal tetramethylsilane (0 ppm) for ^1H and ^{13}C NMR spectra and external H_3PO_4 (0 ppm) for ^{31}P NMR spectra.

UV/Vis/NIR spectra were recorded on a Varian Cary 5 UV/Vis/NIR spectrometer. For spectroelectrochemistry, samples (1 mM) were dissolved in CH_2Cl_2 (with 0.5 M [Bu^n_4N][PF_6] supporting electrolyte). The OTTLE cell consists of a 1 mm path length with a platinum gauze working electrode, platinum wire counter and pseudo-reference electrodes.

Cyclic voltammograms were recorded using either a MacLab/400 or a PAR model 263 apparatus (using a platinum working electrode, platinum wire counter and pseudo-reference electrode). Solutions were made up in CH_2Cl_2 using a 0.1 M solution of [Bu^n_4N][PF_6] as the supporting electrolyte, at a scan rate 0.1 V s^{-1}. Ferrocene was used as an internal calibrant, $[FeCp_2]/[FeCp_2]^+ = +0.46V$.

Electrospray mass spectra (ES-MS) were recorded on either a VG Platform 2 or a Finnigan LCQ spectrometer. Methanol solutions were directly infused into the instrument, using chemical aids to ionisation as required.

X-ray crystal structures were determined by Professor Allan White and Dr Brian Skelton, University of Western Australia, Australia. Structural data were received in CIF format and the ORTEP plots of the individual molecules or cations were generated using ORTEP for Windows, showing 50% ellipsoid probability with non-essential hydrogen atoms removed for clarity. Throughout this thesis, ORTEP plots adhere to the following colour scheme: osmium and ruthenium in orange, carbon in red, halides in blue, phosphorus in green, iron in purple and nitrogen in cyan.

Reagents: The compounds $[Cp^*(dppe)Os{=}C{=}CH_2][PF_6]$,[77] $Cp^*(dppe)RuC{\equiv}CH$,[31] $Cp^*(dppe)FeC{\equiv}CH$,[63] $[FeCp_2][PF_6]$,[75] $TMSC{\equiv}CC{\equiv}CH$,[78],$OsCl(dppe)Cp^*$,[77] were all prepared using standard literature procedures. The compounds $Na[BPh_4]$ and proton sponge™ were use as received from Aldrich.

$Cp^*(dppe)OsC{\equiv}CH$ (8).[79]

To a suspension of $[Cp^*(dppe)Os{=}C{=}CH_2][PF_6]$ (88 mg, 0.098 mmol) in THF (15 mL) was added KO^tBu (12 mg, 0.098 mmol). After the mixture was stirred for 30 min, the solvent was removed under vacuum. The residue was then extracted with benzene and the solvent was again removed under vacuum to yield yellow $Cp^*(dppe)OsC{\equiv}CH$ (44 mg, 60%). Anal. Calcd. ($C_{38}H_{40}P_2Os$): C: 60.95, H: 5.38, Found C: 60.81, H: 5.39. IR (nujol, cm^{-1}): 3274 s ν(≡CH); 1929 w ν(C≡C). ^1H NMR (d_6-benzene): δ 7.95-7.03 (m, 20H, Ph); 2.71-2.65, 2.08-1.99 (2 x m, 2 x 2H, CH_2CH_2); 2.10 (s, 1H, ≡CH); 1.73 (s, 15H, Cp*). ^{13}C NMR (d_6-benzene): δ 139.37-127.02 (m, Ph); 92.91 (t, $^2J_{CP}$ 16.6 Hz, C_α); 89.88 (s, C_β); 88.79 (t, $^2J_{CP}$ 2.7 Hz, C_5Me_5); 31.16 (m, CH_2CH_2); 10.04 (s, C_5Me_5). ^{31}P NMR (d_6-benzene): δ 43.6 (s, dppe). ES-MS (positive ion mode, MeOH, *m/z*): 751, $[M + H]^+$.

[Cp*(dppe)Os=C=CHCH=C=Os(dppe)Cp*][PF_6]$_2$ (9).[79]

To a cooled suspension (-78°C) of Cp*(dppe)OsC≡CH (150 mg, 0.20 mmol) in CH_2Cl_2 (20 mL) was added [$FeCp_2$][PF_6] (63 mg, 0.19 mmol). The reaction mixture was stirred at -78°C for 1 h before the product was precipitated directly from the reaction mixture upon the slow addition of Et_2O (50 mL). The solid was filtered by cannula and dried under vacuum to yield [Cp*(dppe)Os=C=CHCH=C=Os (dppe)Cp*][PF_6]$_2$ (126 mg, 74%). IR (nujol, cm^{-1}): 1611 w ν(C=C); 841 s ν(PF). ^{1}H NMR ($CDCl_3$): δ 7.56-7.00 (m, 40H, Ph); 2.72-2.60(m, 8H, CH_2CH_2); 1.73 (s, 30H, Cp*); 1.00 (s, 2H, =CH). ^{13}C NMR ($CDCl_3$): δ 309.69 (s, C_α); 134.32-128.62 (m, Ph); 100.37 (s, C_β); 88.21 (s, C_5Me_5); 31.87-30.21 (m, CH_2CH_2); 9.46 (s, C_5Me_5). ^{31}P NMR ($CDCl_3$): δ 39.4 (s, dppe); -143.7 (sept, $^1J_{PF}$ 711 Hz, PF_6). ES-MS (positive ion mode, MeOH *m/z*): 749, $[M]^{2+}$.

{Cp*(dppe)Os}$_2$(μ-C≡CC≡C) (6).[79]

To a suspension of [Cp*(dppe)Os=C=CHCH=C=Os(dppe)Cp*][PF_6]$_2$ (125 mg, 0.07 mmol) in THF (20 mL) was added KO^{t}Bu (15.5 mg, 0.139 mmol). After the mixture was stirred for 30 min, the solvent was removed under vacuum. The residue was then extracted with hexane and the solvent was again removed under vacuum to yield orange {Cp*(dppe)Os}$_2$(μ-C≡CC≡C) (65 mg, 66%). Anal. Calcd. ($C_{76}H_{78}P_4Os_2$): C: 61.03, H: 5.26, Found C: 61.15, H: 5.34. IR (nujol, cm^{-1}): 1965 s, 1867 w ν(C≡C). ^{1}H NMR (d_6-benzene): δ 7.99-7.06 (m, 40H, Ph); 2.69-2.62, 2.05-1.99 (2 x m, 2 x 4H, CH_2CH_2); 1.75 (s, 30H, Cp*). ^{13}C NMR (d_6-benzene): δ 139.99-127.16 (m, Ph); 95.46 (s, C_β); 88.68 (s, C_5Me_5); 71.32 (t, $^2J_{CP}$ 19.1 Hz, C_α); 31.42-31.35 (m, CH_2CH_2); 10.08 (s, C_5Me_5). ^{31}P NMR (d_6-benzene): δ 43.5 (s, dppe). ES-MS (positive ion mode, MeOH, *m/z*): 1497, $[M]^+$.

{Cp*(dppe)Os}C≡CC≡C{Ru(dppe)Cp*} (10).

To a cooled suspension (-78°C) of Cp*(dppe)OsC≡CH (17 mg, 0.023 mmol) and Cp*(dppe)RuC≡CH (15 mg, 0.023 mmol) in CH_2Cl_2 (10 mL) was added $[FeCp_2][PF_6]$ (15 mg, 0.046 mmol). The reaction mixture was stirred at -78°C for 1 h before the product was precipitated directly from the reaction mixture upon the slow addition of Et_2O (50 mL). The solid was filtered by canula and dried under vacuum. THF (10 mL) was then added to the solid followed by KO^{t}Bu (6 mg, 0.046 mmol). The reaction mixture was stirred at r.t. for 30 min before the solvent was removed. The crude solid was extracted with hexane to give bright orange solution. The solvent was then removed under vacuum to yield a mixture of {Cp*(dppe)Os}C≡CC≡C{Ru(dppe)Cp*}, {Cp*(dppe)Os}$_2$(μ-C≡CC≡C), and {Cp*(dppe)Ru}$_2$(μ-C≡CC≡C). ^{1}H NMR (d_6-benzene): δ 8.01-7.07 (m, 40H, Ph); 2.78-2.63 and 2.02-1.95 (m, 8H, CH_2CH_2); 1.74 (s, 15H, Os-Cp*); 1.69 (s, 15H, Ru-Cp*). ^{31}P NMR (d_6-benzene): δ 82.5 (s, Ru-dppe); 43.5 (s, Os-dppe). ES-MS (positive ion mode, MeOH, *m/z*): 1317, [{Cp*(dppe)Ru}$_2$(μ-C≡CC≡C)]$^+$; 1408, [{Cp*(dppe)Os}C≡CC≡C{Ru(dppe)Cp*}]$^+$; 1496, [{Cp*(dppe)Os}$_2$(μ-C≡CC≡C)]$^+$.

{Cp*(dppe)Os}C≡CC≡C{Fe(dppe)Cp*} (11).

Similarly, to a cooled suspension (-78°C) of Cp*(dppe)OsC≡CH (17 mg, 0.023 mmol) and Cp*(dppe)FeC≡CH (14 mg, 0.023 mmol) in CH_2Cl_2 (10 mL) was added $[FeCp_2][PF_6]$ (15 mg, 0.046 mmol). The reaction mixture was stirred at -78°C for 1 h before the product was precipitated directly from the reaction mixture upon the slow addition of Et_2O (50 mL). The solid was then filtered by canula and dried under vacuum. THF (10 mL) was then added to the solid followed by KO^{t}Bu (6 mg, 0.046 mmol). The reaction mixture was stirred at r.t. for 30 min before the solvent was removed. The crude solid was extracted with hexane to give bright orange solution. The solvent was then removed under vacuum to yield a mixture of {Cp*(dppe)Os}C≡CC≡C{Fe(dppe)Cp*}, {Cp*(dppe)Os}$_2$(μ-C≡CC≡C), and {Cp*(dppe)Fe}$_2$(μ-C≡CC≡C). ^{1}H NMR (d_6-benzene): δ 8.12-7.06 (m, 40H, Ph); 2.81-2.73 and 2.11-1.98 (m, 8H, CH_2CH_2); 1.73 (s, 15H, Os-Cp*); 1.56 (s, 15H, Fe-

Cp*). ^{31}P NMR (d_6-benzene): δ 101.4 (s, Fe-dppe); 43.5 (s, Os-dppe). ES-MS (positive ion mode, MeOH, *m/z*): 1226, $[\{Cp^*(dppe)Fe\}_2(\mu\text{-}C{\equiv}CC{\equiv}C)]^+$; 1362, $[\{Cp^*(dppe)Os\}C{\equiv}CC{\equiv}C\{Fe(dppe)Cp^*\}]^+$; 1496, $[\{Cp^*(dppe)Os\}_2(\mu\text{-}C{\equiv}CC{\equiv}C)]^+$.

Cp*(dppe)RuC≡CC≡CTMS (5).

To a suspension of RuCl(dppe)Cp* (100 mg, 0.15 mmol), Na[BPh_4] (51 mg, 0.15 mmol) and proton sponge™ (32 mg, 0.15 mmol) in ^{t}BuOH (15 mL) was added HC≡CC≡CTMS (92 mg, 0.75 mmol). The suspension was heated at 50°C in a sealed flask for one hour before allowing to cool. The yellow suspension was filtered warm to yield Cp*(dppe)RuC≡CC≡CTMS (97 mg, 86%). IR (nujol, cm^{-1}): 2170 w, 2094 m, 1989 w ν(C≡C). ^{1}H NMR (d_6-benzene): δ 7.79-6.91 (m, 20H, Ph); 2.52-2.46, 1.80-1.73 (2 x m, 2 x 2H, CH_2CH_2); 1.52 (t, $^3J_{HP}$ 2 Hz, 15H, Cp*); 0.21 (s, 9H, TMS). ^{31}P NMR (d_6-benzene): δ 81.4 (s, dppe). Lit values.[72] IR (Nujol, cm^{-1}): ν(C≡C) 2171 w, 2095 m, 1990 w. ^{1}H NMR ($CDCl_3$): δ 7.86-6.89 (m, 20H, Ph); 2.49, 1.78 (2 x m, 2 x 2H, CH_2CH_2); 1.53 (t, $^3J_{HP}$ 2 Hz, 15H, Cp*); 0.23 (s, 9H, TMS). ^{31}P NMR ($CDCl_3$): δ 81.3 (s, dppe).

Cp*(dppe)OsC≡CC≡CTMS (12).

To a suspension of OsCl(dppe)Cp* (100 mg, 0.137 mmol), Na[BPh_4] (51 mg, 0.145 mmol) and proton sponge™ (31 mg, 0.145 mmol) in ^{t}BuOH (8 mL) was added HC≡CC≡CTMS (32 mg, 0.264 mmol). The suspension was heated at 50°C in a sealed flask for 18 h before the solvent was removed under vacuum. The residue was extracted with hot hexane until the extracts were no longer coloured. Solvent was again removed under vacuum to yield yellow Cp*(dppe)Os(C≡CC≡CTMS) (2 mg, 2%). IR (nujol, cm^{-1}): 2182 w, 2131 m, 2106 w ν(C≡C). ^{1}H NMR (d_6-benzene): δ 7.87-6.92 (m, 20H, Ph); 2.46-2.41, 1.91-1.87 (2 x m, 2 x 2H, CH_2CH_2); 1.63 (s, 15H, Cp*); 0.29 (s, 9H, TMS). ^{31}P NMR (d_6-benzene): δ 43.1 (s, dppe). ES-MS (positive ion mode, MeOH *m/z*): 847, $[M + H]^+$; 725 $[Os(dppe)Cp^*]^+$.

[{Cp*(dppe)Os}$_2$(μ-CCCC)][PF$_6$] (6[PF$_6$]).

To a solution of {Cp*(dppe)Os}$_2$(μ-C≡CC≡C) (26 mg, 0.017 mmol) in CH_2Cl_2 (10 mL) was added [FeCp$_2$][PF$_6$] (5.4 mg, 0.016 mmol) causing an immediate change in colour from orange to green. After the mixture was stirred for 30 min, the solvent was concentrated to 2 mL and hexane (25 mL) was added dropwise to yield green [{Cp*(dppe)Os}$_2$(μ-CCCC)][PF$_6$] (20 mg, 72%). IR (nujol, cm^{-1}): 1860 w ν(CC); 839 s ν(PF). ^{1}H NMR (d_6-acetone): δ 12.16 (br, 30H, Cp*); 10.68 (br, 8H, CH_2CH_2); 8.22-7.36 (br m, 40H, Ph). ES-MS (positive ion mode, MeOH, *m/z*): 1496, [M]$^+$; 725 [Os(dppe)Cp*]$^+$.

[{Cp*(dppe)Os}$_2$(μ-CCCC)][PF$_6$]$_2$ (6[PF$_6$]$_2$).

To a solution of {Cp*(dppe)Os}$_2$(μ-C≡CC≡C) (10 mg, 0.007 mmol) in CH_2Cl_2 (10 mL) was added [FeCp$_2$][PF$_6$] (4.3 mg, 0.013 mmol) causing a change in colour from orange to blue. After the mixture was stirred for 30 min, the solvent was concentrated to 2 mL and hexane (25 mL) was added dropwise to yield green [{Cp*(dppe)Os}$_2$(μ-C=C=C=C)][PF$_6$]$_2$ (8 mg, 67%). Anal. Calcd. ($C_{76}H_{70}F_{12}P_6Os_2$): C: 51.12, H: 4.40, Found C: 51.09, H: 4.31. IR (nujol, cm^{-1}): 1781 w ν(C=C); 836 s ν(PF). ^{1}H NMR (d_6-acetone): δ 7.80-6.99 (m, 40H, Ph); 3.69-3.58. 3.31-3.19 (2 x m, 2 x 4H, CH_2CH_2); 2.13 (br, 30H, Cp*). ^{31}P NMR (d_6-acetone): δ 80.9 (br, dppe); -143.0 (sept, $^1J_{PF}$ 707 Hz, PF$_6$). ES-MS (positive ion mode, MeOH, *m/z*): 748, [M]$^{2+}$; 725 [Os(dppe)Cp*]$^+$.

Chapter Three

Redox-active complexes containing Group 8 metal centres linked by C_2 bridges

3.1. Introduction.

Continuing interest in redox-active metal complexes containing all carbon ligands has been spurred on by the synthesis of complexes such as Cp*(dppe)RuC≡CC≡CFe(dppe)Cp* [32], and other such complexes of the formula $[L_nM]$-C_x-$[M'L'_m]$. This interest has been further enhanced due to the possible involvement of these complexes in molecular devices.

Development of these complexes has centred around carbon ligands from -C≡CC≡C- and longer (see Chapter 2 for synthetic strategies), with electron-rich metal termini. There is also a wide range of -C≡C- complexes, of the general formula $[ML_n]C{\equiv}C[M'L'_m]$, containing metal termini such as $Cr(CO)_3Cp$,[80] $Mn(CO)_5$,[81] and $Fe(CO)_2Cp^*$.[82] As a result of the electron withdrawing ligands on the metal termini however, these complexes have no significant electrochemistry, which would allow comparison to higher order complexes such as $\{Cp(dppe)Ru\}_2(\mu\text{-}C{\equiv}CC{\equiv}C)$.[83]

There are few examples of $[ML_n]C{\equiv}C[M'L'_m]$ complexes containing electron-rich metal termini such as $Ti(PMe_3)Cp^*_2$,[84] and $Au(PR_3)$ (where R = Me or Et),[85] which has been further extended by the recent synthesis of $(MeC_5H_4)(dmpe)Mn{=}C{=}C{=}Mn(dmpe)(MeC_5H_4)$[86]. Complexes of the general formula $[ML_n]C{\equiv}C[M'L'_m]$ can exist in three different valence bond forms (see Figure 3.1). The first two valence bond forms show alternating single and triple bonds (**D** and **E**), where the third is a completely double-bonded cumulenic form **F**).

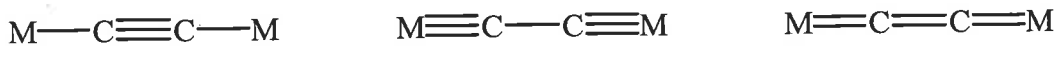

(D) **(E)** **(F)**

Figure 3.1. *Possible valence bond structures for complexes of the general formula MC_2M.*

3.1.1. Synthetic strategies for C_2 bridged complexes.

Taking into account these possible valence bond structures there have been limited synthetic approaches into the synthesis of these short carbon chain complexes. At present there are three main synthetic approaches used in the synthesis of these short even-numbered carbon chain complexes.

1. Metal-catalysed alkyne metathesis.

2. Coupling between a substituted C_2 fragment and two equivalents of the desired metal-ligand fragment.

3. Coupling between a [M]C≡CH fragment and a metal ligand fragment.

3.1.1.1. Synthetic strategy one. Metal-catalysed alkyne metathesis.

When considering metal-catalysed alkyne metathesis for the synthesis of $[ML_n]C{\equiv}C[ML_n]$ complexes, there are several important factors, namely the correct choice of metal catalyst, the desired metal alkyne and reaction solvent.

The product $\{Cp(CO)_2Ru\}_2(\mu\text{–}C{\equiv}C)$ was synthesised from $Cp(CO)_2RuC{\equiv}CMe$ and $(Me_3CO)_3W{\equiv}W(OCMe_3)_3$, in *iso*-octane in a moderate yield of 66% (see Scheme 3.1).[87] The reaction proceeds through the ruthenium-tungsten intermediate $Cp(CO)_2Ru\text{–}C{\equiv}W(OCMe_3)_3$, with the driving force of the reaction being the production of volatile C_2Me_2.

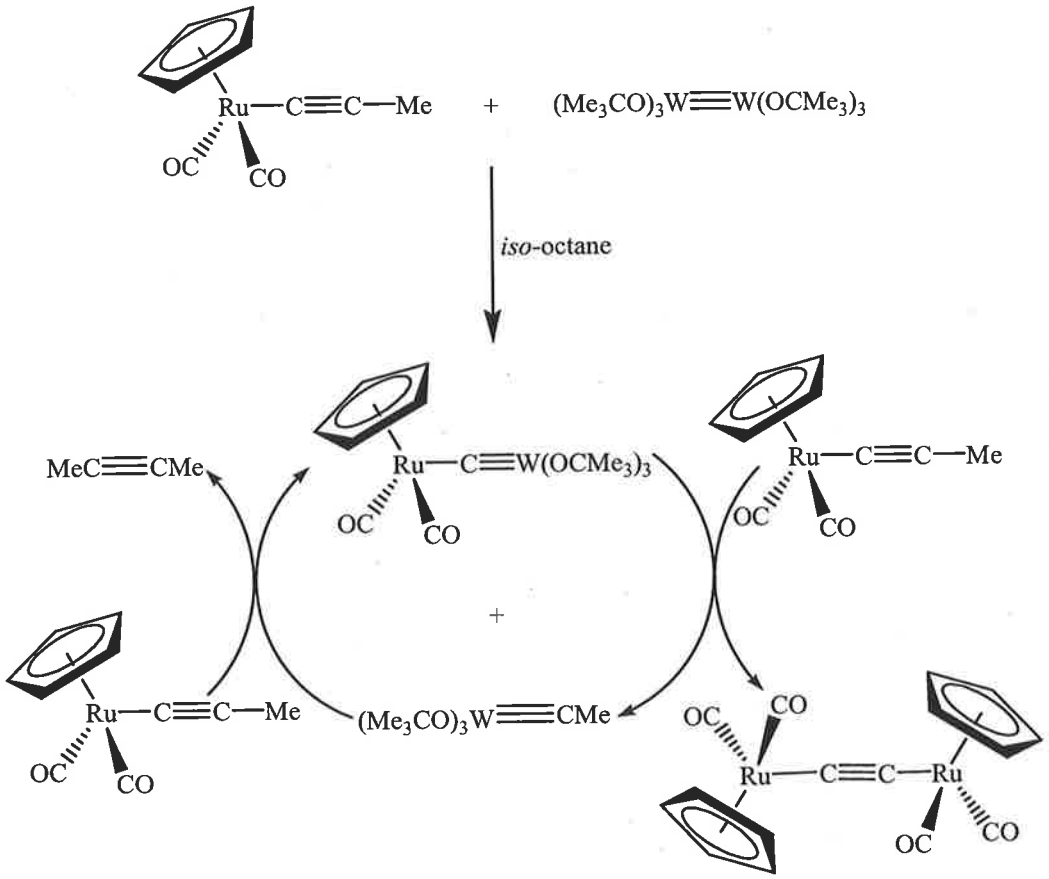

Scheme 3.1. *Metal-catalyzed alkyne metathesis.*

The above reaction makes use of the tungsten complex $(Me_3CO)_3W{\equiv}W(OCMe_3)_3$, which has been previously reported to be a useful reagent for alkyne metathesis reactions.[88] Complexes such as $Cp(CO)_2RuC{\equiv}CMe$ are also relatively simple synthetic targets by reaction of the lithium salt with MeI (see Scheme 3.2).[89] However the choice of solvent is equally important, by conducting the reaction in toluene instead of *iso*-octane, the catalytic cycle of the tungsten complex does not proceed and the formation of the desired product is not observed.

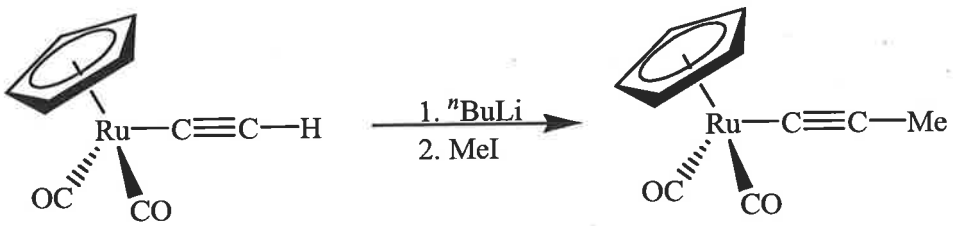

Scheme 3.2. *Synthesis of $Cp(CO)_2RuC{\equiv}CMe$.*

3.1.1.2. Synthetic strategy two. Coupling between a substituted C_2 fragment and two equivalents of the desired metal-ligand fragment.

The coupling of two metal-ligand fragments to an appropriately substituted C_2 fragment is a simple yet effective method of making C_2 complexes. This method possesses great versatility with a wide range of substituted C_2 fragments such as TMSC≡CH,[90] $Me_3SnC{\equiv}CSnMe_3$,[91] and IC≡CI.[92]

Acetylene is the simplest available C_2 fragment. The greatest difficulty in using acetylene is its high volatility, which makes maintaining a significant amount within the reaction mixture problematic. This restricts reactions so they must be either done using an excess of acetylene or in a sealed flask, which exposes the user to possibile explosions. Substitution of one or both of the protons reduces some of the difficulty associated with acetylene, as most products are either non-volatile liquids or solids.

The complex $[(MeC_5H_4)(dmpe)MnC_2Mn(dmpe)(MeC_5H_4)]^+$ was synthesised from a slight excess of $(MeC_5H_4)_2Mn(dmpe)$ and the bis-substituted acetylene $Me_3SnC{\equiv}CSnMe_3$, in THF at room temperature in a good yield of 69% (see Scheme 3.3).[86]

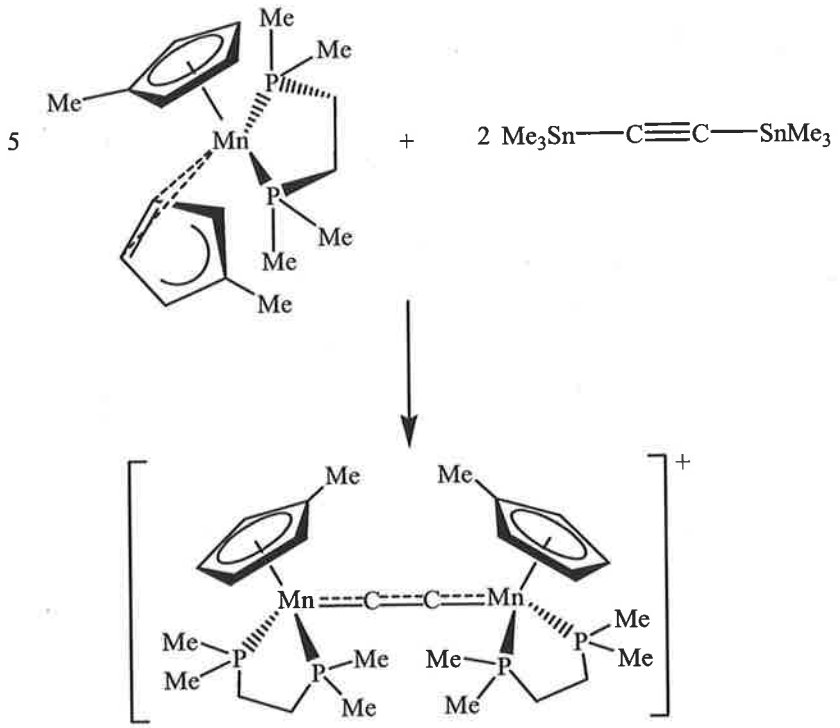

Scheme 3.3. *Synthesis of an electron-rich C_2 complex.*

Another method using a disubstituted acetylene fragment was in the synthesis of $(OC)_5MnC{\equiv}CMn(CO)_5$, from $[Mn(CO)_5]^-$[93] and IC≡CI, in THF, but in a poor yield of 15% (see Scheme 3.4).[81]

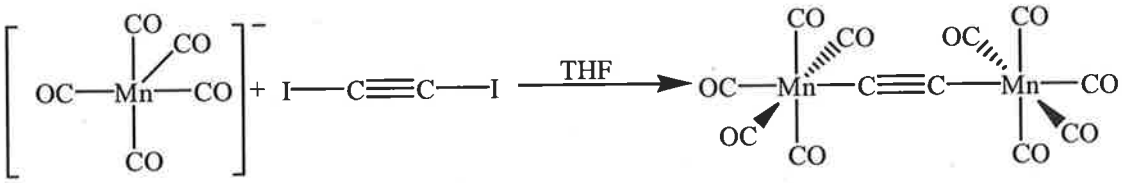

Scheme 3.4. *Synthetic route to $(CO)_5MnC{\equiv}CMn(CO)_5$.*

3.1.1.3. Synthetic strategy three. Coupling between a $[ML_n]C{\equiv}CH$ fragment and a metal ligand fragment.

Coupling between a $[ML_n]C{\equiv}CH$ fragment and another metal-ligand fragment possesses greater flexibility than the strategies outlined above, with the added possibility of forming hetero-metallic species. There is a wide range of complexes of the general formula $[ML_n]{=}C{=}CH_2$ such as $[Cp(dppe)Os{=}C{=}CH_2][PF_6]$ (see Chapter Six), which can be readily deprotonated to give the desired $[ML_n]C{\equiv}CH$ fragment. The $[ML_n]C{\equiv}CH$ fragment can be further deprotonated using ^{n}BuLi, which activates the C_β to further electrophilic attack. Metal halides of the general formula $[ML_n]X$ (where X = Cl, Br, I) can also be activated by reaction with AgOTf. Such silver salts abstract the halide from the metal to give the solvated cation, which is susceptible to nucleophilic attack.

The complex $Cp^*(NO)(PPh_3)ReC{\equiv}CRh(CO)(PPh_3)_2$ was prepared from the reaction of $Cp^*(NO)(PPh_3)ReC{\equiv}CH$ with ^{n}BuLi and $RhCl(CO)(PPh_3)_2$, in THF at –80°C in a yield of 72% (see Scheme 3.5).[89]

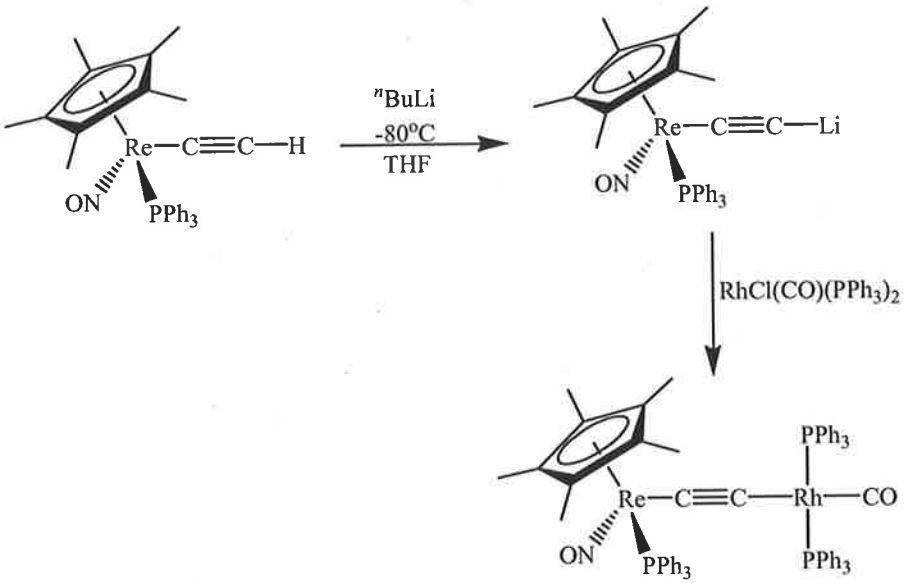

Scheme 3.5. *Synthesis of Cp*(NO)(PPh₃)ReC≡CRh(CO)(PPh₃)₂.*

The complex $\{Cp^*(CO)_2Fe\}_2(\mu\text{–}C\equiv C)$ was synthesised from $FeC\equiv CH(CO)_2Cp^*$ and $[Fe(CO)_2Cp^*(THF)]BF_4$ (prepared by the reaction of $FeCl(CO)_2Cp^*$ with $Ag[BF_4]$ in THF), in CH_2Cl_2 stirred overnight and then treated with NEt_3 to deprotonate the cation complex in a moderate yield of 57% (see Scheme 3.6).[82,94]

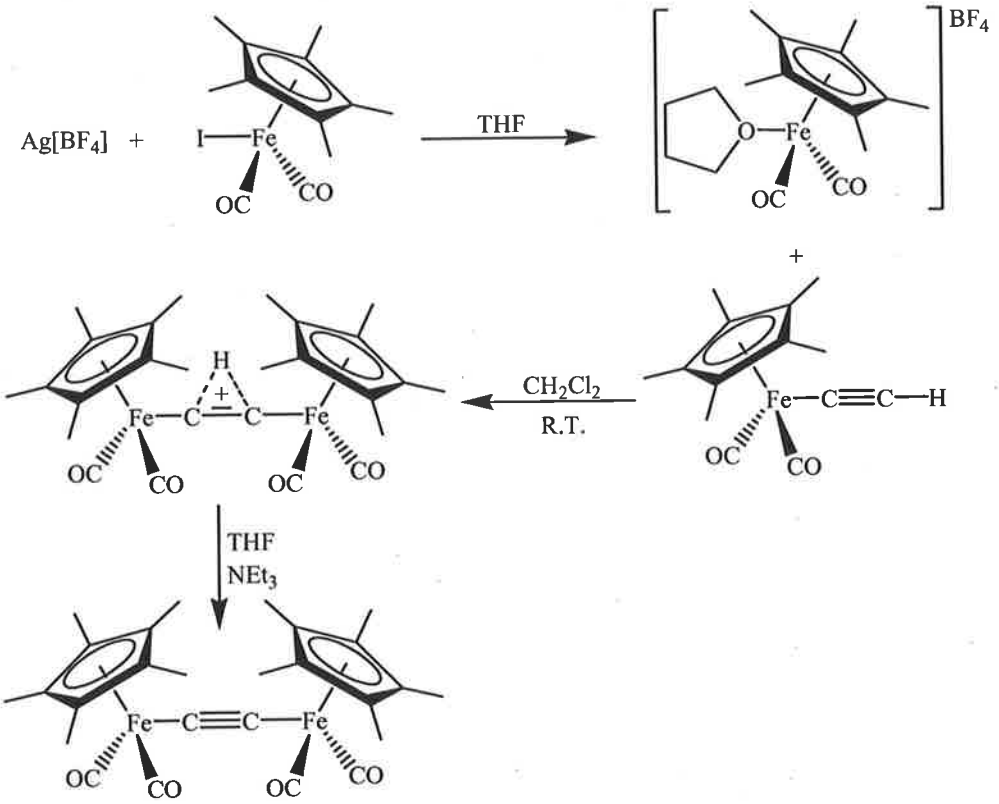

Scheme 3.6. *Synthetic route to {Cp*(CO)₂Fe}₂(μ-C≡C).*

3.1.2. Properties of C_2 complexes.

Bimetallic complexes bridged by a C_2 fragment are of particular interest for their potential as models for molecular wires. Their synthesis will also allow comparisons to be drawn with longer chain analogues.

The cyclic voltammetry of these complexes has been particularly limited due to the nature of the electron-withdrawing ligands on the metal termini. Complexes containing electron donating ligands such as $[(MeC_5H_4)(dmpe)MnC_2Mn(dmpe)(MeC_5H_4)]^+$, have demonstrated large separation between redox events (988mV), which indicates significant interactions between the two metal termini through the bridging carbon chain.

3.2. Aims of this work.

The aim of this work is to develop syntheses for several redox-active Group 8 complexes linked by C_2 bridges. The effect of having a shorter carbon chain will be compared to their corresponding analogues. The metal-metal interactions will also be investigated, by comparing the separation between redox events via cyclic voltammetry.

3.3. Results and Discussion.

3.3.1. Synthesis of C_2 complexes.

The synthesis of Cp(dppe)RuC≡CRu(dppe)Cp (**15**)[72] has been previously reported starting from [Cp(dppe)Ru=C=CH_2[PF_6] (**16**) and RuCl(dppe)Cp (**17**). This method was utilized to incorporate other metals, such as iron and osmium and ligands such as Cp* (see Scheme 3.7).

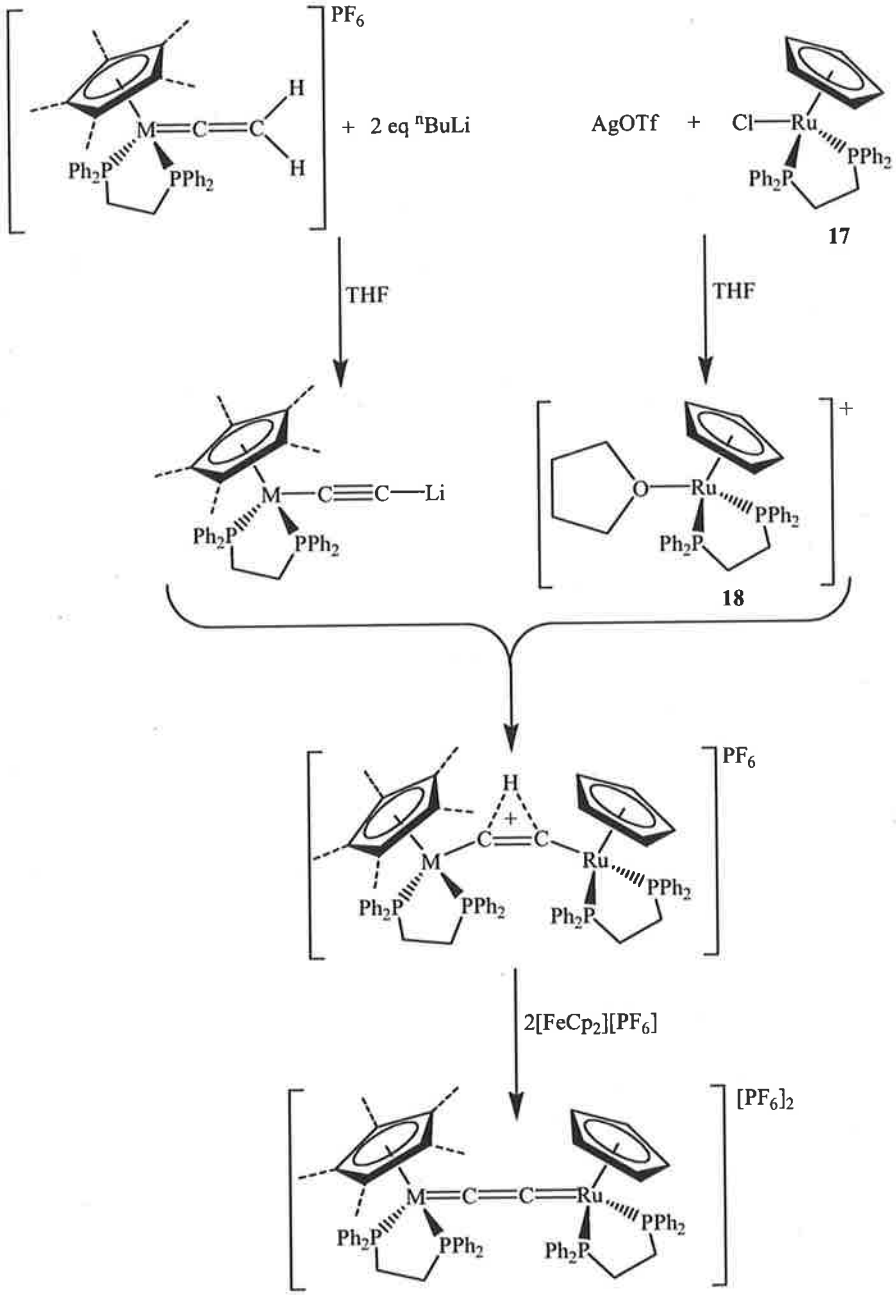

Scheme 3.7. *General synthesis for the complexes [Cp(dppe)RuCCM(dppe)Cp'], where M = Fe Cp' = Cp, M = Ru Cp' = Cp/Cp*, M = Os Cp' = Cp/Cp*.*

The first goal was to prepare several complexes end-capped with the Ru(dppe)Cp moiety, by generating the THF stabilised cation $[Ru(THF)(dppe)Cp]^+$ (**18**) (by treatment of **17** with AgOTf) and reacting it with the desired Cp'(dppe)MC≡CLi. Thus the relevant $[Cp'(dppe)MCCH_2][PF_6]$ (where M = Fe Cp' = Cp, M = Ru Cp' = Cp/Cp*, M = Os Cp' = Cp/Cp*) complex was treated with two equivalents of ^{n}BuLi to produce the lithio complex and reacted *in situ* with **18**. The resulting solution was chromatographed (silica gel) to yield forest-green $[Cp(dppe)RuCCHM(dppe)Cp'][PF_6]$. Previously these protonated complexes were seen as the most suitable synthetic targets due to the reactivity of the neutral complexes.[72]

Isolation of the desired complexes was then achieved through oxidation of the protonated complexes using two equivalents of $[FeCp_2][PF_6]$. Silica gel chromatography eluting with 50% acetone / hexane yielded the desired complexes, except where M = Fe which was precipitated from the reaction upon addition of Et_2O. Conversion of the di-cation **15[PF$_6$]$_2$** to either the mono-cation or the neutral complex was achieved by the treatment with one or two equivalents of KO^{t}Bu (see Scheme 3.8).[95-97]

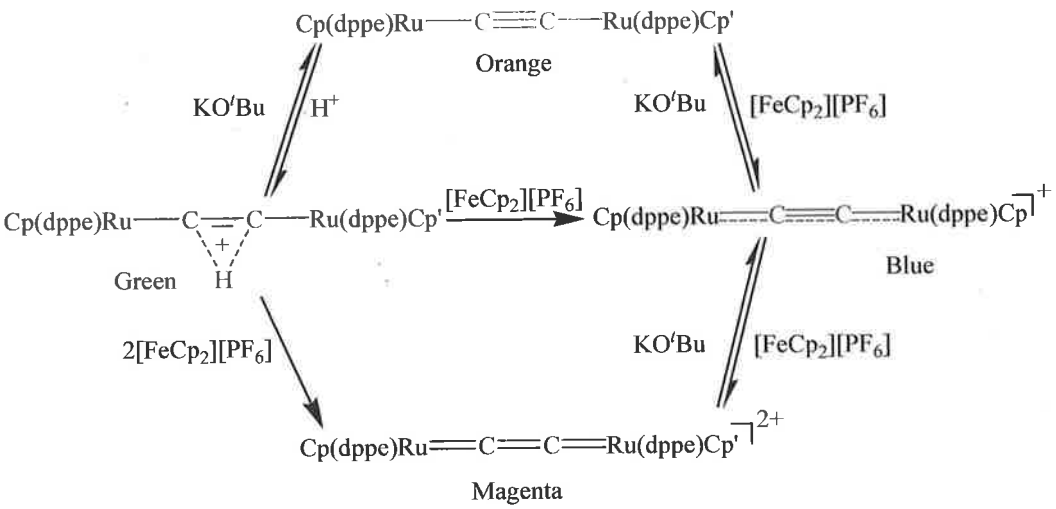

Scheme 3.8. *Chemical oxidation and reduction of Cp(dppe)RuC$_2$Ru(dppe)Cp', where Cp' = Cp/Cp**.

3.3.2. Spectral properties of C_2 complexes.

The IR spectrum for the mono-cation **15[PF$_6$]** showed a weak ν(CC) band at 1713 cm^{-1}. This peak shifts to longer wavelengths in **15[PF$_6$]$_2$** to 1651 cm^{-1}, which is consistent with a decrease in the carbon-carbon bond order as seen for the C_4 complexes. All the di-cations **19[PF$_6$]$_2$**, **20[PF$_6$]$_2$**, **21[PF$_6$]$_2$**, and **22[PF$_6$]$_2$** gave bands in the IR spectra between 1672-1630 cm^{-1} corresponding to ν(CC) of a cumulenic structure **F**.

Due to the paramagnetic nature of the mono- and di-cations, the ^{1}H NMR spectra could not be collected for **15[PF$_6$]**, **15[PF$_6$]$_2$**, **19[PF$_6$]$_2$**, **20[PF$_6$]$_2$**, **21[PF$_6$]$_2$** and **22[PF$_6$]$_2$**. For **19** the ^{1}H NMR spectrum contained a multiplet between δ 7.93-6.76 corresponding to the aromatic protons on both dppe ligands. The CH_2CH_2 protons in dppe appeared as two multiplets at δ 2.15-2.08 and 1.98-1.87. The Cp and Cp* protons were observed at δ 4.60 and 1.69 respectively.

The ^{13}C NMR spectrum contains peaks at δ 147.46-126.07, corresponding to the aromatic carbons. The Cp* and Cp carbons were found at δ 92.82, 10.97 and 83.01 respectively. The CH_2CH_2 bridging carbons in dppe were also found as a multiplet between δ 27.98-27.59, but like that found for **15** the carbons in the chain were not observed due to the relaxation times.

The ^{31}P NMR spectrum of **19** shows two peaks at δ 88.74 and 83.01, corresponding to the different dppe ligands, as a result of the different environments due to the effect of Cp versus Cp*, on the ruthenium termini.

Mass spectrometry proved a useful diagnostic tool in determining the nature of the complexes with the molecular ion observed for all complexes. The molecular ion for **19** appeared at *m/z* 1224, while for the mono-cation **15[PF$_6$]** it appeared at *m/z* 1154. For the di-cations **15[PF$_6$]$_2$**, **19[PF$_6$]$_2$**, **20[PF$_6$]$_2$**, **21[PF$_6$]$_2$** and **22[PF$_6$]$_2$** peaks were observed at *m/z* 577, 611, 656, 621 and 554 each corresponding to $[M]^{2+}$. These complexes also underwent similar fragmentation with peaks corresponding to

$[M(dppe)Cp']^+$ (where M = Ru Cp' = Cp / Cp*, Os Cp' = Cp / Cp*, and Fe Cp' = Cp) observed at *m/z* 565, 635, 655, 725 and 519 respectively.

3.3.3. Molecular structures.

It has proved difficult to obtain crystals of sufficient quality for X-ray studies, although determinations of reasonable precision have been successfully carried out with a dichloromethane solvate of **15** and water and acetone solvates of **15[PF_6]$_2$** (see Figure 3.2). The determination on **15[PF_6]**, also reported here, is of lower precision. Comparisons between these four determinations provided some information on the changes occurring within the Ru-C-C-Ru fragment as oxidation proceeds.

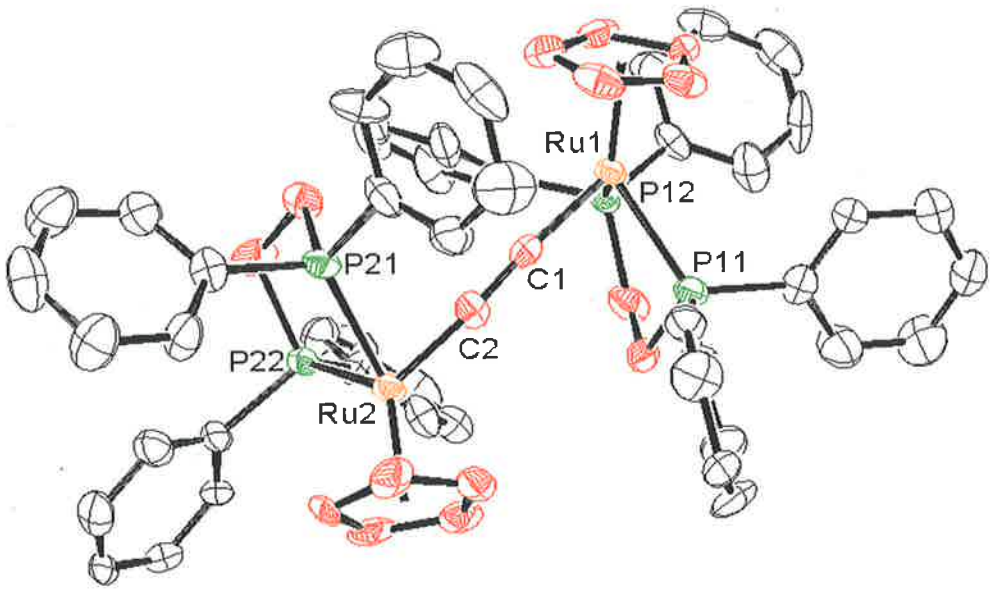

Figure 3.2. *X-ray crystal structure of [{Cp(dppe)Ru}$_2$(μ-CC)][PF_6]$_2$.*

For the neutral complex **15**, two Ru(dppe)Cp groups are linked by the C_2 fragment, with the dihedral angle between the two Ru…C(0) vectors [C(0) is the mid-point of

the Cp ring] being 101.9(3)°. The Ru-C(1,2) and C(1)-C(2) distances are 2.046(5), 2.051(5) and 1.230(7) Å, respectively, with angles at C(1, 2) being 174.0(4) and 170.2(4)°. The four Ru-P distances fall between 2.234(1) and 2.243(1) Å (av. 2.237 Å). In the corresponding mono-cation, the Ru-C(1,2) distances are 2.00(3), 2.02(3) Å, with C(1)-C(2) lengthening to 1.28(4) Å, with angles at C(1,2) similar to those in **15**. Lengthening of the Ru-P distances to between 2.317 and 2.329(10) Å is found (av. 2.321 Å). The two di-cations have essentially identical geometries, with Ru-C(1,2) 1.878(8), 1.881(8) Å and C(1)-C(2) 1.30(1) Å, with angles at C(1,2) being 172.6(7) and 175.6(6)°, respectively (values for acetone solvate given). The Ru-P distances are between 2.287(3) and 2.315(3) Å (av. 2.298 Å). The torsion angles C(0)...Ru...Ru...C(0) are all around 60° and reflect steric congestion between the two organoruthenium groups.

Table 3.1 compares the M-CC-M systems in **15**, $[\mathbf{15}]^{+}$ and $[\mathbf{15}]^{2+}$, and of the Mn complexes $[\{Mn(dmpe)(\eta\text{-}C_5H_4Me)\}_2(\mu\text{-}CC)]^{n+}$ (n = 0-2)[86]. In the latter case the structural data has been interpreted as indicating that the di-cation is an example of the bis-carbyne resonance form. Overall, for the ruthenium complexes, these structural data are consistent with a gradual shortening of the Ru-C bond and lengthening of the C-C bond, which may be represented in valence bond terms as a change from the ethynediyl structure **D** [-Ru-C≡C-Ru-] towards the cumulenic structure **F** [-Ru=C=C=Ru-] as oxidation proceeds. This interpretation is also supported by theoretical calculations carried out on $[\{Cp(dHpe)Ru\}_2(\mu\text{-}CC)]^{n+}$ (**15-H**$^{n+}$, n = 0-2) at the density functional theory (DFT) level of theory (see below).

	15[72]	**[15]PF$_6$**	**[15](PF$_6$)$_2$**[a]	**[15](PF$_6$)$_2$**[b]
Bond distances (Å)				
Ru(1)-P(11)	2.234(1)	2.320(9)	2.287(3)	2.285(2)
Ru(1)-P(12)	2.234(1)	2.321(10)	2.294(2)	2.299(2)
Ru(2)-P(21)	2.243(1)	2.317(10)	2.296(3)	2.281(2)
Ru(2)-P(22)	2.239(1)	2.329(10)	2.315(3)	2.301(2)
Ru(1)-C(cp)	2.202-2.263(5)	2.27-2.35(3)	2.255-2.282(7)	2.244-2.287(9)
(av.)	2.24	2.30	2.27	2.26
Ru(2)-C(cp)	2.232-2.266(5)	2.26-2.31(3)	2.235-2.282(9)	2.243-2.282(9)
(av.)	2.24	2.29	2.26	2.25
Ru(1)-C(1)	2.046(5)	2.00(3)	1.878(8)	1.89(1)
C(1)-C(2)	1.230(7)	1.28(4)	1.30(1)	1.28(2)
C(2)-Ru(2)	2.051(5)	2.02(3)	1.881(8)	1.88(1)
Bond angles (°)				
P(11)-Ru(1)-P(12)	84.04(4)	83.0(3)	81.97(9)	80.88(8)
P(21)-Ru(2)-P(22)	83.43(4)	83.0(3)	80.72(8)	82.27(7)
P(11)-Ru(1)-C(1)	84.04(13)	85.6(8)	81.4(3)	81.3(2)
P(12)-Ru(1)-C(1)	84.99(13)	85.2(9)	91.6(2)	96.7(3)
P(21)-Ru(2)-C(2)	83.19(12)	90.7(8)	82.0(3)	82.8(2)
P(22)-Ru(2)-C(2)	90.10(12)	79.4(8)	97.5(3)	92.4(3)
Ru(1)-C(1)-C(2)	174.0(4)	170.8(24)	174.8(7)	172.6(7)
C(1)-C(2)-Ru(2)	170.2(4)	177.1(22)	174.6(6)	175.6(6)

Table 3.1. *Relative bond distances and angles of* **15**, **[15]**$^+$ *and* **[15]**$^{2+}$. [a] *acetone solvate,* [b] *water solvate.*

3.3.4. Magnetic properties.

Solutions of the di-cations give broad NMR spectra, which sharpen somewhat upon cooling the solutions and suggest a degree of paramagnetism. This has been confirmed in the case of **15[PF_6]$_2$** by measurements of the magnetic susceptibilities of two freshly prepared samples over the temperature range 4-300 K. The samples gave rather similar plots of the magnetic moment μ_{eff} (per Ru_2) vs temperature, one having a room temperature moment of 0.46 μ_B, the other 0.26 μ_B. The former, shown in Figure 3.3, remains constant between 300 and 100 K, then decreases gradually to reach 0.3 μ_B at 4 K. The corresponding μ_M data follow a Curie temperature dependence. These values are very small and close to being diamagnetic after allowing for the diamagnetic corrections of the ligands. Susceptibilities are bulk measurements that indicate the presence of weak paramagnetism but they cannot specify if unpaired electron spins are or are not localised on the Ru or C_2 fragments.

Small paramagnetic susceptibilities can originate from a variety of sources, a possible one being the presence of paramagnetic impurities in an otherwise diamagnetic material. In principle they can originate from second-order Zeeman effects on the Ru centres, but these would be expected to be independent of temperature, which is not the case in Figure 3.3. Of particular relevance to the present and related μ-C_2 species, is the occurrence of spin-triplet, as well as spin-singlet states (*vide infra*). What is clear is that the present μ_{eff} values are much smaller than those reported for the related μ-C_2-manganese complexes [{Cp'(dmpe)Mn}-CC-{Mn(dmpe)Cp'}]$^{n+}$, where n = 0 or 1,[21] the former having a value of 2.47 μ_B at room temperature which decreased to 2.28 μ_B at 2 K, and ascribed to a population of a spin-triplet state at all temperatures, which should lead to a μ_{eff} value of 2.8 μ_B. The authors proposed a spin-triplet / singlet equilibrium with S = 1 close in energy above S = 0 to explain the temperature dependence in μ_{eff}. The n = 1 cation showed a most unusual increase in μ_{eff} from 0.69 μ_B at 300 K to 1.67 μ_B at 5 K and this was ascribed to one unpaired spin. An alternative possibility is that ferromagnetic coupling of two spins is occurring in that case combined with a spin-triplet / singlet equilibrium. Returning to the results obtained for the present di-cation, the data could be indicative of a triplet / singlet equilibrium with the S = 1 state at energy >> kT above the ground S = 0 state.

However, since μ_{eff} does not approach zero at intermediate temperatures, because of the population of the singlet state, it is more likely that a mixture of singlet and triplet state molecules exists in these solid samples with the singlet being dominant.

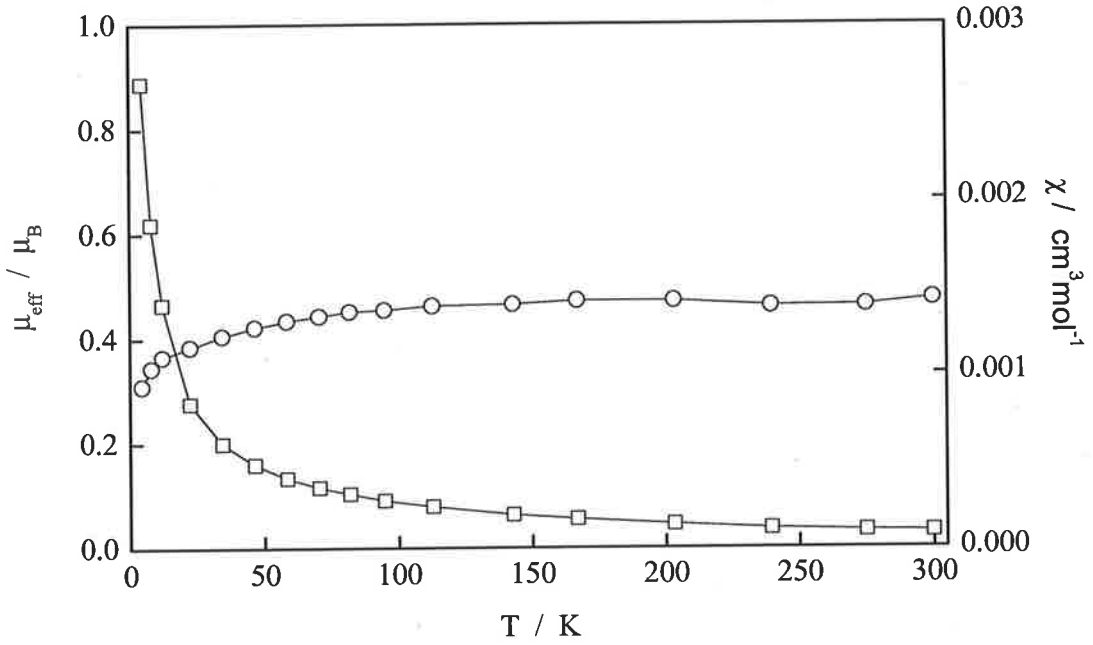

Figure 3.3.

3.3.5. Theory.

In order to better understand some of the experimental results a theoretical investigation was conducted at the DFT level. First on the model system $[\{Ru(dHpe)Cp\}_2(\mu\text{-}CC)]^{n+}$, **15-H**$^{n+}$ (n = 0-2, dHpe = $PH_2CH_2CH_2PH_2$) used to mimic $[\{Ru(dppe)Cp\}_2(\mu\text{-}CC)]^{n+}$, **15**$^{n+}$. Optimised distances and angles computed for the neutral and cationic models compare rather well with available experimental data obtained from X-ray crystallography. Experimentally measured changes in the Ru-C and C-C bond distances of **15** upon oxidation can be rationalised by the nodal properties of the two nearly degenerate HOMOs (Highest Occupied Molecular Orbital) computed for **15-H** (see Figure 3.4). As shown earlier,[98] they are delocalised over the Ru_2C_2 backbone, π-type in character and anti-bonding between ruthenium and carbon and bonding between the two carbon atoms. It turns out that removal of

electrons leads to some lengthening of the carbon-carbon bond and to some shortening of the metal-carbon bonds.

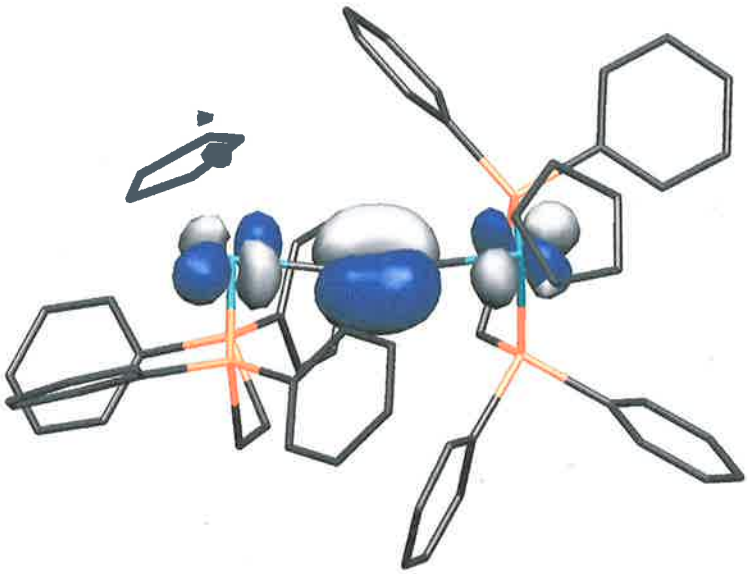

HOMO (-2.93 eV; 39 / 42)

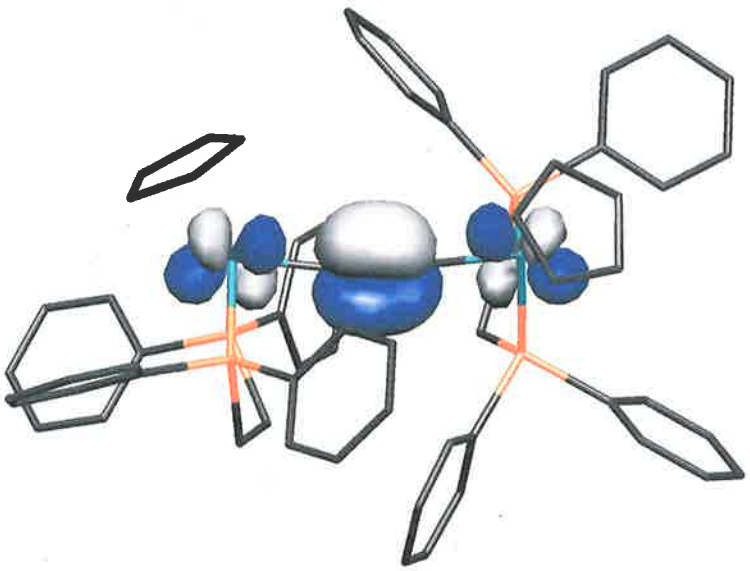

HOMO-1 (-3.10 eV; 40 / 43)

Figure 3.4. *HOMO and HOMO-1 of {Cp(dppe)Ru}$_2$(μ-CC).*

An interesting point too, is the position of one metallic fragment Ru(dHpe)Cp with respect to the other. Energy of the neutral system **15-H** seems to be hardly affected

upon rotation around the C_2 vector of one metallic moiety relative to the other. Indeed, a rather flat potential energy surface is computed for **15-H** with the energetically most favoured arrangement found for α = 180° (*transoid* geometry), only 0.03 eV (0.7 kcal/mol) below the most unfavored one. This indicates that the orientation of one Ru(dHpe)Cp fragment relative to the other in the neutral complex **15-H** has a negligible influence on the electronic and structural features of the metal-carbon core under investigation.

The same conclusion can be reached for the di-cationic high-spin (HS) **15-H**$^{2+}$ species. A flat potential energy surface is computed with a shallow minimum found for a CpRuRuCp torsion angle α of 62°. Here again no noteworthy energy difference (less than 1 kJ/mol) is computed between the different conformers. Identical observations were made for the triplet state of model complex $[(MeC_5H_4)(dHpe)Mn]_2C_2$, isoelectronic to (HS) **15-H**$^{2+}$, i.e., a flat potential energy curve with an energy minimum (α = 90 and 270°) and an energy maximum (α = 0°) separated by less than 5 kJ/mol.[86] In contrast, the energy of the low-spin (LS) **15-H**$^{2+}$ di-cation and, to a lesser extent that of the cation **15-H**$^{+}$, are much more dependent upon the adopted conformation. For instance, in the case of (LS) **15-H**$^{2+}$ a maximum energy difference of 20 kJ/mol is calculated between the most stable rotamer (α = 2°) and the less stable one (α = 56°). An even higher energy difference, ca. 36 kJ/mol, was found for the LS complex $[(MeC_5H_4)(dHpe)Mn]_2C_2$, isoelectronic to **15-H**$^{2+}$, but for different angles since the most stable conformer is computed for α = 180° (*transoid* geometry) whereas the less stable is for α = 90° (*gauche* geometry).[86] The energy dependence upon the conformation in these M_2C_2 complexes (M = Mn or Ru) is attributed to the fact that the shape and the metal character of the two π-type fragment orbitals of the pseudo-octahedral $\{M(dHpe)Cp\}^{+}$ fragment are not fully equivalent.[98] Consequently the HOMOs of the complexes in which these FOs are involved (see Figure 3.4) are not degenerate but slightly energetically separated in the *transoid* geometry. On the other hand, they become nearly degenerate in the *gauche* geometry with some energy stabilisation of the HOMO and some destabilisation of the HOMO-1. If both are doubly (neutral) or singly (HS di-cation) occupied, the total energy is hardly affected by changes of conformation. On the other hand, if one is

doubly occupied and one vacant (LS di-cation) or partially filled (mono-cation), the *transoid* configuration becomes more stable.

Steric hindrance of the bulky dppe ligands as well as solvation effects, also play a role in the conformer arrangements of **15**. QM/MM geometry optimisations followed by full DFT single point calculations were performed on $[\mathbf{15}]^{n+}$ (n = 0-2) series. An energy minimum is found for a CpRuRuCp torsion angle of 61° for **15**, very close to the value of 59.25° experimentally measured. For the di-cationic low-spin species $\mathbf{15}^{2+}$, the *transoid* form is now calculated 28 kJ/mol higher in energy than the most stable arrangement which is computed for α = 55° (angles of 52.4 and 60.8° are experimentally measured). We were not able to calculate *cisoid* forms (α = 0°) because of high steric repulsion. Obviously, the observed conformation of $\mathbf{15}^{n+}$ results from steric hindrance of the bulky dppe ligands, which seem to overcome the electronic effects previously described for the $\mathbf{15\text{-}H}^{n+}$ series.

It was important to calculate the energies of the different conformers of $\mathbf{15\text{-}H}^{2+}$ with accuracy since the energy differences are of the same order that those computed between different spin configurations. Indeed, theoretical results reveal that overall, singlet and triplet states of the di-cationic Ru_2C_2 species $\mathbf{15\text{-}H}^{2+}$ as well as the hetero-bimetallic model $[\{Cp(dHpe)Ru\}(CC)\{Os(dHpe)Cp\}]^{2+}$, $\mathbf{21\text{-}H}^{2+}$, are very close in energy. DFT/B3LYP calculations give the triplet state slightly favoured over the singlet state by 3 kJ/mol and 2 kJ/mol for $\mathbf{15\text{-}H}^{2+}$ and $\mathbf{21\text{-}H}^{2+}$, respectively (see computational details). This is an interesting result which strongly contrasts with di-cationic di-ruthenium complexes containing longer carbon chain spacers such as $\{Cp(dppe)Ru\}_2(\mu\text{–}C{\equiv}CC{\equiv}C)$, which are diamagnetic.[47,66,99] This behaviour which recalls that of magnetic di-iron carbon complexes,[32,33] is attributed to the high metal character of the "magnetic" orbitals. It turns out the HOMO and LUMO (HOMO-1 and HOMO in the neutral system) of (LS) $\mathbf{15\text{-}H}^{2+}$ are much more metallic in character than their corresponding MOs in the C_4-containing species (LS) $[\{Cp(dHpe)Ru\}_2(\mu\text{–}CCCC)]^{2+}$ (38 and 42 % vs 26 and 21%). This presumably contributes to the metal-centred diradical character of the former. Indeed, the computed metal spin density is more important in (HS) $\mathbf{15\text{-}H}^{2+}$ than in (HS) $[\{Cp(dHpe)Ru\}_2(\mu\text{–}CCCC)]^{2+}$ (0.49 vs 0.39). Similar results are obtained for the

hetero-bimetallic Ru/Os model **21-H**$^{2+}$, with an important metallic character in the HOMO and LUMO (44 and 43%, respectively), and large atomic spin densities located on Ru and Os (0.49 and 0.51, respectively) for the HS configuration. It is noteworthy that QM/MM-DFT calculations performed on **15**$^{2+}$ show the ferromagnetic triplet state 3 kJ/mol lower in energy than the antiferromagnetic singlet state (broken symmetry calculation).

As said earlier, it is known that carbon chain containing di-iron species are magnetic.[32,33] Concomitantly, the triplet state of the hetero-bimetallic Ru/Fe model [{Cp(dHpe)Ru}(CC){Fe(dHpe)Cp}]$^{2+}$, **22-H**$^{2+}$, is calculated to be 20 kJ/mol more stable than the singlet state. Again, the HOMO and LUMO are heavily weighted on the metal atoms, 49 and 46%, respectively, and in the triplet state, the metallic spin densities are 0.49 and 0.79 electron on Ru and Fe atoms respectively. Our theoretical results carried out at 0 K predict a magnetic behaviour for **22-H**$^{2+}$, whereas for **15-H**$^{2+}$ and **21-H**$^{2+}$, a singlet-triplet equilibrium is expected.

Time-dependent density functional theory (TD-DFT) was used to calculate the first vertical electronic transition energies for the mono-cationic model **15-H**$^{+}$ with its most stable conformation (α = 55°) and with the *transoid* arrangement. The lowest significative excitation was found in both at 16200 cm^{-1} (oscillator strength f = 0.17). This excitation, energetically isolated from other absorptions, involves for 70% an electronic transition from the highest occupied spin-orbital (HOSO)-1 (β) to the lowest unoccupied spin-orbital (LUSO), and for 13% an electronic transition from the HOSO-3 (β) to LUSO. Interestingly the LUSO is equally distributed on the metal atoms and the C_2 chain. This low energy excitation can be described as a metal-to-metal-C_2 transition rather than intervalence charge transfer (IVCT) transition.

3.3.6. Electrochemistry.

The aim of this work was to further extend the chemistry of {Cp(dppe)Ru}$_2$(μ–C≡C), by looking at substitution of one ruthenium centre with another group 8 metal, along with the effect of adding the more electron-rich Cp* ligand versus Cp and what effects these have on the electrochemistry of the isolated complexes (see Table 3.2).

The cyclic voltammogram of **15** has been previously reported as containing three fully reversible redox events (i_c / i_a = 1, current proportional to (scan rate)$^{1/2}$), and one quasi-reversible redox event (i_c / i_a = 0.9).[72] These four redox events show large peak-to-peak separations (large values of ΔE) of approximately 800mV. This gives rise to a large comproportionation constant (K_c = 1.02 x 10^{14}) indicating the high thermal stability of both the mono- and di-cations.[72] Both the mono- and di-cations were found to be stable as solids, but in solution the blue mono-cation changes to a magenta colour indicating conversion to the di-cation. The cyclic voltammogram for the di-cation **15[PF$_6$]$_2$** not surprisingly showed three fully reversible and one quasi-reversible redox events as found for the neutral complex (see Figure 3.5).

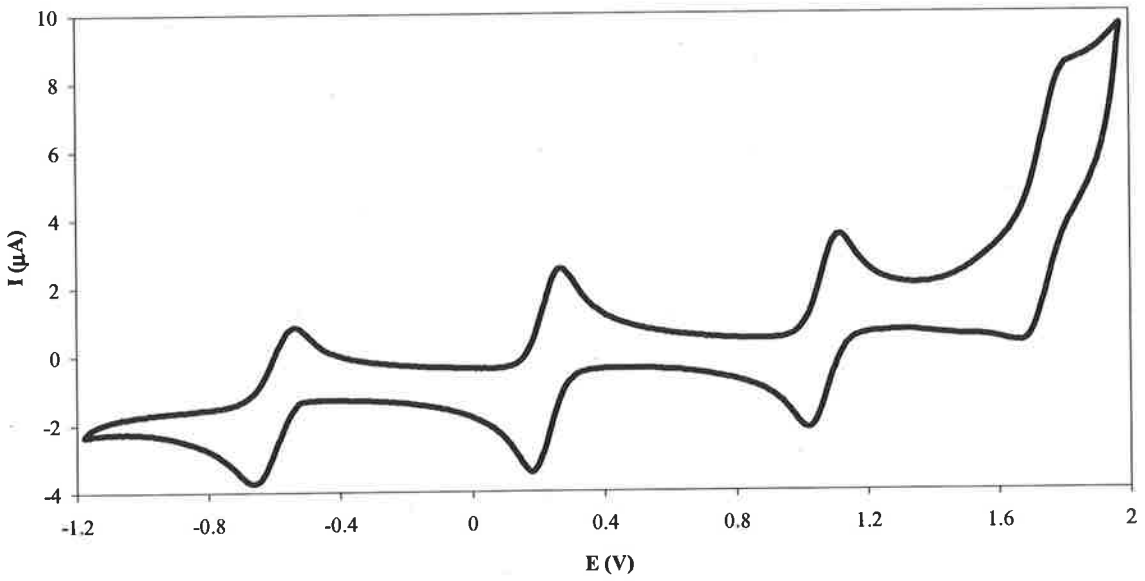

Figure 3.5. *Cyclic voltammogram of* **15[PF$_6$]$_2$** *recorded in 0.1M [Bu$^n_4$N][PF$_6$] / CH$_2$Cl$_2$ at 100 mV s^{-1}.*

As expected from observations made from the chloro complexes (see Chapter 6) exchange of one ruthenium centre for either iron or osmium has a dramatic effect on the oxidation potentials. Both **22[PF$_6$]$_2$** and **21[PF$_6$]$_2$** display three well separated fully reversible redox events (i_c / i_a = 1) at –0.75, +0.16, +1.04 and –0.67, +0.09, +1.00 V respectively (see Figure 3.6, 3.7).

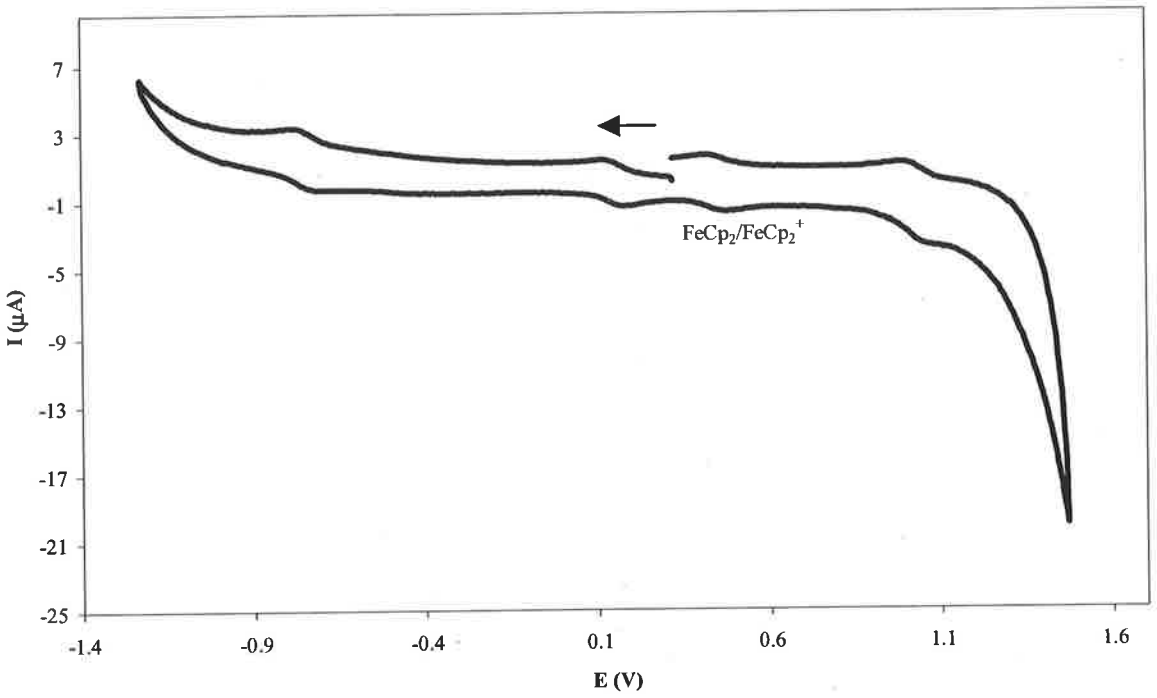

Figure 3.6. *Cyclic voltammograms of* **22[PF$_6$]$_2$** *measured in 0.1M [Bu^n$_4$N][PF$_6$] in CH_2Cl_2 at 100 mV s^{-1}.*

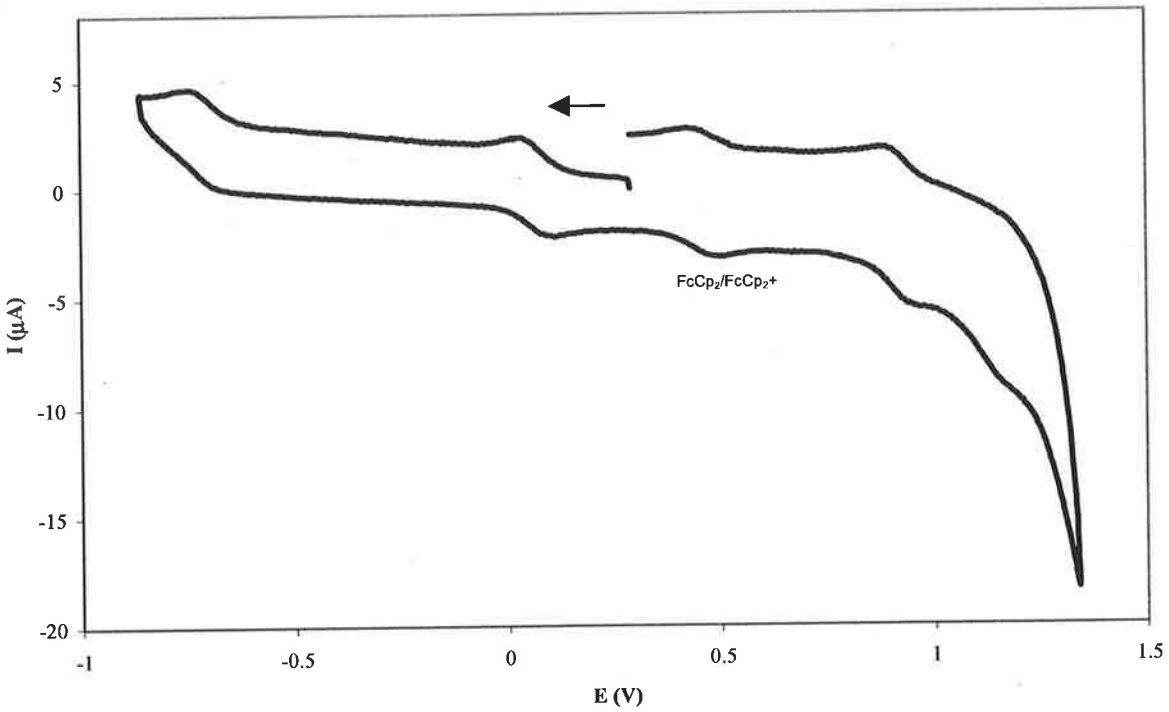

Figure 3.7. *Cyclic voltammograms of* **21[PF$_6$]$_2$** *measured in 0.1M [Bu^n$_4$N][PF$_6$] in CH$_2$Cl$_2$ at 100 mV s^{-1}.*

Exchange of ruthenium for iron shows slightly greater separation in the redox events than that found in **15[PF$_6$]$_2$**. These large separations also indicate high thermal stability, which is seen in the significant comproportionation constants (K_c = 2.39 x 10^{15}). Substitution of the ruthenium for iron also renders the first oxidation potential 140 mV more favourable, but shows similar second and third oxidation potentials of +0.16 and +1.04 V.

This same pattern is seen with the exchange of one ruthenium by osmium in **21[PF$_6$]$_2$**. The complex **21[PF$_6$]$_2$** shows similar separation between the redox events again with high comproportionation constants (K_c = 6.97 x 10^{12}). Substitution of the ruthenium for osmium also renders the first oxidation potential 60 mV more favourable along with the second and third oxidation potentials of +0.09 and +1.00 V.

The exchange of Cp for the more electron-donating Cp* ligand in **19**, has no effect on the first three oxidation potentials for those seen in **15[PF$_6$]$_2$** (see Figure 3.8). Notably though with the exchange of Cp in {Cp(dppe)Ru}$_2$(μ-C≡CC≡C) to Cp* in

{Cp*(dppe)Ru}$_2$(μ-C≡CC≡C) the first oxidation potential is 190 mV more favourable. Even with this shift, the first oxidation potential in both complexes display very similar comproportionation constants. This indicates that even with the increase in electron density within the complex, there is no significant difference in the interactions between the two ruthenium centres.

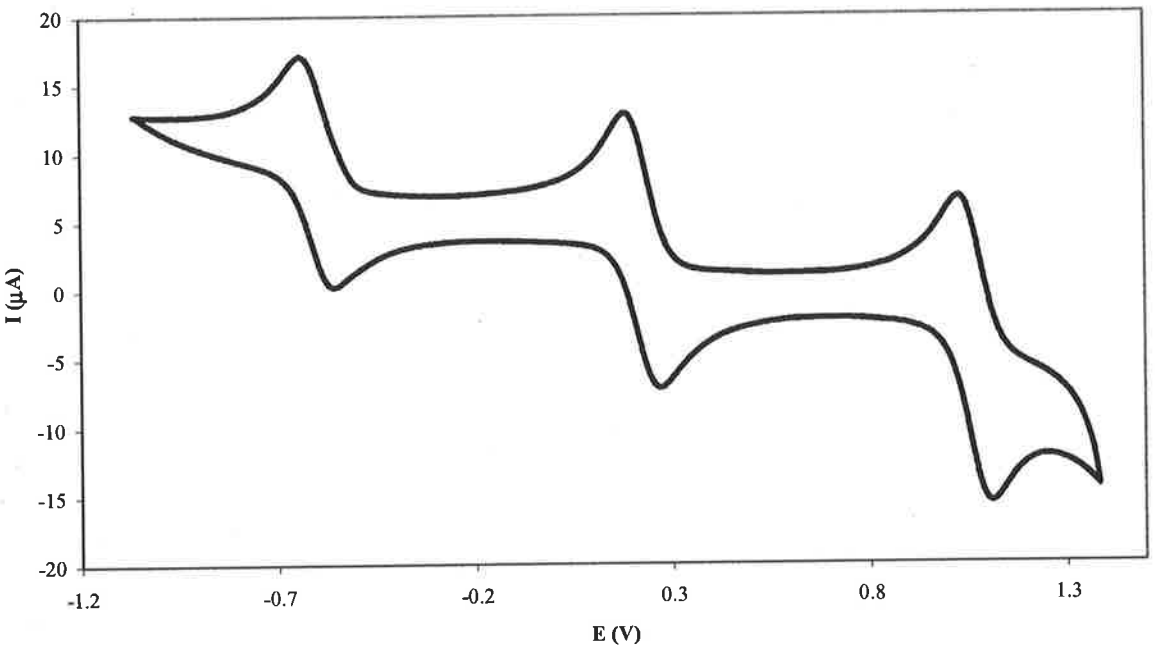

Figure 3.8. *Cyclic voltammogram of* **19[PF$_6$]$_2$** *recorded in 0.1M [Bu$^n_4$N][PF$_6$] / CH$_2$Cl$_2$ at 100 mV s^{-1}.*

In contrast there is a decrease in the first oxidation potential with the exchange of Cp for the more electron donating Cp* from **21[PF$_6$]$_2$** to **20[PF$_6$]$_2$** (see Figure 3.9). The first oxidation potential appears 110 mV lower than that found for **21[PF$_6$]$_2$**. However both complexes show similar second and third oxidation potentials of approximately +0.05 and +0.97 V. The complex **20[PF$_6$]$_2$** shows very similar comproportionation constants to those found in **21[PF$_6$]$_2$**.

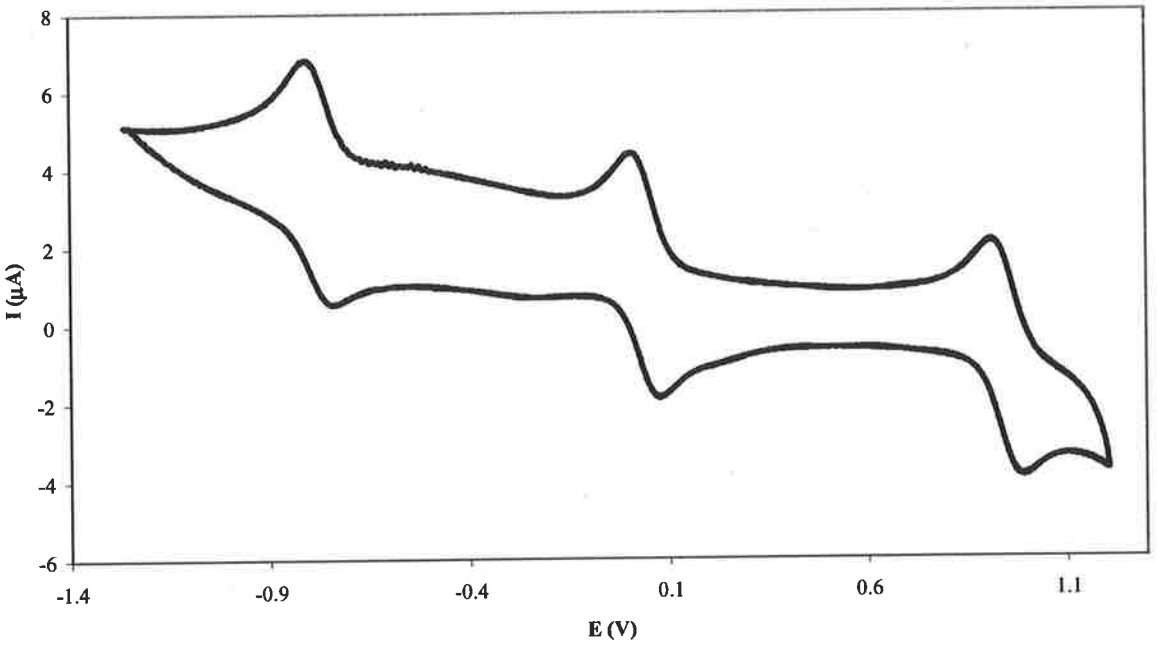

Figure 3.9. *Cyclic voltammogram of* **20[PF$_6$]$_2$** *recorded in 0.1M [Bu$^n_4$N][PF$_6$] / CH$_2$Cl$_2$ at 100 mV s^{-1}.*

Complex	[M]	E_1	E_2	$E_{1/2}$	E_3	E_4[a]	K_c(0/1+/2+)	[REF]
22	Fe(dppe)Cp	-0.75	+0.16	0.91	+1.04		2.39×10^{15}	This work
15	Ru(dppe)Cp	-0.61	+0.21	0.82	+1.06	+1.74	7.19×10^{13}	72
21	Os(dppe)Cp	-0.67	+0.09	0.76	+1.00		6.97×10^{12}	This work
19	Ru(dppe)Cp*	-0.60	+0.22	0.82	+1.07		7.19×10^{13}	This work
20	Os(dppe)Cp*	-0.78	+0.04	0.82	+0.95		7.19×10^{13}	This work

Table 3.2. *Electrochemical data for Cp(dppe)RuC≡C[M] recorded in CH_2Cl_2 0.1M $[Bu^n{}_4N][PF_6]$ and 100 mV s^{-1}.* [a] *peak potential of a quasi-reversible wave.*

3.3.6. Spectroelectrochemistry.

The high thermodynamic stability of the various electrochemically detected species prompted an investigation of their electronic spectra by spectrochemical means. The spectroelectrochemical spectrum of the mono-cation $[\mathbf{15}]^{+}$ (obtained by electrochemical reduction of the isolable di-cation $[\mathbf{15}]^{2+}$ in a standard OTTLE cell at -30°C) is dominated by an asymmetric band at 14150 cm^{-1} (see Figure 3.10). As there are no bands at lower energy, it seems reasonable to assume that this band is related to the IVCT band of mixed-valence complexes or possibly a metal to metal-carbon band. The band-width at half-height is 4300 cm^{-1}, considerably narrower than that predicted by the Hush relationship for a weakly-coupled (Class II) mixed-valence complex (5700 cm^{-1}). The analysis is, however, somewhat complicated by the difficulty in determining whether the NIR band envelope represents a single transition or comprises several overlapping bands. As has been demonstrated on previous occasions, strongly coupled (organic) mixed-valence systems give rise to asymmetric IVCT bands, whilst the combination of spin-orbit coupling and the relatively low symmetry of the metal centre can lead to the observation of multiple transitions in organometallic systems.[54]

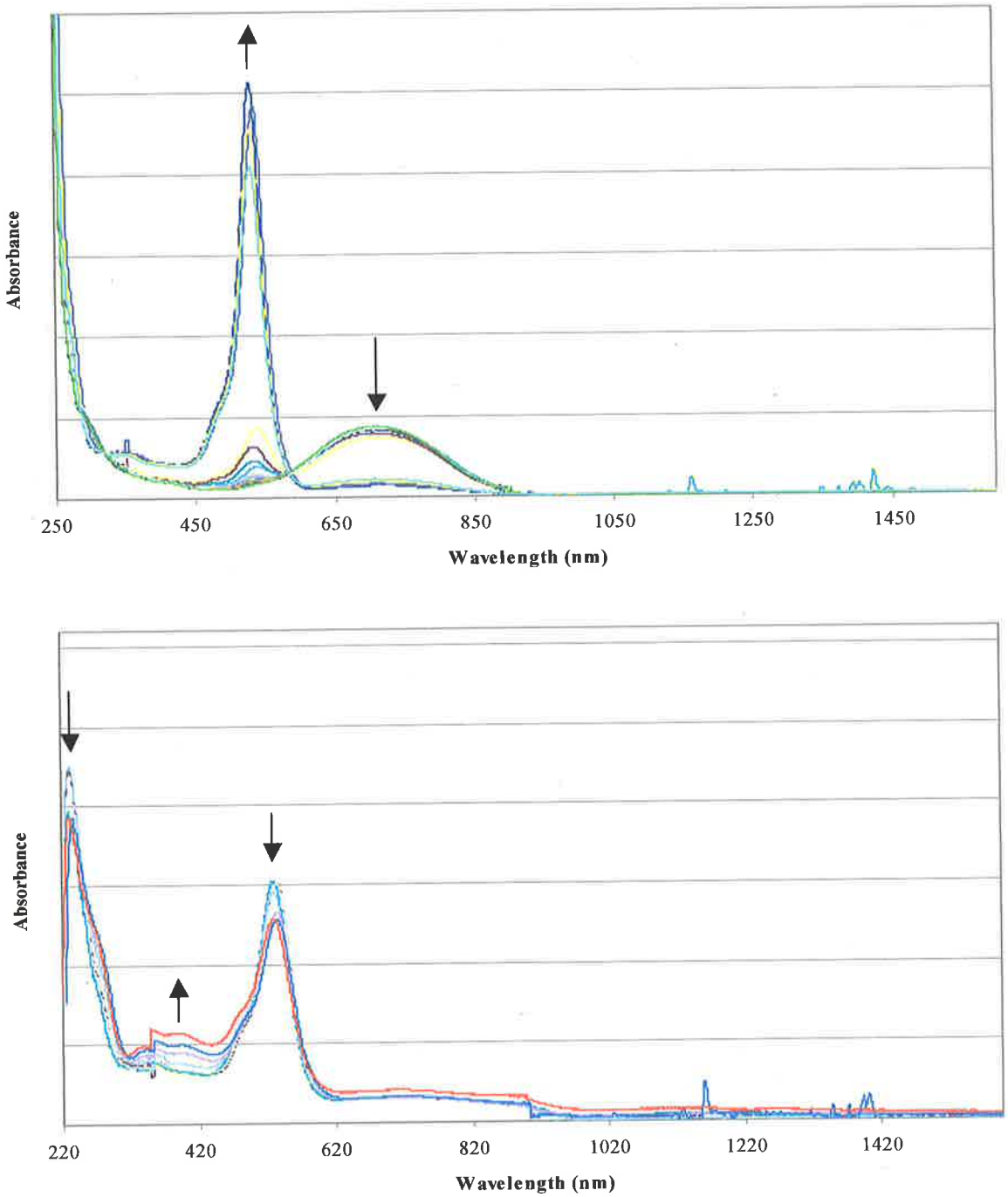

Figure 3.10. *UV/VIS/NIR spectra of {Cp(dppe)Ru}$_2$(μ-C≡C)* **15** *as oxidation proceeds. Top: [***15***]$^+$ to [***15***]$^{2+}$. Bottom: [***15***]$^{2+}$ to [***15***]$^{3+}$.*

In the present case there are several solutions when the band shape is deconvoluted into a sum of Gaussian-shaped curves. In the light of this and to permit direct comparison with previously reported data from related C_4-bridged species, we have elected to treat the band envelope as a single transition and to use the same Hush-style analysis as that described previously for closely-related systems.[31] In that event, the coupling term H_{ab} = 7075 cm^{-1} (or 0.88 eV). This is considerably larger than that observed for the Ru-C_4-Ru complexes (H_{ab} = ca 0.6-0.7 eV) which is consistent with the concept that the shorter polycarbon bridge, the stronger the coupling. However, given the nature of the assumptions made in this analysis, we caution over-reliance on the numerical result.

Nevertheless, the conclusions drawn from the simple analysis presented here are entirely consistent with the TD-DFT-based computational work which shows an electronic transition at 16200 cm^{-1} (see above).

An intense band at 18900 cm^{-1} develops upon oxidation of the mono-cation $[\mathbf{15}]^+$, with concomitant collapse of the lower energy feature associated with the mono-cation. Clean interconversion of the mono- and di-cations is evidenced by the isosbestic point near 17200 cm^{-1}. The new band is identical to that observed for the chemically formed and isolated di-cation. The profile of this band is virtually identical to that observed for the C_4 cases, but it is found at somewhat lower energy. The electronic origin of the visible band has not been fully assigned, but it is dependent upon both the length of the carbon chain and the nature of the metal-ligand fragments. This suggests significant contribution from the carbon-based orbitals - possibly a transition between filled and empty π orbitals delocalised along the Ru-C_n-Ru backbone.

Oxidation to the tri-cation was also achieved. The spectral profile is again, not surprisingly, similar to that of the C_4 case, but the shift in the visible band is less pronounced. However, the decrease in band intensity and small shift in the band maximum are obvious (see Table 3.3).

Complex	ν max (cm^{-1}) / ε ($M^{-1}dm^{-3}$)
$\mathbf{15}^{+}$	14150 / 4400 34000 / 5000
$\mathbf{15}^{2+}$	18900 / 26000 20750 / 5500 28000 / 2800
$\mathbf{15}^{3+}$	18970 / 20200 25500 / 6700

Table 3.3. *UV-Vis-NIR data of* $\mathbf{15}^{n+}$ *(n = 1-3).*

3.4. Conclusions.

The synthesis of several novel complexes in which the C_2 ligand is end-capped by redox-active Group 8 metal centres was achieved. These complexes show three or four successive one-electron oxidation processes. NMR and magnetic measurements of **15[PF$_6$]$_2$**, show that this di-cation has a triplet ground state, which is consistent with theoretical calculations. Structural studies confirm that a change from M-C≡C-M in the neutral towards M=C=C=M in the di-cation occurs as oxidation proceeds. Electrochemical studies confirm that there is a large electronic interaction between the end-groups along the carbon chain, which decreases as the carbon chain is lengthened, further emphasising that these compounds may be considered as models for molecular wires.

3.5. Experimental.

General experimental conditions are detailed on page 45.

Reagents: The compounds TMSC≡CH,[90] OsCl(dppe)Cp,[77] RuCl(dppe)Cp,[100] FeCl(dppe)Cp,[101] OsCl(dppe)Cp*,[77] $[FeCp_2][PF_6]$,[75] $[\{Cp(dppe)Ru\}_2(\mu\text{-}CCH)](PF_6)$,[72] AgOTf,{Dixon #146} $[Cp^*(dppe)Ru{=}C{=}CH_2][PF_6]$,[31] were all prepared using standard literature procedures. The compound KO^{t}Bu was used as received from Aldrich.

$[\{Cp(dppe)Ru\}_2(\mu\text{-}CC)][PF_6]$ (15[PF_6]).

$[FeCp_2][PF_6]$ (38 mg, 0.115 mmol) was added to a solution of $[\{Cp(dppe)Ru\}_2(\mu\text{-}CCH)](PF_6)$ (150 mg, 0.115 mmol) in CH_2Cl_2 (15 mL) and the mixture was stirred for 30 min. The solvent was then removed under vacuum and the residue dissolved in a minimum amount of benzene and submitted to silica gel column chromatography eluting with 10% acetone/hexane to remove $FeCp_2$ and then 30% acetone/hexane to yield $[\{Cp(dppe)Ru\}_2(\mu\text{-}CC)](PF_6)$ (137 mg, 92%). Anal. Calcd ($C_{64}H_{58}F_6P_5Ru_2$): C, 59.21; H, 4.50. Found: C, 59.30; H, 4.53. IR (nujol, cm^{-1}): 1713 w ν(CC); 839 s ν(PF). ES-MS (positive ion mode, MeOH, *m/z*): 1154, $[M]^+$.

$[\{Cp(dppe)Ru\}_2(\mu\text{-}CC)][PF_6]_2$ (15[PF_6]$_2$)

$[FeCp_2][PF_6]$ (76 mg, 0.23 mmol) was added to a solution of $[\{Cp(dppe)Ru\}_2(\mu\text{-}CCH)](PF_6)$ (150 mg, 0.115 mmol) in CH_2Cl_2 (15 mL) and the mixture was stirred for 30 min. The solvent was then removed under vacuum, and the residue dissolved in a minimum amount of benzene and submitted to silica gel column chromatography eluting with 10% acetone/hexane to remove $FeCp_2$ and then 50% acetone/hexane to yield $[\{Cp(dppe)Ru\}_2(\mu\text{-}CC)](PF_6)_2$ (166 mg, 89%). Anal. Calcd ($C_{64}H_{58}F_{12}P_6Ru_2$): C, 53.18;

H, 4.05. Found: C, 53.09; H, 4.07. IR (nujol, cm^{-1}): 1651 w ν(C=C); 840 s ν(PF). ES-MS (positive ion mode, MeOH, m/z): 577, $[M]^{2+}$; 565, $[Ru(dppe)Cp]^{+}$.

$[Cp^*(dppe)Ru=C=C=Ru(dppe)Cp][PF_6]_2$ ($19[PF_6]_2$)

Solution 1:
AgOTf (190 mg, 0.741 mmol) was added to stirred RuCl(dppe)Cp (445 mg, 0.741 mmol) in THF (15 ml) while in the dark.

Solution 2:
^{n}BuLi (0.6 ml, 1.5 mmol, 2.5 M) was added to stirred $[Cp^*(dppe)Ru=C=CH_2][PF_6]$ (597 mg, 0.741 mmol) in THF (15 ml).

Both solutions were stirred for 30 min before Solution 1 was filtered through celite into Solution 2. The resulting reaction mixture was stirred for a further 18 h before being submitted to silica gel column chromatography, eluting with acetone to remove all bands. The solvent was then removed and solid redissolved in CH_2Cl_2 (30 ml) and $[FeCp_2][PF_6]$ (491 mg, 1.48 mmol) added turning the solution pink. This solution was then submitted to silica gel column chromatography eluting first with 10% acetone/hexane to remove any excess RuCl(dppe)Cp and $FeCp_2$ then with 50% acetone/hexane remove the pink band which was collected and the solvent removed to yield $[Cp^*(dppe)Ru=C=C=Ru(dppe)Cp](PF_6)_2$ (426 mg, 38%). Anal. Calc. ($C_{69}H_{68}F_{12}P_6Ru_2$): C: 54.77, H: 4.53, Found C: 54.63, H: 4.51. IR (nujol, cm^{-1}): 1639 w ν(C=C); 841 s ν(PF). ES-MS (positive ion mode, MeOH, *m/z*): 611, $[M]^{2+}$; 635, $[Ru(dppe)Cp^*]^{+}$; 565, $[Ru(dppe)Cp]^{+}$.

Cp*(dppe)Ru-C≡C-Ru(dppe)Cp (19).

To a solution of [Cp*(dppe)RuCCRu(dppe)Cp][PF_6]$_2$ (100 mg, 0.066 mmol) in THF (10 ml) excess KO^{t}Bu (23 mg, 0.198 mmol) was added. The solution was stirred for 30 min before the solvent was removed under vacuum. The residue was extracted with hot hexane until the fractions were no longer coloured. Solvent was removed under vacuum to yield an orange solid identified as Cp*(dppe)Ru-C≡C-Ru(dppe)Cp (60 mg, 75%). Anal Calc. ($C_{69}H_{68}P_4Ru_2 \cdot 1/2CH_2Cl_2$): C: 65.95, H: 5.49, Found C: 66.40, H: 5.21. ^{1}H NMR (d_6-benzene): δ 7.93-6.76 (m, 40H, Ph); 4.60 (s, 5H, Cp); 2.15-2.08, 1.98-1.87 (2m, 8H, CH_2CH_2); 1.69 (s, 15H, Cp*). ^{13}C NMR (d_6-benzene): δ 147.46-128.07 (m, Ph); 92.84 (s, C_5Me_5); 83.01 (s, Cp); 27.98-27.59 (m, CH_2CH_2); 10.97 (s, C_5Me_5). ^{31}P NMR (d_6-benzene): δ 88.7, 83.3 (br, dppe). ES-MS (positive ion mode, MeOH, *m/z*): 1224, $[M]^+$; 635, $[Ru(dppe)Cp^*]^+$; 565, $[Ru(dppe)Cp]^+$.

[Cp*(dppe)Os=C=C=Ru(dppe)Cp][PF_6]$_2$ (20[PF_6]$_2$).

Solution 1:
AgOTf (190 mg, 0.741 mmol) was added to stirred RuCl(dppe)Cp (445 mg, 0.741 mmol) in THF (15 ml) while in the dark.

Solution 2:
^{n}BuLi (0.6 ml, 1.5 mmol, 2.5 M) was added to stirred [Cp*(dppe)Os=C=CH_2][PF_6] (663 mg, 0.741 mmol) in THF (15 ml).

Both solutions were stirred for 30 min before Solution 1 was filtered through celite into Solution 2. The resulting reaction mixture was stirred for a further 18 h before being submitted to silica gel column chromatography, eluting with acetone to remove all bands. The solvent was then removed and solid redissolved in CH_2Cl_2 (30 ml) and [$FeCp_2$][PF_6] (491 mg, 1.48 mmol) added turning the solution pink. This solution was then submitted to silica gel column chromatography eluting first with 10% acetone/hexane to remove

any excess RuCl(dppe)Cp and $FeCp_2$ then with 50% acetone/hexane to remove the pink band which was collected and the solvent removed to yield $[Cp^*(dppe)Os{=}C{=}C{=}Ru(dppe)Cp][PF_6]_2$ (510 mg, 43%). Anal Calc. ($C_{69}H_{68}F_{12}P_6Ru_1Os_1$): C: 51.72, H: 4.28, Found C: 51.68, H: 4.30. IR (nujol, cm^{-1}): 1672 w ν(C=C); 838 s ν(PF). ES-MS (positive ion mode, MeOH, *m/z*): 656, $[M]^{2+}$; 725, $[Os(dppe)Cp^*]^+$; 565, $[Ru(dppe)Cp]^+$.

$[Cp(dppe)Os{=}C{=}C{=}Ru(dppe)Cp][PF_6]_2$ (21$[PF_6]_2$).

Solution 1:
AgOTf (9.5 mg, 0.037 mmol) was added to stirred RuCl(dppe)Cp (22 mg, 0.037 mmol) in THF (10 ml) while in the dark.

Solution 2:
^{n}BuLi (0.04 ml, 0.10 mmol, 2.5 M) was added to stirred $[Cp(dppe)Os{=}C{=}CH_2[PF_6]$ (30 mg, 0.037 mmol) in THF (10 ml).

Solution 1 was stirred for 30 min while Solution 2 was only stirred for 5 min before Solution 1 was filtered through celite into Solution 2. The resulting reaction mixture was stirred for a further 18 h before been submitted to silica gel column chromatography, eluting with acetone to remove all bands. The solvent was then removed and solid redissolved in CH_2Cl_2 (10 ml) and $[FeCp_2][PF_6]$ (24 mg, 0.074 mmol) added turning the solution pink. This solution was then submitted to silica gel column chromatography eluting first with 10% acetone/hexane to remove any excess RuCl(dppe)Cp and $FeCp_2$ then with 50% acetone/hexane remove the pink band which was collected and the solvent removed to yield $[Cp(dppe)Os{=}C{=}C{=}Ru(dppe)Cp][PF_6]_2$ (34 mg, 62%). Anal. Calcd. ($C_{64}H_{58}F_{12}P_6Ru_1Os_1$): C: 50.17, H: 3.82, Found C: 49.99, H: 3.88. IR (nujol, cm^{-1}): 1630 w ν(C=C); 844 s ν(PF). ES-MS (positive ion mode, MeOH, *m/z*): 621, $[M]^{2+}$; 655, $[Os(dppe)Cp]^+$; 565, $[Ru(dppe)Cp]^+$.

[Cp(dppe)Fe=C=C=Ru(dppe)Cp][PF_6]$_2$ (22[PF_6]$_2$).

Solution 1:
AgOTf (19 mg, 0.073 mmol) was added to stirred RuCl(dppe)Cp (44 mg, 0.073 mmol) in THF (10 ml) while in the dark.

Solution 2:
^{n}BuLi (0.06 ml, 0.15 mmol, 2.5 M) was added to stirred [Cp(dppe)Fe=C=CH_2][PF_6] (50 mg, 0.073 mmol) in THF (10 ml).

Solution 1 was stirred for 30 min while Solution 2 was only stirred for 5 min before Solution 1 was filtered through celite into Solution 2. The resulting reaction mixture was stirred for a further 18 h before being submitted to a basic alumina column, eluting with acetone to remove all bands. The solvent was then removed and solid redissolved in CH_2Cl_2 (10 ml) and [$FeCp_2$][PF_6] (14 mg, 0.04 mmol) added turning the solution blue. Stirring was continued for 30 min before Et_2O (15 mL) was added and the resulting precipitate was collected on a sinter to yield [Cp(dppe)Fe=C=C=Ru(dppe)Cp][PF_6]$_2$ (27 mg, 27%). Anal. Calcd. ($C_{64}H_{58}F_{12}P_6Ru_1Fe_1$): C: 54.99, H: 4.18, Found C: 55.04, H: 4.12. IR (nujol, cm^{-1}): 1645 w ν(C=C); 840 s ν(PF). ES-MS (positive ion mode, MeOH, *m/z*): 554, $[M]^{2+}$; 565, $[Ru(dppe)Cp]^+$; 519, $[Fe(dppe)Cp]^+$.

Chapter Four

Towards the synthesis of an organo-iron complex with a trapped singlet state: some 9,10-anthracenediyl-iron complexes

4.1. Introduction.

Even though recent work has centred around complexes of the general formula [M]–$(C\equiv C)_n$–[M] (where n = 2, 13),[52,57] interest has extended to inserting other organic fragments[103] and metal centres into these unsaturated carbon chains. Insertion of organic fragments with appropriate overlapping π–orbitals such as 1,4-C_6H_4[104] and 2,5-thiophenediyl[105] have been reported previously. These organic fragments act as partial insulators when compared to the metal-metal interactions seen in the poly-yndiyl complexes.[36,106] However, organic fragments contain other interesting properties, which make them worthy of closer examination. One such property is the interconversion between a high-spin (triplet state) and low-spin (singlet state) state. This interconversion can be initiated by a simple rearrangement of electrons either electrochemically or through external forces such as variation in temperature, pressure or irradiation with light. All these methods allow for the interconversion by overcoming the energy gap between the two states (see Figure 4.1).

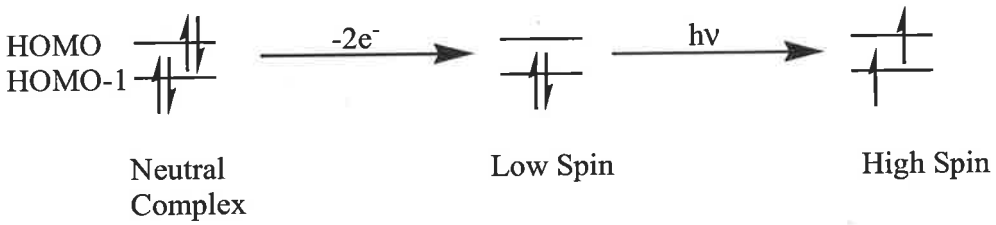

Figure 4.1. *Low-spin high-spin interconversion.*

This property has been observed in the iron complex [Cp*(dppe)Fe=C=C=C=C=Fe (dppe)Cp*]$^{2+}$ which has a small triplet-singlet energy gap –18.2 cm^{-1}.[63] A similar small energy gap was observed in [Cp*(dppe)FeC(OMe)CHCHC(OMe)Fe(dppe)Cp*]$^{2+}$[107] which undergoes conversion from a spin-opposed state (low spin) to a spin-aligned state (high spin) through a rearrangement of its electronic configuration (see Scheme 4.1).

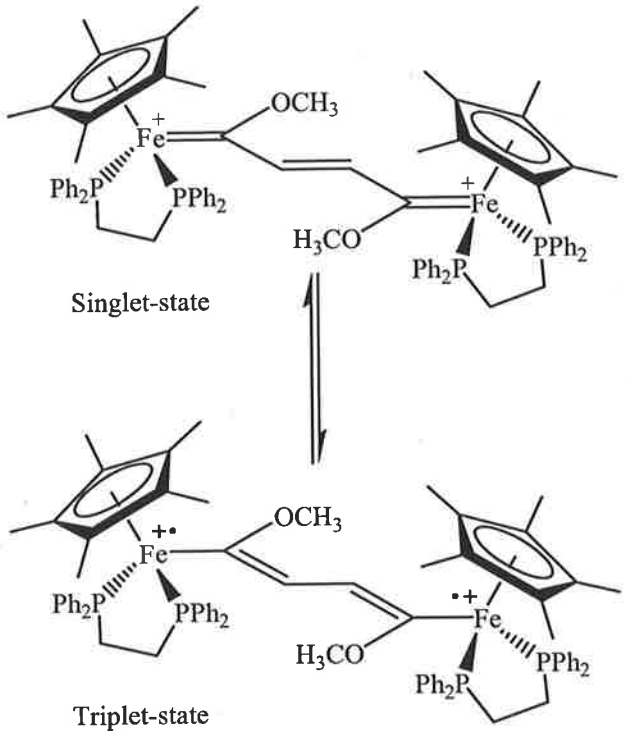

Scheme 4.1. *Singlet-state / triplet-state interconversion in* $[Cp^*(dppe)FeC(OMe)CHCHC(OMe)Fe(dppe)Cp^*]^{2+}$.

The inclusion of the 9,10-anthracenediyl moiety in the complex $[Cp^*(dppe)Fe{=}C{=}C{=}C_{14}H_8{=}C{=}C{=}Fe(dppe)Cp^*]^{2+}$ prevented this interconversion. Further study found that this complex has a large band gap between the triplet-singlet state of at least 1200 cm^{-1}.[108] The large energy gap is a result of the anthracene fragment, which makes the HOMO comparatively higher in energy and separates it significantly from the rest of the occupied molecular orbitals.[108]

4.1.1. Synthetic strategies for bridged complexes containing organic fragments.

At present there are three main synthetic routes into bridged complexes containing organic fragments other than simple yndiyl units (see Scheme 4.2).

1. Coupling between a substituted bridge fragment and two equivalents of the desired metal-ligand fragment.

2. Coupling between a metal-containing bridging fragment and another metal-ligand fragment.

3. Coupling between two substituted metal-ligand fragments and the desired organic centre spacer.

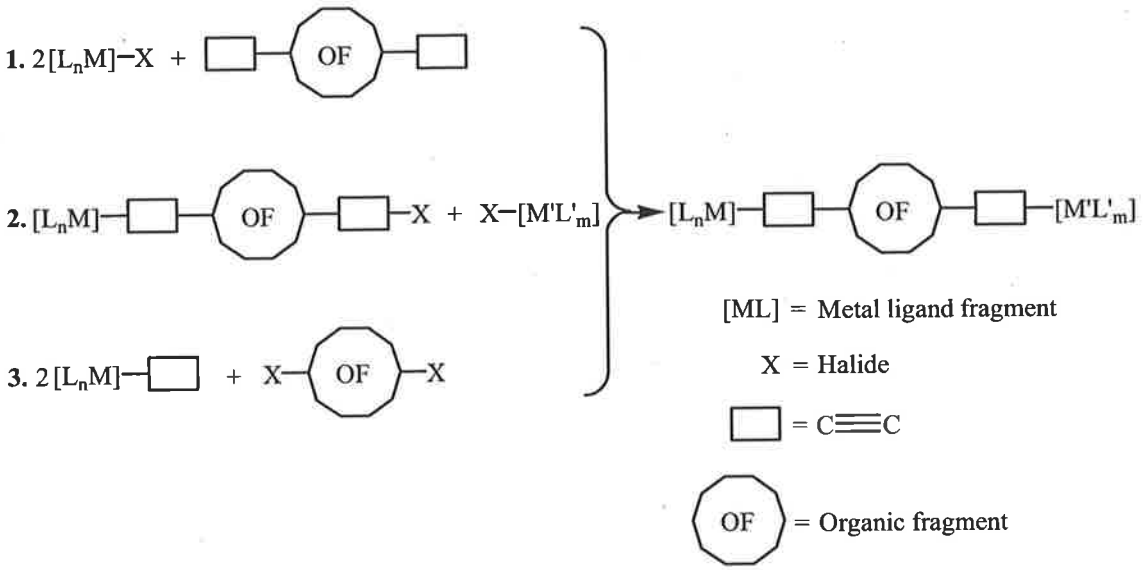

Scheme 4.2. *Synthetic strategies for the synthesis of [ML$_n$]-(C≡C)-OF-(C≡C)-[M'L'$_m$].*

4.1.1.1. Synthetic strategy one. Coupling between a substituted bridge fragment and two equivalents of the desired metal-ligand fragment.

Coupling between a substituted bridge fragment and two equivalents of the desired metal-ligand fragment possesses great flexibility. With many organic reactions such as the Sonogashira reaction, which allow the addition of the appropriate coupling fragments to the organic group.

Commercially available 9,10-dibromoanthracene can be coupled with HC≡CTMS under Sonogashira conditions (CuI, $PdCl_2(PPh_3)_2$ in THF / NEt_3 mixture) to give 9,10-bis(trimethylsilylethynyl)anthracene. Subsequent *in situ* desilylation with K_2CO_3 in methanol and then further coupling with FeCl(dppe)Cp* (**23**) in the presence of $Na[BPh_4]$ yields Cp*(dppe)FeC≡$CC_{14}H_8$C≡CFe(dppe)Cp* (**24**) in 91% yield (see Scheme 4.3).[108]

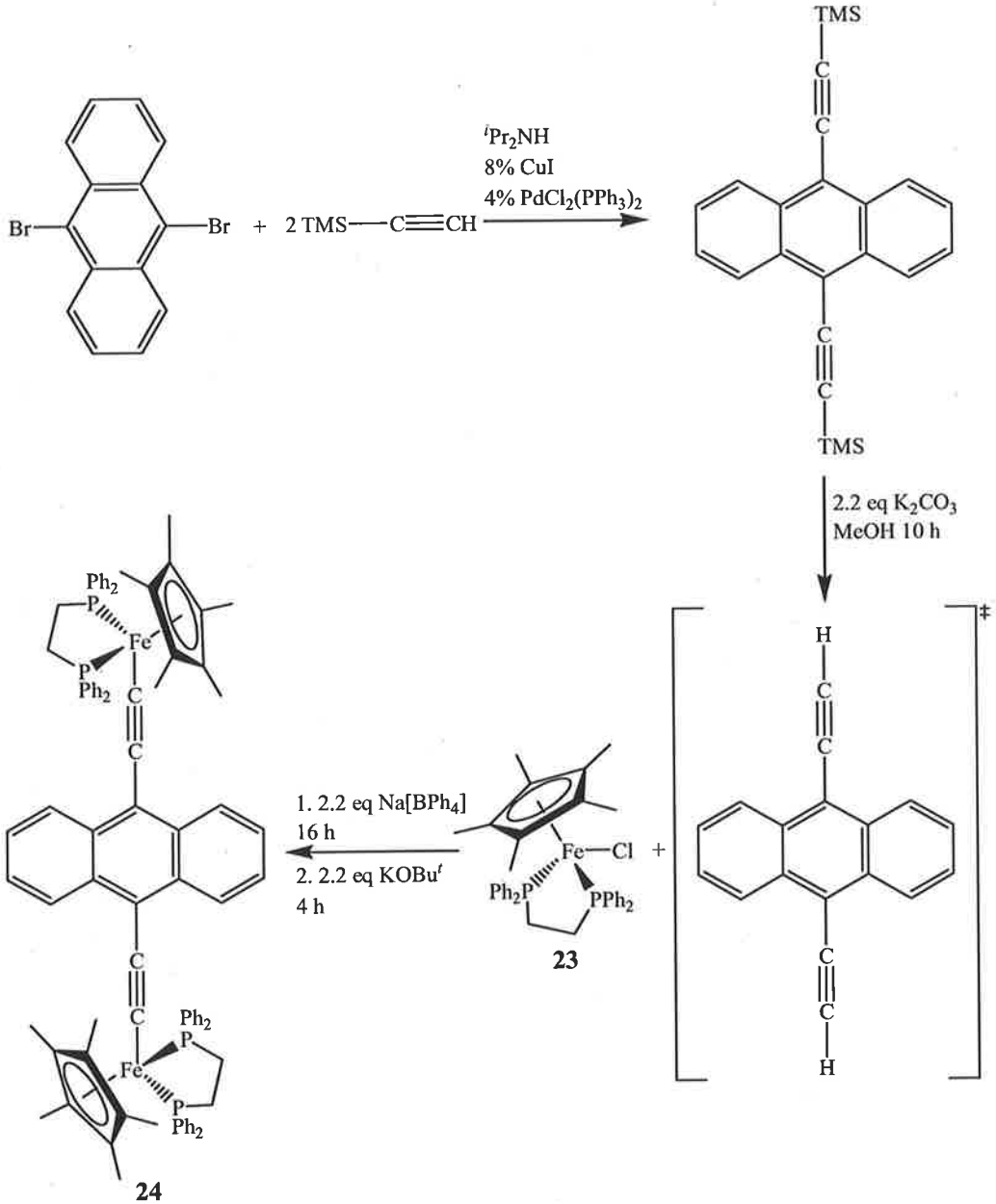

Scheme 4.3. *Synthetic route to Cp*(dppe)FeC≡$CC_{14}H_8$C≡CFe(dppe)Cp*.*

4.1.1.2. Synthetic strategy two. Coupling between a metal-containing bridging fragment and another metal-ligand fragment.

Coupling between a metal-ligand fragment which contains the bridging group and another metal-ligand halide offers the greatest extension. This strategy leads to the possibility of making heterometallic complexes. Great flexibility in the bridging group can be achieved through the use of two terminal groups that have different reactivities, such as TMS and triisopropylsilyl (TIPS). Symmetrical organic bridges can also be used in the synthesis of heterometallic complexes by considering the relative solubility of the intermediates.

The stepwise synthesis of $\{Cp(PPh_3)_2Ru\}_2(\mu\text{-}C{\equiv}CC_6H_4C{\equiv}C)$,[109] has been reported by reaction of $Cp(PPh_3)_2RuC{\equiv}CC_6H_4C{\equiv}CTMS$,[110] with $RuCl(PPh_3)_2Cp$ in THF. Direct substitution of both termini using $TMSC{\equiv}CC_6H_4C{\equiv}CTMS$ and two equivalents of $RuCl(PPh_3)_2Cp$ fails due to poor solubility of the intermediate $Cp(PPh_3)_2RuC{\equiv}CC_6H_4C{\equiv}CTMS$ in MeOH (see Scheme 4.4).

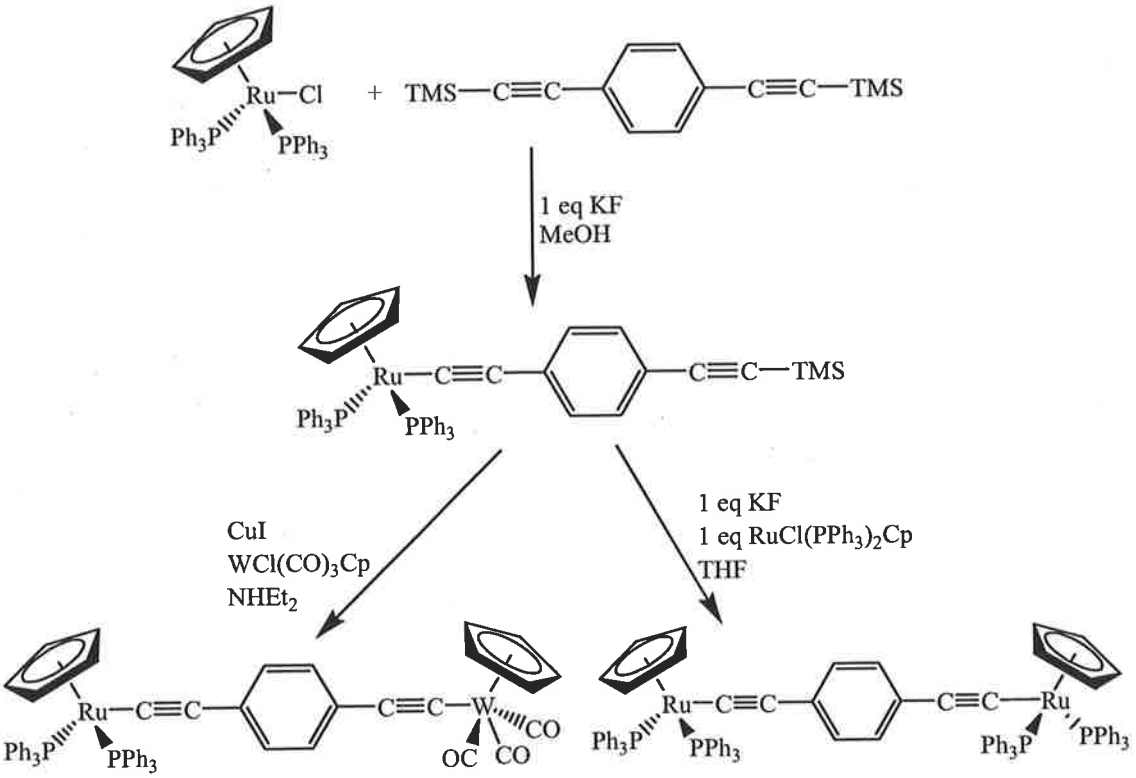

Scheme 4.4. *Coupling between a metal-ligand fragment containing the organic bridge and another metal-ligand fragment.*

4.1.1.3. Synthetic strategy three. Coupling between two substituted metal-ligand fragments and the desired organic centre spacer.

Through the use of the recent gold coupling reaction substituted metal-ligand fragments can be coupled to the desired organic fragment.[111]

Coupling between (dppm-μ_2)$(OC)_7Co_3(\mu_3$-CC≡CAuPPh_3) and di-iodobenzene under Sonogashira type conditions (CuI, $Pd(PPh_3)_4$ in THF) results in the formation of {(dppm-μ_2)$(OC)_7Co_3(\mu_3$-CC≡C)$\}_2C_6H_4$ in 11% yield (see Scheme 4.5).[111,112]

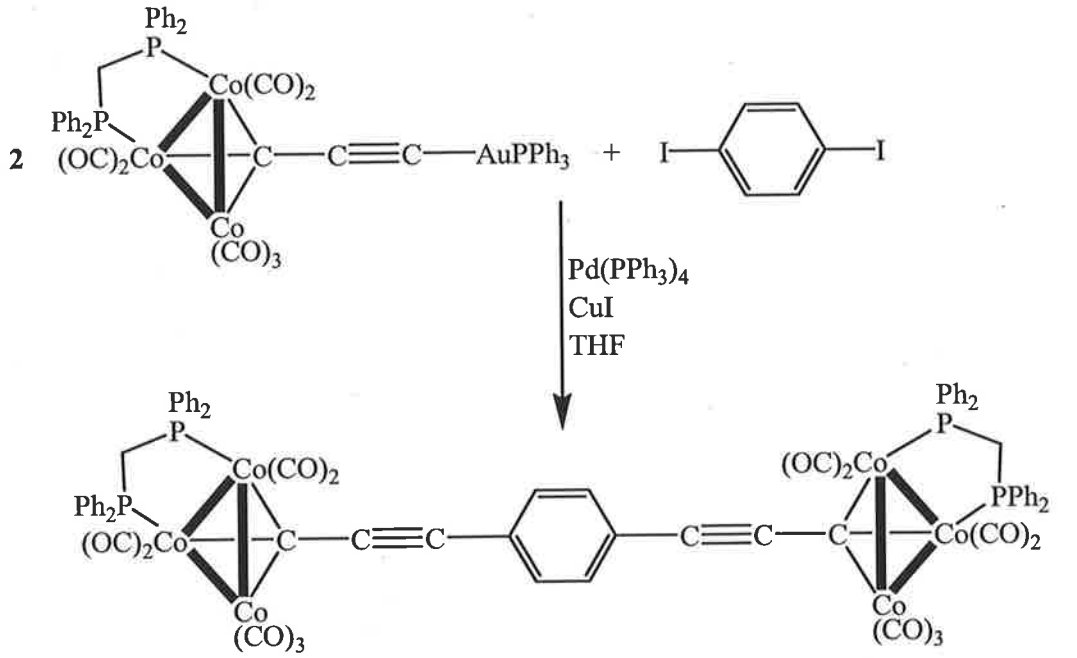

Scheme 4.5. *Coupling between (dppm-μ_2)(OC)$_7$Co$_3$(μ_3-CC≡CAuPPh$_3$) and di-iodobenzene.*

4.2. Aims.

The first aim of this work is to investigate the effect of inserting an anthracenediyl fragment into the C_4 bridging carbon chain of both $\{Cp^*(dppe)Ru\}_2(\mu\text{-}C{\equiv}CC{\equiv}C)$ and $Cp^*(dppe)FeC{\equiv}CC{\equiv}CRu(dppe)Cp^*$ and then draw comparisons with the previously reported complex **24**. The insertion of anthracene into $\{Cp^*(dppe)Fe\}_2(\mu\text{-}C{\equiv}CC{\equiv}C)$ making **24** has a significant effect on the singlet-triplet interconversion that is observed in the doubly oxidised species. Ruthenium has also been shown to have a similar effect over this interconversion when going from $[Cp^*(dppe)Fe{=}C{=}C{=}C{=}C{=}Fe(dppe)Cp^*]^{2+}$ to $[Cp^*(dppe)Fe{=}C{=}C{=}C{=}C{=}Ru(dppe)Cp^*]^{2+}$ with a singlet ground state.[32]

The second aim of this work was to develop a synthetic route to an organo-iron complex that possesses a trapped singlet state (see Figure 4.2). As mentioned above there is an observed triplet-singlet state interconversion for organo-iron complexes, such as $[Cp^*(dppe)Fe{=}C{=}C{=}C{=}C{=}Fe(dppe)Cp^*][PF_6]_2$.[63] The ground state for this complex is the singlet state, but even at liquid nitrogen temperatures the triplet state was still found to be populated.[113] This triplet state is not seen when anthracene is inserted into this C_4 bridging chain in $[Cp^*(dppe)Fe{=}C{=}C{=}C_{14}H_8{=}C{=}C{=}Fe(dppe)Cp^*][PF_6]_2$,[108] due to the increase in the energy gap between the HOMO and the rest of the occupied molecular orbitals.

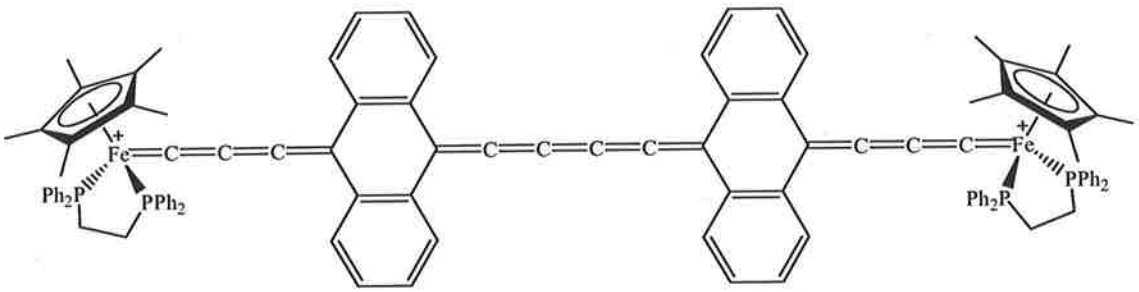

Figure 4.2. *Complex* **25** *target organo-iron complex with a trapped singlet state.*

Within this Chapter the synthesis of two novel anthracene-containing complexes containing the Ru(dppe)Cp* and Fe(dppe)Cp* terminal groups is reported. Comparisons

between these complexes and **[24][PF_6]$_2$** are made, focusing on the paramagnetic nature of the doubly oxidised species. Several novel iron allenylidene complexes are also reported along with the synthesis of several organic bridging ligands en route to the synthesis of the desired final complex **25**.

4.3. Results and Discussion.

4.3.1. Synthesis of anthracenediyl complexes.

4.3.1.1. Synthesis of Cp*(dppe)RuC≡CC$_{14}$H$_8$C≡CRu(dppe)Cp* and Cp*(dppe)FeC≡CC$_{14}$H$_8$C≡CRu(dppe)Cp*.

The synthesis of Cp*(dppe)RuC≡CC$_{14}$H$_8$C≡CRu(dppe)Cp* (**26**) was achieved by treatment of TMSC≡CC$_{14}$H$_8$C≡CTMS with two equivalents of RuCl(dppe)Cp* (**4**) in the presence of potassium fluoride in refluxing methanol. The desired complex precipitated from the reaction mixture and was filtered to give **26** in a 74% yield.

The synthesis of Cp*(dppe)FeC≡CC$_{14}$H$_8$C≡CRu(dppe)Cp* (**27**) was achieved by treatment of Cp*(dppe)FeC≡CC$_{14}$H$_8$C≡CTIPS in the presence of **4** and [Bu^n$_4$N]F.3H$_2$O. After removal of the solvent and washing the residue with ice-cold methanol the desired complex **27** was obtained in 44% yield.

Treatment of either **26** or **27** with two equivalents of [FeCp$_2$][PF$_6$] in THF at –78°C resulted in the doubly oxidised species of both complexes. After the reaction mixture was allowed to warm and recooled to –78°C the addition of hexane facilitated the precipitation of the desired di-cation, which was filtered to yield **26[PF$_6$]$_2$** and **27[PF$_6$]$_2$** in 70% and 60% respectively.

4.3.1.2. Spectral properties of anthracenediyl complexes.

The IR spectrum of **26** showed a band at 2023 cm^{-1} assigned to ν(C≡C). This band shifts to longer wavelengths in **26[PF$_6$]$_2$** (1636 cm^{-1}), which corresponds to a decrease in the carbon-carbon triple bond order, which is consistent with the proposed metallacumulene structure.

The ^{1}H NMR spectrum of **26** shows unresolved multiplets at approximately δ 8.00-7.00 corresponding to the anthracene and phenyl protons. The peak corresponding to the Cp* protons appeared at δ 1.77, whereas the multiplets for the CH_2CH_2 bridge in dppe appear as two multiplets at δ 3.08-2.97 and 2.06-1.92.

The double oxidation of **26** to **26[PF$_6$]$_2$** results in no distinctive change in the ^{1}H NMR spectra with unresolved multiplets at approximately δ 8.00-7.00 corresponding to the anthracene and phenyl protons. The Cp* protons appear at δ 1.77 with the CH_2CH_2 bridge coalescing into one multiplet at δ 3.38-2.97. The well resolved sharp peaks observed in the ^{1}H NMR spectrum for **26[PF$_6$]$_2$** indicates that there is no low-lying paramagnetic triplet state allowing a singlet-triplet state interconversion at room temperature.

In the ^{13}C NMR spectrum for **26** none of the acetylenic carbons were seen due to its poor solubility, whereas for **26[PF$_6$]$_2$** two cumulenic carbons were seen at δ 277.59 and 142.14 corresponding to C_α and C_β respectively. Both spectra contained peaks at approximately δ 140-125, 100 and 11, corresponding to the aromatic carbons and the Cp* carbons respectively.

The ^{31}P NMR spectra were similar with peaks for the neutral and di-cation at approximately δ 80. This is an unusual result with the ^{31}P peaks for **24** and $[\mathbf{24}]^{2+}$ at δ 102 and δ 69 respectively, differing by 33 ppm, which is similar to that seen going from **2** to $[\mathbf{2}]^{2+}$ which differ by 35 ppm.

The mass spectra for **26** and **26[PF$_6$]$_2$** contained ions at *m/z* 1494 and 747, which corresponded to $[M]^+$ and $[M]^{2+}$ respectively. Both complexes underwent similar fragmentation with the appearance of a peak at *m/z* 635, assigned to $[Ru(dppe)Cp^*]^+$.

The IR spectrum for **27** showed two ν(C≡C) bands at 2007 and 2000 cm^{-1} corresponding to the two different carbon-carbon triple bonds due to the different termini. Double

oxidation to **27[PF$_6$]$_2$** resulted in a dramatic shift in the carbon-carbon bond stretching frequencies as found in the conversion of **26** to **26[PF$_6$]$_2$**. **27[PF$_6$]$_2$** displayed two bands at 1948 and 1940 cm^{-1}, which indicates there is still significant carbon-carbon triple bonding rather than the cumulenic bonding observed in **26[PF$_6$]$_2$**.

The ^{1}H NMR spectrum of **27** shows well resolved peaks with multiplets at δ 8.88-7.06, 2.91-2.85 and 2.70-2.64 corresponding to the aromatic hydrogens and the CH_2CH_2 bridge in the two dppe ligands respectively. Sharp peaks are also observed at δ 1.60 and 1.53 corresponding to the two Cp* ligands. After double oxidation the ^{1}H NMR spectrum of the di-cation **27[PF$_6$]$_2$** shows very broad and unresolved peaks at δ 8.00-6.97, 4.03-3.91, and 2.97-2.78 corresponding to the aromatic and CH_2CH_2 bridge hydrogens. The Cp* peaks are observed as broad singlets at δ 1.80 and 1.56. The appearance of these broad peaks in the ^{1}H NMR spectrum indicates significant population of a low-lying paramagnetic triplet state. At -78°C the ^{1}H NMR spectrum still contains broad unresolved peaks, which indicates population of the triplet state is still significant. This result is somewhat surprising when compared to other ruthenium/iron complexes. For [Cp*(dppe)FeCCCCFe(dppe)Cp*][PF$_6$]$_2$ a triplet state is observed while addition of the 9,10-anthracenediyl fragment resulted in an increase in the energy gap between the singlet and triplet states.[108] This is also observed when one iron terminal is substituted by ruthenium,[32] which would indicate a further increase in this energy gap by the addition of the 9,10-anthracenediyl fragment whereas the ^{1}H NMR spectrum indicates the opposite.

The mass spectra of the two complexes displayed peaks at *m/z* 1448 and 724 corresponding to $[M]^+$ and $[M]^{2+}$ for **27** and **27[PF$_6$]$_2$**, respectively.

4.3.2. Synthesis of precursors for an organo-iron complex with a trapped singlet state.

Previously allenylidene complexes have been synthesised by reaction of the corresponding chloro-complex and the related alkynol in the presence of $[NH_4][PF_6]$ in ethanol.[114] This method was then extended in the synthesis of iron allenylidene complexes (see Scheme 4.5).[115] Reaction of **23** with the desired di-substituted-prop-2-yn-1-ol in the presence of $Na[BPh_4]$ or $K[PF_6]$ results in formation of an iron hydroxyvinylidene complex. Addition of amberlyst-15 to the hydroxyvinylidene complex facilitates its dehydration to form the iron allenylidene complex.

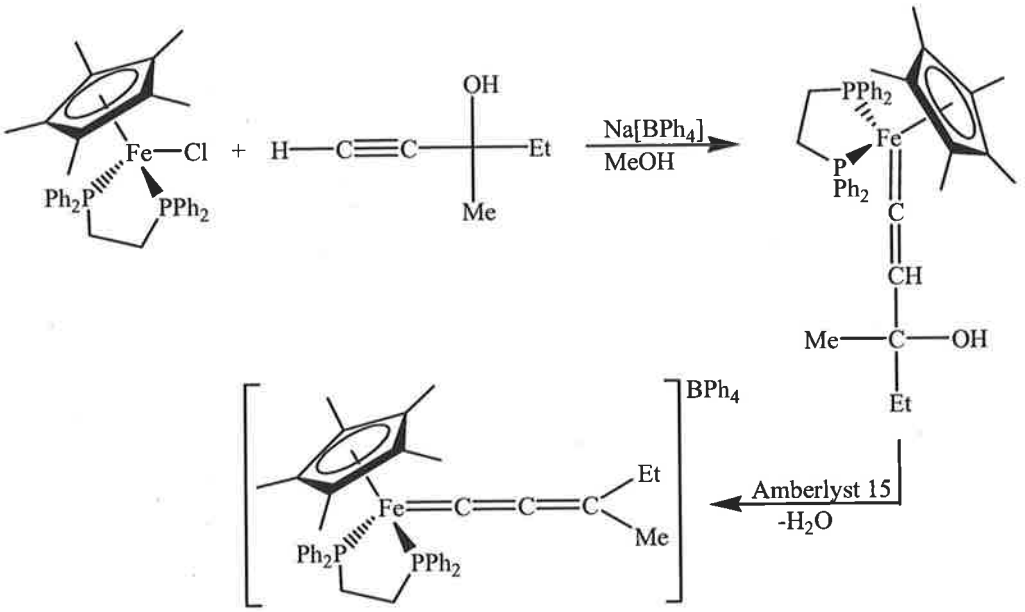

Scheme 4.5. *Synthetic route into iron allenylidenes.*

Using this approach the appropriate starting materials were devised. Treatment of 9-anthraldehyde with LiC_2TMS (from the reaction of ^{n}BuLi and HC≡CTMS) in THF gives orange $C_{14}H_9CH(OH)C_2TMS$ (**28**) after chromatography (silica gel) eluting with 1:1 CH_2Cl_2 / heptane. Further treatment with K_2CO_3 results in desilylation affording, after chromatography (silica gel), $C_{14}H_9CH(OH)C_2H$ (**29**). Compound **29** reacts with **23** in the presence of $Na[BPh_4]$ undergoing spontaneous dehydration without the need for

amberlyst-15 to yield the iron allenylidene complex $[Cp^*(dppe)Fe{=}C{=}C{=}CHC_{14}H_9][BPh_4]$ (**30**) in 80% yield (see Scheme 4.6).

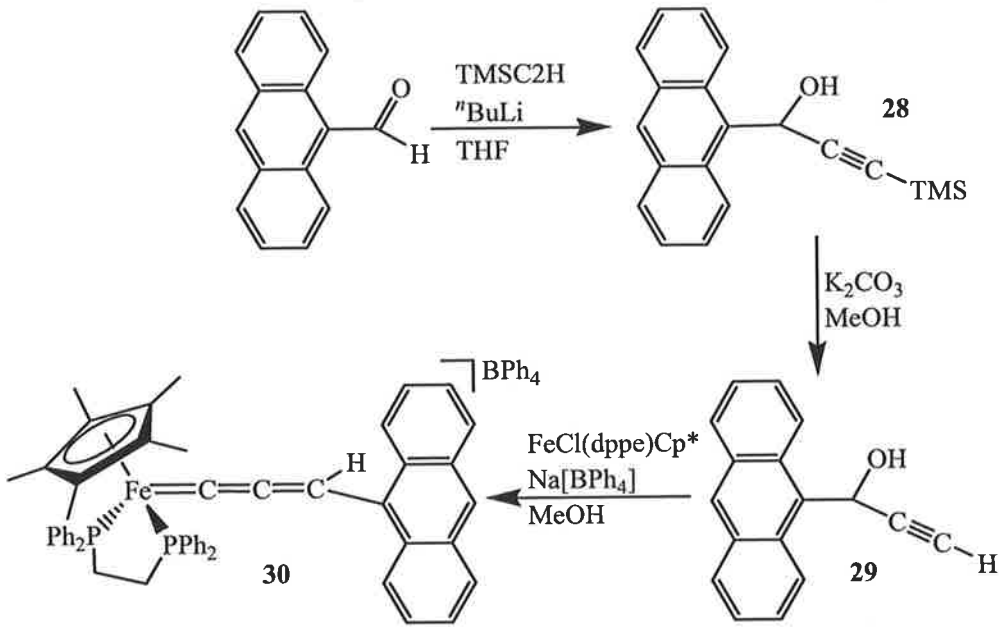

Scheme 4.6. *Synthetic route to* **30**.

This synthetic method was then extended to incorporate the appropriate organic bridging group containing two anthracene fragments (see Scheme 4.7). 9-Bromo-10-formylanthracene (**31**) can be obtained from 9,10-dibromoanthracene by treatment with one equivalent ^{n}BuLi in THF at low temperature followed by the addition of DMF.[116]

The extension of this synthetic method was achieved using a Sonogashira coupling between TMSC≡CH and **31**. After chromatography (silica gel) eluting with CH_2Cl_2 : hexane (1:1) yielded 9-trimethylsilylethynyl-10-formylanthracene (**32**) in 94% yield. Like that shown above, TIPSC≡CH can be treated with ^{n}BuLi in THF to produce TIPSC≡CLi, which was further reacted with **32** to yield $TMSC{\equiv}CC_{14}H_8CH(OH)C{\equiv}C$ TIPS (**33**) in 97% yield after chromatography (silica gel) eluting with CH_2Cl_2 : hexane (1:1). The difference in rate of desilylation of TMS and TIPS allowed treatment of **33** with potassium carbonate in methanol to yield the mono-deprotected organic fragment $HC{\equiv}CC_{14}H_8CH(OH)C{\equiv}CTIPS$ (**34**) in 94% yield.

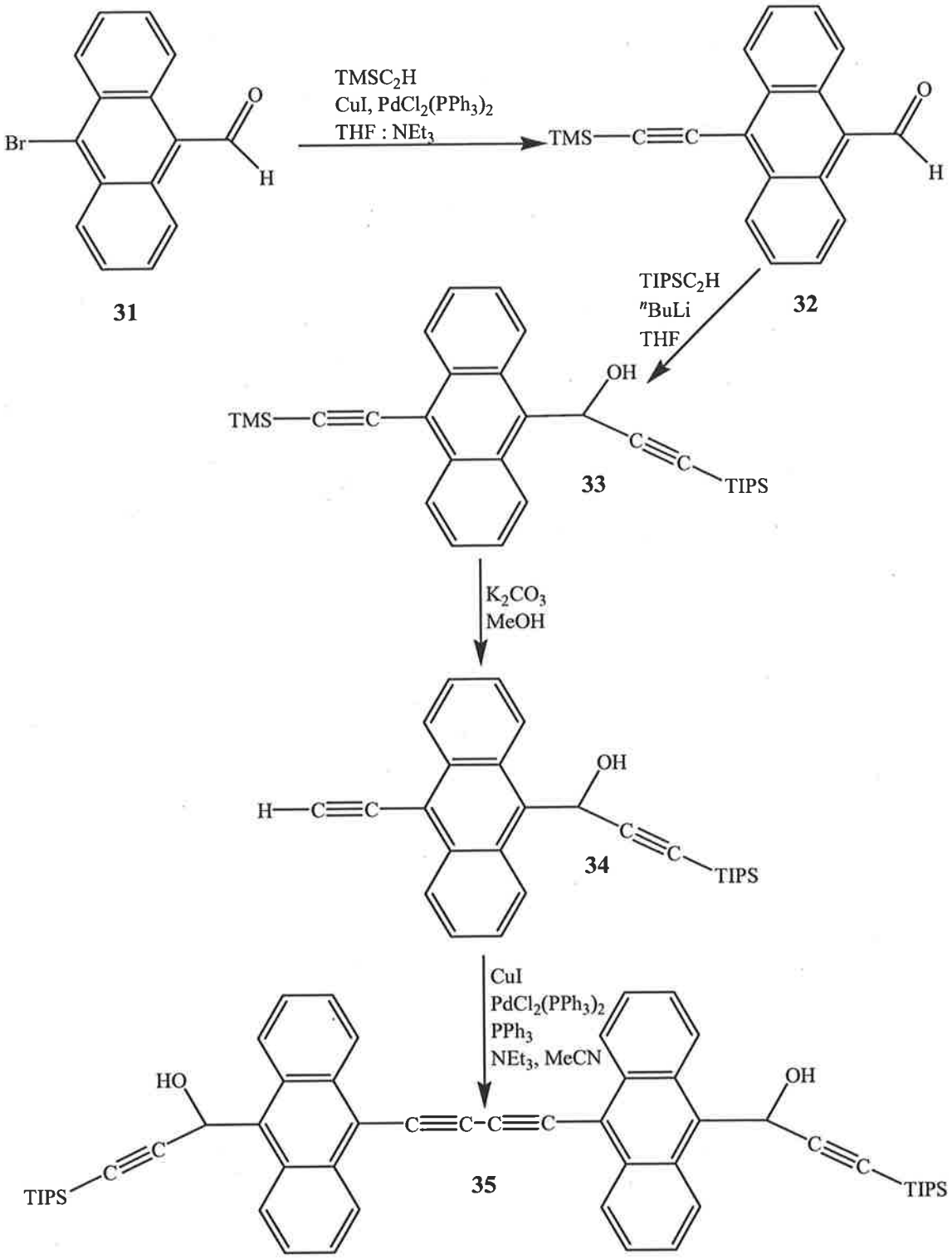

Scheme 4.7. *Synthesis of (-C≡CC$_{14}$H$_8$CH(OH)C≡CTIPS)$_2$.*

Oxidative-coupling of **34** was achieved through the Sonogashira coupling in the presence of CuI, $PdCl_2(PPh_3)_2$ and PPh_3 in a mixture of NEt_3 and MeCN. The desired product (-$C{\equiv}CC_{14}H_8CH(OH)C{\equiv}CTIPS)_2$ (**35**) was isolated in 70% yield after chromatography (silica gel) eluting with CH_2Cl_2 : heptane (4:1). Unfortunately removal of both TIPS protecting groups with $[Bu^n{}_4N]F$ in THF resulted in complete decomposition of the starting material and therefore isolation of $(-C_2C_{14}H_8CH(OH)C_2H)_2$ was not achieved.

To overcome this problem a one-pot synthesis was devised (see Scheme 4.8), as has been previously reported for TMS-containing compounds.[108] Reaction of $TIPSC{\equiv}CLi$ with 9-formylanthracene gave $C_{14}H_9CH(OH)C{\equiv}CTIPS$ (**36**) in 97% yield, after chromatography (silica gel) eluting with CH_2Cl_2 : heptane (1:1). Several attempts were made at a one-pot synthesis from **36** to yield $[Cp^*(dppe)Fe{=}C{=}C{=}CHC_{14}H_9]^+$ using different desilylating reagents, which resulted in either no reaction, recovery of starting organic compound or decomposition of the starting materials. Considering the problems encountered with the mono-iron allenylidene complex this one-pot synthesis was not attempted with the bis-anthracene organic compound **35**.

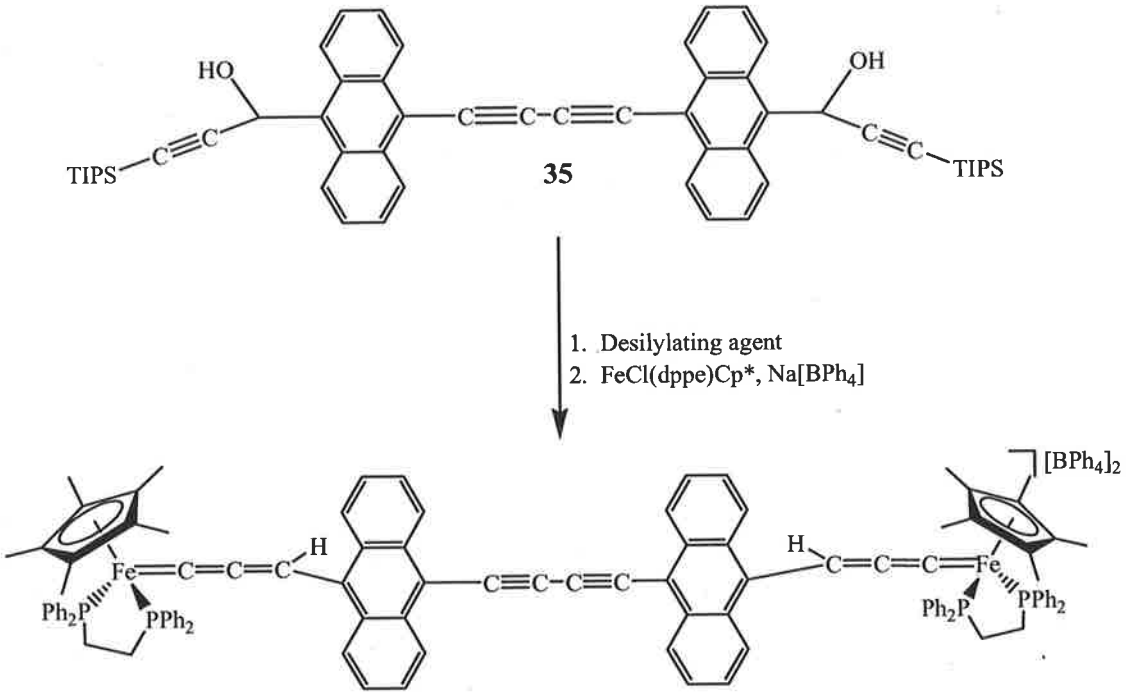

Scheme 4.8. *Devised one-pot synthesis of* $[Cp^*(dppe)Fe{=}C{=}C{=}CH(C_{14}H_8)C{\equiv}CC{\equiv}C(C_{14}H_8)HC{=}C{=}C{=}Fe(dppe)Cp^*][BPh_4]_2$.

To overcome the problem with the TIPS protecting group and the success that has been reported with the TMS protecting group,[108] a one-pot synthesis was attempted starting from **28**. Compound **28** was first treated with potassium carbonate in methanol for four hours, after which time **23**, amberlyst-15 and $Na[BPh_4]$ were added to the solution. The desired product, **30**, was then isolated by precipitation and recrystallised from CH_2Cl_2 : pentane in 65% yield. This yield is lower than that found previously starting from **29**, but offers a direct route to the desired complex.

Direct replacement of TIPS for TMS in **33** would result in both termini containing the TMS protecting group. Treatment with potassium carbonate, as done previously, would afford desilylation of both TMS groups. The resulting compound would not undergo the controlled oxidative-coupling, seen above, due to the two acetylenic hydrogens. Also direct addition of TMSC≡CLi to 9-ethynyl-10-anthracenealdehyde may participate in side reactions due to the acidic acetylenic proton.

Treatment of **32** with potassium carbonate in methanol yielded 9-ethynyl-10-anthraldehyde (**37**) in 98% yield. Initially this reaction was carried out in a THF / methanol mixture, which resulted in poor yields and required purification by chromatography (silica gel). Under these conditions the THF stabilises the intermediate, $^{-}C_2C_{14}H_8CHO$, which can then undergo electrophilic attack of the aldehyde carbon.

A previously reported source of $TMSC{\equiv}C^{-}$ is $[(TMSC{\equiv}C)_2CuLi]$,[117] this compound is nucleophilic and non-basic thus opening up a new synthetic route to the organic bridged anthracenyl complex containing TMS protecting groups (see Scheme 4.9).

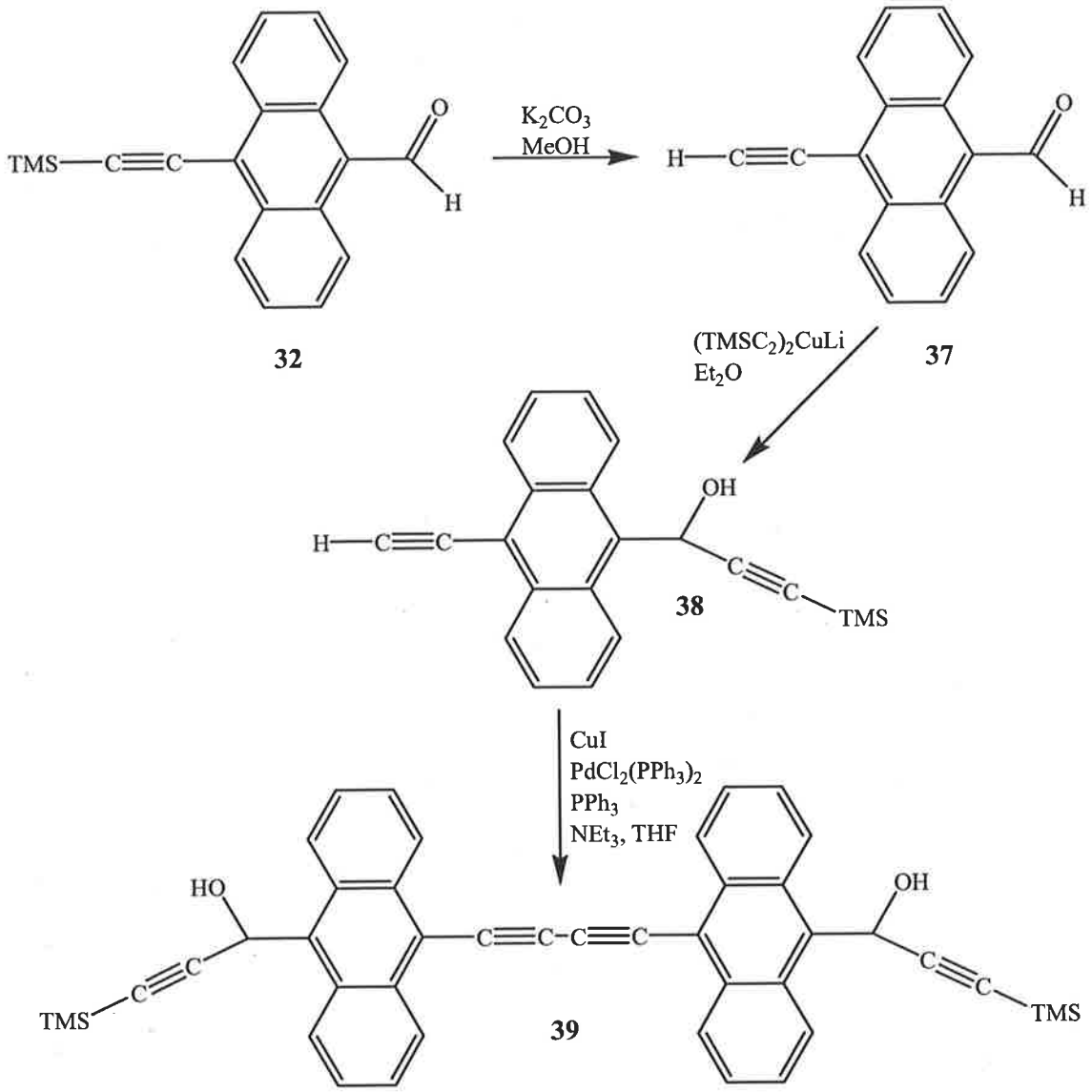

Scheme 4.9. *Synthetic route to (-C≡CC$_{14}$H$_8$CH(OH)C≡CTMS)$_2$.*

Treatment of **37** with [(TMSC≡C)$_2$CuLi] (from the reaction of TMSC≡CH with ^{n}BuLi in Et_2O, which is then added to a solution of copper(I) iodide in Et_2O resulting in a yellow milky suspension) yielded HC≡CC$_{14}$H$_8$CH(OH)C≡CTMS (**38**) in 98% yield. The oxidative coupling of this product was performed under previously reported conditions, all resulting in average yields (see Table 4.1).[118] The best yield 43% of (-C$_2$C$_{14}$H$_8$CH(OH)C$_2$TMS)$_2$ (**39**) was achieved using CuI (12%), $PdCl_2(PPh_3)_2$ (12%) and PPh_3 (36%) in a THF / NEt_3 (1:1) mixture.

Reagents	% of reagent to starting material	Solvent	Yield
CuI $PdCl_2(PPh_3)_2$ PPh_3	3 3 9	NEt_3 / THF 1 : 1	25%
CuI $PdCl_2(PPh_3)_2$ PPh_3	3 3 9	NEt_3 / MeCN 1 : 1	23%
CuI $PdCl_2(PPh_3)_2$ PPh_3	2 additions of 3 2 additions of 3 2 additions of 9	NEt_3 / MeCN 1 : 1	40%
CuI $PdCl_2(PPh_3)_2$ PPh_3	12 12 36	NEt_3 / THF 1 : 1	43%
CuI $PdCl_2(PPh_3)_2$ PPh_3	12 12 36	NEt_3 / THF 1 : 1 60°C	18%
CuI $PdCl_2(PPh_3)_2$ PPh_3	3 100 0	NEt_3 / THF 1 : 1	0%

Table 4.1. *Reaction conditions for the homo coupling of* $HC{\equiv}CC_{14}H_8CHOHC{\equiv}CTMS$.

A different approach might use the possibility of the gold coupling reaction,[111] to isolate the desired organo-iron complex (see Scheme 4.10), but this has not yet been attempted.

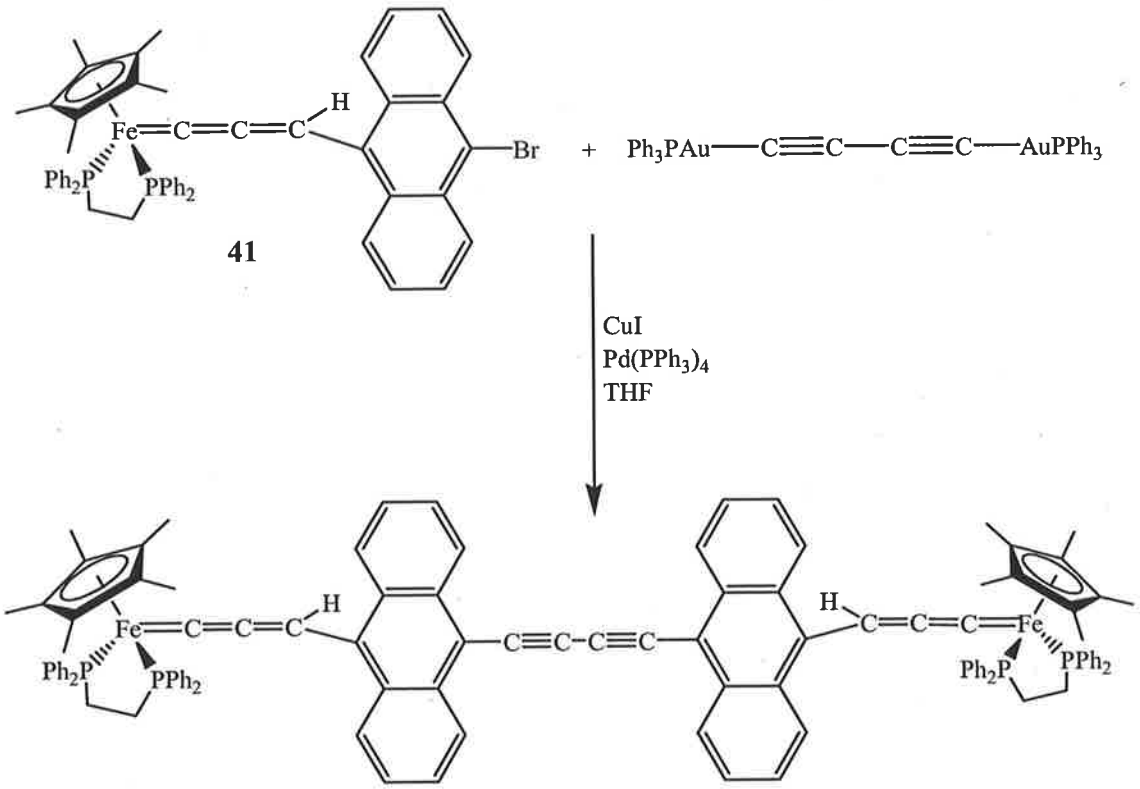

Scheme 4.10. *Proposed synthesis using the gold coupling reaction.*

TMSC≡CLi reacts with **31** to yield $BrC_{14}H_8CH(OH)C{\equiv}CTMS$ (**40**) after chromatography (silica gel) eluting with CH_2Cl_2 / hexane (1:1) in 65% yield. The decrease in yield is a result of the bromine group on the anthracene, which can undergo attack by the organo-lithium reagent in solution similar to that found in the conversion of 9,10-dibromo-anthracene to **31**. Compound **40** was then treated directly with potassium carbonate for 18 h before the product was extracted and used without further purification in a reaction with **23** in the presence of sodium tetraphenylborate to yield the desired iron allenylidene, $[Cp^*(dppe)Fe{=}C{=}C{=}CHC_{14}H_8Br][BPh_4]$ (**41**), after precipitation and recrystallisation in 65% yield.

4.3.2.1. Spectral properties of allenylidene complexes.

The IR spectra for **30** and **41** contained a diagnostic band at 1888 cm^{-1} assigned to ν(=C=C=C) which is similar to that found previously for allenylidene complexes such as [Cp*(dppe)Fe=C=C=CPh_2][BPh_4] (1888 cm^{-1}).[115]

The organic bridges also showed diagnostic bands in their IR spectra. For compounds **28** **36** and **40**, which are all closely related, broad peaks at 3418, 3424 and 3314 cm^{-1} respectively can be assigned to ν(OH). The other distinctive peaks were at 2115, 2168, and 2171 cm^{-1}, respectively, assigned to ν(C≡C). The deprotected compound **29** has an IR spectrum containing peaks at 3396 ν(OH), 2115 ν(C≡C) and 3292 ν(≡CH) cm^{-1}.

Compound **32** displayed peaks in the IR spectrum at 2136 and 1675 cm^{-1} corresponding to ν(C≡C) and ν(CO) respectively. In **33**, the band at 1675 cm^{-1} disappears and two new bands at 3386 (broad) ν(OH) and 2136 cm^{-1} ν(C≡C) appear indicating conversion from the aldehyde to the alcohol. Removal of the TMS group with potassium carbonate to give **34** results in a significant shift in one ν(C≡C) band from 2139 to 2096 cm^{-1} and the appearance of ν(≡CH) from the acetylenic proton at 3270 cm^{-1}. Deprotection of **32** to **37** results in a similar effect with an observed shift in ν(C≡C) from 2136 to 2079 cm^{-1} and the acetylenic proton giving a ν(≡CH) band at 3228 cm^{-1}, with only a small shift in ν(CO) to 1673 cm^{-1}. In **38** a similar change occurs with the disappearance of ν(CO) and appearance of ν(OH) at 3418 cm^{-1} (broad). There is however an observed shift in ν(C≡C) with the two peaks at 2170 and 2096 cm^{-1}, but there is only a small shift seen in ν(≡CH) to 3239 cm^{-1}.

Oxidative coupling of both **34** and **38** to give **35** and **39**, result in a shift of ν(C≡C) from 2096 to 2126 cm^{-1} and 2096 to 2123 cm^{-1} respectively.

The ^1H NMR spectra for **30** and **41** showed a peak at δ 10.28 and 10.18, respectively, corresponding to the cumulenic proton. The anthracene and phenyl peaks for **41**

appeared as unresolved multiplets between δ 8.80 and 6.85. For **30**, however, the anthracene peaks appeared as a doublet at δ 8.42 ($^3J_{HH}$ 7.8 Hz) and 8.21 ($^3J_{HH}$ 7.8 Hz), a singlet at δ 8.92 along with a multiplet at δ 7.63-6.95 for the phenyl protons. The dppe CH_2CH_2 protons appeared as two distinct multiplets at δ 3.06-3.02, 2.44-2.40 and 3.01-2.95, 2.43-2.37 for **30** and **41** respectively. Also the Cp* protons gave peaks at δ 1.52 and 1.47.

The ^{1}H NMR spectra for **28**, **29** and **36** display similar peaks with doublets at approximately δ 8.75 ($^3J_{HH}$ ca. 9 Hz), 8.00 ($^3J_{HH}$ 9 Hz), a singlet at δ 8.40 and a multiplet at δ 7.60-7.50 all corresponding to the anthracene protons. Similar peaks are also observed for the CHOH protons at approximately δ 7.00 (CH) and 3.20 (OH). The three complexes display differences in the terminal protons with peaks at δ 0.37, 2.71, and 1.28-1.04 for **28**, **29** and **36** respectively. The ^{1}H NMR spectrum for **40** showed two unresolved multiplets δ 8.68-8.58 and 7.58-7.50 corresponding to the anthracene protons. The other three peaks are similar to those seen for **28** at δ 6.89 (CH), 3.31 (COH) and 0.26 (TMS).

The ^{1}H NMR spectra for **32**, **33**, **34**, **37** and **38** showed either two sets of doublets and a multiplet (for **32** and **37**) or two unresolved multiplets (for **33**, **34** and **38**) arising from the anthracene protons. Diagnostic peaks in the ^{1}H NMR relate to the substitutions on the anthracene moiety. The spectrum of **32** showed peaks at δ 11.51 for the aldehyde proton and at δ 0.43 corresponding to the TMS group. Addition of TIPSC≡C fragment resulted in the disappearance of the aldehyde proton and the appearance of peaks at δ 6.98 (CH), 2.93 (OH) and a multiplet at 1.08-0.97 (TIPS). The deprotection of either **33** or **32** resulted in the TMS peak being replaced by peaks at δ 4.08 and 4.23, respectively, assigned to the acetylenic proton. A similar effect is observed with the addition of the TMSC≡C fragment in **38**, as seen in **33**, where the aldehyde peak has been displaced by peaks at δ 6.99, 2.74 and 0.18 assigned to the CH, COH and TMS protons respectively.

Oxidative coupling of both **34** and **38** to give **35** and **39** resulted in only one significant change in the ^{1}H NMR spectra with the peak assigned to the acetylenic proton no longer present.

In the ^{13}C NMR spectra of **28**, **36** and **29**, the anthracene carbons resonate between δ 134 and 118. Differences included peaks at approximately δ 107 and 90 for both **28** and **36**, which were assigned to the C≡C carbons. A peak at δ 60 was also observed which was assigned to the CH(OH) carbon. The TMS and TIPS groups have characteristic peaks at δ 0.43 (TMS) and δ19.1 and 11.7 (TIPS). Removal of the TMS group in **29** shows a significant shift in only the C≡C resonances peaks to δ 84.4 and 75.7.

In **32** the aldehyde carbon appeared at δ 193.1 and the C≡C atoms at δ 111.0 and 101.4 with the TMS group at δ 0.6. Addition of the TIPSC≡C fragment sees a shift in the related aldehyde carbon to δ 60 and new C≡C peaks at δ 107.8 and 89.5, which is similar to that observed for **36**, with no significant shift in the other C≡C signals. Deprotection of either **32** or **33** resulted in an observed upfield shift of the C≡C resonances to δ 92.3, 80.2 and 89.7, 80.9, respectively. Addition of the TMSC≡C fragment to **37** has a similar effect in the ^{13}C NMR spectra of **32** with the related aldehyde carbon shifted upfield to δ 60, along with two new C≡C peaks at δ 106.0 and 89.8 and the TMS group at δ 0.2.

Oxidative coupling of both **34** and **38** to give **35** and **39** resulted in a shift in the C≡C resonances from δ 89.7, 80.9 to δ 86.5, 82.6 in **35** and from δ 93.0, 80.9 to δ 86.4 and 82.5 in **39**.

4.3.3. Electrochemistry.

The redox potentials of complexes **26** and **27** were measured under similar conditions (see Table 4.2).

For **26** two fully reversible waves (i_a / i_c = 1, current proportional to (scan rate)$^{1/2}$) are observed at –0.19 V and +0.12 V and one fully non-reversible wave (i_a / i_c = 0, current proportional to (scan rate)$^{1/2}$) at +0.85 V (see Figure 3). Further analysis of the electrochemical data allowed the thermodynamic stabilities of the oxidised species to be determined by calculating the comproportionation constant K_c. Complex **26** gives rise a significant but not large equilibrium constant of K_c = 1.75 x 10^5, indicating considerable thermodynamic stability for the corresponding di-cation **[26]**$^{2+}$.

Complex	[M]/[M']	E_1	E_2	$\Delta E_{½}$	K_c(0/+1/+2)	E_3	[REF]
24	Fe/Fe	-0.40	-0.04	0.36	1.22 x 10^6		108
26	Ru/Ru	-0.19	+0.12	0.31	1.75 x 10^5	+0.85[a]	This work
27	Fe/Ru	-0.07	+0.28	0.35	8.30 x 10^5	+1.08[b]	This work

Table 4.2. *Cyclic voltammetry data for Cp*(dppe)MC≡CC$_{14}$H$_8$C≡CM'(dppe)Cp*, measured in 0.1M [Bu$^n_4$N][PF$_6$] in CH$_2$Cl$_2$ at 100mV s^{-1}.* [a] *Peak potential of a fully non-reversible wave.* [b] *Peak potential of a quasi-reversible wave.*

The cyclic voltammogram for **27** did not display intermediate waves between **26** and **24**, but two fully reversible waves (i_a / i_c = 1, current proportional to (scan rate)$^{1/2}$) at –0.07 V and +0.28 V and a quasi reversible wave (i_c / i_a = 0.3, current proportional to (scan rate)$^{1/2}$) at +1.08 V were observed (see Figure 4.3). Further analysis of the electrochemical data gave a comproportionation constant of K_c = 8.30 x 10^5.

Despite the insertion of the 9,10-anthracenediyl fragment, both complexes **26** and **27** show strong electronic interactions between the metal centres with $\Delta E_{1/2}$ of approximately 320 mV. This strong interaction is comparable to other straight-chain complexes such as $\{Cp^*(dppe)Ru\}_2(\mu\text{-}C{\equiv}C)_4$ with $\Delta E_{1/2}$ = 350 mV, which is considered a Class III complex by the Robin and Day classification system.

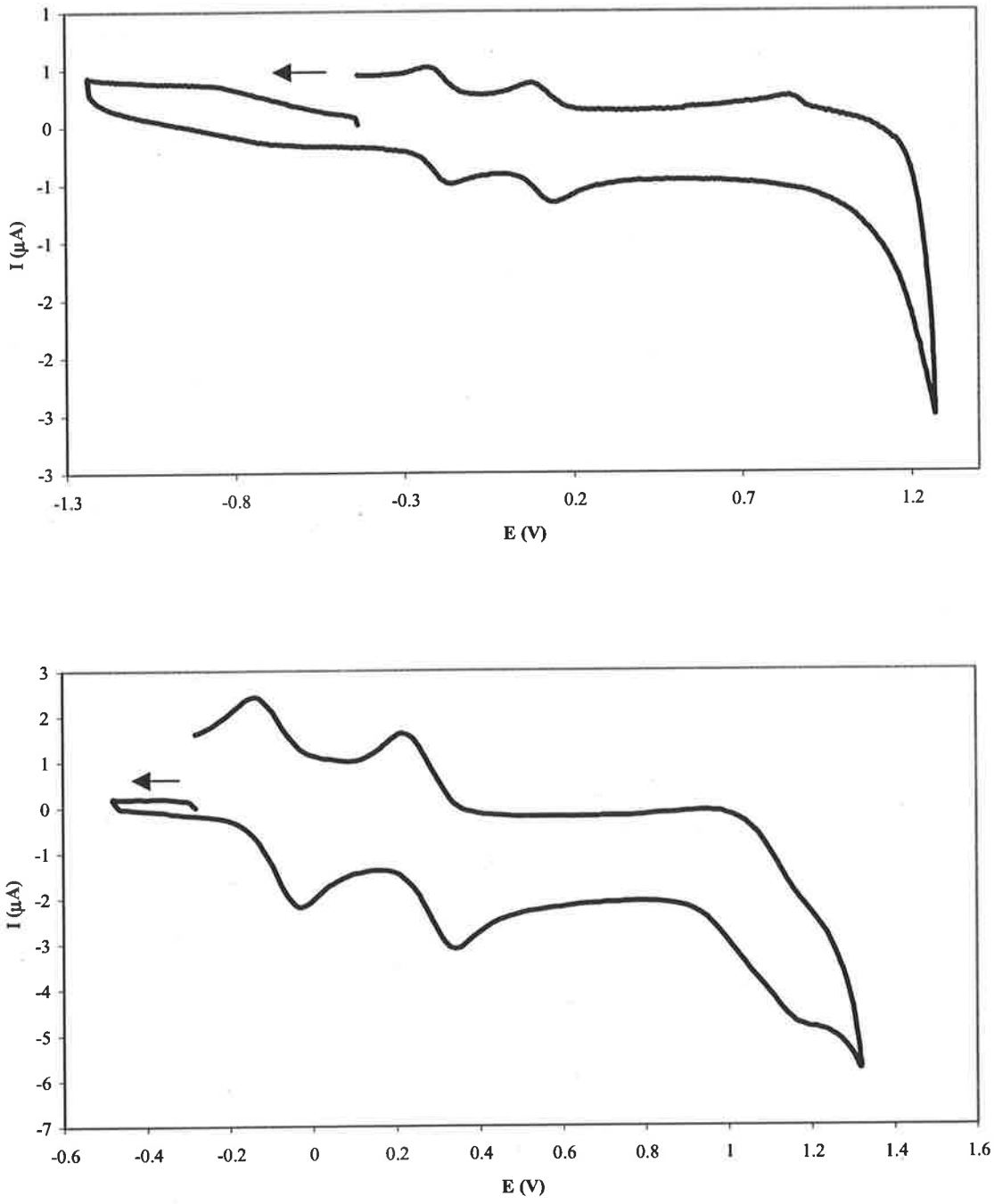

Figure 4.3. *Cyclic voltammograms of Top:* ***26****, Bottom:* ***27****, recorded in 0.1M* $[Bu^n_4N][PF_6]$ *in* CH_2Cl_2 *at 100 mV* s^{-1}.

4.4. Conclusions.

In summary, this work has described the synthesis of two new organometallic complexes containing the 9,10-anthracenediyl bridging ligand. Cyclic voltammetry has shown that significant electronic interactions exist between the two metal termini, which are comparable to those found for straight-chain analogues such as $\{Cp^*(dppe)Ru\}_2(\mu\text{-}C{\equiv}C)_4$. The di-cations of both **26** and **27** were also prepared by two-electron oxidation of the neutral complexes.

The di-cation **27[PF$_6$]$_2$** was shown by ^{1}H NMR spectroscopy to have a low-lying triplet state when compared to **24[PF$_6$]$_2$** and **26[PF$_6$]$_2$** which is dominant even at low temperatures.

This work has also described many organic compounds and organoiron complexes obtained in work towards the synthesis of an organoiron complex with a trapped singlet state **25**. The synthetic route described has demonstrated some of the difficulties that could be encountered through the stability or lack thereof in some compounds and complexes. The most achievable synthetic method would be either the one-pot synthesis from **39** or the gold coupling reaction in Scheme 4.9. The product from either reaction could undergo a singlet (low-spin) / triplet state (high-spin) interconversion, which could make determining the precise nature of the complex difficult. However this complex should undergo radical abstraction of two hydrogen atoms to give the organoiron complex **25** (see Scheme 4.11).

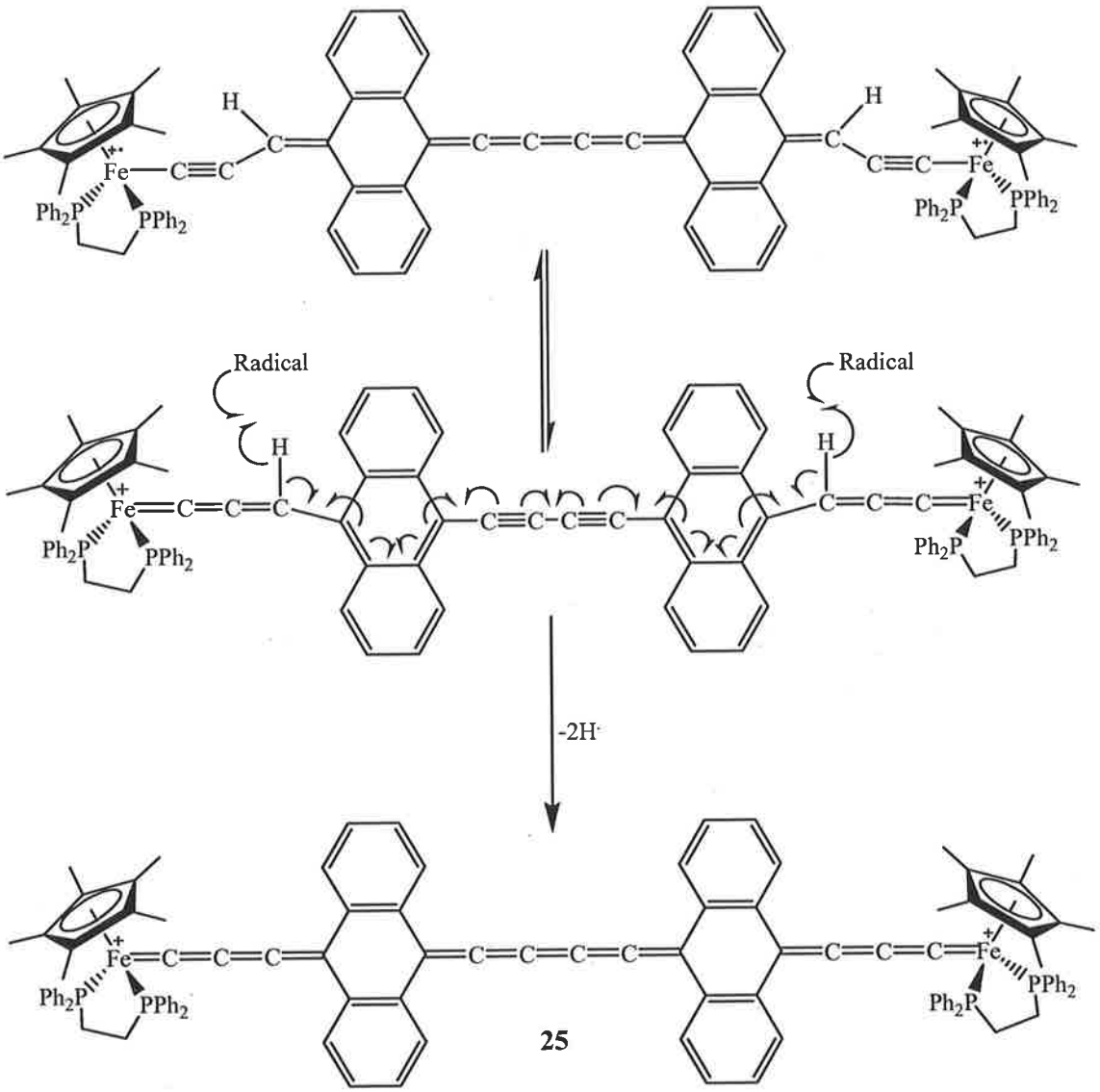

Scheme 4.11. *Proposed synthetic method to* ***25****.*

4.5. Experimental.

General experimental conditions are detailed on page 45.

Reagents: The compounds RuCl(dppe)Cp*,[72,119] 9,10-bis(trimethylsilylethynyl)anthracene,[101] Cp*(dppe)FeC≡CC$_{14}$H$_8$C≡CTIPS,[120] [FeCp$_2$][PF$_6$],[75] TMSC≡CH,[90] FeCl(dppe)Cp*,[121,122] BrC$_{14}$H$_8$CHO,[116] PdCl$_2$(PPh$_3$)$_2$[123] were all prepared using standard literature procedures. The compounds KF, [Bu$^n_4$N]F.3H$_2$O, K$_2$CO$_3$, Na[BPh$_4$], CuI, ^{n}BuLi, PPh$_3$ were all used as received from Aldrich.

Cp*(dppe)RuC≡CC$_{14}$H$_8$C≡CRu(dppe)Cp* (26).

A solution of RuCl(dppe)Cp* (388 mg, 0.58 mmol), TMSC≡CC$_{14}$H$_8$C≡CTMS (100 mg, 0.28 mmol) and KF (34 mg, 0.58 mmol) in MeOH (20 mL) was heated at reflux point for 16 h. The resulting precipitate was collected, washed with MeOH and dried to yield Cp*(dppe)RuC≡CC$_{14}$H$_8$C≡CRu(dppe)Cp* (304 mg, 74%). Anal. Calcd (C$_{90}$H$_{86}$P$_4$Ru$_2$): C, 72.37; H, 5.80. Found: C, 72.39; H, 5.86. IR (nujol, cm^{-1}): 2023 m ν(C≡C). ^{1}H NMR (d_6-benzene): δ 8.30-6.89 (m, 48H, Ph, C$_{14}$H$_8$); 3.08-2.97, 2.06-1.92 (2 x m, 2 x 4H, CH$_2$CH$_2$); 1.77 (s, 30H, Cp*). ^{13}C NMR (d_6-benzene): δ 141.14-123.85 (m, Ph); 93.50 (s, *C*$_5$Me$_5$); 30.46-29.84 (m, CH$_2$CH$_2$); 11.02 (s, C$_5$*Me*$_5$). ^{31}P NMR (d_6-benzene): δ 82.7 (s, dppe). ES-MS (positive ion mode, MeOH, *m/z*): 1494, [M]$^+$; 635, [Ru(dppe)Cp*]$^+$.

[Cp*(dppe)Ru=C=C=C$_{14}$H$_8$=C=C=Ru(dppe)Cp*][PF$_6$]$_2$ (26[PF$_6$]$_2$).

A solution of Cp*(dppe)RuC≡CC$_{14}$H$_8$C≡CRu(dppe)Cp* (40 mg, 0.027 mmol) in THF was cooled to -78°C before adding [FeCp$_2$][PF$_6$] (17 mg, 0.053 mmol) and stirring continued at –78°C for 30 min. The solution was allowed to warm to r.t. before again being cooled to –78°C and hexane (20 mL) was added. The resulting precipitate was

collected washed with hexane and dried to yield $[Cp^*(dppe)Ru{=}C{=}C{=}C_{14}H_8{=}C{=}C{=}Ru(dppe)Cp^*][PF_6]_2$ (66 mg, 70%). Anal. Calcd ($C_{90}H_{86}P_6F_{12}Ru_2$): C, 60.61; H, 4.86. Found: C, 60.58; H, 4.82. IR (nujol, cm^{-1}): 1636 m ν(C=C); 839 s ν(PF). ^1H NMR (d_6-acetone): δ 7.63-7.26 (m, 48H, Ph, $C_{14}H_8$); 3.38-2.97 (m, 8H, CH_2CH_2); 1.78 (s, 30H, Cp*). ^{13}C NMR (d_6-acetone): δ 277.59 (s, C_α); 142.14 (s, C_β); 136.57-128.79 (m, Ph); δ 105.43 (s, C_5Me_5); δ 10.75 (s, C_5Me_5). ^{31}P NMR (d_6-acetone): δ 78.9 (s, dppe); -143.6 (sept, $^1J_{PF}$ 689 Hz, PF_6). ES-MS (positive ion mode, MeOH, *m/z*): 747, $[M]^{2+}$; 635, $[Ru(dppe)Cp^*]^+$.

$Cp^*(dppe)RuC{\equiv}CC_{14}H_8C{\equiv}CFe(dppe)Cp^*$ (27).

A solution of $RuCl(dppe)Cp^*$ (46 mg, 0.068 mmol), $Cp^*(dppe)FeC{\equiv}CC_{14}H_8C{\equiv}CTIPS$ (60 mg, 0.062 mmol) and $[Bu^n{}_4N]F.3H_2O$ (22 mg, 0.068 mmol) in THF (5 mL) was heated at reflux point for 16 h. The solvent was removed under vacuum and the residue washed with cold (0°C) MeOH and dried to yield $Cp^*(dppe)RuC{\equiv}C$ $C_{14}H_8C{\equiv}CFe(dppe)Cp^*$ (40 mg, 44%). IR (nujol, cm^{-1}): 2007 m, 2000 m ν(C≡C). ^1H NMR (d_6-benzene): δ 8.88-7.06 (m, 48H, Ph, $C_{14}H_8$); 2.91-2.85, 2.70-2.64 (2 x m, 2 x 4H, CH_2CH_2); 1.60, 1.53 (2 x s, 2 x 15H, Cp*). ^{13}C NMR (d_6-benzene): δ 141.14-123.85 (m, Ph); 93.50 (s, C_5Me_5); 30.46-29.84 (m, CH_2CH_2); 11.02 (s, C_5Me_5). ^{31}P NMR (d_6-benzene): δ 100.4 (s, Fe-dppe); 75.5 (s, Ru-dppe). ES-MS (positive ion mode, MeOH, *m/z*): 1448, $[M]^+$.

$[Cp^*(dppe)Ru{=}C{=}C{=}C_{14}H_8{=}C{=}C{=}Fe(dppe)Cp^*][PF_6]_2$ (27$[PF_6]_2$).

A solution of $Cp^*(dppe)RuC{\equiv}CC_{14}H_8C{\equiv}CFe(dppe)Cp^*$ (35 mg, 0.024 mmol) in THF (2 mL) was cooled to -78°C before adding $[FeCp_2][PF_6]$ (15 mg, 0.046 mmol) and stirring continued at –78°C for 30 min. The solution was allowed to warm to r.t. before again being cooled to –78°C and adding hexane (20 mL). The resulting precipitate of $[Cp^*(dppe)Ru{=}C{=}C{=}C_{14}H_8{=}C{=}C{=}Fe(dppe)Cp^*][PF_6]_2$ (25 mg, 60%) was collected

washed with hexane and dried. IR (nujol, cm^{-1}): 1948 w, 1940 w ν(C=C); 839 s ν(PF). ^1H NMR (d_6-acetone): δ 8.00-6.97 (m, 48H, Ph, $C_{14}H_8$); 4.03-3.91, 2.97-2.78 (2 x m, 2 x 4H, CH_2CH_2); 1.80, 1.56 (2 x br s, 2 x 15H, Cp*). ^{31}P NMR (d_6-acetone): δ 88.4, 86.7 (2 x br s, dppe); -143.6 (sept, $^1J_{PF}$ 689 Hz, PF_6). ES-MS (positive ion mode, MeOH, *m/z*): 724, $[M]^{2+}$.

$C_{14}H_9CHOHC{\equiv}CTMS$ (28).

To a stirred solution of $TMSC{\equiv}CH$ (3.7 mL, 26.19 mmol) in THF (30 mL) at –10°C was added ^{n}BuLi (14.55 mL, 23.28 mmol, 1.6 M in hexane). The resulting solution was allowed to warm to 25°C and added via a cannula to a stirred solution of $C_{14}H_9CHO$ (3.00 g, 14.55 mmol) in THF (50 mL) at –10°C. The resulting solution was stirred for a further 18 h allowing the reaction to warm to 25°C. The solution was then neutralised with NH_4Cl(aq), extracted with CH_2Cl_2 and washed with NH_4Cl(aq). The organic fractions were combined and dried over $MgSO_4$. The solvent was then removed and the residue submitted to silica gel column chromatography eluting with 1:1 CH_2Cl_2 / heptane to yield orange $C_{14}H_9CH(OH)C{\equiv}CTMS$ (3.52 g, 80%). IR (KBr/nujol, cm^{-1}): 3418 br ν(OH); 2170 s ν(C≡C). ^1H NMR ($CDCl_3$): δ 8.78 (d, $^3J_{HH}$ 10 Hz, 2H, $C_{14}H_8$); 8.31 (s, 1H, $C_{14}H_8$); 7.93 (d, $^3J_{HH}$ 8.0 Hz, 2H, $C_{14}H_8$); 7.61-7.45 (m, 4H, $C_{14}H_8$); 7.00 (s, 1H, C-H); 3.69 (s, 1H, OH); 0.37 (s, 9H, TMS). ^{13}C NMR ($CDCl_3$): δ 132.08, 131.32, 129.65, 129.50, 126.44, 125.38, 125.29 (two overlapping peaks, $C_{14}H_8$); 106.93, 92.28 (C≡C); 59.98 (CHOH); 0.43 (TMS).

$C_{14}H_9CH(OH)C{\equiv}CH$ (29).

A suspension of $C_{14}H_9CH(OH)C{\equiv}CTMS$ (500 mg, 1.64 mmol) and K_2CO_3 (272 mg, 1.97 mmol) in MeOH (50 mL) was stirred for 18 h in the absence of light before removing the solvent and extracting the residue with CH_2Cl_2 and washed with H_2O and dried over $MgSO_4$. The solvent was then removed and the residue submitted to silica gel column

chromatography eluting with 9:1 CH_2Cl_2 / heptane to yield orange $C_{14}H_9CH(OH)C{\equiv}CH$ (358 mg, 94%). IR (KBr/nujol, cm^{-1}): 3396 br ν(OH); 3292 s ν(≡CH); 2115 m ν(C≡C). ^1H NMR ($CDCl_3$): δ 8.66 (d, $^3J_{HH}$ 8.8 Hz, 2H, $C_{14}H_8$); 8.45 (s, 1H, $C_{14}H_9$); 8.02 (d, $^3J_{HH}$ 7.6 Hz, 2H, $C_{14}H_8$); 7.62-7.47 (m, 4H, $C_{14}H_8$); 6.93 (s, 1H, CH); 3.13 (s, 1H, COH); 2.71 (s, 1H, C≡CH). ^{13}C NMR ($CDCl_3$): δ 132.01, 130.64, 129.72, 129.51, 126.73, 125.49, 124.82 (two overlapping peaks, $C_{14}H_8$); 84.43, 75.75 (C≡C); 59.41 (CHOH).

[Cp*(dppe)Fe=C=C=CHC$_{14}$H$_9$][BPh$_4$] (30).

Method one.

A solution of FeCl(dppe)Cp* (200 mg, 0.32 mmol), Na[BPh_4] (120 mg, 0.35 mmol) and $C_{14}H_9CH(OH)C{\equiv}CH$ (81 mg, 0.35 mmol) in MeOH (30 mL) was stirred for 18 h before the solvent was removed, $MgSO_4$ added, and the residue extracted with CH_2Cl_2. The crude product was precipitated from solution with the addition of pentane and the product recystallised from CH_2Cl_2 / pentane to yield [Cp*(dppe)Fe=C=C=CHC$_{14}$H$_9$][BPh_4] (287 mg, 80%). IR (KBr/nujol, cm^{-1}): 1888 m ν(=C=C=C). ^1H NMR ($CDCl_3$): δ 10.28 (s, 1H, =CH); 8.92 (s, 1H, $C_{14}H_9$); 8.42 (d, $^3J_{HH}$ 7.8 Hz, 2H, $C_{14}H_8$); 8.21 (d, $^3J_{HH}$ 7.6 Hz, 2H, $C_{14}H_8$); 7.63-6.95 (m, 44H, $C_{14}H_8$/dppe/BPh_4); 3.06-3.02, 2.44-2.40 (2m, 4H, CH_2CH_2); 1.52 (s, 15H, Cp*). ^{31}P NMR ($CDCl_3$): δ 90.8 (s, dppe).

Method two.

A solution of $C_{14}H_9CH(OH)C{\equiv}CTMS$ (55 mg, 0.18 mmol) and K_2CO_3 (29 mg, 0.21 mmol) in MeOH (20 mL) was stirred for 4 h before the addition of Amberlyst 15 (250 mg), FeCl(dppe)Cp* (100 mg, 0.16 mmol) and Na[BPh_4] (62 mg, 0.18 mmol). Stirring was continued for a further 18 h. The solvent was then removed, $MgSO_4$ added and the residue extracted with CH_2Cl_2 before the product was precipitated with the addition of pentane to yield [Cp*(dppe)Fe=C=C=C HC$_{14}$H$_9$][BPh_4] (117 mg, 65%).

TMSC≡C$C_{14}H_8$CHO (32).

A solution of Br$C_{14}H_8$CHO (3.00 g, 10.53 mmol), TMSC≡CH (1.8 mL, 12.64 mmol), $PdCl_2(PPh_3)_2$ (295 mg, 0.42 mmol) and CuI (160 mg, 0.84 mmol) in a mixture of THF (80 mL) and NEt_3 (20 mL) was stirred at 25°C for 18 h. The solvent was then removed and the residue extracted with CH_2Cl_2 and washed with NH_4Cl(aq) and dried over $MgSO_4$. The solvent was then removed and the residue submitted to silica gel column chromatography eluting with 1:1 CH_2Cl_2 / hexane to yield orange TMSC≡C$C_{14}H_8$CHO (2.98 g, 94%). IR (KBr/nujol, cm^{-1}): 2136 m ν(C≡C); 1675 s ν(C=O). ^{1}H NMR ($CDCl_3$): δ 11.51 (s, 1H, CHO); 8.94 (d, $^3J_{HH}$ 8 Hz, 2H, $C_{14}H_8$); 8.70 (d, $^3J_{HH}$ 8 Hz, 2H, $C_{14}H_8$); 7.70-7.63 (m, 4H, $C_{14}H_8$); 0.43 (s, 9H, TMS). ^{13}C NMR ($CDCl_3$): δ 193.10 (CHO); 132.13, 131.01, 129.05, 127.87, 126.86, 125.32, 125.19, 124.03 ($C_{14}H_8$); 111.05, 101.41 (C≡C); 0.63 (TMS).

TMSC≡C$C_{14}H_8$CH(OH)C≡CTIPS (33).

To a stirred solution of TIPSC≡CH (1.34 mL, 6.00 mmol) in THF (20 mL) at –10°C was added ^{n}BuLi (3.31 mL, 5.30 mmol, 1.6 M in hexane). The resulting solution was allowed to warm to 25°C and then added via a cannula to a stirred solution of TMSC≡C$C_{14}H_8$CHO (1.00 g, 3.31 mmol) in THF (40 mL) at –10°C. The resulting solution was stirred for a further 18 h allowing the reaction to warm to 25°C. The solution was then neutralised with NH_4Cl(aq), extracted with CH_2Cl_2 and washed with NH_4Cl(aq) and dried over $MgSO_4$. The solvent was then removed and the residue submitted to silica gel column chromatography eluting with 1:1 CH_2Cl_2 / hexane to yield orange TMSC≡C$C_{14}H_8$CH(OH)C≡CTIPS (1.55 g, 97%). IR (KBr/nujol, cm^{-1}): 3386 br ν(OH); 2163 m, 2139 s ν(C≡C). ^{1}H NMR ($CDCl_3$): δ 8.80-8.71 (m, 4H, $C_{14}H_8$); 7.70-7.58 (m, 4H, $C_{14}H_8$); 6.98 (s, 1H, CH); 2.93 (s, 1H, COH); 1.08-0.97 (m, 21H, TIPS); 0.54 (s, 9H, TMS). ^{13}C NMR ($CDCl_3$): δ 133.21, 132.87, 129.01, 128.03, 126.75,

126.69, 125.52, 119.84 ($C_{14}H_8$); 108.01, 107.87, 102.19, 89.54 (2 x C≡C); 60.01 (CHOH); 19.05, 11.68 (TIPS); 0.73 (TMS).

HC≡C$C_{14}H_8$CH(OH)C≡CTIPS (34).

A suspension of TMSC≡C$C_{14}H_8$CH(OH)C≡CTIPS (1.60 g, 3.31 mmol) and K_2CO_3 (550 mg, 3.97 mmol) in MeOH (70 mL) was stirred for 18 h in the absence of light. The solvent was removed and the residue extracted with CH_2Cl_2 and washed with H_2O and dried over $MgSO_4$. The solvent was then removed and the residue submitted to silica gel column chromatography eluting with 1:1 CH_2Cl_2 / heptane to yield orange HC≡C$C_{14}H_8$CH(OH)C≡CTIPS (1.29 g, 94%). IR (KBr/nujol, cm^{-1}): 3398 br ν(OH); 3270 s ν(≡CH); 2171 s, 2096 m ν(C≡C). ^{1}H NMR ($CDCl_3$): δ 8.80-8.65 (m, 4H, $C_{14}H_8$); 7.65-7.53 (m, 4H, $C_{14}H_8$); 6.98 (s, 1H, CH); 4.08 (s, 1H, C≡CH); 3.03 (s, 1H, COH); 1.19-0.97 (m, 21H, TIPS). ^{13}C NMR ($CDCl_3$): δ 133.42, 133.21, 128.90, 127.87, 126.75, 126.64, 125.52, 118.75 ($C_{14}H_8$); 108.01, 89.75, 80.93 (two overlapping peaks at 89.75, 2 C≡C); 60.01 (CH(OH)); 19.07, 11.63 (TIPS).

(-C≡C$C_{14}H_8$CH(OH)C≡CTIPS)$_2$ (35).

A solution of HC≡C$C_{14}H_8$CH(OH)C≡CTIPS (110 mg, 0.27 mmol), $PdCl_2(PPh_3)_2$ (7 mg, 0.01 mmol), CuI (2 mg, 0.01 mmol) and PPh_3 (7 mg, 0.03 mmol) in NEt_3 (2.5 mL) and MeCN (1.5 mL) was stirred for 24 h at 25°C before removing the solvent and the residue extracted with CH_2Cl_2 and washed with NH_4Cl(aq) and dried over $MgSO_4$. The solvent was then removed and the residue submitted to silica gel column chromatography eluting with 4:1 CH_2Cl_2 / heptane to yield orange (-C≡C$C_{14}H_8$CH(OH)C≡CTIPS)$_2$ (77 mg, 70%). IR (KBr/nujol, cm^{-1}): 3382 br ν(OH); 2168 s, 2126 m ν(C≡C). ^{1}H NMR ($CDCl_3$): δ 8.82-8.67 (m, 8H, $C_{14}H_8$); 7.73-7.60 (m, 8H, $C_{14}H_8$); 7.02 (s, 2H, CH); 2.74 (S, 2H, COH); 1.05-0.93 (m, 42H, TIPS). ^{13}C NMR ($CDCl_3$): δ 134.19, 133.54, 128.87, 127.86,

127.12, 126.75, 125.63, 118.34 ($C_{14}H_8$); 107.87, 89.89, 86.54, 82.63 (2 x C≡C); 60.01 (CHOH); 19.09, 11.63 (TIPS).

$C_{14}H_9CH(OH)C{\equiv}CTIPS$ (36).

To a stirred solution of TIPSC≡CH (1.97 mL, 8.73 mmol) in THF (20 mL) at –10°C was added ^{n}BuLi (4.85 mL, 7.76 mmol, 1.6 M in hexane). The resulting solution was allowed to warm to 25°C and then added via a cannula to a stirred solution of $C_{14}H_9CHO$ (1.00 g, 4.85 mmol) in THF (30 mL) at –10°C. The resulting solution was stirred for a further 18 h allowing the reaction to warm to 25°C. The solution was then neutralised with NH_4Cl(aq), extracted with CH_2Cl_2 and washed with NH_4Cl(aq) and dried over $MgSO_4$. The solvent was then removed and the residue submitted to silica gel column chromatography eluting with 1:1 CH_2Cl_2 / heptane to yield orange $C_{14}H_9CH(OH)C{\equiv}CTIPS$ (1.83 g, 97%). IR (KBr/nujol, cm^{-1}) 3424 br ν(OH); 2168 s ν(C≡C). ^{1}H NMR ($CDCl_3$): δ 8.80 (d, $^3J_{HH}$ 8.0 Hz, 2H, $C_{14}H_8$); 8.40 (s, 1H, $C_{14}H_9$); 7.99 (d, $^3J_{HH}$ 8.0 Hz, 2H, $C_{14}H_8$); 7.60-7.46 (m, 4H, $C_{14}H_8$); 7.02 (s, 1H C-H); 3.17 (s, 1H, COH); 1.28-1.04 (m, 21H, TIPS). ^{13}C NMR ($CDCl_3$): δ 132.01, 131.54, 129.56, 129.48, 126.43, 125.32, 125.31 (two overlapping peaks, $C_{14}H_9$); 108.56, 88.91 (C≡C); 60.05 (CHOH); 19.10, 11.73 (TIPS).

$HC{\equiv}CC_{14}H_8CHO$ (37).

A suspension of $TMSC{\equiv}CC_{14}H_8CHO$ (1.40 g, 4.63 mmol) and K_2CO_3 (768 mg, 5.56 mmol) in MeOH (100 mL) was stirred for 18 h in the absence of light before removing the solvent, extraction into CH_2Cl_2 followed by washing with H_2O and drying over $MgSO_4$. The solvent was then removed to yield orange $HC{\equiv}CC_{14}H_8CHO$ (990 mg, 98%). IR (KBr/nujol, cm^{-1}): 3228 s ν(≡CH); 2079 m ν(C≡C); 1673 s ν(C=O). ^{1}H NMR ($CDCl_3$): δ 11.56 (s, 1H, CHO); 8.96 (d, $^3J_{HH}$ 8 Hz, 2H, $C_{14}H_8$); 8.75 (d, $^3J_{HH}$ 8 Hz, 2H,

$C_{14}H_8$); 7.79-7.66 (m, 4H, $C_{14}H_8$); 4.23 (s, 1H, C≡C-H). ^{13}C NMR ($CDCl_3$): δ 193.72 (CHO); 134.54, 129.41, 128.49, 127.97, 127.64, 127.36, 126.37, 124.32 ($C_{14}H_8$); 92.31, 80.33 (C≡C).

HC≡C$C_{14}H_8$CH(OH)C≡CTMS (38).

To a solution of TMSC≡CH (1.93 mL, 13.68 mmol) in Et_2O (20 mL) at –10°C was added ^{n}BuLi (8.55 mL, 13.68 mmol, 1.6 M in hexane) and stirred for 15 min. The resulting solution was added via a cannula to a solution of CuI (1.30 g, 6.84 mmol) in Et_2O (20 mL) at –10°C. The resulting solution was then stirred for a further 1 h before powdered HC≡C$C_{14}H_8$CHO (1.05 g, 4.65 mmol) was added and stirred for a further 80 min. The solution was then neutralised with NH_4Cl(aq) and extracted with Et_2O and washed with NH_4Cl(aq). The organic fractions where then combined and the solvent removed to yield orange HC≡C$C_{14}H_8$CH(OH)C≡CTMS (1.50 g, 98%). IR (KBr/nujol, cm^{-1}): 3418 br ν(OH); 3239 s ν(≡CH); 2170 s, 2096 m ν(C≡C). ^1H NMR ($CDCl_3$): δ 8.79-8.69 (m, 4H, $C_{14}H_8$); 7.65-7.59 (m, 4H, $C_{14}H_8$); 6.99 (s, 1H, CH); 4.08 (s, 1H, C≡C-H); 2.74 (s, 1H, COH); 0.18 (s, 9H, TMS). ^{13}C NMR ($CDCl_3$): δ 133.41, 132.91, 128.95, 127.87, 126.86, 126.64, 125.54, 118.83 ($C_{14}H_8$); 106.09, 93.05, 89.80, 80.91 (2 C≡C); 59.94 (CHOH); 0.23 (TMS).

(-C≡C$C_{14}H_8$CH(OH)C≡CTMS)$_2$ (39).

A solution of HC≡C$C_{14}H_8$CH(OH)C≡CTMS (120 mg, 0.37 mmol), $PdCl_2(PPh_3)_2$ (28 mg, 0.04 mmol), CuI (8 mg, 0.04 mmol) and PPh_3 (34 mg, 0.13 mmol) in NEt_3 (10 mL) and THF (10 mL) was stirred for 24 h at 25°C before removing the solvent and extracting the residue with CH_2Cl_2 and washing with NH_4Cl(aq). The residue was then submitted to column chromatography eluting with 4:1 CH_2Cl_2 / hexane to yield orange (-C≡C$C_{14}H_8$CH(OH)C≡CTMS)$_2$ (52 mg, 43%). IR (KBr/nujol, cm^{-1}) 3407 br ν(OH); 2170

s, 2123 m ν(C≡C). ^{1}H NMR ($CDCl_3$): δ 8.82-8.73 (m, 8H, $C_{14}H_8$); 7.72-7.58 (m, 8H, $C_{14}H_8$); 6.97 (s, 2H, C-H); 2.74 (s, 2H, OH); 0.19 (s, 18H, TMS). ^{13}C NMR ($CDCl_3$): δ 134.32, 133.38, 129.07, 127.92, 127.21, 126.89, 125.63, 118.54 ($C_{14}H_8$); 105.62, 93.37, 86.42, 82.54 (2 C≡C); 60.08 (CHOH); 0.13 (TMS).

$BrC_{14}H_8CH(OH)C{\equiv}CTMS$ (40).

To a stirred solution of TMSC≡CH (0.45 mL, 3.15 mmol) in THF (20 mL) at −10°C was added ^{n}BuLi (1.75 mL, 2.80 mmol, 1.6 M in hexane). The resulting solution was allowed to warm to 25°C and then added via a cannula to a stirred solution of $BrC_{14}H_8CHO$ (500 mg, 1.75 mmol) in THF (30 mL) at −10°C. The resulting solution was stirred for a further 18 h allowing the reaction to warm to 25°C. The solution was then neutralised with NH_4Cl(aq), extracted with CH_2Cl_2 and washed with NH_4Cl(aq) and dried over $MgSO_4$. The solvent was then removed and the residue submitted to silica gel column chromatography eluting with 1:1 CH_2Cl_2 / hexane to yield yellow $BrC_{14}H_8CH(OH)C{\equiv}CTMS$ (436 mg, 65%). IR (KBr/nujol, cm^{-1}): 3314 br ν(OH); 2171 m ν(C≡C). ^{1}H NMR ($CDCl_3$): δ 8.68-8.58 (m, 4H, $C_{14}H_8$); 7.58-7.50 (m, 4H, $C_{14}H_8$); 6.89 (s, 1H, CH); 3.31 (s, 1H, COH); 0.26 (s, 9H, TMS).

$[Cp^*(dppe)Fe{=}C{=}C{=}CHC_{14}H_8Br][BPh_4]$ (41).

A solution of $BrC_{14}H_8CHOHC{\equiv}CTMS$ (160 mg, 0.42 mmol) and K_2CO_3 (64 mg, 0.46 mmol) in MeOH (20 mL) was stirred for 18 h in the absence of light before removing the solvent and the residue extracted with CH_2Cl_2, washed with H_2O and dried over $MgSO_4$. The solvent was then removed and the residue taken up in MeOH (30 mL). FeCl(dppe)Cp* (212 mg, 0.34 mmol) and $Na[BPh_4]$ (128 mg, 0.37 mmol) was added and stirring continued for a further 18 h. The solvent was then removed and $MgSO_4$ added. The residue was extracted with CH_2Cl_2 and the crude product was precipitated from solution with the addition of pentane. The product was then recrystallized from CH_2Cl_2 /

Et_2O to yield [Cp*(dppe)Fe=C=C=$CHC_{14}H_8Br$][BPh_4] (266 mg, 65%). IR (KBr/nujol, cm^{-1}): 1888 m ν(=C=C=C). ^1H NMR ($CDCl_3$): δ 10.18 (s, 1H, =CH); 8.80-8.74 (m, 2H, $C_{14}H_8$); 8.36-8.30 (m, 2H, $C_{14}H_8$); 7.59-6.85 (m, 44H, $C_{14}H_8$/dppe/BPh_4); 3.01-2.95, 2.43-2.37 (2m, 4H, CH_2CH_2); 1.47 (s, 15H, Cp*).

Chapter Five

Some ferrocenylethynyl and ruthenocenylethynyl complexes

5.1. Introduction.

While much work has centred around complexes containing all organic bridges capped by redox-active metal termini, the focus has also shifted to the addition of ferrocenyl and ruthenocenyl groups into these bridging ligands, as a result of the effect the redox-active sandwich complex has over the strong electronic interactions seen in straight chain complexes. Complexes of the general formula $[ML_n](\mu\text{-}C{\equiv}C)_xMc$ and $[MLn](\mu\text{-}C{\equiv}C)_xMc'(C{\equiv}C\text{-}\mu)_n[M'L'_m]$ (where Mc = $CpM(\mu_5\text{-}C_5H_4\text{-})$ M = Fc and Mc' = $M(\mu_5\text{-}C_5H_4\text{-})_2$ M = Ru) have driven this interest.[124-126]

5.1.1. Synthetic strategies for metallocenyl complexes.

Complexes containing these redox-active sandwich moieties have been prepared through one main synthetic pathway, starting from a substituted metallocenyl and the desired metal ligand end cap.

Both metallocenyl fragments FcC≡CH and 1,1'-Rc'$(C{\equiv}CTMS)_2$ are well known and allow a wide range of products due to the extensive number of metal ligand end caps. Treatment of FcC≡CH with $RuCl(PPh_3)_2Cp$ in the presence of $[NH_4][PF_6]$, in a dichloromethane / methanol solution for one hour followed by the addition of sodium methoxide results in the formation of $Ru(C{\equiv}CFc)(PPh_3)_2Cp$ (see Scheme 5.1).[124]

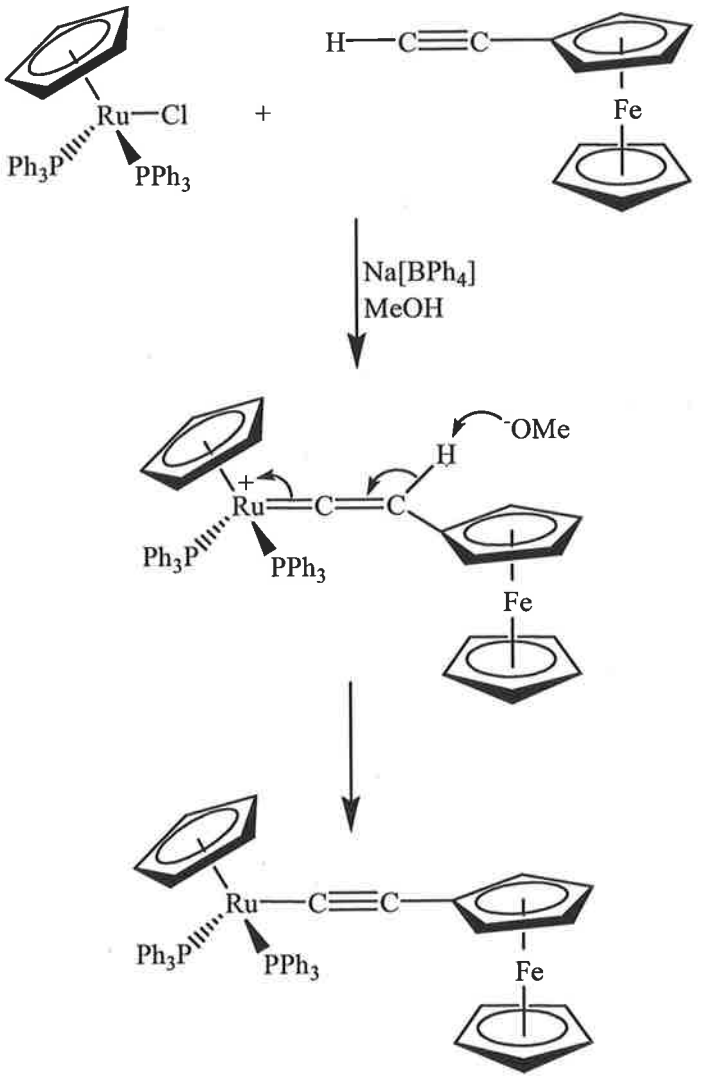

Scheme 5.1. *Synthesis of Ru(C≡CFc)(PPh$_3$)$_2$Cp.*

This complex can be further oxidised by treatment with [FeCp$_2$][PF$_6$] to [Ru(CCFc)(PPh$_3$)$_2$Cp][PF$_6$]. The IR spectrum shows bands intermediate between an acetylide or allenylidene type complex demonstrating some interaction between the two centres (see Scheme 5.2).

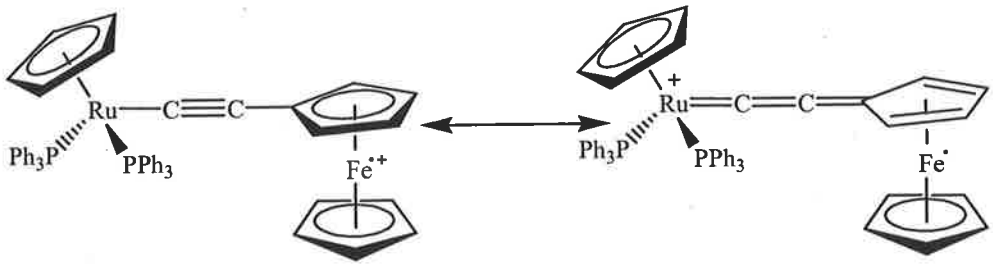

Scheme 5.2. *Limiting structures of [Ru(CCFc)(PPh$_3$)$_2$Cp][PF$_6$].*

However the addition of ferrocenyl into {Cp(PPh$_3$)$_2$Ru}$_2$(μ-C≡CC≡C) to give 1,1'-{Cp(PPh$_3$)$_2$RuC≡C}$_2$Fc' shows different interactions than those observed above. The cyclic voltammogram of 1,1'-{Cp(PPh$_3$)$_2$RuC≡C}$_2$Fc' shows some decoupling of the two ruthenium termini, but the UV-Vis-NIR data indicates that ferrocenyl moiety does act as an insulator to the electronic interactions observed in {Cp(PPh$_3$)$_2$Ru}$_2$(μ-C≡CC≡C). The synthetic method is very similar to above with a mixture of RuCl(PPh$_3$)$_2$Cp, 1,1'-(TMSC≡C)$_2$Fc' and KF heated at reflux in a methanol / THF solution (see Scheme 5.3.).

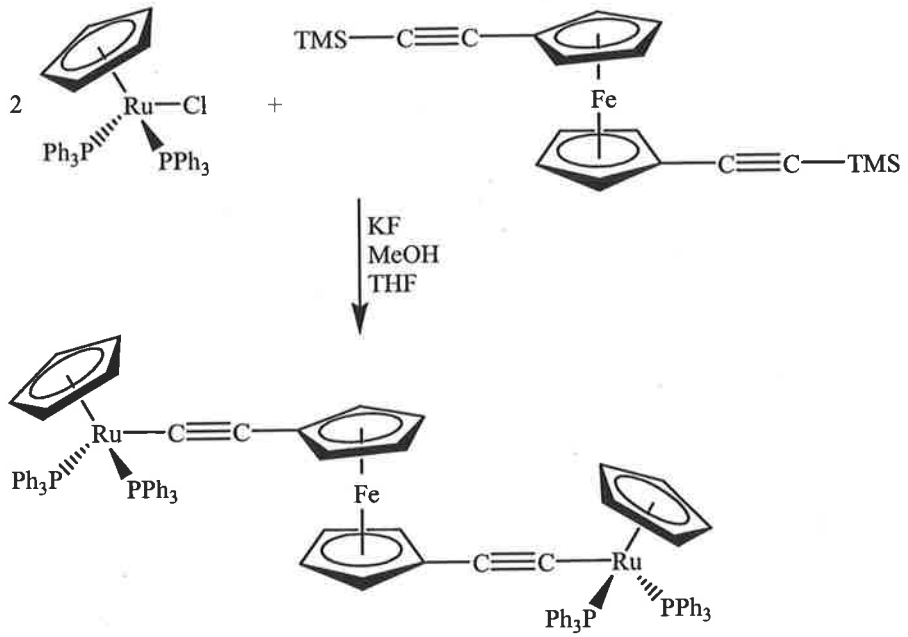

Scheme 5.3. *Synthesis of 1,1'-{Cp(PPh$_3$)$_2$RuC≡C}$_2$Fc'.*

5.2. Aims.

The primary aim of this work was to synthesise complexes containing either the ferrocenyl or ruthenocenyl moiety within the bridging ligand. The reactivity of the carbon chain would then be tested using the electron-deficient compound tetracyanoethene (TCNE), which can undergo a [2 + 2] cycloaddition with electron-rich carbon-carbon triple bonds.

Cyclic voltammetry would also be used to determine what effect the inclusion of these sandwich complexes have over the strong electronic interactions observed in the straight-chain analogues.

5.3. Results and Discussion.

5.3.1. Synthesis and properties of Os(C≡CFc)(dppe)Cp and 1,1'-(Cp[P*m*-tol$_3$]$_2$RuC$_2$)$_2$Rc.

OsC≡CFc(dppe)Cp (**42**) was prepared by treatment of HC≡CFc (**43**) with OsCl(dppe)Cp (**44**) in the presence of Na[BPh$_4$], which assists in the ionisation of the Os-Cl bond, heated at reflux in methanol. After 18 h the solution was cooled on ice before the addition of sodium methoxide, which deprotonates the vinylidene complex, giving the neutral complex after basic alumina column chromatography, eluting with 9/1 acetone-hexane, in 78% yield (see Scheme 5.4).

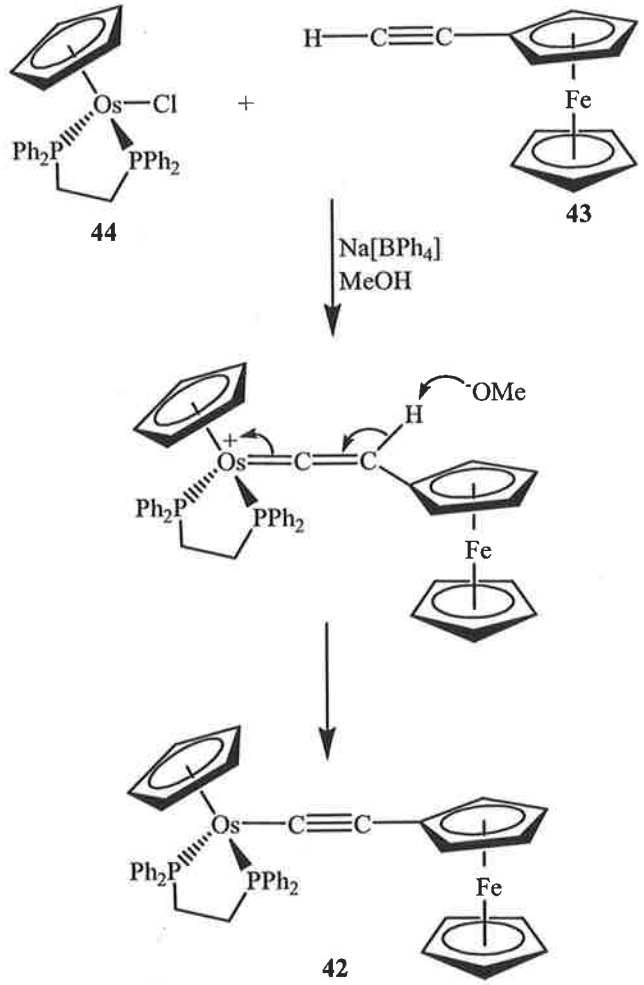

Scheme 5.4. *Synthetic route to OsC≡CFc(dppe)Cp.*

The IR spectrum of **42** showed ν(C≡C) at 2078 cm^{-1}, which is consistent with a triple bond of this nature.

The ^{1}H NMR spectrum of **42** displayed two unresolved multiplets between δ 2.23-2.29, 2.51-2.62 corresponded to the CH_2CH_2 in dppe. Broad signals at δ 3.85 and δ 3.90, correspond to an overlap of the unsubstituted Cp ring and two hydrogens from the substituted Cp ring in Fc, along with the other two hydrogens from the substituted Cp ring respectively. The Cp on the osmium was observed as a singlet at δ 4.62, while the aromatic hydrogens were seen between δ 6.97-8.11.

The ^{13}C NMR spectrum of **42** displayed multiplets between δ 30.05-30.67 and 126.62-143.89 corresponded to the CH_2CH_2 in dppe and the aromatic carbons respectively. The ferrocenyl carbons appeared at δ 66.66 and 70.69, which corresponded to the four carbons containing hydrogens of the substituted Cp ring. A peak at δ 69.72 corresponded to the unsubstituted Cp ring, along with δ 77.42 corresponding to C_{ipso}. The Os-Cp carbons appeared as a triplet at δ 78.62 ($^{2}J_{CP}$ 2.3 Hz). The ethynyl carbons could be differentiated by the splitting seen for C_α a triplet at δ 83.41 ($^{2}J_{CP}$ 18.6 Hz), due to the coupling of the phosphorus through osmium, while C_β appeared as a singlet at δ 102.15.

The ^{31}P NMR spectrum of **42** showed a peak at δ 47.2 corresponding to the dppe ligand. The mass spectrum shows a peak corresponding to $[M]^+$ at *m/z* 864, which undergoes fragmentation to give $[Os(dppe)Cp]^+$ at *m/z* 655.

Due to the instability of Rc'(C≡CH)$_2$ the TMS protected ruthenocenyl was used. Thus reaction with RuCl[P*m*-tol$_3$]$_2$Cp in the presence of the desilylating agent KF, resulted in the precipitation of 1,1'-{Cp[*m*-tol$_3$P]$_2$RuC≡C}$_2$Rc' (**45**) from the reaction mixture in a yield of 86%.

The IR spectrum of **45** showed ν(C≡C) at 2081 cm^{-1} and another band at 1591 cm^{-1} corresponding to aromatic ν(C=C).

The ^{1}H NMR spectrum displayed a peak at δ 2.05 corresponding to the methyl hydrogens, along with a multiplet between δ 6.84-7.71 corresponding to the aromatic hydrogens. A peak at δ 4.58 was found for the Ru-Cp group. While as a result of the symmetry of the complex, looking down the carbon chain and through the ruthenocenyl rings, the hydrogens of the ruthenocenyl rings appeared as two broad singlets at δ 4.54 and 5.12.

The ^{31}P NMR spectrum showed a peak corresponding to the P*m*-tol$_3$ ligands at δ 51.8 and the molecular ion was observed in the mass spectrum at *m/z* 1827.

5.3.2. Reactions of Os(C≡C)Fc(dppe)Cp and 1,1'-{Cp[*m*-tol$_3$P]$_2$RuC≡C}$_2$Rc' with tetracyanoethene.

Reactions of the electron-deficient alkene tetracyanoethene (TCNE) with electron rich carbon-carbon triple bonds are well known.[127-130] Reactions of these triple bonds adjacent to metal centres can give rise to several different complexes such as tetracyano-cyclobutenyl or –butadienyl or allylic (vinylcarbene) complexes, under various conditions (see Figure 5.1).

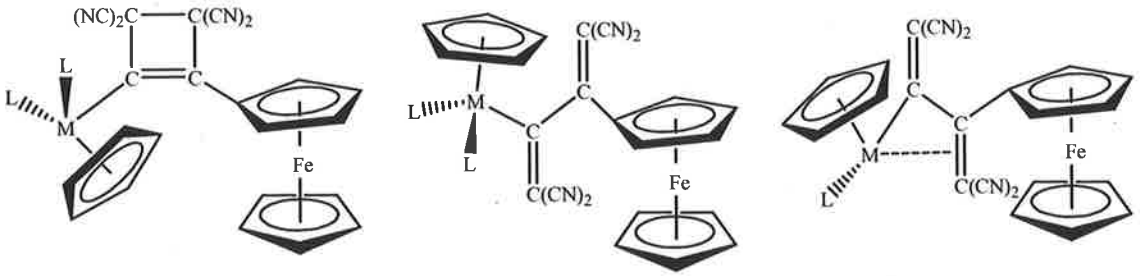

G **H** **J**

Figure 5.1. *Possible reaction products upon the addition of TCNE, G. Tetracyano-cyclobutenyl. H. Tetracyano-butadienyl. J. Vinylcarbene.*

Treatment of **42** with TCNE in benzene at room temperature results in addition across the electron-rich carbon-carbon triple bond and ring opening to give Os{C[=C(CN)$_2$]=CFc=C(CN)$_2$}dppeCp (**46**) in 37% yield. The cyclobutenyl complex **G** and the vinylcarbene complex **J** were not observed for this reaction. Displacement is observed however for RuC≡CFc(PPh$_3$)$_2$Cp due to triphenylphosphine being a more labile ligand compared to dppe, which is bi-dentate instead of mono-dentate. A similar displacement also occurs for RuC≡CFc(dppe)Cp* to give the vinylcarbene complex **J** (see Scheme 5.5).[120] This is a result of the extra steric hindrance of Cp* compared to Cp, which offers some further protection against electrophilic and nucleophilic attack at C_α and C_β (also discussed in Chapter 6).

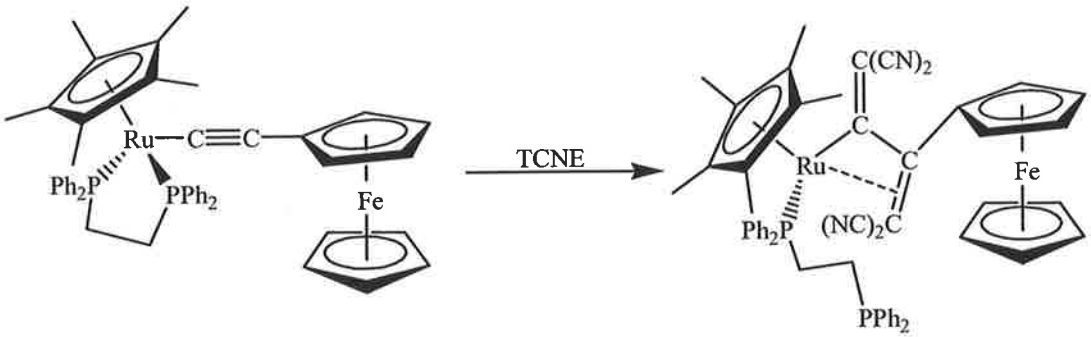

Scheme 5.5. *Ligand displacement caused by the addition of TCNE.*

The IR spectrum of **46** showed three bands at 2214, 2199 cm^{-1} corresponding to ν(CN) along with a ν(C=C) band at 1508 cm^{-1}.

The ^{1}H NMR spectrum of **46** showed one multiplet corresponding to the CH_2CH_2 in dppe between δ 2.00-2.50. The aromatic hydrogens appeared as a series of multiplets between δ 6.41-7.95 and the two Cp peaks from the unsubstituted FeCp and OsCp groups were observed at δ 4.13 and 5.03 respectively. With the addition of TCNE the symmetry through carbons C_α, C_β, and C_{ipso} (see X-ray crystal structure Figure 5.3) is broken resulting in the protons of the Fe(C_5H_4) ring appearing as four broad singlets at δ 2.26, 3.98, 4.49 and 5.53 instead of the two peaks observed in **42**. This addition also affects

the ^{31}P NMR spectrum, which contained an AB quartet at δ 29.03 and 40.79 (d, *J* 6.8 Hz).

The mass spectrum showed $[M + Na]^+$ at *m/z* 1015 along with the fragment at *m/z* 655 corresponding to $[Os(dppe)Cp]^+$.

Treatment of 1,1'-{Cp[*m*-tol$_3$P]$_2$RuC≡C}$_2$Rc' with TCNE in dichloromethane at room temperature results in the displacement of one *m*-tol$_3$P ligand from each ruthenium centre to give the adducts **47** and **48** (in a ratio of 36:64) in 44% yield. The TCNE adducts **47** and **48** are isolated as an inseparable mixture of the two diastereomeric conformers of the vinylcarbene form (see Figure 5.2).

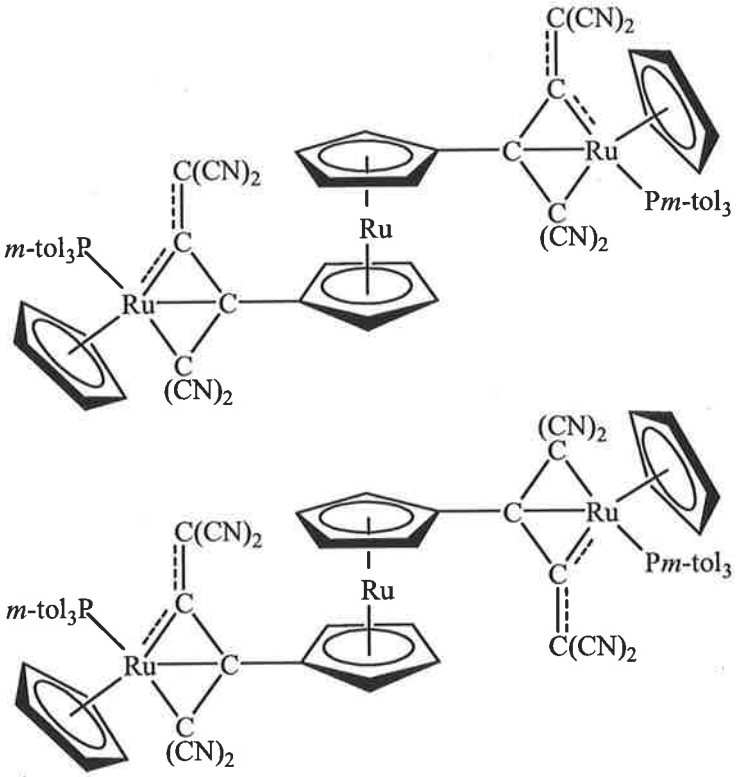

Figure 5.2. *Structure of the products from the reaction between 1,1'-(Cp[m-tol$_3$P]$_2$RuC$_2$)$_2$Rc' and TCNE.*

The two diastereomers differ in the relative stereochemistries about the two-ruthenium centres. The cyano groups in the minor conformer are on the same face, whereas for the

major conformer they are on opposite faces. The major conformer is assigned by comparison with the results of the previously reported reaction of 1,1'-$\{Cp(Ph_3P)_2FeC{\equiv}C\}_2Fc$' with TCNE.[120]

The IR spectra of **47** and **48** both show one band at 2213 cm^{-1} corresponding to ν(CN), along with a ν(CC) stretch at 1614 cm^{-1} corresponding to the vinylcarbene.

The ^1H NMR spectrum showed peaks at δ 1.30 and 2.44 corresponding to the methyl protons of the major and minor isomer, respectively. For the major isomer the hydrogens of the ruthenocenyl rings appeared as four broad singlets at δ 5.08, 5.23, 5.39, 6.09, whereas for the minor isomer they appeared as only three peaks, with two overlapping peaks at δ 5.23, along with δ 5.32 and 5.92. The Cp peaks appeared at δ 4.65 and 4.63 for the major and minor isomer, respectively, with the aromatic hydrogens between δ 7.18-7.41.

The ^{31}P NMR spectra were similar with peaks at δ 39.4 and 39.4 corresponding to the major and minor isomer, respectively.

5.3.3. Molecular Structure.

Single crystals suitable for X-ray diffraction studies of complex **46** were grown from dichloromethane and hexane. The ORTEP plot of the complex along with relative bond distances and angles can be seen in Figure 5.3 and Table 5.1.

The osmium-phosphorus bonds lengths are shown to be ca. 2.3 Å, with the osmium Cp bonds (av 2.255(7) Å) and the ferrocenyl terminal (2.033(4) Å FeCp and 2.044(6) Å FeCp').

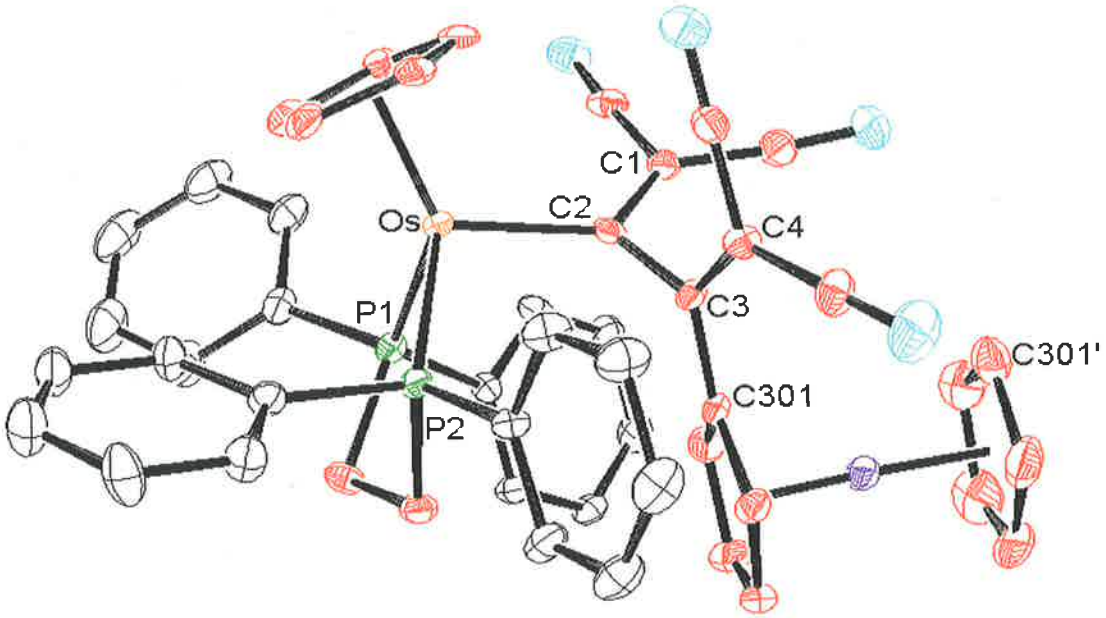

Figure 5.3. *ORTEP plot of* ***46****.*

Bond distance (Å)			
Os-P(1)	2.2978(9)	C(3)-C(301)	1.372(5)
Os-P(2)	2.3278(9)	Fe-Cp	2.017-2.047(4)
Os-Cp	2.241-2.273(4)	(av)	2.033(4)
(av)	2.255(7)	Fe-Cp'	2.022-2.058(7)
Os-C(2)	2.065(3)	(av)	2.044(6)
C(2)-C(3)	1.495(5)	C-CN	1.417-1.433(6)
C(3)-C(4)	1.459(5)	(av)	1.428(6)
C(2)-C(1)	1.396(5)		
Bond Angle (°)			
Os-C(2)-C(3)	122.6(2)	C(1)-C(2)-C(3)	117.4(3)
C(2)-C(3)-C(301)	117.4(3)	C(2)-C(3)-C(4)	119.1(1)
P(1)-Os-P(2)	82.25(3)		

Table 5.1. *Bond distances and angles of* ***46****.*

The Os-C(2) bond distance of 2.065(3) Å is very similar to other reported Os-C single bond distances.[131] The C(2)-C(3) and C(3)-C(301) bond distances of 1.495(5) and 1.459(5) Å respectively indicate carbon-carbon single bonds. This is expected with both C(2) and C(3) undergoing a conversion from C(*sp*) linear to C(sp^2) trigonal. This change is observed with bond angles of Os-C(2)-C(3) and C(2)-C(3)-C(301) at 122.6(2) and 117.4(3)°, respectively.

5.3.4. Electrochemistry.

The cyclic voltammogram of **42** displayed three well-separated peaks. The first two peaks at +0.03 and +0.59 V demonstrated complete reversibility ($i_a / i_c = 1$ along with the current proportional to (scan rate)$^{1/2}$). These two redox events are assigned to an oxidation at the osmium and ferrocenyl centres respectively. The third redox event at +1.20 V appeared fully non-reversible ($i_c / i_a = 0$) even at faster scan rates and is assigned to the second oxidation of the osmium centre. The change in the first oxidation potential for the osmium centre, when compared to that found for **43** (see Chapter 6), may be explained by the electron-donating effect of the ferrocenyl centre. This indicates that there is some interaction between the two metal centres ($\Delta E_{1/2}$ = 0.64V), which has been further demonstrated by other complexes such as M(C≡CFc)(LL)Cp' (where M = Ru, LL = $(PPh_3)_2$, dppe, dppm, Cp' = Cp, Cp* and M = Os, LL = $(PPh_3)_2$, Cp ' + Cp) (see Table 5.2). Determination of the comproportionation constant K_c for the mono-cation (n = 1, K_c = 2.95 x 10^6) and di-cation (n = 2, Kc = 2.07 x 10^{10}) indicates high thermal stability of both these cations with respect to disproportionation.

Complex [M]	E_1	E_2	$\Delta E_{1/2}$	K_c(0/+1/+2)	E_3	[REF]
$Ru(PPh_3)_2Cp$	+0.13	+0.82	0.69	3.5×10^{11}		120
$Os(PPh_3)_2Cp$	+0.05	+0.69	0.64	6.7×10^{10}	+1.40[a]	120
Ru(dppm)Cp	+0.13	+0.69	0.56	3.0×10^{9}	+1.40[a]	120
Ru(dppe)Cp	+0.14	+0.72	0.58	8.0×10^{9}		120
Os(dppe)Cp	+0.03	+0.59	0.56	3.0×10^{9}		This work
Ru(dppe)Cp*	+0.05	+0.68	0.63	4.6×10^{10}	+1.21[a]	120

Table 5.2. *Cyclic voltammetry data for [M]C_2Fc, measured in 0.1M [Bu^n_4N][PF_6] in CH_2Cl_2 at 100mV s^{-1}. [a] Peak potential of a fully non-reversible wave.*

The cyclic voltammogram of **45** displayed three well-separated and fully reversible (i_a / i_c = 1, current proportional to (scan rate)$^{1/2}$) redox events at +0.12, +0.36 and +0.69V (see Figure 5.4).

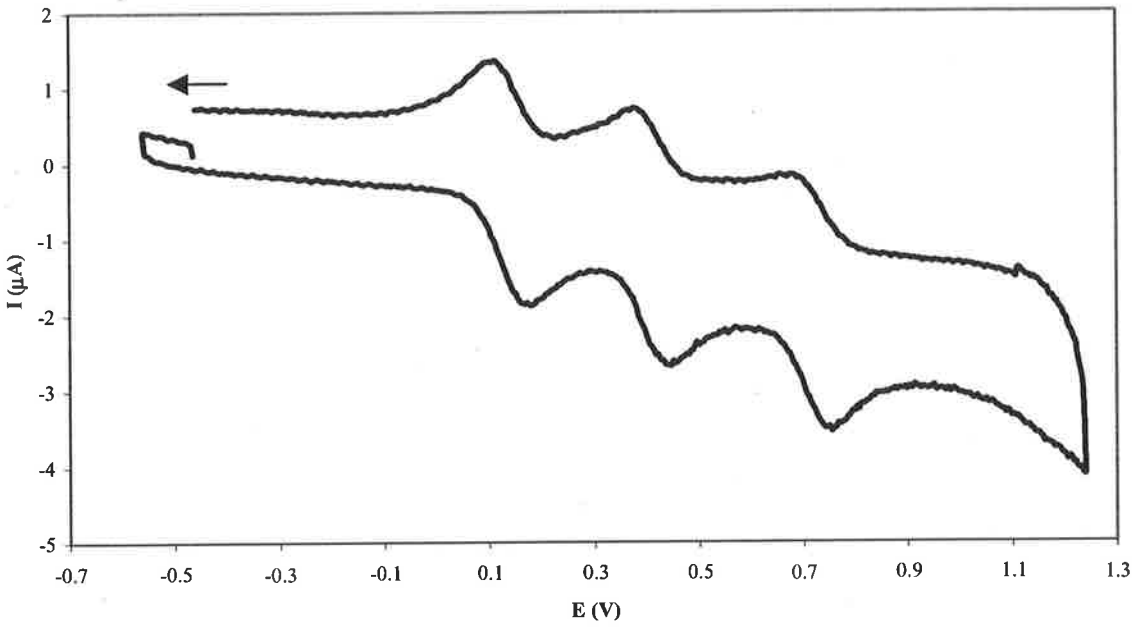

Figure 5.4. *Cyclic voltammogram of **45** recorded in CH_2Cl_2, 0.1M [Bu$^n_4$N][PF_6] at 100 mV s^{-1}.*

Further examination of the cyclic voltammogram current ratios and peak areas indicate that the three redox events are associated with a one-electron process. This clearly points to there being significant interactions mediated by the bridging ruthenocenediyl moiety ($\Delta E_{1/2}$ = 0.24V), which decouples the oxidation potentials despite the identical nature of the two metal termini. However the first redox event is assigned to an oxidation at a ruthenium terminal, followed by an oxidation at the ruthenocenediyl centre. As a result of the decoupling though, the third redox event can not be assigned directly from the cyclic voltammogram. This same observation was made with other such complexes containing the ruthenocenediyl bridging moiety (see Table 5.3).[132]

Complex [M]	E_1	E_2	$\Delta E_{1/2}$	K_c(0/+1/+2)	E_3	E_4	[REF]
$Ru(PPh_3)_2Cp$	+0.18	+0.44	0.26	2.5×10^4	+0.61	+0.75	132
Ru(dppe)Cp	+0.16	+0.30	0.14	2.3×10^2	+0.66	+1.21[a]	132
Ru(dppe)Cp*	+0.02	+0.27	0.25	1.7×10^4	+0.59	+1.16[a]	132
$Ru[P(m\text{-tol})_3]_2Cp$	+0.12	+0.36	0.24	1.1×10^4	+0.69		This work

Table 5.3. *Cyclic voltammetry data for 1,1'-([M]C≡C)$_2$Rc', measured in 0.1M [Bu$^n_4$N][PF$_6$] in CH_2Cl_2 at 100mV s^{-1}.* [a] *Peak potential of a fully non-reversible wave.*

5.4. Conclusions.

This work summarises the synthesis of novel di-metallic ferrocenyl and tri-metallic ruthenocenediyl complexes **42** and **45**. Further reactions of these complexes with the electrophilic alkene TCNE produced either η^1-tetracyanobutadienyl or η^3-vinylcarbene complexes, which is confirmed by the X-ray crystal structure of **46**.

The cyclic voltammogram of **42** demonstrates significant interactions between the bridging moiety and the metal termini, observed by the large value of $\Delta E_{1/2}$, of 640 mV. The cyclic voltammogram of **45**, shows some interactions between the metal termini and the bridging moiety, demonstrated by the decoupling of the two termini, but acts as a total insulator when compared to straight-chain complexes such as $\{Cp^*(dppe)Ru\}_2(\mu\text{-}C{\equiv}C)_4$.

5.5. Experimental.

General experimental conditions are detailed on page 45.

Reagents: The compounds HC≡CFc,[133,134] RuCl[*m*-tol$_3$P]$_2$Cp,[135] and Rc'(C≡CTMS)$_2$[136] were all prepared using standard literature procedures. The compounds Na[BPh$_4$], TCNE, KF were all used as received from Aldrich.

Os(C≡CFc)(dppe)Cp (42).

A mixture of OsCl(dppe)Cp (62 mg, 0.093 mmol), HC≡CFc (32 mg, 0.152 mmol) and Na[BPh$_4$] (57 mg, 0.167 mmol) in MeOH (10 mL) was heated at reflux point for 18 h. After cooling in an ice bath, NaOMe [(Na (5 mg) in MeOH (2 mL)] was added dropwise and the mixture was stirred for 15 min. The solvent was then removed under vacuum and the residue purified by column chromatography (basic alumina, acetone-hexane 9/1) to give Os(C≡CFc)(dppe)Cp (61 mg, 78%) as an orange powder. IR (nujol, cm^{-1}): 2078 s ν(C≡C). ^{1}H NMR (*d*$_6$-benzene): δ 2.23-2.29, 2.51-2.62 (2 x m, 2 x 2H, dppe); 3.85 (s br, 7H, C$_5$H$_4$ + FcCp); 3.90 (s, 2H, C$_5$H$_4$); 4.62 (s, 5H, OsCp); 6.97-8.11 (m, 20H, Ph). ^{13}C NMR (*d*$_6$-benzene): δ 30.05-30.67 (m, CH$_2$ of dppe); 66.66, 70.69 (C$_5$H$_4$ of Fc); 69.72 (FcCp); 77.42 (C$_{ipso}$ of Fc); 78.62 (t, $^2J_{CP}$ 2.3 Hz, OsCp); 83.41 (t, $^2J_{CP}$ 18.6 Hz, C$_\alpha$); 102.15 (C$_\beta$); 126.62-143.89 (m, Ph). ^{31}P NMR (*d*$_6$-benzene): δ 47.2. ES-MS (positive ion, MeOH, *m/z*); 864, [M]$^+$; 655 [Os(dppe)Cp]$^+$.

Os{C[=C(CN)$_2$]=CFc=C(CN)$_2$}(dppe)Cp (46).

A mixture of Os(C≡CFc)(dppe)Cp (59 mg, 0.068 mmol) and TCNE (11 mg, 0.082 mmol) was stirred in benzene (10 mL) at r.t. for 24 h. The solvent was removed and the residue purified by preparative TLC (2% acetone, dichloromethane). A dark red-brown fraction was collected and identified as Os{C[=C(CN)$_2$]=CFc=C(CN)$_2$}(dppe)Cp (25 mg, 37%).

Anal. Calcd ($C_{49}H_{38}FeN_4OsP_2.0.5CH_2Cl_2$): C, 57.54; H, 3.80; N, 5.42. Found: C, 57.58; H, 3.88; N, 4.74. IR (nujol, cm^{-1}): 2214 s, 2199 s ν(CN); 1508 s ν(CC). ^1H NMR ($CDCl_3$): δ 2.00-2.50 (m, 4H, CH_2CH_2); 2.26, 3.98, 4.49, 5.53 (4 x m, 4 x 1H, C_5H_4); 4.13 (s, 5H, FeCp); 5.03 (s, 5H, OsCp); 6.41-6.47, 7.04-7.14, 7.26-7.58, 7.73, 7.89-7.95 (6 x m, 2 + 3 + 10 + 3 + 2H, Ph). ^{31}P NMR ($CDCl_3$): δ 29.0 (d, *J* 6.8 Hz); 40.7 (d, *J* 6.8 Hz) (AB q). ES-MS (positive ion, MeOH + NaOMe, *m/z*); 1015, $[M + Na]^+$; 655, $[Os(dppe)Cp]^+$.

1,1'-(Cp[*m*-tol$_3$P]$_2$RuC≡C)$_2$Rc' (45).

A degassed solution of RuCl[Pm-tol$_3$]$_2$Cp (171 mg, 0.232mmol), KF (12 mg, 0.207 mmol) and Rc'(C≡CTMS)$_2$ (49 mg, 0.116 mmol) were heated at reflux for 18 h. The precipitate was collected on a sinter and washed with methanol to afford 1,1'-(Cp[*m*-tol$_3$P]$_2$RuC≡C)$_2$Rc' as a yellow solid (182 mg, 86%). Anal. Calcd ($C_{108}H_{102}Ru_3P_4$): C, 71.00; H, 5.63, Found: C, 70.93, H, 5.61. IR (nujol, cm^{-1}); 2081 s ν(C≡C); 1591 m ν(C=C). ^1H NMR (d_6-benzene): δ 2.05 (s, 36H, tol); 4.54 and 5.12 (s, 2 x 4H, C_5H_4 of Rc); 4.58 (s, 10H, Cp); 6.84-7.71 (m, 48H, Ph). ^{31}P NMR (d_6-benzene): δ 51.8. ES-MS (positive ion, MeOH, *m/z*): 1827, $[M]^+$.

Reaction of 1,1'-(Cp[*m*-tol$_3$P]$_2$RuC$_2$)$_2$Rc with TCNE (47 and 48).

To a solution of 1,1'-(Cp[*m*-tol$_3$P]$_2$RuC$_2$)$_2$Rc (100 mg, 0.055 mmol) in dry dichloromethane (20 mL) was added TCNE (17 mg, 0.137 mmol) and the reaction mixture was stirred for 24 h. The solvent was removed under vacuum and the crude residue purified by preparative TLC (1% acetone / dichloromethane) to afford a mixture of **47** and **48** as an orange solid (36 mg, 44%). The ratio of diastereomers was 36:64. Anal. Calcd ($C_{78}H_{60}N_8Ru_3P_2$): C, 65.23; H, 3.91; N, 7.25, Found: C, 65.23; H, 3.98; N,

7.28. IR (nujol, cm^{-1}): 2213 s ν(CN); 1614 m ν(C=C). ES-MS (positive ion, MeOH, *m/z*): 1498, $[M + Na]^+$.

Minor isomer **47**

^1H NMR ($CDCl_3$): δ 2.44 (s, 36H, *m*-tol); 5.23 (s, 4H, C_5H_4 of Rc), 5.32, 5.92 (s, 2 x 2H, C_5H_4 of Rc); 4.63 (s, 10H, Cp); 7.18-7.41 (m, 48H, Ph). ^{31}P NMR ($CDCl_3$): δ 39.4.

Major isomer **48**

^1H NMR ($CDCl_3$): δ 1.30 (s, 36H, *m*-tol); 5.08, 5.23, 5.39, 6.09 (s, 2 x 4H, C_5H_4 of Rc); 4.65 (s, 10H, Cp); 7.18-7.41 (m, 48H, Ph). ^{31}P NMR ($CDCl_3$): δ 39.4.

Chapter Six

Some improved syntheses

(A) Osmium precursors

(B) Group 8 vinylidenes

A. New synthetic routes into osmium precursors.

A.6.1. Introduction.

There is increasing interest in the organometallic chemistry of osmium as the nature of the differences from its lighter congenor ruthenium becomes more apparent. The usual precursor for these complexes is osmium(VIII) oxide, OsO_4, a pale yellow solid (m.p. 31°C) which has an appreciable vapour pressure at ambient temperatures and which can cause severe physiological problems if appropriate care is not taken.[137,138] The use of dilute solutions for staining or other preparation of organic samples for histological study is well-known.[139] Conversion of OsO_4 to other starting materials has been documented from the rather insoluble $(NH_4)_2[OsBr_6]$ (by direct reduction with conc. aqueous HBr)[139] or $(NH_4)_2[OsCl_6]$ [by treatment with conc. HCl and Fe(II)][140].

The difficulty in reduction of OsO_4 directly by concentrated HCl has resulted in bromo-osmium complexes being generally prepared for use as precursors. The intermediate $H_2[OsBr_6]$ can be used for the synthesis of some cyclopentadienyl-osmium complexes, such as $OsBr(PPh_3)_2Cp$,[140] or $OsCp_2$,[141] the further reduction to osmium(II) being achieved with an excess of PPh_3 or zinc, respectively.

Recent changes to rules covering transport of hazardous materials by air have resulted in there being some reluctance to transport OsO_4 and other starting materials which are less dangerous have been sought. One of these is so-called "potassium osmate" which is formulated as the tetrahydroxo-dioxo-osmate(VI), $K_2[OsO_2(OH)_4]$. Conversion of OsO_4 to this salt is effected in ethanolic KOH.[142]

A.6.2. Aims of this work.

The primary aim of this work was to find a new synthetic route into suitable osmium reagents for organometallic synthesis from the more readily available potassium osmate $K_2[OsO_2(OH)_4]$ (**49**). X-ray structure determinations of both OsCl(dppe)Cp (**44**) and OsCl(dppe)Cp* (**13**) are reported along with their electrochemistry and comparison to other related group 8 complexes.

A.6.3. Results and Discussion.

A.6.3.1. Synthesis of organo-osmium starting materials.

Previously the synthesis of OsBr(dppe)Cp* (**50**) has been described through the reduction of OsO_4 by HBr.[131] Starting from potassium osmate instead, it is possible to reduce the osmium by refluxing it in concentrated HCl overnight. The excess HCl is removed by distillation to leave a brick-red solid, which is assumed to be $K_2[OsCl_6]$. This brick-red osmium salt can be treated with either triphenylphosphine or pentamethylcyclopentadiene depending on the desired product (see Scheme 6.1).

Reaction of $K_2[OsCl_6]$ with PPh_3 in refluxing aqueous *t*-butanol for 18 h resulted in the precipitation of green $OsCl_2(PPh_3)_3$ (**51**) in 99% yield. The PPh_3 plays an important role in this reaction as it not only acts as a co-ordinating ligand, but as the reducing agent as well. This complex has also been made from the reaction of $(NH_4)_2[OsCl_6]$ with PPh_3 in aqueous *t*-butanol.{Elliott #149}

Addition of the cyclopentadienyl group was achieved through the treatment of $OsCl_2(PPh_3)_3$ with LiCp, which was synthesised through the reaction of ^{n}BuLi with CpH for 15 min in THF. After removal of the solvent the residue was extracted into a minimal amount of benzene and purified by column chromatography (silica gel). Excess PPh_3 was removed with elution of hexane and pure yellow $OsCl(PPh_3)_2Cp$ (**52**),[144] was eluted with a 10% acetone-hexane mixture.

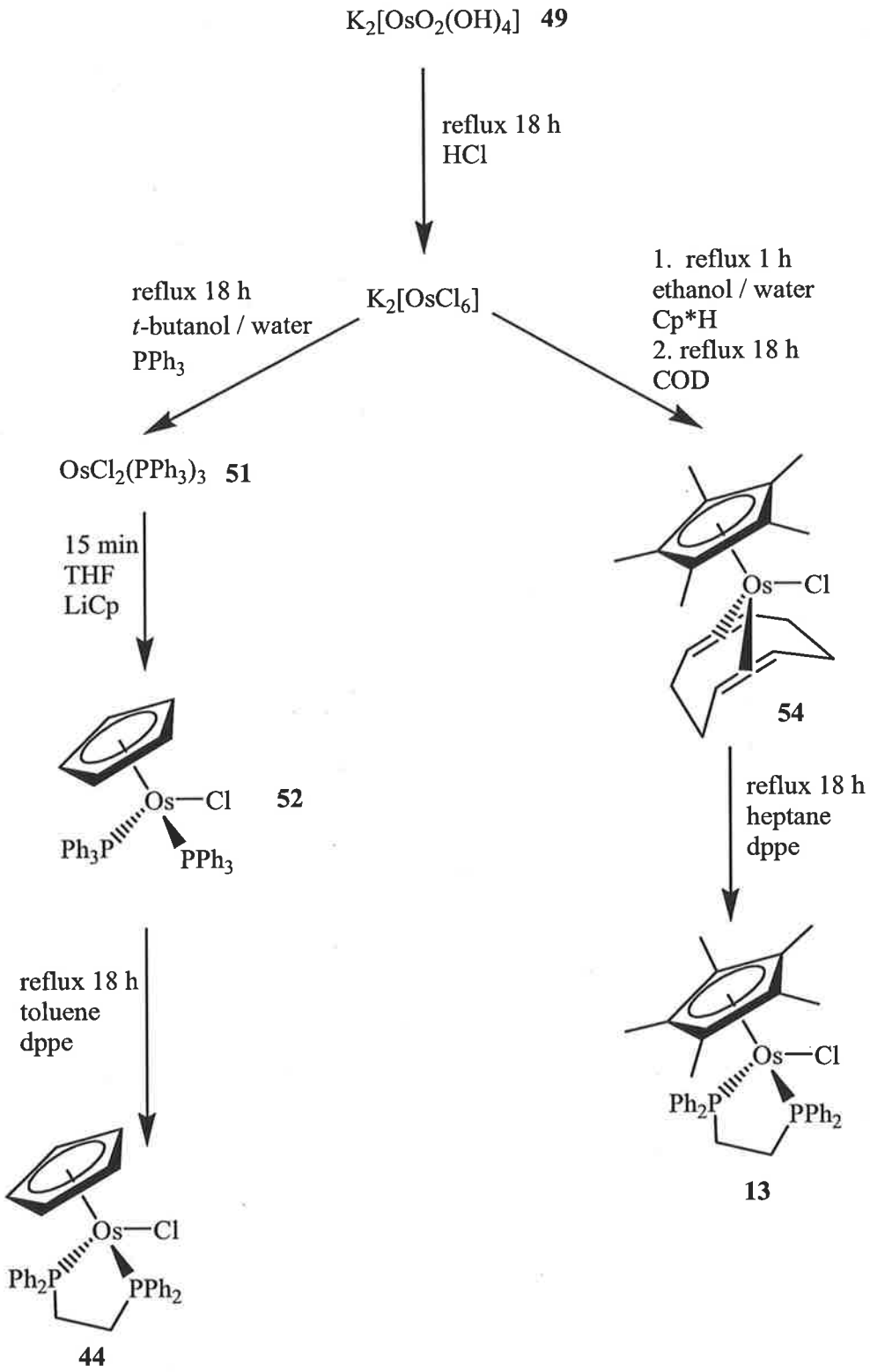

Scheme 6.1. *Synthetic routes to both OsCl(dppe)Cp and OsCl(dppe)Cp* from $K_2[OsO_2(OH)_4]$.*

The ready exchange of PPh_3 ligands for dppe has been demonstrated before from $RuCl(PPh_3)_2Cp$ (**53**) to RuCl(dppe)Cp (**16**).[100] The use of benzene, as described previously, affords a mixture of the desired product and starting material However heating both reactants (**51** and dppe) in refluxing toluene overnight yielded a suspension, which was filtered and the filtrate chromatographed to afford pure yellow **44** in 81% yield. The solid which was filtered from the reaction mixture may be the dimer $[OsCl(dppe)Cp]_2$, which is observed in the ligand exchange of **53** with dppe to **16**.[100]

The pentamethylcyclopentadienyl analogue was prepared by treatment of $K_2[OsCl_6]$ with a degassed solution of pentamethylcyclopentadiene in aqueous ethanol. The mixture was heated at reflux point for 1 h before the addition of 1,5-cyclooctadiene and refluxing continued for a further 18 h. After this time the solvent was evaporated under vacuum and the residue extracted with hot diethyl ether. Again the solvent was removed to yield an orange residue, which is most likely OsCl(COD)Cp* (**54**). This residue was then treated directly with a solution of dppe in heptane and heated at reflux for 18 h. The resulting suspension was filtered to give **13**, chromatography (silica gel) of the filtrate afforded a further amount of pure yellow **13** (total yield of 61%).

A.6.3.2. Spectral properties.

The ^1H NMR spectra for **52** and **44** show multiplets between δ 7.39-7.15 and δ 8.02-6.84 respectively, corresponding to the aromatic protons on the phenyl groups. Multiplets for the CH_2CH_2 groups in dppe were found at δ 2.41-2.33 and δ 2.22-2.14. The Cp protons were found as singlets at δ 4.37 and 4.52 for **52** and **44** respectively. The small shift downfield is a result on the more electron-donating affect of the dppe in comparison to the two PPh_3 ligands.

The ^1H NMR spectrum of **13** shows multiplets between δ 7.82-7.05 corresponding to the aromatic protons in dppe, while multiplets between δ 2.59-2.49 and δ 2.09-1.97 are assigned to the CH_2CH_2 protons in dppe. The ^1H NMR spectra of **50** showed multiplets

in similar regions to **13** between δ 7.92-6.97, 2.62 and 2.09 all corresponding to the relevant protons of dppe.[131] Singlets arising from the Cp* protons are found at δ 1.57 and 1.61 for **13** and **50**, respectively.

The ^{13}C NMR spectra for **44** and **13** show resonances at δ 143.56-128.07 and 140.78-127.77 for the aromatic carbons on the phenyl groups in dppe. Carbons of the Cp group appear as a triplet ($^2J_{CP}$, 2.5 Hz) at δ 75.75. The Cp* ring carbons of **13** give a triplet at δ 86.10 ($^2J_{CP}$, 2.6 Hz). The CH_2CH_2 carbons of the dppe bridge also show coupling to the phosphorus atoms appearing as multiplets at δ 30.44-29.12 and 31.24-30.63 for **44** and **13**, respectively. The other carbons in the Cp* ligand for **13** occur as a singlet at δ 10.18. These regions are very similar to those seen for **50**.

The ^{31}P NMR spectra show a shift from δ -1.2 to 46.6, with the ligand exchange from PPh_3 to dppe, in **52** to **44** respectively. Exchange of Cp for Cp* has little effect with singlets arising in the ^{31}P NMR spectra at δ 43.4 and 43.0 for **13** and **50**, respectively.

Both **52** and **44** undergo very similar fragmentations in their mass spectra, with ions corresponding to $[M - Cl]^+$ at *m/z* 781 and 655 respectively. Complex **52** also undergoes loss of PPh_3 (*m/z* 519 $[OsPPh_3Cp]^+$). The mass spectrum of **13** displays peaks at *m/z* 760 corresponding to $[M]^+$, and at m/z 725, which corresponds to loss of Cl ($[M - Cl]^+$).

A.6.3.3. Molecular structures.

In the course of this work the molecular structures of **44** and **13** (crystallised from dichloromethane / hexane) were determined. These molecules are illustrated in Figure 6.1 and selected bond distances are presented in Table 6.1 and 6.2, together with values previously reported for the associated ruthenium analogues. As can be seen, these are further examples of Group 8 complexes of the type MX(PP)Cp', all having pseudo-octahedral geometry at the metal centre.

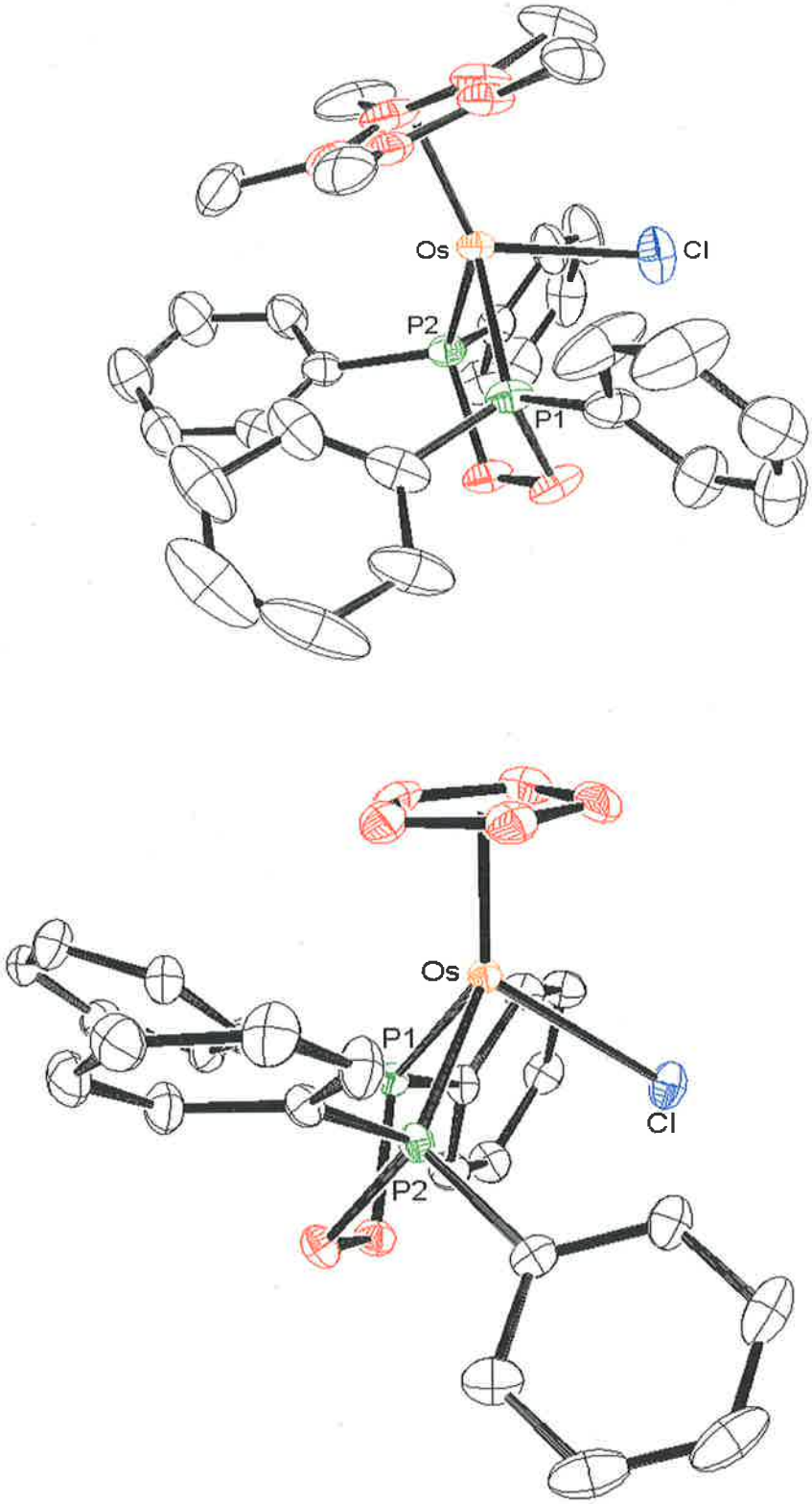

Figure 6.1. *ORTEP diagram of Top: OsCl(dppe)Cp* and Bottom: OsCl(dppe)Cp.*

The structure of $OsBr(PPh_3)_2Cp$ (**55**) as its dichloromethane solvate has been reported previously, together with the isomorphous and isostructural ruthenium compound.[145,146] The present study was carried out on solvent-free crystals and shows some significant differences in the coordination geometry around the osmium centre. As expected, the similarity of the covalent radii of ruthenium and osmium (Ru: 1.26, Os 1.28 Å)[147] results in there being essentially no differences in the M-P and M-Cl bond lengths in MCl(dppe)Cp and MX(dppe)Cp*, with the exception of the Os-Br and Ru-Cl bonds in the latter, which differ by 0.13 Å (cf. the difference in covalent radii of Cl and Br, 0.15 Å). The M-C(cp) distances are somewhat shorter than the M-C(cp*) separations on account of the increased bulk of the permethylated ligand. Significant differences are found in the P-M-X angle pair between the PPh_3 and dppe complexes, contingent on the effects of the Ru-P-C-C-P ring conformation in the latter.

Complex	**53**[148]	**52**[145]	**17**[149]	**44**	**4**[31]	**13**
MX	RuCl	OsCl	RuCl	OsCl	RuCl	OsCl
PP	$(PPh_3)_2$	$(PPh_3)_2$	dppe	dppe	dppe	dppe
Cp'	Cp	Cp	Cp	Cp	Cp*	Cp*
Solvate	CH_2Cl_2	CH_2Cl_2	$CHCl_3$	CH_2Cl_2	-	-
Bond distances (Å)						
M-P(1)	2.323(1)	2.320(2)	2.2688(7)	2.2705(7)	2.2882(5)	2.2714(9)
M-P(2)	2.329(1)	2.319(2)	2.2863(7)	2.2797(7)	2.2812(5)	2.2694(8)
M-X	2.448(1)	2.460(2)	2.4466(7) [Cl]	2.4488(8) [Cl]	2.4532(5) [Cl]	2.4437(9) [Cl]
M-C(Cp)	2.159-2.218(3)	2.183-2.235(6)	2.169-2.227(4)	2.172-2.243(4)	2.219-2.252(2)	2.214-2.250(4)
(av.)	2.20(1)	2.21(2)	2.20(3)	2.22(5)	2.24(1)	2.230(14)
Bond angles (°)						
P(1)-M-P(2)	103.79(3)	103.23(6)	83.48(2)	83.43(3)	82.15(2)	82.12(3)
P(1)-M-X	88.29(3)	88.44(6) [Cl]	83.04(3) [Cl]	84.00(3) [Cl]	81.93(2) [Cl]	82.22(3) [Cl]
P(2)-M-X	89.15(3)	89.77(5) [Cl]	93.28(3) [Cl]	93.33(3) [Cl]	90.93(2) [Cl]	90.74(3) [Cl]

Table 6.1. *Selected bond distances (Å) and angles (°) in MX(PP)Cp'.*

Complex	**53-Br**[146]	**52-Br**[131]	**4-Br**[146]	**50**[131]	**13/50**[131]
MX	RuBr	OsBr	OsBr	OsBr	Os(Br/Cl)
PP	$(PPh_3)_2$	$(PPh_3)_2$	$(PPh_3)_2$	dppe	dppe
Cp'	Cp	Cp	Cp	Cp*	Cp*
Solvate	CH_2Cl_2	-	CH_2Cl_2	-	-
Bond distances (Å)					
M-P(1)	2.323(2)	2.327(2)	2.290(2)	2.2870(6)	2.2851(5)
M-P(2)	2.329(2)	2.318(2)	2.297(2)	2.2780(7)	2.2781(5)
M-X	2.5683(8) [Br]	2.585(1) [Br]	2.5438(9) [Br]	2.5818(4) [Br]	2.5708(3) [Br/Cl]
M-C(Cp)	2.172-2.220(5)	2.19-2.24(1)	2.150-2.197(6)	2.229-2.260(3)	2.228-2.261(2)
(av.)	2.20(2)	2.22(2)	2.18(2)	2.242(13)	2.240(14)
Bond angles (°)					
P(1)-M-P(2)	103.18(5)	104.28(8)	103.13(7)	82.11(2)	82.13(2)
P(1)-M-X	88.36(4) [Br]	89.50(6) [Br]	88.45(5) [Br]	82.39(2) [Br]	82.42(1) [Br/Cl]
P(2)-M-X	90.77(4) [Br]	90.94(6) [Br]	90.48(5) [Br]	91.84(2) [Br]	91.95(1) [Br/Cl]

Table 6.2. *Selected bond distances (Å) and angles (°) in MX(PP)Cp'.*

A.6.3.4. Electrochemisty.

The successful synthesis of **13** and **44** completes the Group 8 series of the general formula MCl(dppe)Cp' (where M = Fe Cp' = Cp[101] / Cp*,[122] M = Ru, Cp' = Cp[100] / Cp*,[72,119] M = Os Cp' = Cp / Cp*). This allows the direct comparison of their redox properties and a determination of the effect of the exchange of Cp for Cp* and the differences that occur due to the change of metal down the group (for comparison all CV's were remeasured using the same potentiostat and cell setup).

From the data summarised in Table 6.3 there are several interesting comparisons that can be drawn. Looking down the series of complexes for either Cp or Cp*, the first oxidation potential (M(II) / M(III)) does not increase uniformly on going from Fe to Os. Instead the ease of oxidation increases as Fe > Os > Ru (see Graph 6.1). As expected on changing of Cp for the more electron-donating Cp* ligand, the first oxidation becomes easier by approximately 280 (Fe), 220 (Ru) and 210 mV (Os)(see Graph 6.1). Second oxidation events are not observed for all complexes, which may be a result of an electrochemical reaction occuring after the first redox event within the cell making these processes either quasi or fully non-reversible.

Complex	E_1	E_2
FeCl(dppe)Cp	+0.04	+0.68[a]
FeCl(dppe)Cp*	-0.24	
RuCl(dppe)Cp	+0.46	
RuCl(dppe)Cp*	+0.28	+1.37[a]
OsCl(dppe)Cp	+0.38	+1.18[b]
OsCl(dppe)Cp*	+0.17	+1.19[b]

Table 6.3. *Redox potentials (V) of FeCl(dppe)Cp,* **23**, **17**, **4**, **44** *and* **13** *recorded in 0.1 M* $[Bu^n_4N][PF_6]$ */* CH_2Cl_2 *at 100 mV* s^{-1}*, 293 K using Pt electrodes.* [a] *Peak potential of a fully non-reversible process.* [b] *Peak potential of a quasi-reversible process.*

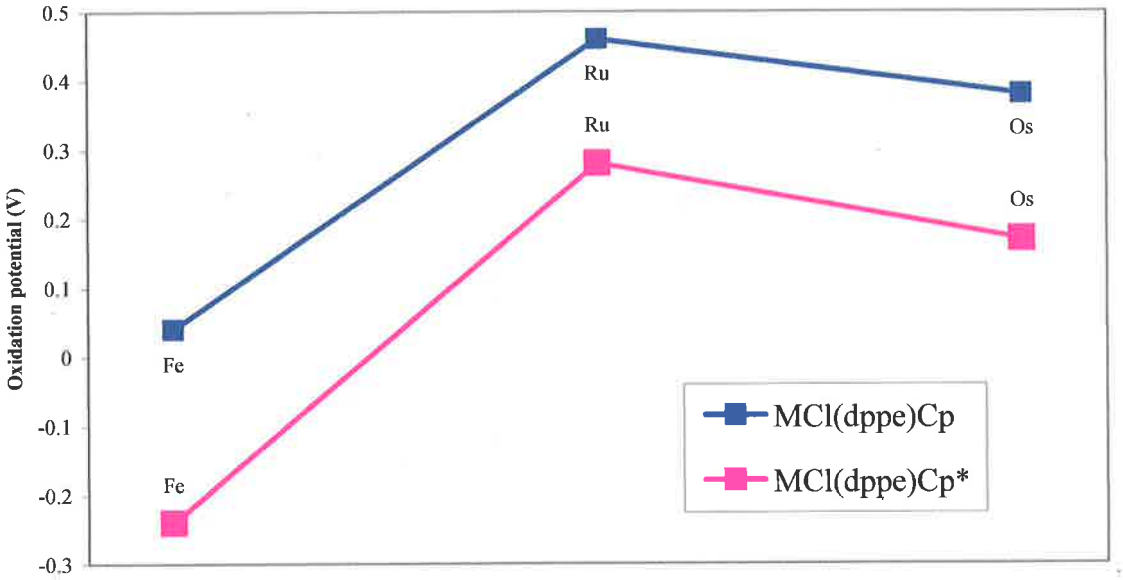

Graph 6.1. *First oxidation potentials of the group 8 series MCl(dppe)Cp', where M = Fe, Ru, Os, and Cp' = Cp / Cp*.*

The first redox event for all complexes was found to be fully reversible and ranges from –0.24 V in FeCl(dppe)Cp* (**22**) to +0.46 V in RuCl(dppe)Cp (**16**) (see Table 6.3). The osmium complexes **43** and **12** show two redox events at +0.38 V (fully reversible) and at +1.18 V (quasi reversible) for **43** and at +0.17 V (fully reversible) and +1.19 (quasi reversible) (see Figure 6.2).

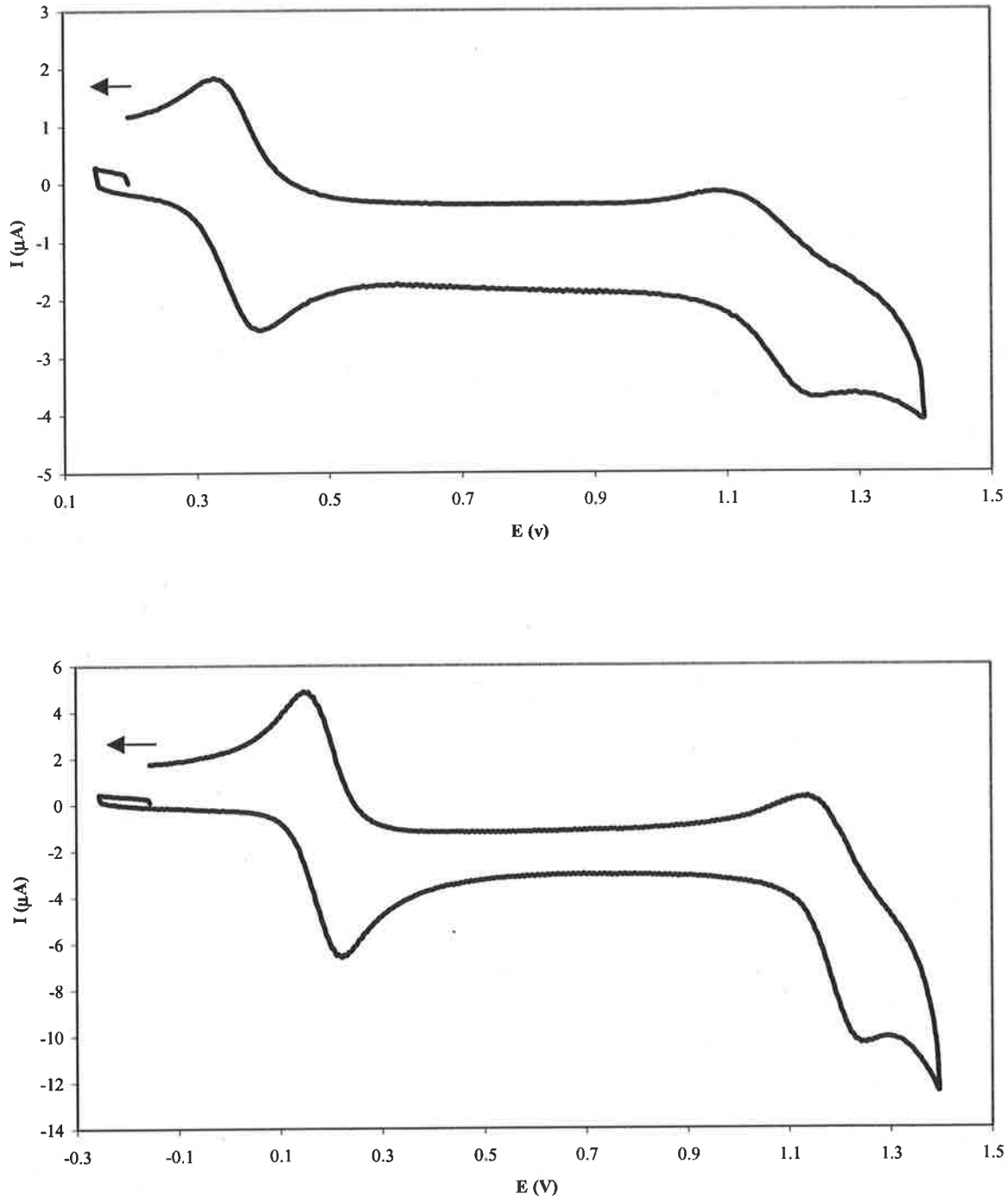

Figure 6.2. *Cyclic voltammograms of Top:* ***44****, Bottom:* ***13****, recorded in 0.1M* $[Bu^n_4N][PF_6]$ *in* CH_2Cl_2 *at 100 mV* s^{-1}.

A.6.4. Conclusions.

The synthesis of OsCl(dppe)Cp and OsCl(dppe)Cp* was achieved starting from potassium osmate (see Scheme 6.1). Single-crystal X-ray structure determinations revealed marked similarities to both ruthenium analogues (see Table 6.1 and 6.2). These two osmium complexes have significantly lower first oxidation potentials than their ruthenium analogues instead of a continuing increase from iron to osmium as was expected.[74]

B. Improved syntheses of some Group 8 vinylidene complexes.

B.6.1. Introduction.

Group 8 vinylidene complexes of the general formula [Cp'(dppe)M=C=CH_2][PF_6] (where M = Ru Cp' = Cp, and M = Os Cp' = Cp*) have been previously prepared in solvents such as dichloromethane.[131,150] Mixtures of the halide starting material are heated at reflux point for three days in a sealed flask in the presence of TMSC≡CH, which must be done behind a safety shield due to the possibility of explosion. However both [Cp*(dppe)M=C=CH_2][PF_6] (where M = Ru and Fe)[30,31] have been synthesised using methanol with a dramatic decrease in the reaction times.

B.6.2. Aims of this work.

The aim of this work is to use a bulky alcohol solvent, such as ^{t}BuOH, for the synthesis of several vinylidene complexes containing Group 8 metals of the general formula [Cp'(dppe)M=C=CH_2][PF_6] (where M = Ru, Fe Cp' = Cp and M = Os Cp' = Cp/Cp*) and thereby overcome the problematic and dangerous synthesis that have been designed previously.

B.6.3. Results and discussion.

B.6.3.1. Synthesis of vinylidene complexes.

The vinylidene complexes $[Cp(dppe)M{=}C{=}CH_2][PF_6]$ (where M = Fe (**56**), Ru (**57**), Os (**58**)) were prepared from the reactions of the corresponding chloro complexes and TMSC≡CH in ^{t}BuOH, in the presence of $[NH_4][PF_6]$ proceeding in 90, 91 and 56% yields respectively. For the Cp* derivative, $[Cp^*(dppe)Os{=}C{=}CH_2][PF_6]$ (**59**), this same reaction was carried out in MeOH instead with a 85% yield. These reactions proceed quickly (within 4 h) with the products precipitating directly as the PF_6 salts from the hot reaction mixture.

Complex **57** has been previously synthesised using dichloromethane instead of ^{t}BuOH.[150] The use of dichloromethane not only increases the reaction time to 3 d, but also must be done in a sealed flask to prevent evaporation of the volatile TMSC≡CH. This sealed flask was then heated to reflux, which must be done behind a safety shield for protection against explosion. The use of the high boiling ^{t}BuOH allows the reaction to be done with an effective condenser instead of the sealed flask because the reaction times are much shorter than those needed when using dichloromethane.

Due to the steric protection that Cp* gives when compared to Cp, **59** was synthesised using methanol instead of ^{t}BuOH. This lack of steric protection given by Cp prevents the use of primary alcohols, such as MeOH, in the preparation of $[Cp(dppe)M{=}C{=}CH_2][PF_6]$ (where M = Fe, Ru, Os) because the complex is rapidly converted into the corresponding methoxy-carbene complex (see Scheme 6.2).[150]

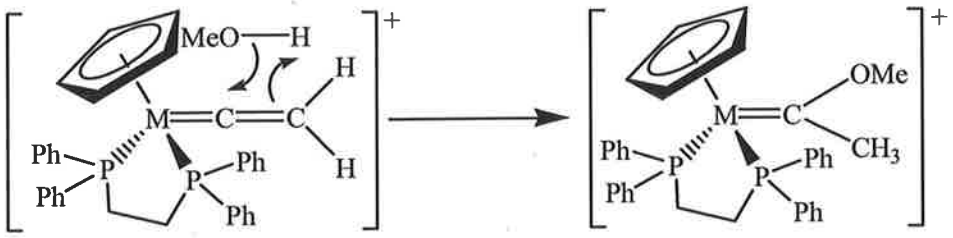

Scheme 6.2. *MeOH addition to* $[Cp(dppe)M{=}C{=}CH_2]^+$.

B.6.3.2. Spectroscopic properties of vinylidene complexes.

Most informative in the IR spectra was the ν(C=C) stretching bands. For complexes **56**, **57**, **58** and **59** this band appears at 1626, 1640, 1641, and 1633 cm^{-1}, respectively. A noticeable difference can be seen in this band between iron and ruthenium, but not between ruthenium and osmium. There is a small difference also observed with the exchange from Cp to Cp*, as a result of the more electron-donating nature of Cp*. All spectra contained ν(PF) at ca 840 cm^{-1}.

The ^{1}H NMR spectra of **56**, **57**, **58** and **59** are all similar. Multiplets are observed between δ 7.73-7.42, 7.83-7.34, 7.91-7.14, and 7.63-7.24 for **56**, **57**, **58** and **59** respectively, corresponding to the aromatic protons of the dppe ligand. The Cp protons all appear at δ 5.25 (**56**), δ 5.65 (**57**), and δ 5.76 (**58**), while for **59** the Cp* protons appear at δ 1.74. The CH_2CH_2 protons of dppe appear as multiplets at δ 3.37-3.06 (**56**), δ 3.24-3.08 (**57**), δ 3.22-2.94 (**58**), and δ 3.06-2.86 (**59**). Significant differences are found in the vinylidene protons, which are found at δ 3.99 (**56**), 3.20 (**57**), 0.62 (**58**) and 0.60 (**59**). Those for **57** and **58** are triplets ($^{4}J_{HP}$, 1.5 Hz) and ($^{4}J_{HP}$, 0.2 Hz), respectively.

In the ^{13}C NMR spectra significant deshielding is found for C_α. This is seen with a dramatic downfield shift to δ 354.71, 342.28 and 302.91 in **56**, **57** and **58** respectively. The dramatic deshielding is a result of the large HOMO-LUMO energy gap rather than the electron-deficient nature of C_α, which has been shown by theoretical studies.[74] The aromatic carbons in the dppe ligand give multiplets between δ 137.47-129.42, 137.27-129.47 and δ 139.29-126.73 for **56**, **57** and **58** respectively. This similarity is also seen in the Cp carbons at δ 90.15 for **56**, δ 93.19 for **57** and δ 90.79 for **58**. Carbon C_β is observed at δ 106.93 for **56**, δ 96.56 for **57** and δ 95.06 for **58**. The CH_2CH_2 bridging carbons in dppe are not seen because of the NMR solvent (d_6-acetone ca δ 30), which masks these peaks.

The ^{31}P NMR are very similar, all containing a peak at ca δ –142 (septet) from the PF_6 anion. For the dppe ligand peaks appeared at δ 97.9, δ 80.7, δ 42.9, and δ 40.7 for **56**, **57**,

58 and **59** respectively. Only a small difference between **58** and **59** results from exchanging Cp for Cp*.

The mass spectra for the two vinylidenes **56** and **58** contain parent ions at *m/z* 545 and 681, assigned to the cations $[Cp(dppe)M=C=CH_2]^+$, respectively. Both show fragmentation by loss of $=C=CH_2$ to give $[M(dppe)Cp]^+$ at *m/z* 519 and 655 for **56** and **58**, respectively.

B.6.4. Conclusions.

In summary, this work has demonstrated an improved synthetic approach to form vinylidenes containing unprotected carbon chains, as in the cases of **56**, **57** and **58**. The use of ^{t}BuOH or methanol, which are higher boiling solvents than dichloromethane aids in the ionization of the metal-halide bond.

6.5. Experimental.

General experimental conditions are detailed on page 45.

Reagents: The compounds TMSC≡CH,[90] RuCl(dppe)Cp,[100] FeCl(dppe)Cp,[101] LiCp,[151] and dppe[108]were all prepared using standard literature procedures. The compound $K_2[OsO_4(OH_2)_2]$ was used as received from Johnson Matthey. The compounds PPh_3, Cp*H, $[NH_4][PF_6]$ were used as received from Aldrich.

$OsCl_2(PPh_3)_3$ (51).

A solution of $K_2[OsO_4(OH_2)_2]$ (2.00 g, 5.43 mmol) in conc. HCl (300 ml) was heated at reflux for 18 h. Excess HCl was distilled away and a degassed solution of PPh_3 (10.00 g, 38.13 mmol) in ^{t}BuOH (420 ml) and water (150 ml) was added to the solid residue. After heating at reflux point for 18 h, after which time a green suspension had formed, the mixture was cooled and the precipitate filtered off, washed with EtOH and hexane and dried under vacuum to yield $OsCl_2(PPh_3)_3$ (5.63g, 99%).

$OsCl(PPh_3)_2Cp$ (52).

To a solid mixture of LiCp (30 mg, 0.45 mmol: from ^{n}BuLi and C_5H_6 in hexane, followed by filtration of the white LiCp and drying) and $OsCl_2(PPh_3)_3$ (468 mg, 0.45 mmol) was added THF (50 mL) and the solution stirred for 15 min. After removal of the solvent under vacuum, the residue was taken up in a minimum amount of benzene and chromatographed (silica gel). Eluting with hexane removed excess PPh_3 as the first fraction and 10% acetone/hexane eluted yellow $OsCl(PPh_3)_2Cp$ (279 mg, 76%). ^{1}H NMR ($CDCl_3$): δ 7.39-7.15 (m, 30H, PPh_3); 4.37 (s, 5H, Cp). ^{31}P NMR ($CDCl_3$): δ -1.2 (s, 2P, PPh_3). ES-MS (positive ion mode, MeOH, *m/z*): 781, $[Os(PPh_3)_2Cp]^+$; 519, $[Os(PPh_3)Cp]^+$.

OsCl(dppe)Cp (44).

A solution of $OsCl(PPh_3)_2Cp$ (1.8 g, 2.2 mmol) and dppe (964 mg, 2.42 mmol) in toluene (100 ml) was heated at reflux point for 18 h. The mixture was filtered and the filtrate was chromatographed on silica gel, washing off displaced PPh_3 with hexane and eluting the product with 10% acetone/hexane to give yellow OsCl(dppe)Cp (1.23 g, 81%). Anal. Found: C, 49.63; H, 4.10. Calcd ($C_{36}H_{39}ClOsP_2.CH_2Cl_2$): C, 49.65; H, 4.04. IR (nujol, cm^{-1}): 1306w, 1180w, 1095s, 1026w, 998w, 791m, 749m, 696s, 671w. ^1H NMR (d_6-benzene): δ 8.02-6.84 (m, 20H, Ph); 4.52 (s, 5H, Cp); 2.41-2.33 (m, 2H, CH_2CH_2); 2.22-2.14 (m, 2H, CH_2CH_2). ^{13}C NMR (d_6-benzene): δ 143.56-128.07 (m, Ph); 75.75 (t, $^2J_{CP}$, 2.5 Hz, Cp); 30.44-29.12 (m, CH_2CH_2). ^{31}P NMR (d_6-benzene): δ 46.6. ES-MS (positive ion mode, MeOH, *m/z*): 655, $[Os(dppe)Cp]^+$.

OsCl(dppe)Cp* (13).

A solution of $K_2[OsO_4(OH_2)_2]$ (138 mg, 0.42 mmol) in conc. HCl (20 ml) was heated at reflux point for 18 h. The excess HCl was then distilled away before adding a degassed solution of pentamethylcyclopentadiene (0.1 mL, 0.62 mmol) in aqueous ethanol (2 + 15 mL). This mixture was heated at reflux point for 1 h, 1,5-cyclooctadiene (0.26 mL, 2.10 mmol) was added and the mixture heated for a further 18 h. After removal of the solvent, the residue was extracted with hot Et_2O and the filtered solution was again evaporated. After the addition of dppe (182 mg, 0.46 mmol) in heptane (20 mL) and heating at reflux point for 18 h, the yellow precipitate which had separated was filtered off (176 mg). The filtrate was then chromatographed (silica gel column, eluted with 1% acetone-hexane) to give a further amount of yellow OsCl(dppe)Cp* (total yield 192 mg, 61%). Anal. Found: C; 56.83, H; 5.23. Calcd ($C_{36}H_{39}P_2ClOs$): C; 56.95, H; 5.18. IR (nujol, cm^{-1}): 1306w, 1155w, 1094s, 1027m, 867w, 788m, 744s, 693s, 668vs, 646w. ^1H NMR (d_6-benzene): δ 7.82-7.05 (m, 20H, Ph); 2.59-2.49, 2.09-1.97 (2 x m, 2 x 2H, CH_2CH_2); 1.57 (s, 15H, Cp*). ^{13}C NMR (d_6-benzene): δ 140.78-127.77 (m, Ph); 86.10 (t, $^2J_{CP}$, 2.6 Hz, C_5Me_5);

31.24-30.63 (m, CH_2CH_2); 10.18 (s, C_5Me_5). ^{31}P NMR (d_6-benzene): δ 43.4. ES-MS (positive ion mode, *m/z*): 760, $[M]^+$; 725, $[Os(dppe)Cp^*]^+$.

[Cp(dppe)Fe=C=CH$_2$][PF$_6$] (56).

A solution of FeCl(dppe)Cp (500 mg, 0.90 mmol), $[NH_4][PF_6]$ (294 mg, 1.80 mmol) and TMSC≡CH (0.64 mL, 4.50 mmol) in ^{t}BuOH (10 mL) was heated at reflux point for 2 h before filtering off the resulting precipitate and washing with Et_2O to yield $[Cp(dppe)Fe=C=CH_2](PF_6)$ (559 mg, 90%). IR (nujol, cm^{-1}): 1626 w ν(=C=C); 842 s ν(PF). ^1H NMR (d_6-acetone): δ 7.73-7.42 (m, 20H, Ph); 5.25 (s, 5H, Cp); 3.99 (s, 2H, $=C=CH_2$); 3.37-3.06 (m, 4H, CH_2CH_2). ^{13}C NMR (d_6-acetone): δ 354.71 (t, $^2J_{CP}$ 33 Hz, C_α); 137.47-129.42 (m, Ph); 106.93 (s, C_β); 90.15 (s, Cp). ^{31}P NMR (d_6-acetone): δ 98.0 (s, dppe); -142.4 (septet, $^1J_{PF}$ 703 Hz, PF_6). ES-MS (positive ion mode, MeOH, *m/z*): 545, $[Fe=C=CH_2(dppe)Cp]^+$; 519, $[Fe(dppe)Cp]^+$.

[Cp(dppe)Ru=C=CH$_2$][PF$_6$] (57).

Similarly a solution of RuCl(dppe)Cp (500 mg, 0.83 mmol), $[NH_4][PF_6]$ (272 mg, 1.67 mmol) and TMSC≡CH (0.59 mL, 4.15 mmol) in ^{t}BuOH (10 mL) yielded $[Cp(dppe)Ru=C=CH_2](PF_6)$ (554 mg, 91%). IR (nujol, cm^{-1}): 1640 w ν(=C=C); 839 s ν(PF). ^1H NMR (d_6-acetone): δ 7.83-7.34 (m, 20H, Ph); 5.65 (s, 5H, Cp); 3.24-3.08 (m, 4H, CH_2CH_2); 3.20 (t, $^4J_{HP}$ 1.5 Hz, 2H, $=C=CH_2$). ^{13}C NMR (d_6-acetone): δ 342.28 (t, $^2J_{CP}$ 17 Hz, C_α); 137.27-129.47 (m, Ph); 96.56 (s, C_β); 93.19 (s, Cp). ^{31}P NMR (d_6-acetone): δ 80.8 (s, dppe); -142.4 (septet, $^1J_{PF}$ 703 Hz, PF_6). Lit values:[150] IR (nujol, cm^{-1}): 1641 w ν(C=C); 841 s ν(PF). ^1H NMR (CD_2Cl_2): δ 7.57-7.16 (m, 20H, Ph); 5.37 (s, 5H, Cp); 3.19 (t, $^4J_{HP}$ 1.5 Hz, 2H, $=C=CH_2$); 2.95 (m, 4H, CH_2CH_2).

[Cp(dppe)Os=C=CH$_2$][PF$_6$] (58).

A solution of OsCl(dppe)Cp (100 mg, 0.145 mmol), [NH$_4$][PF$_6$] (48 mg, 0.29 mmol) and TMSC≡CH (0.1 mL, 0.725 mmol) in ^{t}BuOH (2.5 mL) was heated at reflux point for 4 h before the solvent was removed under vacuum. The residue was dissolved in a minium amount of CH_2Cl_2 and filtered into Et_2O. The resulting precipitate was collected to yield [Cp(dppe)Os=C=CH$_2$](PF$_6$) (40 mg, 56%). The filtrate was then submitted to silica gel column chromatography eluting with 30% acetone/hexane to recover unreacted OsCl(dppe)Cp (40 mg). IR (nujol, cm^{-1}): 1641 w ν(=C=C); 837 s ν(PF). ^{1}H NMR (d_6-acetone): δ 7.91-7.14 (m, 20H, Ph); 5.76 (s, 5H, Cp); 3.22-2.94 (m, 4H, CH_2CH_2); 0.62 (t, $^4J_{HP}$ 0.2 Hz, 2H, =C=CH_2). ^{13}C NMR (d_6-acetone): δ 302.91 (s, C_α); 139.29-126.73 (m, Ph); 95.06 (s, C_β); 90.79 (s, Cp). ^{31}P NMR (d_6-acetone): δ 42.9 (s, dppe); -141.6 (septet, $^1J_{PF}$ 703 Hz, PF_6). ES-MS (positive ion mode, MeOH, *m/z*): 681, [Os=C=CH$_2$(dppe)Cp]$^+$; 655, [Os(dppe)Cp]$^+$.

[Cp*(dppe)Os=C=CH$_2$][PF$_6$] (59).

Similarly a solution of OsCl(dppe)Cp* (160 mg, 0.211 mmol), [NH$_4$][PF$_6$] (69 mg, 0.422 mmol) and TMSC≡CH (0.14 mL, 1.054 mmol) in MeOH (15 mL) heated at reflux for 3 h yielded [Cp*(dppe)Os=C=CH$_2$](PF$_6$) (160 mg, 85%). IR (nujol, cm^{-1}): 1633 w ν(=C=C); 836 s ν(PF). ^{1}H NMR (d_6-acetone): δ 7.63-7.24 (m, 20H, Ph); 3.06-2.86 (m, 4H, CH_2CH_2); 1.74 (s, 15H, Cp*); 0.60 (s, 2H, CCH_2). ^{31}P NMR (d_6-acetone): δ 40.8 (s, dppe); -142.5 (septet, $^1J_{PF}$ 703 Hz, PF_6). Lit values;[131] IR (nujol, cm^{-1}): 1633 w ν(C=C), 836 s ν(PF). ^{1}H NMR (CD_2Cl_2): δ 7.65-7.15 (m, 20H, Ph); 2.94-2.70 (m, 4H, CH_2CH_2); 1.73 (t, $^4J_{HP}$ 10.3 Hz, 15H, Cp*); 0.66 (s, 2H, CCH_2). ^{31}P NMR ($CDCl_3$): δ 40.8 (s, dppe); -143.2 (septet, $^1J_{PF}$ 711Hz, PF_6).

General Conclusions.

In summary this Thesis describes a rich study of Group 8 alkynyl organometallic complexes, which serves to increase the understanding of the chemistry of these complexes. The use of electron donating ligands, such as Cp*, Cp and dppe, has provided a wide variety of termini that are redox-active, allowing further investigation by cyclic voltammetry. This process has enabled the electronic interactions between the two metal termini along the bridge to be evaluated and comparisons to be drawn with related complexes.

The series of complexes of the general formula $[LM](C{\equiv}C)_n[M'L'_m]$ (where n = 1, 2) show very strong interactions between the two metal termini. The addition of an extra carbon-carbon triple bond (going from n = 1 to n = 2) decreases the electronic interactions, however the demonstrated communication between the metal termini for both C_2 and C_4 complexes does indicate their potential as one-dimensional molecular wires.

The synthesis of several heterometallic complexes such as Cp*(dppe)OsC≡CC≡CM(dppe)Cp* (where M = Ru / Fe) has not only allowed direct comparison to other hetero- and homo-metallic Group 8 complexes, but also completed this series. Cyclic voltammetry of these complexes revealed four one-electron redox events from the neutral through to the tetra-cation. Chemical oxidation and isolation of the homo-metallic mono- and di-cation complexes proved possible with the tri-cation being too unstable. The infrared results of these complexes allowed a relationship to be drawn between the vibrational frequencies of the carbon-carbon bonds and the electronic structure demonstrating a change from acetylenic to cumulenic when going from the neutral to di-cation.

This work has examined the effect of insertion of different organic and inorganic fragments into these straight carbon chains. It was found that despite there still being significant interactions between the termini and the inorganic centre, such as

ruthenocenyl, the centre still acts as an insulator. The addition of the anthracenyl fragment, however demonstrates comparable electronic interactions when compared to straight-chain analogues.

Work within this thesis also looked at the synthetic problems encountered in the synthesis of several known and novel complexes. These results revealed the effect of different solvents on the metal-halide bond. Through the synthesis of these complexes an interesting pattern was observed as you travel down Group 8 with both osmium and iron demonstrating very similar redox chemistry while ruthenium proved to be much more resistant to oxidation.

References.

(1) Wassel, R. A.; Gorman, C. B. *Angew. Chem. Int. Ed.* **2004**, *43*, 5120-5123.

(2) Gutmann, A. *Electronic Materials Chemistry, Marcel Dekker, New York.* **1996**, 199.

(3) Tour, J. M. *Acc. Chem. Res.* **2000**, *33*, 791.

(4) Ward, M. D. *Chem. Ind.* **1997**, 640.

(5) Donhauser, Z. J.; Montooth, B. A.; Kelly, K. F.; Bumm, L. A.; Monnell, J. D.; Stapleton, J. J.; Price, D. W.; Rawlett, A. M.; Allara, D. L.; Tour, J. M.; Weiss, P. S. *Science* **2001**, *292*, 2303.

(6) Fraysse, S.; Coudret, C.; Launay, J. P. *Eur. J. Inorg. Chem.* **2000**, 1581.

(7) Chen, J.; Reed, M. A.; Rawlett, A. M.; Tour, J. M. *Science* **1999**, 1550.

(8) Roth, K. M.; Dontha, N.; Dabke, R. B.; Gryko, D. T.; Clausen, C.; Lindsey, J. S.; Bocian, D. F.; Kuhr, W. G. *J. Vac. Sci. Technol. B* **2000**, *18*, 2359.

(9) Morales, G. M.; Jiang, P.; Yuan, S.; Lee, Y.; Sanchez, A.; You, W.; Yu, L. *J. Am. Chem. Soc.* **2005**, *127*, 10456.

(10) Robertson, N.; McGowan, C. A. *Chem. Soc. Rev.* **2003**, *32*, 96.

(11) Ward, M. D. *Chem. Ind.* **1996**, 568.

(12) Paul, F.; Lapinte, C. *Coord. Chem. Rev.* **1998**, *178-180*, 431.

(13) Tour, J. M.; Rawlett, A. M.; Kozaki, M.; Yao, Y.; Jagessar, R. C.; Dirk, S. M.; Price, D. W.; Reed, M. A.; Zhou, C. W.; Chen, J.; Wang, W.; Campbell, I. *Chem. Eur. J.* **2001**, *7*, 5118.

(14) Aviram, A.; Ratner, M. A. *Chem. Phys. Lett.* **1974**, *29*, 277.

(15) Xu, Z.; Moore, J. S. *Angew. Chem. Int. Ed. Engl.* **1993**, *32*, 1354.

(16) Tour, J. M. *Chem. Rev.* **1996**, *96*, 537.

(17) Valasek, M.; Pecka, J.; Jindrich, J.; Calleja, G.; Craig, P. R.; Michl, J. *J. Org. Chem.* **2005**, *70*, 405.

(18) Seifert, G.; Kohler, T.; Frauenheim, T. *Appl. Phys. Lett.* **2000**, *77*, 1313.

(19) Launay, J. P. *Chem. Soc. Rev.* **2001**, *30*, 386.

(20) Fink, H. W.; Schonenberger, C. *Nature* **1999**, *398*, 407.

(21) Williams, D. J.; Colquhoun, H. M.; O'Mahoney, C. A. *J. Chem. Soc., Chem. Commun.* **1994**, 1643.

(22) Schumm, J. S.; Pearson, D. L.; Tour, J. M. *Angew. Chem. Int. Ed.* **1994**, *33*, 1360.

(23) Iijima, S. *Nature* **1991**, *56*, 354.

(24) Tans, S. J.; Devoret, M. H.; Dai, H.; Thess, A.; Smalley, R. E.; Geerligs, L. J.; Dekker, C. *Nature* **1997**, *386*, 474.

(25) Robertson, N.; McGowan, C. A. *Chem. Soc. Rev.* **2003**, *32*, 96.

(26) Rueches, T.; Kim, K.; Joselevich, E.; Tseng, G. Y.; Cheung, C.-L.; Lieber, C. M. *Science* **2000**, *289*, 94.

(27) Collins, P. G.; Avouris, P. *Sci. Am.* **2000**, *283*, 62.

(28) Odom, T. W.; Huang, J.; Kim, P.; Leiber, C. M. *Nature* **1998**, *392*, 62.

(29) Dong, T. Y.; Chen, K.; Lin, M. C.; Lee, L. *Organometallics* **2005**, *24*, 4198.

(30) Narvor, N. L.; Toupet, L.; Lapinte, C. *J. Am. Chem. Soc.* **1995**, *117*, 7129.

(31) Bruce, M. I.; Ellis, B. G.; Low, P. J.; Skelton, B. W.; White, A. H. *Organometallics* **2003**, *22*, 3184.

(32) Bruce, M. I.; Costuas, K.; Davin, T.; Ellis, B. G.; Halet, J. F.; Lapinte, C.; Low, P. J.; Smith, M. E.; Skelton, B. W.; Toupet, L.; White, A. H. *Organometallics* **2005**, *24*, 3864.

(33) Jiao, H.; Costuas, K.; Gladysz, J. A.; Halet, J. F.; Guillemot, M.; Toupet, L.; Paul, F.; Lapinte, C. *J. Am. Chem. Soc.* **2003**, *125*, 9511.

(34) Robin, M. B.; Day, P. *Adv. Inorg. Chem. Radiochem.* **1967**, *10*, 247.

(35) Demadis, K. D.; Hartshorn, C. M.; Meyer, T. J. *Chem. Rev.* **2001**, *101*, 2655.

(36) Ghazala, S. I.; Paul, F.; Toupet, L.; Roisnel, T.; Hapiot, P.; Lapinte, C. *J. Am. Chem. Soc.* **2006**, *128*, 2463.

(37) Xu, B.; Xiao, X.; Tao, N. J. *J. Am. Chem. Soc.* **2003**, *125*, 16164.

(38) Xu, B.; Tao, N. J. *Science* **2003**, *301*, 1221.

(39) Reed, M. A.; Zhou, C.; Muller, C. J.; Burgin, T. P.; Tour, J. M. *Science* **1997**, *278*, 252.

(40) Goldsby, K. A.; Meyer, T. J. *Inorg. Chem.* **1984**, *23*, 3002.

(41) Sutton, J. E.; Sutton, P. M.; Taube, M. *Inorg. Chem.* **1979**, *18*, 1017.

(42) Richardson, D. E.; Taube, H. *J. Am. Chem. Soc.* **1983**, *105*, 40.

(43) Astruc, D. *Electron Transfer and Radical Processes in Transition-Metal Chemistry, VCH Pub. Inc., New York.* **1995**, 89.

(44) Best, S. P.; Ciniawsky, S. A.; Humphrey, D. G. *J. Chem. Soc., Dalton Trans.* **1996**, 2945.

(45) Best, S. P.; Clark, R. J. H.; McQueen, R. C. S. *Rev. Sci. Instrum.* **1987**, *58*, 2071.

(46) Duff, C. M.; Heath, G. A. *Inorg. Chem.* **1991**, *30*, 2528.

(47) Bruce, M. I.; Low, P. J.; Costuas, K.; Halet, J. F.; Best, S. P.; Heath, G. A. *J. Am. Chem. Soc.* **2000**, *122*, 1949.

(48) Brunschwig, B. S.; Creutz, C.; Sutin, N. *Chem. Soc. Rev.* **2002**, *31*, 168.

(49) Lambert, C.; Noll, G. *J. Am. Chem. Soc.* **1999**, *121*, 8434.

(50) Hush, N. S. *Coord. Chem. Rev.* **1985**, *64*, 135.

(51) Low, P. J. *Dalton Trans.* **2005**, 2821.

(52) Herrmann, C.; Neugebauer, J.; Gladysz, J. A.; Reiher, M. *Inorg. Chem.* **2005**, *44*, 6174.

(53) Dembinski, R.; Bartik, T.; Bartik, B.; Jaeger, M.; Gladysz, J. A. *J. Am. Chem. Soc.* **2000**, *122*, 810.

(54) Meyer, W. E.; Amoroso, A. J.; Horn, C. R.; Jaeger, M.; Gladysz, J. A. *Organometallics* **2001**, *20*, 1115.

(55) Brady, M.; Weng, W.; Gladysz, J. A. *J. Chem. Soc., Chem. Commun.* **1994**, 2655.

(56) Horn, C. R.; Martin-Alvarez, J. M.; Gladysz, J. A. *Organometallics* **2002**, *21*, 5386.

(57) Zhuravkev, F.; Gladysz, J. A. *Chem. Eur. J.* **2004**, *10*, 6510.

(58) Peters, T. B.; Bohling, J. C.; Arif, A. M.; Gladysz, J. A. *Organometallics* **1999**, *18*, 3261.

(59) Mohr, W.; Stahl, J.; Hampel, F.; Gladysz, J. A. *Chem. Eur. J.* **2003**, *9*, 3324.

(60) Stahl, J.; Bohling, J. C.; Bauer, E. B.; Peters, T. B.; Mohr, W.; Martin-Alvarez, J. M.; Hampel, F.; Gladysz, J. A. *Angew. Chem. Int. Ed.* **2002**, *41*, 1871.

(61) Wong, W.-Y.; Wong, C.-K.; Lu, G.-L.; Cheah, K.-W.; Shi, J.-X.; Lin, Z. *J. Chem. Soc., Dalton Trans.* **2002**.

(62) Szafert, S.; Gladysz, J. A. *Chem. Rev.* **2003**, *103*, 4175.

(63) Le Narvor, N.; Toupet, L.; Lapinte, C. *J. Am. Chem. Soc.* **1995**, *117*, 7129.

(64) Rappert, T.; Nurnberg, O.; Werner, H. *Organometallics* **1993**, *12*, 1359.

(65) Werner, H.; Lass, R. W.; Gevert, O.; Wolf, J. *Organometallics* **1997**, *16*, 4077.

(66) Bruce, M. I.; Hall, B. C.; Kelly, B. D.; Low, P. J.; Skelton, B. W.; White, A. H. *J. Chem. Soc., Dalton Trans.* **1999**, 3719.

(67) Bruce, M. I.; Ke, M.; Low, P. J.; Skelton, B. W.; White, A. H. *Organometallics* **1998**, *17*, 3539.

(68) Roberts, R. L.; Puschmann, H.; Howard, J. A. K.; Yamamoto, J. H.; Carty, A. J.; Low, P. J. *Dalton Trans.* **2003**, 1099.

(69) Coat, F.; Guillevic, M.-A.; Toupet, L.; Paul, F.; Lapinte, C. *Organometallics* **1997**, *16*, 5988.

(70) Bruce, M. I.; Ellis, B. G.; Gaudio, M.; Lapinte, C.; Melino, G.; Paul, F.; Skelton, B. W.; Smith, M. E.; Toupet, L.; White, A. H. *Dalton Trans.* **2004**, 1601.

(71) Bruce, M. I.; Hall, B. C.; Low, P. J.; Smith, M. E.; Skelton, B. W.; White, A. H. *Inorg. Chim. Acta* **2000**, *300-302*, 633.

(72) Ellis, B. G. *PhD Thesis, University of Adelaide* **2003**.

(73) Jevric, M.; Parker, C. R. *Private communication*.

(74) Halet, J. F. *Private communication*.

(75) Connelly, N. G.; Geiger, W. E. *Chem. Rev.* **1996**, *96*, 877.

(76) Guillemot, M.; Toupet, L.; Lapinte, C. *Organometallics* **1998**, *17*, 1928.

(77) This Work, Chapter six.

(78) Bartik, B.; Dembinski, R.; Bartik, T.; Arif, A. M.; Gladysz, J. A. *New J. Chem.* **1997**, *21*, 739.

(79) Work done in conjuction with Kramarczuk, K. A.

(80) Ustynyuk, N. A.; Vinogradova, V. N.; Kravtsov, D. N. *Metallo-org. Khim.* **1988**, *1*, 85.

(81) Davies, J. A.; El-Ghanem, M.; Pinkerton, A. A.; Smith, D. A. *J. Organomet. Chem.* **1991**, *409*, 367.

(82) Akita, M.; Terada, M.; Oyama, S.; Moro-oka, Y. *Organometallics* **1990**, *9*, 816.

(83) Smith, M. E. *PhD Thesis, University of Adelaide* **2002**.

(84) Binger, P.; Muller, P.; Phillips, P.; Gabor, B.; Mynott, R.; Herrmann, A. T.; Langhauser, F.; Kruger, C. *Chem. Ber.* **1992**, *125*, 2209.

(85) Liau, R.-Y.; Schier, A.; Schmidbaur, H. *Organometallics* **2003**, *22*, 3199.

(86) Kheradmandan, S.; Venkatesan, K.; Olivier, B.; Schmalle, H. W.; Berke, H. *Chem. Eur. J.* **2004**, *10*, 4872.

(87) Koutsantonis, G. A.; Selegue, J. P. *J. Am. Chem. Soc.* **1991**, *113*, 2316.

(88) Blau, R. J.; Chisholm, M. H.; Folting, K.; Wang, R. J. *J. Am. Chem. Soc.* **1987**, *109*, 4552.

(89) Ramsden, J. A.; Weng, W.; Arif, A. M.; Gladysz, J. A. *J. Am. Chem. Soc.* **1992**, *114*, 5890.

(90) Holmes, A. B.; Sporikou, C. N. *Org. Synth.* **1987**, *65*, 61.

(91) Brandsma, L. *Preparative Acetylenic Chemistry, 2nd ed., Elsevier Pub. Co., New York* **1988**.

(92) Webb, J. A.; Klijn, J. E.; Hill, P. A.; Bennett, J. L.; Goroff, N. S. *J. Org. Chem.* **2004**, *69*, 660.

(93) Ellis, J. E.; Flom, E. A. *J. Organomet. Chem.* **1975**, *99*, 263.

(94) Akita, M.; Chung, M.-C.; Sakurai, A.; Sugimoto, S.; Terada, M.; Tanaka, M.; Moro-oka, Y. *Organometallics* **1997**, *16*, 4882.

(95) Coto, A.; Rios, I.; Tenorio, M. J.; Puerta, M. C.; Valerga, P. *J. Chem. Soc., Dalton Trans.* **1999**, 4309.

(96) Tenorio, M. A. J.; Tenorio, M. J.; Puerta, M. C.; Valerga, P. *Inorg. Chim. Acta.* **1997**, *259*, 77.

(97) Slugovc, C.; Sapunov, V.; Wiede, P.; Mereiter, K.; Schmid, R.; Kirchner, K. *J. Chem. Soc., Dalton Trans.* **1997**, 4209.

(98) Oudai, N.; Costuas, K.; Bencharif, M.; Saillard, J.-Y.; Halet, J. F. *C. R. Chimie* **2005**, *8*, 1336.

(99) Bruce, M. I.; Hinterding, P.; Tiekink, E. R. T.; Skelton, B. W.; White, A. H. *J. Organomet. Chem.* **1993**, *450*, 209.

(100) Joslin, F. L.; Johnson, M. P.; Mague, J. T.; Roundhill, D. M. *Organometallics* **1991**, *10*, 41.

(101) Low, P. J. *Private communication.*

(102) Dixon, N. E.; Lawrance, G. A.; Lay, P. A.; Sargeson, A. M.; Taube, H. *Inorg. Synth.*,**1986**, *24*, 243.

(103) Weyland, T.; Lapinte, C.; Frapper, G.; Calhorda, M. J.; Halet, J. F.; Toupet, L. *Organometallics* **1997**, *16*, 2024.

(104) Le Narvor, N.; Lapinte, C. *Organometallics* **1995**, *14*, 634.

(105) Le Stang, S.; Paul, F.; Lapinte, C. *Organometallics* **2000**, *19*, 1035.

(106) Roue, S.; Lapinte, C.; Bataille, T. *Organometallics* **2004**, *23*, 2558.

(107) Guillaume, V.; Mahias, V.; Mari, A.; Lapinte, C. *Organometallics* **2000**, *19*, 1422.

(108) Montigny, F. d.; Argouarch, G.; Costuas, K.; Halet, J. F.; Roisnel, T.; Toupet, L.; Lapinte, C. *Organometallics* **2005**, *24*, 4558.

(109) Bruce, M. I.; Hall, B. C.; Low, P. J.; Skelton, B. W.; White, A. H. *J. Organomet. Chem.* **1999**, *592*, 74.

(110) Ghose, B. N. *Synth. React. Inorg. Met. Org. Chem.* **1994**, *24*, 29.

(111) Antonova, A. B.; Bruce, M. I.; Ellis, B. G.; Gaudio, M.; Humphrey, P. A.; Jevric, M.; Melino, G.; Nicholson, B. K.; Perkins, G. J.; Skelton, B. W.; Stapleton, B.; White, A. H.; Zaitseva, N. N. *Chem. Commun.* **2004**, *8*, 960.

(112) Antonova, A. B.; Gaudio, M.; Zaitseva, N. N. *Private communication.*

(113) Paul, F.; Meyer, W. E.; Toupet, L.; Jiao, H.; Gladysz, J. A.; Lapinte, C. *J. Am. Chem. Soc.* **2000**, *122*, 9405.

(114) Selegue, J. P. *Organometallics* **1982**, *1*, 217.

(115) Argouarch, G.; Thominot, P.; Paul, F.; Toupet, L.; Lapinte, C. *C. R. Chimie* **2003**, *6*, 209.

(116) Montigny, F. d.; Argouarch, G. *Private communication.*

(117) Daia, D. E.; Gabbutt, C. D.; Heron, B. M.; D., H. J.; Hursthouse, M. B.; Abdul Malik, K. M. *Tetrahedron Lett.* **2003**, *44*, 1461.

(118) Fairlamb, I. J. S.; Bauerlein, P. S.; Marrison, L. R.; Dickinson, J. M. *Chem. Commun.* **2003**, 632.

(119) Morandini, F.; Dondana, A.; Munari, I.; Pilloni, G.; Consiglio, G.; Sironi, A.; Moret, M. *Inorg. Chim. Acta.* **1998**, *282*, 163.

(120) Bruce, M. I.; Low, P. J.; Hartl, F.; Humphrey, P. A.; Montigny, F.; Jevric, M.; Lapinte, C.; Perkins, G. J.; Roberts, R. L.; Skelton, B. W.; White, A. H. *Organometallics* **2005**, *24*, 5241.

(121) Roger, C.; Marseille, P.; Salus, C.; Hamon, J.-R.; Lapinte, C. *J. Organomet. Chem.* **1987**, *336*, C13.

(122) Roger, C.; Hamon, P.; Toupet, L.; Rabae, H.; Saillard, J.-Y.; Hamon, J.-R.; Lapinte, C. *Organometallics* **1991**, *10*, 1045.

(123) Brandsma, L.; Verkruijsse, H. D.; Vasilevsky, S. F. *Application of Transition Metal Catalysts in Organic Synthesis, Springer-Verlag, Berlin.* **1998**.

(124) Sato, M.; Shintate, H.; Kawata, Y.; Sekino, M.; Katada, M.; Kawata, S. *Organometallics* **1994**, *13*, 1956.

(125) Sato, M.; Hayashi, Y.; Kumakura, S.; Shimizu, N.; Katada, M.; Kawata, S. *Organometallics* **1996**, *15*, 721.

(126) Sato, M.; Kawata, Y.; Shintate, H.; Habata, Y.; Akabori, S.; Unoura, K. *Organometallics* **1997**, *16*, 1693.

(127) Davison, A.; Solar, J. P. *J. Organomet. Chem.* **1979**, *C13*, 166.

(128) Bruce, M. I.; Hambley, T. W.; Snow, M. R.; Swincer, A. G. *Organometallics* **1985**, *4*, 494.

(129) Bruce, M. I.; Low, P. J.; Skelton, B. W.; White, A. H. *New J. Chem.* **1998**, *22*, 419.

(130) Onitsuka, K.; Ose, N.; Ozawa, F.; Takahashi, S. *J. Organomet. Chem.* **1999**, *578*, 169.

(131) Kramarczuk, K. A. *Honours Thesis, University of Adelaide* **2001**.

(132) Bruce, M. I.; Jevric, M. *Unpublished work.*

(133) Doisneau, G.; Balavoine, G.; Fillebeen-Khan, T. *J. Organomet. Chem.* **1992**, *113*, 425.

(134) Yuan, Z.; Stringer, G.; Jobe, I. R.; Kreller, D.; Scott, K.; Koch, L.; Taylor, N. J.; Marder, T. B. *J. Organomet. Chem.* **1993**, *115*, 452.

(135) Baratta, W.; Zotto, A. D.; Rigo, P. *Organometallics* **1999**, *18*, 5091.

(136) Pudelski, J. K.; Callstrom, M. R. *Organometallics* **1994**, *13*, 3095.

(137) Wohler, L.; Metz, L. *Z. Anorg. Chem* **1925**, *149*, 301.

(138) Bailar, J. C.; Emeleus, H. J.; Nyholm, R. S.; Trotman Dickenson, A. F. *Comprehensive Inorganic Chemistry* **1973**, *3*, 1216.

(139) Hanker, J. S.; Romanovicz, D. K.; Padykula, H. *Histochem. J.* **1976**, *49*, 263.

(140) Bruce, M. I.; Windsor, N. J. *Aust. J. Chem.* **1977**, *30*, 1601.

(141) Boeyens, J. C. A.; Levendis, D. C.; Bruce, M. I.; Williams, M. L. *J. Cryst. Spectrosc. Res* **1986**, *16*, 519.

(142) Malin, J. M. *Inorg. Synth.* **1980**, *20*, 61.

(143) Elliott, G. P.; Mcauley, N. M.; Roper, W. R. *Inorg. Synth.*,**1989**, *26*, 184.

(144) Wilczewski, T. *J. Organomet. Chem.* **1986**, *317*, 307.

(145) Bruce, M. I.; Williams, M. L.; Patrick, J. M.; White, A. H. *Aust. J. Chem.* **1983**, *36*, 1353.

(146) Bruce, M. I.; Low, P. J.; Skelton, B. W.; Tiekink, E. R. T.; Werth, A.; White, A. H. *Aust. J. Chem.* **1995**, *48*, 1887.

(147) www.webelement.com.

(148) Tiekink, E. R. T. *Z. Krist* **1992**, *198*, 158.

(149) Pearson, W. H.; Shade, J. E.; Brown, J. E.; Bitterwolf, T. E. *Acta. Crystallogr.* **1996**, *C52*, 1106.

(150) Bruce, M. I.; Koutsantonis, G. A. *Aust. J. Chem.* **1991**, *44*, 207.

(151) Zou, C.; Wrighton, M. S.; Blaha, J. P. *Organometallics* **1987**, *6*, 1452.

Complex Index.

1 $\{Cp^*(dppe)Fe\}_2(\mu\text{–}C{\equiv}CC{\equiv}C)$

2 $\{Cp^*(dppe)Ru\}_2(\mu\text{–}C{\equiv}CC{\equiv}C)$

3 $Cp^*(dppe)FeC{\equiv}CC{\equiv}CRu(dppe)Cp^*$

4 $RuCl(dppe)Cp^*$

5 $Cp^*(dppe)RuC{\equiv}CC{\equiv}CTMS$

6 $\{Cp^*(dppe)Os\}_2(\mu\text{-}C{\equiv}CC{\equiv}C)$

7 $[Cp^*(dppe)Os{=}C{=}CH_2][PF_6]$

8 $Cp^*(dppe)OsC{\equiv}CH$

9 $[Cp^*(dppe)Os{=}C{=}CHCH{=}C{=}Os(dppe)Cp^*][PF_6]_2$

10 $Cp^*(dppe)OsC{\equiv}CC{\equiv}CRu(dppe)Cp^*$

11 $Cp^*(dppe)OsC{\equiv}CC{\equiv}CFe(dppe)Cp^*$

12 $Cp^*(dppe)OsC{\equiv}CC{\equiv}CTMS$

13 $OsCl(dppe)Cp^*$

14 $Cp^*(dppe)OsC{\equiv}CC_4(H)_2(TMS)C{\equiv}COs(dppe)Cp^*$

15 $\{Cp(dppe)Ru\}_2(\mu\text{-}C{\equiv}C)$

16 $[Cp(dppe)Ru{=}C{=}CH_2][PF_6]$

17 $RuCl(dppe)Cp$

18 $[Ru(THF)(dppe)Cp]^+$

19 $Cp(dppe)RuC{\equiv}CRu(dppe)Cp^*$

20 $Cp(dppe)RuC{\equiv}COs(dppe)Cp^*$

21 $Cp(dppe)RuC{\equiv}COs(dppe)Cp$

22 $Cp(dppe)RuC{\equiv}CFe(dppe)Cp$

23 $FeCl(dppe)Cp^*$

24 $Cp^*(dppe)FeC{\equiv}CC_{14}H_8C{\equiv}CFe(dppe)Cp^*$

25 $\{Cp^*(dppe)Fe(\mu{=}C{=}C{=}C{=}C_{14}H_8{=}C{=}C{=}\}_2$

26 $Cp^*(dppe)RuC{\equiv}CC_{14}H_8C{\equiv}CRu(dppe)Cp^*$

27 $Cp^*(dppe)FeC{\equiv}CC_{14}H_8C{\equiv}CRu(dppe)Cp^*$

28 $C_{14}H_9CH(OH)C{\equiv}CTMS$

29 $C_{14}H_9CH(OH)C{\equiv}CH$

30 $[Cp^*(dppe)Fe(=C=C=CH(C_{14}H_9)][BPh_4]$

31 $BrC_{14}H_8CHO$

32 $TMSC{\equiv}CC_{14}H_8CHO$

33 $TMSC{\equiv}CC_{14}H_8CH(OH)C{\equiv}CTIPS$

34 $HC{\equiv}CC_{14}H_8CH(OH)C{\equiv}CTIPS$

35 $(\text{-}C{\equiv}CC_{14}H_8CH(OH)C{\equiv}CTIPS)_2$

36 $C_{14}H_9CH(OH)C{\equiv}CTIPS$

37 $HC{\equiv}CC_{14}H_8CHO$

38 $HC{\equiv}CC_{14}H_8CH(OH)C{\equiv}CTMS$

39 $(\text{-}C{\equiv}CC_{14}H_8CH(OH)C{\equiv}CTMS)_2$

40 $BrC_{14}H_8CH(OH)C{\equiv}CTMS$

41 $[Cp^*(dppe)Fe(=C=C=CH(C_{14}H_8Br)][BPh_4]$

42 $Os(C{\equiv}CFc)(dppe)Cp$

43 $HC{\equiv}CFc$

44 $OsCl(dppe)Cp$

45 1,1'-$\{Cp[m\text{-}tol_3P]_2RuC{\equiv}C\}_2Rc'$

46 $Os\{C[=C(CN)_2]=CFc=C(CN)_2\}dppeCp$

47 1,1'-$\{Cp[m\text{-}tol_3P]_2RuC{\equiv}C\}_2Rc'$ + TCNE same face

48 1,1'-$\{Cp[m\text{-}tol_3P]_2RuC{\equiv}C\}_2Rc'$ + TCNE opposite face

49 $K_2[OsO_2(OH)_4]$

50 $OsBr(dppe)Cp^*$

51 $OsCl_2(PPh_3)_3$

52 $OsCl(PPh_3)_2Cp$

53 $RuCl(PPh_3)_2Cp$

54 $OsCl(COD)Cp^*$

55 $OsBr(PPh_3)_2Cp$

56 $[Cp(dppe)Fe=C=CH_2][PF_6]$

57 $[Cp(dppe)Ru=C=CH_2][PF_6]$

58 $[Cp(dppe)Os=C=CH_2][PF_6]$

59 $[Cp^*(dppe)Os=C=CH_2][PF_6]$